SANDIA REPORT

SAND98–1016
Unlimited Release
Printed August 1998

Damage Tolerance Assessment of Bonded Composite Doubler Repairs for Commercial Aircraft Applications

Dennis Roach

Prepared by
Sandia National Laboratories
Albuquerque, New Mexico 87185 and Livermore, California 94550

Sandia is a multiprogram laboratory operated by Sandia Corporation, a Lockheed Martin Company, for the United States Department of Energy under Contract DE-AC04-94AL85000.

Sandia National Laboratories

Issued by Sandia National Laboratories, operated for the United States Department of Energy by Sandia Corporation.

Available to DOE and DOE contractors from
Office of Scientific and Technical Information
P.O. Box 62
Oak Ridge, TN 37831

Prices available from (615) 576-8401, FTS 626-8401

Available to the public from
National Technical Information Service
U.S. Department of Commerce
5285 Port Royal Rd
Springfield, VA 22161

NTIS price codes
Printed copy: A07
Microfiche copy: A01

SAND98-1016
Unlimited Release
Printed August 1998

Damage Tolerance Assessment of Bonded Composite Doubler Repairs for Commercial Aircraft Applications *

Dennis Roach
Airworthiness Assurance Department

Sandia National Laboratories
P. O. Box 5800
Albuquerque, NM 87185-0615

Abstract

The Federal Aviation Administration has sponsored a project at its Airworthiness Assurance NDI Validation Center (AANC) to validate the use of bonded composite doublers on commercial aircraft. A specific application was chosen in order to provide a proof-of-concept driving force behind this test and analysis project. However, the data stemming from this study serves as a comprehensive evaluation of bonded composite doublers for general use. The associated documentation package provides guidance regarding the design, analysis, installation, damage tolerance, and nondestructive inspection of these doublers. This report describes a series of fatigue and strength tests which were conducted to study the damage tolerance of Boron-Epoxy composite doublers. Tension-tension fatigue and ultimate strength tests attempted to grow engineered flaws in coupons with composite doublers bonded to aluminum skin. An array of design parameters, including various flaw scenarios, the effects of surface impact, and other "off-design" conditions, were studied. The structural tests were used to: 1) assess the potential for interply delaminations and disbonds between the aluminum and the laminate, and 2) determine the load transfer and crack mitigation capabilities of composite doublers in the presence of severe defects. A series of specimens were subjected to ultimate tension tests in order to determine strength values and failure modes. It was demonstrated that even in the presence of extensive damage in the original structure (cracks, material loss) and in spite of non-optimum installations (adhesive disbonds), the composite doubler allowed the structure to survive more than 144,000 cycles of fatigue loading. Installation flaws in the composite laminate did not propagate over 216,000 fatigue cycles. Furthermore, the added impediments of impact - severe enough to deform the parent aluminum skin - and hot-wet exposure did not effect the doubler's performance. Since the tests were conducting using extreme combinations of flaw scenarios (sizes and collocation) and excessive fatigue load spectrums, the performance parameters were arrived at in a conservative manner.

* This work was performed for the Federal Aviation Administration (FAA) Technical Center under US Department of Transportation Contract DTFA 03-95-X-90002. This document is currently under review by the FAA for parallel publication by the Department of Transportation.

Acknowledgments

Numerous people have contributed to the success of validating bonded composite doublers for commercial aircraft applications. In addition to the FAA Airworthiness Assurance Center (Sandia Labs), team members for the L-1011 door corner repair included Lockheed-Martin Aeronautical Systems (doubler design and analysis - Bob Bell, Surendra Shah, and Kevin Jones), Delta Air Lines (Engineering Repair Authorization document, doubler installation and NDI support - John Marshall, Malcolm Westberry, Chuck Minafo, and Raymond Worley), Textron Systems Div. (specimen fabrication and installation - Tom Shahood and Jeff Brown), the FAA Atlanta Aircraft Certification Office (review and approval - Charles Perry and Paul Sconyers), and the FAA William J. Hughes Technical Center (project oversight - Pete Versage, Chris Smith, and Dave Galella; FAA Chief Scientist NDI - Al Broz). Specific contributions to the damage tolerance information presented here came from Phil Walkington and Darin Graf (Sandia Labs) who assisted in instrumentation and specimen inspections and Marlene Uribe (Sandia Labs) who helped conduct the fatigue tests. These contributions are gratefully acknowledged. This work was funded by the FAA William J. Hughes Technical Center under a U.S. Department of Transportation contract.

FOREWORD

As part of the Federal Aviation Administration's (FAA) National Aging Aircraft Research Program (NAARP), the FAA William J. Hughes Technical Center, established a major center at Sandia National Laboratories (SNL): the Airworthiness Assurance NDI Validation Center (AANC). The AANC conducts numerous projects related to the validation of improved aircraft maintenance practices. The Center also supports technology development initiatives. To facilitate these activities, the AANC has set up a hangar facility at the Albuquerque International Airport.

One of the primary goals of NAARP is to foster new technology associated with the repair of civil aircraft. A typical aircraft can experience over 2,000 fatigue cycles (cabin pressurizations) and even greater flight hours in a single year. The unavoidable by-product of this use is that flaws develop throughout the aircraft's skin and substructure elements. These flaws can take the form of cracks, corrosion, disbonds, dents, and gouges. Composite doublers, or repair patches, provide an innovative repair technique which can enhance the way aircraft are maintained. Instead of riveting multiple steel or aluminum plates to facilitate an aircraft repair, it is possible to bond a single Boron-Epoxy composite doubler to the damaged structure.

Economic barriers to the purchase of new aircraft have created an aging aircraft fleet and placed even greater demands on efficient and safe repair methods. The use of bonded composite doublers offers the airframe manufacturers and airline maintenance facilities a cost effective technique to safely extend the lives of their aircraft. However, before this advanced aircraft repair technique could be accepted for commercial aircraft use, uncertainties surrounding the application, subsequent inspection and long-term endurance of composite doublers had to be addressed.

This document is one in a series of reports covering the AANC's comprehensive evaluation of composite doublers for commercial aircraft use. The development and validation effort addressed the full array of engineering issues including design, material allowables, installation, damage tolerance, quality assurance, in-service surveillance (nondestructive inspection), and FAA/industry requirements. For completeness, beneficial overlaps of information will be presented in each report. The full suite of reports, each containing a similar foreword section, are:

1. *Development and Validation of Nondestructive Inspection Techniques for Composite Doubler Repairs on Commercial Aircraft (SAND98-1014)*
2. *Damage Tolerance Assessment of Bonded Composite Doubler Repairs for Commercial Aircraft (SAND98-1016)*
3. *Full-Scale Structural and NDI Validation Tests on Bonded Composite Doublers for Commercial Aircraft Applications (SAND98-1015)*

Report #1: "Development and Validation of Nondestructive Inspection Techniques for Composite Doubler Repairs on Commercial Aircraft" - The purpose of this report is to document the NDI techniques and procedures which have been assessed to inspect bonded composite doubler installations on aircraft structures. The intent of the inspections are to detect: 1) disbonds, delaminations, and porosity in the composite laminate, and 2) cracks in

the parent aluminum material. An array of conventional and advanced NDI techniques were evaluated. Flaw detection sensitivity studies were conducted on applicable eddy current, ultrasonic, X-ray and thermography based devices. The pulse-echo ultrasonic technique deployed in this program uses the traditional A-scan approach as its basis, however, significant improvements are realized through the adoption of C-scan imaging. An X-ray inspection was modified from its original specification in the L-1011 NDT Manual. A series of tests were performed in order to: 1) verify that composite doublers do not impede X-ray inspections, and 2) study X-ray optimization when inspecting through composite doublers. This study concluded that a team of NDI techniques can identify flaws in composite doubler installations well before they reach critical size. The development of appropriate inspection reference standards, critical to performing proper inspections, is also discussed.

Report #2: "Damage Tolerance Assessment of Bonded Composite Doubler Repairs for Commercial Aircraft" - This report focuses on a series of fatigue and strength tests which were conducted to study the damage tolerance and fatigue life enhancement associated with Boron-Epoxy composite doublers. Tension-tension fatigue and ultimate strength tests attempted to grow engineered flaws in coupons with composite doublers bonded to aluminum skin. An array of design parameters, including various flaw scenarios, the effects of surface impact, and other "off-design" conditions, were studied. The structural tests were used to: 1) assess the potential for interply delaminations and disbonds between the aluminum and the laminate, and 2) determine the load transfer and crack mitigation capabilities of composite doublers in the presence of severe defects. A series of specimens were subjected to ultimate tension tests in order to determine strength values and failure modes. Coupon test configurations, the loads applied, the test procedures, and all associated results are documented in this report.

Report #3: "Full-Scale Structural and NDI Validation Tests on Bonded Composite Doublers for Commercial Aircraft Applications" - This report describes a series of structural and nondestructive inspection (NDI) tests which were conducted to investigate the performance of Boron-Epoxy composite doublers. Full-scale tests were conducted on fuselage panels cut from retired aircraft. These full-scale tests studied stress reductions, crack mitigation, and load transfer capabilities of composite doublers using simulated flight conditions of cabin pressure and axial stress. Also, structures which modeled key aspects of aircraft structure repairs were subjected to extreme tension, shear and bending loads to examine the composite laminate's resistance to disbonds and delaminations especially in high peel stress regions. Nondestructive inspections were conducted throughout the test series in order to validate pertinent techniques on actual aircraft structure.

The test results were also used to verify design and analyses methodologies for composite doubler technology. The primary test article was a large fuselage section cut from a retired All Nippon Airways (ANA) L-1011 aircraft. The fuselage test article included a passenger door cut-out and contained all substructure frame, longeron, and stringer elements. Several other test configurations - consisting of composite doublers mounted on simulated aircraft panels - were examined in order to assess the response of composite doublers in worst-case shear and bending load scenarios. These two test configurations were loaded to failure in order to determine safety factors associated with current doubler design methodologies.

Background and Deliverables - The Federal Aviation Administration sponsored this project at the AANC to determine the viability of bonded composite doublers and to gain FAA approval for their use on commercial aircraft. A specific application was chosen - reinforcement of an L-1011 door frame - in order to provide the proof-of-concept driving force behind this test and analysis project. In addition to the AANC, other project team members included Lockheed-Martin, Delta Air Lines, and Textron Specialty Materials. Appropriate FAA oversight was provided through the Atlanta Aircraft Certification Office (ACO) and the FAA's William J. Hughes Technical Center. The project deliverables will assist the FAA in developing guidance which assures the continued airworthiness of composite doublers.

The data stemming from this study serves as a comprehensive evaluation of bonded composite doublers for general use. The associated documentation package provides guidance regarding the design, analysis, installation, damage tolerance, quality assurance, and nondestructive inspection of these doublers. Although an initial aircraft application was pursued in parallel to this investigation, the overall goal was to provide results that are pertinent to any use of Boron-Epoxy doublers for commercial aircraft reinforcement or repair. In order to streamline the use of composite doublers in other applications, the documentation package for this validation effort resides in the public domain. The FAA's Atlanta ACO maintains the documents under the FAA project number SP1798AT-Q. The documentation package includes:

	Report	Report Number
1.	Boron-Epoxy Material Allowables	LG95ER0193
2.	Damage Tolerance Assessment	SNL96ER0189
3.	Full-Scale Structural and NDI Testing	SNL96ER0006
4.	Boron-Epoxy Doubler Installation Process Specification	TSM 2000,008-001
5.	Design and Analysis of L-1011 Composite Doubler	LG95ER0157
6.	L-1011 Composite Doubler Drawing (Upper Fwd. Corner, P-3 Passenger Door)	LCC-7622-378
7.	Nondestructive Inspection Procedures	AANC-PEUT-Comp-5521/4-004

The first use of the above documentation package was to support the installation of an FAA-approved Boron-Epoxy composite repair on a Lockheed L-1011 aircraft. The repair has been installed on the upper forward corner of a P3 passenger door frame. The aircraft is currently operating in the Delta Air Lines fleet. Three post-installation inspections, spanning one year of aircraft operation, have shown the doubler to be free of flaws. A second important product of the results cited above is the Lockheed-Martin Service Bulletin 093-53-278 which allows the door corner composite doubler to be installed on all L-1011 aircraft. With the successful completion of the L-1011 door corner application, the FAA and AANC are now conducting a program with Boeing and Federal Express to develop, certify, and install a more generic set of composite doubler applications for a variety of common aircraft repairs.

This Page Left Intentionally Blank

Damage Tolerance Assessment of Bonded Composite Doubler Repairs for Commercial Aircraft Applications

Table of Contents

Damage Tolerance Assessment of Bonded Composite Doubler Repairs for Commercial Aircraft Applications

List of Figures

Figure Page

This Page Left Intentionally Blank

1.0 Background

In 1991, the FAA's William J. Hughes Technical Center established The Airworthiness Assurance NDI Validation Center (AANC) at Sandia National Laboratories. Its primary mission is to support technology development, validation, and transfer to industry in order to enhance the airworthiness and improve the aircraft maintenance practices of the U.S. commercial aviation industry. The Center conducts projects in a myriad of engineering disciplines. The results are placed in the public domain so that the industry at-large can reap the benefits of FAA-funded R & D efforts. To support the Center's goals, the FAA/AANC has set up a hangar facility at the Albuquerque International Airport which contains a series of transport and commuter aircraft. The facility replicates a working maintenance environment by incorporating both the physical inspection difficulties as well as the environmental factors which influence maintenance reliability. Sandia's charter with the FAA includes a wide array of airworthiness assurance disciplines such as nondestructive inspection, structural mechanics, computer science, fire safety, and corrosion.

The development and application of new aircraft repair techniques needs to keep pace with the growing understanding of aircraft structural aging phenomena. One of the primary goals of the Federal Aviation Administration's (FAA) National Aging Aircraft Research Program (NAARP) is to foster new technology associated with the repair of civil aircraft. A typical aircraft can experience over 2,000 fatigue cycles (cabin pressurizations) and even greater flight hours in a single year. The unavoidable by-product of this use is that flaws develop throughout the aircraft's skin and substructure elements. These flaws can take the form of cracks, corrosion, disbonds, dents, and gouges. Composite doublers, or repair patches, provide an innovative repair technique which can enhance the way aircraft are maintained. The high modulus of Boron-Epoxy composite material enables a doubler to pick up load efficiently and effectively when bonded to a metal structure. The load transfer occurs by shear through the adhesive.

In its role as validator of advanced aircraft maintenance techniques, the AANC's main objective is to perform comprehensive, independent, and quantitative evaluations of new repairs and associated inspection techniques. Towards that end, the Federal Aviation Administration sponsored a project at the AANC to validate bonded composite doubler technology and to gain FAA approval for composite doubler use on commercial aircraft. An industry team consisting of an Original Equipment Manufacturer (Lockheed-Martin) and an airline (Delta Air Lines) was formed. FAA oversight was provided through the Atlanta Aircraft Certification Office (ACO) and the FAA's William J. Hughes Technical Center. The overall goal of this project was to establish the capabilities of composite doublers and to assist the FAA in developing guidance which will assure the continued airworthiness of these aircraft repairs.

Two focal points of this study were the effects of non-optimum installations and the certification of adequate inspection procedures. This document addresses the first item: effects of non-optimum installations or damage tolerance. A companion document under

the auspices of this same FAA project discusses nondestructive inspections of Boron-Epoxy composite doubler installations.

A series of fatigue and strength tests were performed in order to establish the damage tolerance of composite doublers. Fatigue and ultimate strength tests were carried out on specimens with crack, disbond, and impact flaws. Environmental conditions representing temperature and humidity exposure were also included in some of the coupon tests. The structural tests were used to: 1) assess the potential for interply delaminations and disbonds between the aluminum and the laminate, and 2) determine the load transfer and crack mitigation capabilities of composite doublers in the presence of severe defects. A series of specimens were subjected to ultimate tension tests in order to determine strength values and failure modes. The damage tolerance was determined in light of the inspection requirements and resolution for flaw detection. In this project, close consultation with the FAA and the air transport industry was pursued in order to meet the necessary requirements. Active industry involvement was essential to the efficient execution of the AANC activities and ensured the relevance of any resulting recommendations.

In addition to developing general information to support composite doubler use, this program introduced composite doubler technology to the U.S. commercial aircraft fleet. A specific application was chosen - reinforcement of an L-1011 door frame - in order to provide the proof-of-concept driving force behind this test and analysis project. By focusing on a particular commercial aircraft application - reinforcement of the L-1011 door frame - and encompassing all "cradle-to-grave" issues such as design, analysis, installation, long term durability, and nondestructive inspection, this program was designed to comprehensively evaluate the capabilities of composite doublers. The first use of the damage tolerance assessment presented herein was to support the structural analysis of the L-1011 composite doubler (Reference [1]).

AANC and Validation Issues for Bonded Composite Doublers - The use of composite doublers in commercial aviation must address issues such as installation, subsequent inspection and long-term endurance. Because of the rapidly increasing use of composites on commercial airplanes, coupled with the potential for economic savings associated with their use in aircraft structures, it appears that the demand for validated composite repair technology will increase.

Efforts to bring newly developed technology to the field can encounter some obstacles. Field personnel may be reluctant to accept new repair practices and associated NDI procedures for several reasons. The technology may not be fully field tested; there may not be enough experience under field conditions. It may require the purchase of new equipment and aircraft maintenance facilities want proof that the capital outlay is justified. Further, it may require retraining personnel. The AANC was set up to comprehensively address these obstacles and reduce the risks involved in introducing new maintenance practices to the field. The Center does this by evaluating the performance of new hardware, software, and NDI procedures; by demonstrating and

documenting the performance of systems; and by supporting the economic analyses of new maintenance practices.

Bonded Composite Doublers on Aircraft Structure - The number of commercial airframes exceeding twenty years of service continues to grow. In addition, Service Life Extension Programs are becoming more prevalent and test and evaluation programs are presently being conducted to extend the "economic" service life of commercial airframes to thirty years. The use of bonded composites may offer the airframe manufacturers and airline maintenance facilities a cost effective technique to safely extend the lives of their aircraft. Flight demonstrations and operational testing have confirmed that under proper conditions, composite doublers can provide a long lasting and effective repair or structural reinforcement [2-6]. Reference [6] describes a series of analytical models which were developed to study the stress field in and around composite doublers and the crack growth life extension resulting from composite doubler use.

The comprehensive goal of these AANC validation efforts are to address any remaining uncertainties about composite doublers and thus, assure: 1) proper design and installation processes, and 2) the continued safe operation of the doublers over time. Through the use of laboratory test structures and flight demonstrations on an in-service L-1011 airplane, this study investigated general composite doubler design, fabrication, installation, structural integrity, and nondestructive evaluation.

Repairs and reinforcing doublers using bonded composites have numerous advantages over mechanically fastened repairs. Adhesive bonding eliminates stress concentrations, and new potential crack initiation sites, caused by additional fastener holes. Composites are readily formed into complex shapes permitting the repair of irregular components. Also, composite doublers can be tailored to meet specific anisotropy needs thus eliminating the undesirable stiffening of a structure in directions other than those required. Other advantages include corrosion resistance, a high strength-to-weight ratio, and potential time savings in installation. The economic advantages stem primarily from time savings in installation and the secondary effect of reduced aircraft downtime. Exact dollar values depend on the complexity of the repair installation and the number of repairs installed.

Typical Composite Doubler Installation and NDI - Figure 1 shows a typical bonded composite doubler repair over a cracked parent aluminum structure. Sample composite doubler installations, showing two families of potential aircraft repair applications, are shown in Figure 2. The number of plies and fiber orientation are determined by the nature of the reinforcement required (i.e. stress field and configuration of original structure). Surface preparation is the most critical aspect of the doubler installation. This consists of paint removal, solvent clean, scotch-brite abrasion and chemical treatment to assure proper adhesion. Since the doubler must be installed in the field, vacuum bag pressure and thermal heat blankets, commonly used on in-situ honeycomb repairs, are used to cure the composite laminate and adhesive layer.

The taper at the edge of the doubler is used to produce a gradually increasing stress gradient in the area of primary load transfer. In some applications, such as the L-1011 door corner doubler design, lightning protection is provided by a copper wire mesh which is imbedded in an adhesive film and applied as a top ply over the doubler. The lightning protection ply has a larger footprint than the composite laminate in order to provide a conductive link between the copper mesh and the surrounding aluminum skin. Finally, a top ply of fiberglass is installed to supply mechanical and environmental protection for the installation.

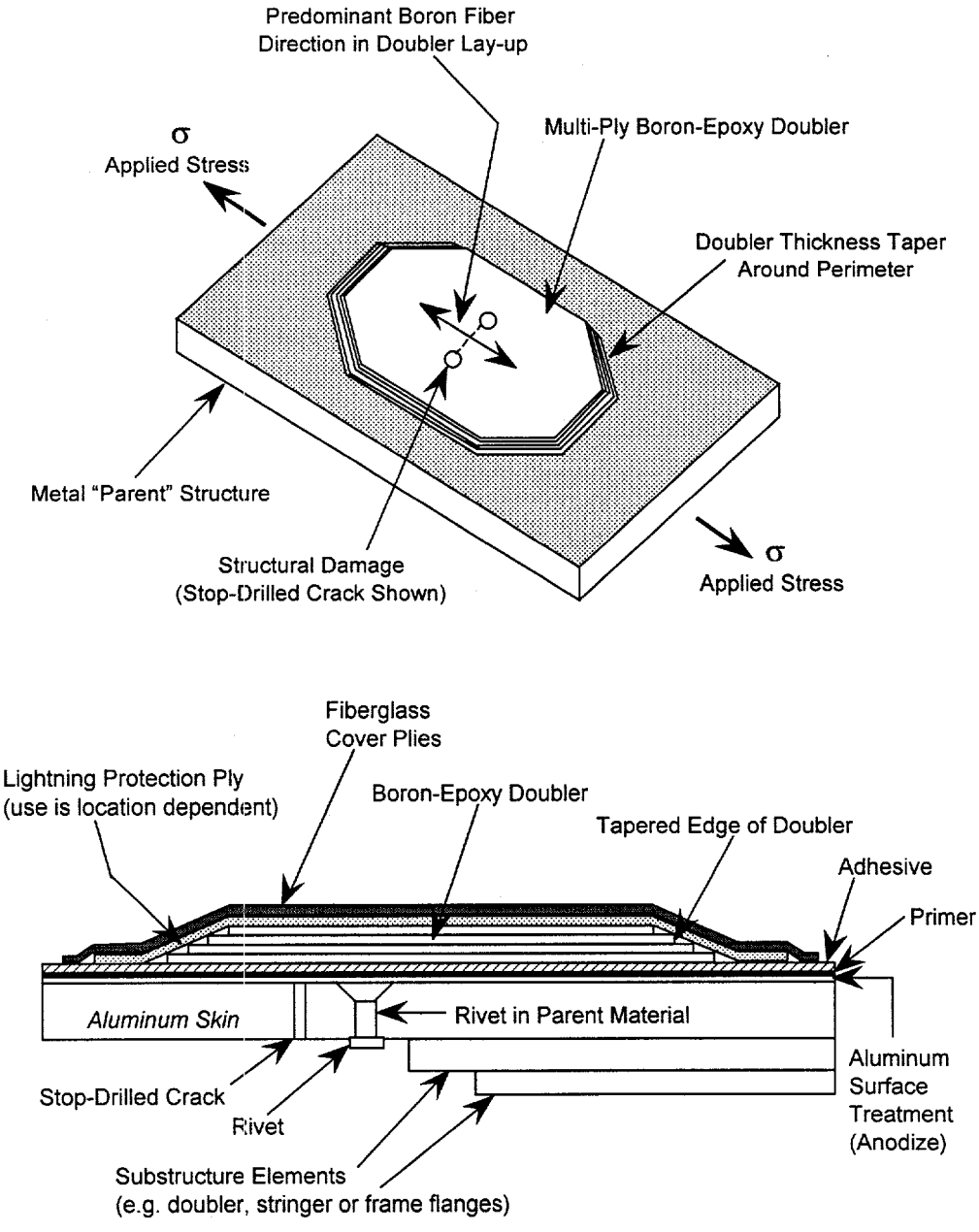

Figure 1: Schematic of Bonded Composite Doubler Installation on an Aluminum Skin

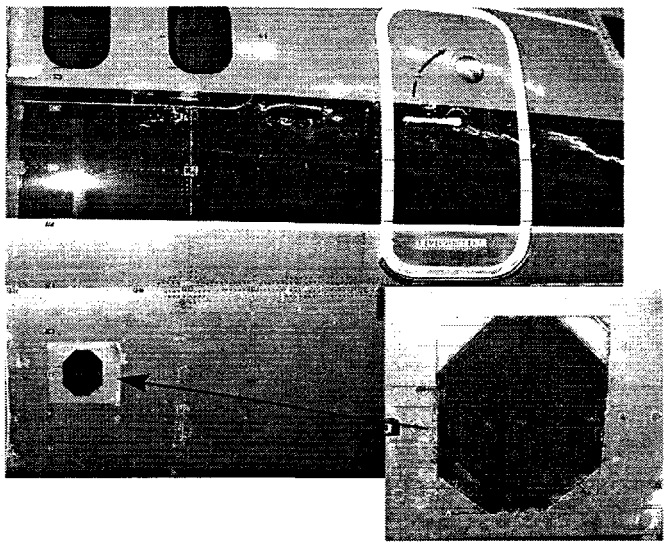

(a) Sample Fuselage Skin Repair (composite doubler approx. 12" X 10")

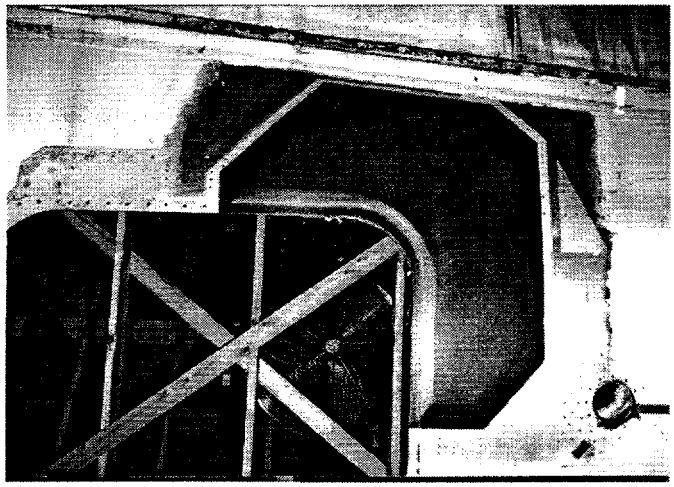

(b) Sample Door Corner Repair (composite doubler approx. 5 ft.^{2} footprint)

Figure 2: Sample Bonded Composite Doubler Installations Showing Two Families of Potential Repair Applications

1.1 Doubler Design Guidelines

Moving Technology into Routine Maintenance Progams - Reference [7] describes airframe maintenance programs from an airlines' perspective. It describes sources of aircraft damage and how the damage is addressed through inspection and repair tasks. A detailed maintenance program is required to ensure that an aircraft can be operated safely for an extended period of time. The emphasis of the maintenance program must be

constantly adjusted to cater to the age of the fleet [7]. These revisions require the co-operation of the aircraft manufacturers, the airlines, and the airworthiness authority to ensure that changes made are technically correct, stringent enough to assure the aircraft's continued safety, with due consideration to the cost to the airline. Aircraft structures suffer continuous degradation throughout their service lives. Corrosion, fatigue, impact and accidental damage from assorted ground activities all contribute to this structural degradation. The airlines and aircraft maintenance depots accomplish permanent and interim repairs suited to the situation and in line with current industry practices. These acceptable repair practices must be continuously revisited and expanded to take advantage of new materials, new processes, and new techniques that offer both engineering and economic advantages. Through the steady and comprehensive introduction of test data, analyses, and in-service composite doubler installations on commercial aircraft a critical database is being assembled to accurately guide enhancements to formal maintenance programs. This is an important step in the evolution of composite doubler applications since it will eventually eliminate the need for each bonded composite repair to be preceded by a lengthy research and testing program.

Doubler Design Guidelines – References [8-11] provide an excellent set of guidelines for designing composite doubler repairs. The primary issues to be addressed include the optimum location, size, shape, and laminate taper for the patches. The major factors that determine the patch design parameters are the stress levels at the repaired flaw, the stress levels in the composite doubler (maximum allowable fiber stresses), and the stress levels in the adhesive layer between the doubler and the aluminum skin. The important, fundamental results produced by Jones and Callinan in ref. [8] are worth reviewing in some detail in order to prepare for the damage tolerance discussions later in this report.

The ref. [8] crack repair study used a unidirectional Boron-Epoxy laminate (fiber perpendicular to crack) as a baseline design. The study found that for patches that cover the entire length of the crack, a one ply (0.0057" thick) patch reduces the stress intensity factor to 33.5% of its value for the unpatched crack. Furthermore, the rate of decrease in the stress intensity factor, K_{IP}, as the patch thickness increases was found to be quite low. A six layer patch, for example, produced a K_{IP} value of 19.5% of the unpatched value. Thus, an increase in patch thickness by a factor of 6 only produces an additional 14% reduction in the stress intensity factor. Another important finding of the ref. [8] study was that in thin patches, the stresses over the flaw (in both the patch and the adhesive) are critical. However, as the patch thickness is increased, the shear stresses in the adhesive at the edges of the patch footprint become critical and may exceed allowable limits.

The findings summarized above produced a series of design requirements that are necessary to maintaining the structural integrity of a composite doubler repair [8].

1) Fiber Strain – For a maximum Boron fiber strain of 5,000 με, the stress in the fibers must satisfy

$$\sigma_f \leq 0.005\, E_{11} \qquad (1)$$

where E_{11} is Young's modulus in the direction of the fibers (28.0 X 10^6 psi). When the fiber stress concentration, K_f, is considered the governing equation for fiber strain becomes

$$\sigma_f = K_f \sigma \leq .14 \text{ lb/in}^2 \qquad (2)$$

Thus, if the applied stress, σ, is known the maximum permissible value of K_f and the minimum permissible patch thickness can be determined.

2) Shear Stress in Adhesive – For a maximum allowable adhesive shear stress of 7 KSI and considering the stress concentrations at the crack and at the edge of the patch, the following design equations must be satisfied

$$\tau_{a(c)} = K_{a(c)} \sigma \leq 7{,}000 \text{ lb/in}^2 \qquad (3)$$

$$\tau_{a(e)} = K_{a(e)} \sigma \leq 7{,}000 \text{ lb/in}^2 \qquad (4)$$

Equations (2) and (3) can be solved to produce a doubler thickness to satisfy the stress requirements at the crack (for both laminate and adhesive). However, this often produces adhesive stresses at the edge of the doubler that exceed those allowed by eq. (4). Ref. [8] showed that the adhesive stresses at the edge of the doubler can be reduced to admissible levels by stepping the thickness of the doubler from one or two plies at the outer perimeter to full thickness over a taper region. The length of the taper region is normally chosen to produce an edge taper ratio (taper depth-to-thickness increase ratio) of 10 to 30. Figure 1 shows a typical doubler edge taper used to gradually transfer load from the aluminum skin and reduce the shear stress in the adhesive. An ongoing study at the AANC regarding the application of composite doublers to DC-10 skin damage encountered this need to balance doubler thickness with an appropriate edge taper [12].

Ref. [8] provides quantitative stress reductions corresponding to the use of stepped doublers. It also lists the effects of varying adhesive thickness and the difference between single- and double-sided repairs.

Doubler Installation Examples - Numerous composite doubler repairs have been installed on military aircraft (both U.S. and foreign). Significant advances have been made on commercial aircraft applications [13-20], however, most of these have occurred on non U.S. certificated aircraft. Hence, the basis of this FAA-sponsored program is to safely and comprehensively introduce the use of composite repairs to the U.S. commercial aircraft fleet. Some examples of successful composite doubler repairs follows. Reference [14] describes a well-documented and extensive composite repair program carried out by the U.S. Air Force. In this program, composite doublers were used to repair cracks emanating from weep holes in the C-141 wing plank risers.

Reference [15] gives an overview of the applications pursued by the Aeronautical and Maritime Research Laboratory in Australia which has pioneered the use of this technology. These composite doubler applications include crack repairs on an F111 wing pivot fitting and stiffening of a corroded keel beam in an Ansett Airlines 767 aircraft. References [17-20] describe the program being led by the FAA's Airworthiness Assurance Center at Sandia National Labs. This program is working to validate the use of composite doublers and streamline their introduction to the U.S. commercial aircraft fleet. An L-1011 door corner repair is now operating in the Delta Air Lines fleet while a family of DC-10 fuselage skin repairs are being readied for a pilot program with Federal Express. A series of demonstration programs [13, 15] have produced hundreds of simulated repair installations on commercial and military aircraft. Since the parent structures were not flawed in these demonstration programs, there were no detrimental effects stemming from stress risers beneath the doublers. However, these composite doubler programs are accumulating thousands of successful flight hours/cycles that can be used to further establish the viability of composite doubler repair technology.

1.2 Damage Tolerance and Fracture Control Plan

1.2.1 Damage Tolerance and Analysis Methodologies

Damage Tolerance of Composite Doublers – Inspection requirements (sensitivity and inspection intervals) are driven by Damage Tolerance Analyses (DTA). However, the stack of metal parent material (isotropic), composite lamina (anisotropic), and adhesive layers makes the analysis quite complex and hinders the calculation of an exact DTA. It is difficult to determine the effects of flaw size and the point at which a flaw size/location becomes critical. This is especially true of disbond, delamination, and porosity flaws. Thus, an increased emphasis is placed on quantifying the probability that a flaw of a particular size and location will be detected by a piece of NDT equipment. *In any surveillance of aircraft structure there are three main aspects to the inspection requirements: 1) the damage tolerance analysis (DTA) which determines the flaw onset and growth data (especially critical flaw size information), 2) the sensitivity, accuracy, and repeatability of NDI techniques which, in concert with the DTA, establishes the minimum inspection intervals, and 3) the impediments that the NDI techniques must contend with while achieving the required level of sensitivity.* In addition to this report, detailed discussions on damage tolerance assessments for composite doubler installations are presented in references [21-25].

The reference [24] observations mirror one of the primary results obtained in the damage tolerance assessment presented in this report: adhesively bonded doublers are extremely damage tolerant to large disbonds and other detrimental conditions such as impact and hot-wet conditioning. These results are quantified in Section 3 of this report. If, in fact, disbond and delamination flaws do not grow even under extreme environmental conditions, then an acceptable design should be predicated on the fact that the stresses in the adhesive are kept below a limiting or threshold value. As a result, reference [24] introduces an essential design methodology that considers damage tolerance. It uses a

fatigue threshold load, P_f, and a fatigue threshold strain, ε_f, below which irreversible damage in the adhesive will not occur. For thin skin repairs, the equations used to determine the threshold load and strain values are as follows:

$$P_f = 2\,(t\,W_f\,ET)^{1/2} \tag{5}$$

$$\varepsilon_f = 2\,(t\,W_f\,E/T)^{1/2} \tag{6}$$

where,

t = thickness of the adhesive
T = thickness of the adherend (skin)
E = Young's modulus of the skin
W_f = threshold value of the strain energy density of the adhesive

W_f can be determined experimentally [25]. Ref. [24] also describes the maximum load, P_{max}, that can be carried by a bond in a symmetrical bonded joint as,

$$P_{max} = 2\,(t\,W_c\,ET)^{1/2} \tag{7}$$

where W_c is the maximum strain energy density of the adhesive. Thus, composite doubler repair design guidelines are that P_{max} is greater than the ultimate load for the repaired structure and that P_f is greater than the limit load. Ref. [24] also points out that these critical design variables are affected by the loading rate. A conservative estimate for P_{max} can be obtained by using the value of the maximum von Mises equivalent stress in the adhesive, σ_e, as measured in high strain rate tests. For FM73, the adhesive used in this study, $\sigma_e = P_{max}$ = 5,800 psi and the threshold stress σ_{th} = 3,600 psi. This analysis approach clearly shows the importance of the adhesive in determining the overall performance of the bonded repair. Ref. [24] goes on to point out the effects of the inelastic strain build-up in the adhesive layer that can accumulate with each load cycle. This hysteresis must be considered when determining the loads and fatigue cycles necessary to reach the maximum strain. The approach outlined above can be used to certify that a composite doubler design will satisfy the damage tolerance provisions of the U.S. Federal Aviation Regulations (FAR) Part 25.

The abilities of nondestructive inspection techniques to meet the DTA flaw detection requirements are presented in references [17-18, 26-28]. The fundamental result from the ref. [18] NDI study is that a team of NDI techniques can identify flaws well before they reach critical size. Crack detection in the parent aluminum material can be accomplished using conventional eddy current and X-ray techniques. Also, ultrasonic and thermography methods have been successfully applied to the problem of disbond and delamination detection.

Analysis of Composite Repairs – Numerous efforts have developed, refined, and advanced the use of methodologies needed to analyze composite doubler installations. Obviously, this is a critical element in the repair process since a badly implemented repair is detrimental to fatigue life and may lead to the near-term loss of structural integrity. The difficulties associated with analyzing the stress fields and flaw tolerance of various composite doubler designs and installations are highlighted in references [5], [21], and [23]. Doubler design and analysis studies [5-6, 24, 29-36] have led to computer codes and turn-key software [37-38] for streamlining the analyses. These developments have taken great strides to eliminate the approximations and limitations in composite doubler DTA. In references [21] and [31], Baker presents an extensive study of crack growth in repaired panels under constant amplitude and spectrum loading. The installation variables evaluated were: 1) doubler disbond size, 2) applied stress, 3) doubler thickness, 4) min-to-max stress ratios (R ratio), and 5) temperature.

In refs. [21] and [31], a predictive capability for the growth of cracks repaired with composite doublers was developed using Rose's analytical model [32] and experimental fatigue studies. The important stress variables include the stress range, $\Delta\sigma_\infty$, and stress ratio, R, where,

$$\Delta\sigma_\infty = \sigma_{max} - \sigma_{min} \tag{8}$$

$$R = \sigma_{min}/\sigma_{max} \tag{9}$$

A Paris-type crack growth relationship is assumed between da/dN and ΔK for the repaired crack such that,

$$da/dN = f(\Delta K,R) = A_R \Delta K^{n(R)} \tag{10}$$

where a is the crack length, N is the number of fatigue cycles, and A_R and $n(R)$ are constants for a given R value. Tests results in [21] and [31] produced crack growth constants and were used to validate the model for crack mitigation effects of composite doublers. It was determined that Rose's model for predicting the stress-intensity range, ΔK, provides a good correlation with measured crack growth data (da/dN), however, anomalies were observed in the cases of temperature and R-ratio effects. Estimates of crack growth in composite doublers containing various disbond sizes were also determined.

In lieu of using computationally expensive, three-dimensional finite elements, reference [33] presents the use of a simple analysis using Mindlin plate theory. The aluminum parent plate and composite doubler are modeled separately by the Mindlin plate finite element (using ANSYS) and the adhesive layer is modeled with effective springs connecting the doubler to the aluminum plate. The model showed excellent agreement with existing boundary element solutions and three-dimensional finite element solutions when calculating the stress intensity factors for double-sided patches. However, the Mindlin plate theory produced appreciably different K values than a three-dimensional

FEM for single-sided doubler repairs. These results highlight some of the difficulties in modeling composite doubler repairs and the need for innovative schemes to address single-sided repairs.

Complete three dimensional FEM analyses of composite doubler repairs are provided in reference [34]. Ref. [34] addressed one-sided repairs and showed that the stress intensity factor reaches an asymptotic value, rather than increasing indefinitely as would be the case for an unrepaired crack. Furthermore, the stress intensity factor can be approximated by an analytical expression that provides a close, yet conservative, estimate for repairs over all crack lengths. While the stress intensity factor for a one-sided repair is much less than the unrepaired configuration, it exceeds the value for the corresponding two-sided repair. This analytical finding supports test results that show the secondary bending induced by the shift in neutral axis in one-sided patch has a detrimental effect on the efficiency of bonded composite repairs.

No discussion of design and analysis methodologies is complete without a mention of a closely-coupled validation program. Reference [35] presents a detailed design and analysis validation effort to substantiate a safety-critical repair to an F-111 lower wing skin. The repair substantiation involved both detailed FEM stress analysis and structural testing ranging from coupons to quasi full-scale specimens representing a spar-stiffened wing box structure. The intercomparison of results provides a high level of confidence that the static residual strength has been restored to the original ultimate strength levels. It also provides a good foundation for the subsequent management of the repaired structure by establishing inspection intervals with sufficient safety factors.

The test results presented in this document and in reference [17] supplement the composite doubler analyses efforts described above and provide a basis of comparison with computational models. Analysis improvements, however, must be validated by successful flight performance of operational doublers. This can only be accumulated over a long period of time. Continued surveillance of installed doublers will provide quantitative flight performance history and produce a conservative safety factor. Thus, regardless of the excellent damage tolerance results accumulated to date, NDI will continue to play a critical role in the use of composite doublers.

This damage tolerance assessment report, along with references [17-19], describes the validation program that accompanied the L-1011 door corner repair. In these four documents, the attempts to generalize the performance test results are discussed. Every effort was made to design the test specimens and extrapolate the results to as wide a range of composite doubler repairs as possible. The overall goal in this approach is to minimize and optimize the testing that must compliment each new composite doubler installation. In order for composite doubler technology to be useful to the commercial aircraft industry, the design-to-installation cycle must be streamlined. An ongoing study at the AANC is addressing composite doubler repairs on DC-10 fuselage skin [20] with the goal of streamlining the design, validation, and certification process. The end result will be the revision of the DC-10 Structural Repair Manual (alternate repairs for existing riveted metallic doublers) thus allowing more rapid and widespread use of specific

doubler repairs. It should be noted that a closely monitored pilot program will be completed prior to any revision of the DC-10 Structural Repair Manual.

Need for Damage Tolerance Assessments - One of the primary concerns surrounding composite doubler technology pertains to long-term survivability, especially in the presence of non-optimum installations. This test program demonstrated the damage tolerance capabilities of bonded composite doublers. The fatigue and strength tests quantified the structural response and crack abatement capabilities of Boron-Epoxy doublers in the presence of worst case flaw scenarios. The engineered flaws included cracks in the parent material, disbonds in the adhesive layer, and impact damage to the composite laminate. Environmental conditions representing temperature and humidity exposure were also included in the coupon tests.

1.2.2 Damage Tolerance Establishes Fracture Control Plan

Establishing Damage Tolerance - Damage tolerance is the ability of an aircraft structure to sustain damage, without catastrophic failure, until such time that the component can be repaired or replaced. The U.S. Federal Aviation Requirements (FAR 25) specify that the residual strength shall not fall below limit load, P_L, which is the load anticipated to occur once in the life of an aircraft. This establishes the minimum permissible residual strength $\sigma_P = \sigma_L$. To varying degrees, the strength of composite doubler repairs are affected by crack, disbond, and delamination flaws. The residual strength as a function of flaw size can be calculated using fracture mechanics concepts. Figure 3 shows a sample residual strength diagram. The residual strength curve is used to relate this minimum permissible residual strength, σ_P, to a maximum permissible flaw size a_P.

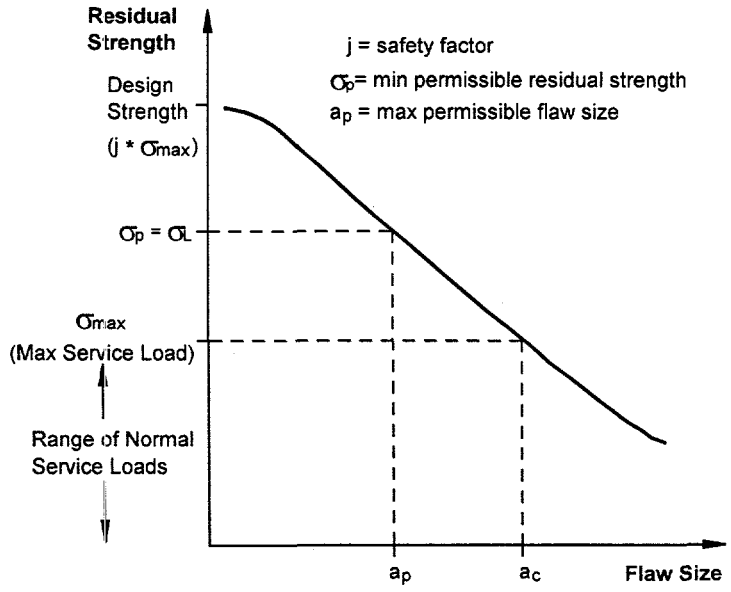

Figure 3: Residual Strength Curve

A fracture control plan is needed to safely address any possible flaws which may develop in a structure. Nondestructive inspection is the tool used to implement the fraction control plan. Once the maximum permissible flaw size is determined, the additional information needed to properly apply NDI is the flaw growth versus time or number of cycles. Figure 4 contains a flaw growth curve. The first item of note is the total time, or cycles, required to reach a_P. A second parameter of note is a_d which is the minimum detectable flaw size. A flaw smaller than a_d would likely be undetected and thus, inspections performed in the time frame prior to n_d would be of little value. The time, or number of cycles, associated with the bounding parameters a_d and a_P is set forth by the flaw growth curve and establishes *H(inspection)*. Safety is maintained by providing at least two inspections during *H(inspection)* to ensure flaw detection between a_d and a_P.

Inspection Intervals - An important NDI feature highlighted by Fig. 4 is the large effect that NDI sensitivity has on the required inspection interval. Two sample flaw detection levels $a_{d\,(1)}$ and $a_{d\,(2)}$ are shown along with their corresponding intervals $n_{d\,(1)}$ and $n_{d\,(2)}$. Because of the gradual slope of the flaw growth curve in this region, it can be seen that the inspection interval H_1*(inspection)* can be much larger than H_2*(inspection)* if NDI can produce just a slightly better flaw detection capability. Since the detectable flaw size provides the basis for the inspection interval, it is essential that quantitative measures of flaw detection are performed for each NDI technique applied to the structure of interest. This quantitative measure is represented by a Probability of Detection (PoD) curve such as the one shown in Figure 5. Regardless of the flaw size, the PoD never quite reaches 1 (100% possibility of detection). Inspection sensitivity requirements normally ask for a 90-95% PoD at a_P. For any given inspection task, the PoD is affected by many factors such as: 1) the skill and experience of the inspector, 2) accessibility to the structure, 3) exposure of the inspection surface, and 4) confounding attributes such as underlying structure or the presence of rivets. Thus, the effects of circumstances on PoD must be accounted for in any NDI application and associated fracture control plan.

As an example of the DTA discussed above, reference [1] describes the design and analysis process used in the L-1011 program. It presents the typical data - stress, strength, safety factors, and damage tolerance - needed to validate a composite doubler design. The design was analyzed using a finite element model of the fuselage structure in the door region along with a series of other composite laminate and fatigue/fracture computer codes. Model results predicted the doubler stresses and the reduction in stress in the aluminum skin at the door corner. Peak stresses in the door corner region were reduced by approximately 30% and out-of-plane bending moments were reduced by a factor of 6. The analysis showed that the doubler provided the proper fatigue enhancement over the entire range of environmental conditions. The damage tolerance analysis indicated that the safety-limit of the structure is increased from 8,400 flights to 23,280 flights after the doubler installation (280% increase in safety-limit). It established an inspection interval for the aluminum and composite doubler of 4,500 flights.

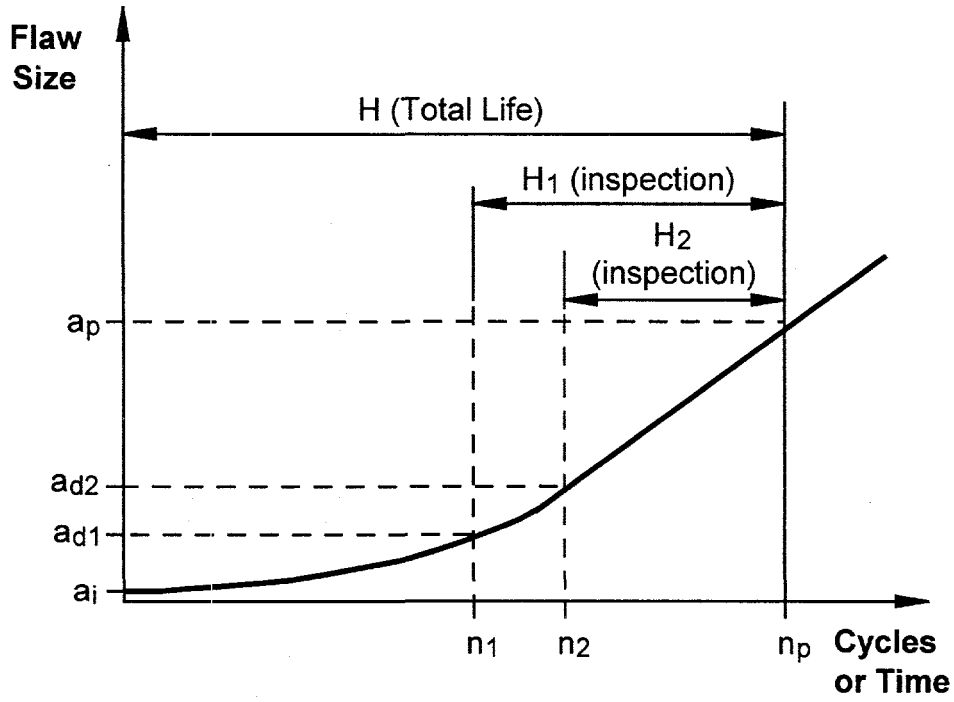

Figure 4: Crack Growth Curve Showing Time Available for Fracture Control

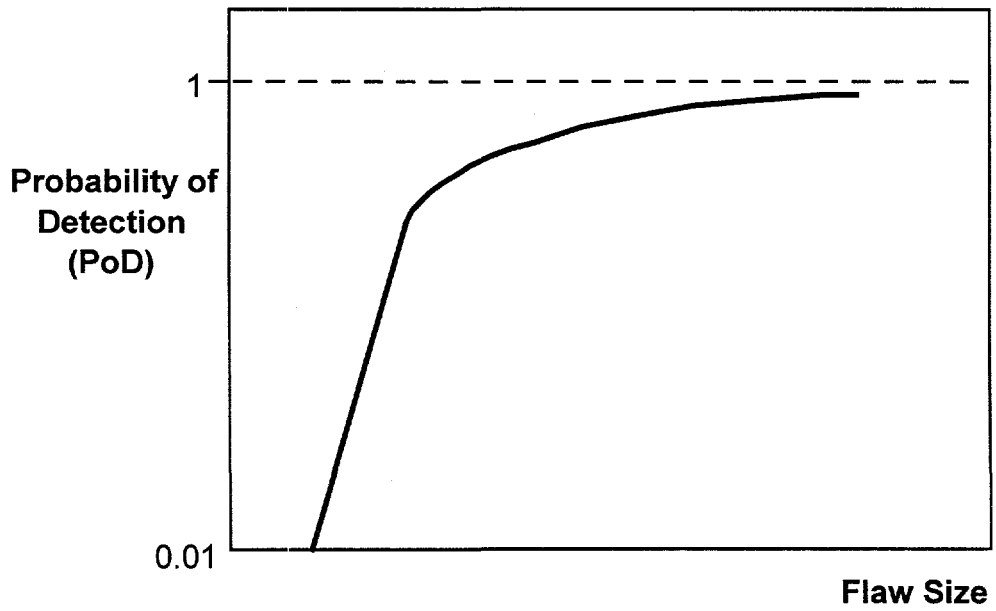

Figure 5: Probability of Flaw Detection vs. Flaw Size

1.2.3 Damage Tolerance Testing

A series of fatigue coupons were designed to evaluate the damage tolerance performance of bonded composite doublers. The general issues addressed were: 1) doubler design - strength, durability, 2) doubler installation, and 3) NDI techniques used to qualify and accept installation. Each specimen consisted of an aluminum "parent" plate, representing the original aircraft skin, with a bonded composite doubler. The doubler was bonded over a flaw in the parent aluminum. The flaws included fatigue cracks (unabated and stop-drilled), aluminum cut-out regions, and disbond combinations. The most severe flaw scenario was an unabated fatigue crack which had a co-located disbond (i.e. no adhesion between doubler and parent aluminum plate) as well as two, large, 1" diameter disbonds in the critical load transfer region of the doubler perimeter. Tension-tension fatigue and residual strength tests were conducted on the laboratory specimens. The entire damage tolerance assessment program and the test results are presented in the following chapters. Through-transmission ultrasonics, resonance UT, and eddy current inspection techniques were interjected throughout the fatigue test series in order to track the flaw growth.

General Use of Results - The objective of this test effort was to obtain a generic assessment of the ability of Boron-Epoxy doublers to reinforce and repair cracked aluminum structure. By designing the specimens using the nondimensional stiffness ratio, it is possible to extrapolate these results to various parent structure and composite laminate combinations. The number of plies and fiber orientations used in these tests resulted in an extensional stiffness ratio of 1.2:1 $\{(Et)_{BE} = 1.2\ (Et)_{Al}\}$. Independent Air Force [39] and Boeing studies [40-41] have determined that stiffness ratios of 1.2 to 1.5 produce effective doubler designs. Lockheed-Martin has also used this range of stiffness ratios in military composite doubler designs.

1.3 Conformity Inspection and FAA Oversight

Appropriate conformity checks and FAA oversight was obtained on all aspects of specimen fabrication, testing, and data acquisition. The following items were witnessed by the FAA or an FAA designated representative. The test plan was reviewed and approved by a Designated Engineering Representative.

1. Fabrication of the test specimens - composite doubler fabrication and installation.
2. Impact and hot-wet conditioning of test specimens.
3. Conformity inspection of coupon test articles to assure adherence to specified structural configuration.
4. Verification that the calibration and operation of test equipment was current.
5. Verification of strain gage locations.

1.4 Technical and Economic Considerations

Cost-Benefit Assessment - A complete validation process must also include an assessment of the cost effectiveness of the new maintenance technique in light of the engineering advantages. This includes an analysis of the implementation costs represented by dollars, time, and resources that are used to carry out the maintenance practice (in this case aircraft repair and subsequent inspection). The aircraft repair process using bonded composite doublers has numerous advantages over conventional, mechanically fastened repairs. Following is a summary of the engineering and economic advantages. Table 1 compares the key features of composite doubler repairs with existing metallic doubler repair technology.

Engineering Advantages:

1. adhesive bonding eliminates stress concentrations caused by additional fastener holes
2. crack mitigation performance (improved fatigue life of structure)
3. strength-to-weight ratio (modulus and strength values are three times that of aluminum yet material is 50% lighter and doublers can be up to 50% thinner than metal repairs)
4. flexibility in design (composite doublers can be tailored to meet specific directional strength needs)
5. corrosion resistance (Boron-Epoxy material does not corrode and will not induce corrosion in the parent material)
6. formability (composite laminates are easily formed to fit the contour of fuselage sections and tight radii).

Economic Advantages:

The economic advantages stem primarily from time savings in installation and the secondary effect of reduced aircraft downtime. Exact dollar values depend on the complexity of the repair installation and the number of repairs installed. In general, data accumulated to date using demonstration installations have indicated that it may be possible to realize a 50% - 60% savings in labor when applying composite doublers.

One of the most common aircraft repairs is the application of a doubler to a cracked, corroded, or dented surface skin (scab repairs). Composite doublers are particularly well suited to these type of repairs. Many of these repairs can be completed without accessing the inside of the aircraft structure. This can produce a large time savings if the comparable metallic doubler requires inside access to install the fasteners. These type of surface skin scab repairs can be found many times on a single aircraft. Thus, economies of scale come into play and the cost savings can be substantial when applied over a carrier's entire fleet.

An important by-product of the reduced man-hours needed to effect a composite doubler repair is that it may be possible to return an aircraft to service earlier. In some cases, a composite doubler may allow for an overnight repair and eliminate any loss of service for

an aircraft. Revenue loss for aircraft down time can be upwards of $80,000 per day. With approximately 6,000 aircraft flying in the U.S. commercial fleet, reduced aircraft downtime may represent the greatest potential for cost savings.

Aircraft Repair Feature	Bonded Composite Doublers	Riveted Metal Doublers	Advantage of Composites & Notes
Stress Field	• No need for additional fastener holes in structure • Bond provides a uniform stress filed	• New holes produce stress risers and fatigue crack initiation sites • Load transfer occurs exclusively at edge of doubler	• Produces gradual load transfer and more uniform stress field • Eliminates stress risers (stress magnification of 3 found in riveted doublers)
Fatigue Life	• Composite doubler can be tailored to provide stiffness only in the required directions • Bonded doubler provides uniform stress reduction in immediate vicinity of flaw	• Isotropic material produces uniform & sometimes undesirable stiffening in all directions	• Longer Fatigue Life: crack mitigation tests show less than half the crack growth over the same number of fatigue cycles (fatigue life improved by factor of 2.5) • Improved damage tolerance
Corrosion Resistance	• Boron-Epoxy material does not corrode or induce galvanic reaction in the parent aluminum material • Adhesive bonding process seals off material beneath it from all moisture	• Metal doublers will corrode over time • Installation provides location for water entrapment between doubler and parent aluminum structure; this accelerates corrosion process	• May eliminate follow-up maintenance costs (inspection, corrosion removal, replacement of metal doubler) • Avoids aggravation of initial flawed area
Aerodynamics	• Higher strength at reduced ply thickness allows for thinner doublers	• Typical repairs are two to four plates thick (0.125" to 0.375")	• Up to 50% decrease in thickness improves aerodynamics

Table 1: Comparison Between Bonded Composite Doubler Repair Technique and Riveted Metallic Doubler Aircraft Repairs

Aircraft Repair Feature	Bonded Composite Doublers	Riveted Metal Doublers	Advantage of Composites & Notes
Strength-to Weight	• Modulus = 28 msi • Tensile Strength = 225 ksi • Density = .066 lbs/in^3	• Modulus (alum/steel) = 10 / 30 msi • Tensile Strength (alum/steel) = 64 / 80 ksi • Density (alum/steel) = 0.100 / 0.283 lbs/in^3	• Strength properties exceed aluminum and steel • Improved fuel efficiency through reduction in aircraft weight (50% - 70% reduction in weight per doubler)
Method of Attachment to Aircraft	• Adhesive bonding	• Mechanical fasteners, rivets	• Certain structures, such as wing spars, cannot tolerate the addition of new holes (must be replaced rather than repaired) • Proper surface preparation and adhesive bonding processes are crucial to composite doublers
Formability	• Hand pressure can readily shape doubler to contoured surfaces (e.g. engine cowlings, wing leading edges)	• Machining process must be employed to provide proper contour on metal doublers in tight radii areas	• Eliminates additional step and associated costs

Table 1: Comparison Between Bonded Composite Doubler Repair Technique and Riveted Metallic Doubler Aircraft Repairs (continued)

Aircraft Repair Feature	Bonded Composite Doublers	Riveted Metal Doublers	Advantage of Composites & Notes
Installation Time	• Typical 1 ft.^{2} fuselage skin repair (12 man-hours)	• Typical 1 ft.^{2} fuselage skin repair (40 man-hours)	• Decreased aircraft down time • Maintenance cost savings due to reduced man-hours required
Material Cost	• Cost depends on size of doubler and number of plies • Typical 1 ft.^{2} skin repair doubler: $800 (20 plies)	• Depends on number of plates & rivets, metal type, and forming required • Typical 1 ft.^{2} skin repair doubler: $300 (including machining)	• Costs approximately 2.5 times comparable metal doublers • Greater material costs can be offset by savings in man-hours & decreased aircraft downtime

Table 1: Comparison Between Bonded Composite Doubler Repair Technique and Riveted Metallic Doubler Aircraft Repairs (continued)

This Page Left Intentionally Blank

2.0 Composite Doubler Damage Tolerance Tests

The Composite Coupon test series utilized tension specimens to assess the damage tolerance and strength of composite doublers bonded to aluminum skin. Fatigue and ultimate strength tests were performed on specimens with crack, disbond, and impact flaws. Environmental conditions representing temperature and humidity exposure were also included in some of the coupon tests. The structural tests were used to: 1) assess the potential for interply delaminations and disbonds between the aluminum and the laminate, and 2) determine the load transfer and crack mitigation capabilities of composite doublers in the presence of severe defects. A series of specimens were subjected to ultimate tension tests in order to determine strength values and failure modes. Nondestructive inspections (NDI) were interjected throughout the test series in order to closely monitor the response of the specimens during testing. Photographs of the damage tolerance test set-up and a close-up view of a composite doubler test coupon are shown in Figure 6.

The two main potential causes of structural failure in composite doubler installations are cracks in the aluminum and adhesive disbonds/delaminations. When disbonds or delaminations occur, they may lead to joint failures. By their nature, they occur at an interface and are, therefore, always hidden. A combination of fatigue loads and other environmental weathering effects can combine to initiate these types of flaws. Periodic inspections of the composite doubler for disbonds and delaminations (from fabrication, installation, fatigue, or impact damage) is essential to assuring the successful operation of the doubler over time. The interactions at the bond interface are extremely complex, with the result that the strength of the bond is difficult to predict or measure. Even a partial disbond may compromise the integrity of the structural assembly. Therefore, it is necessary to detect all areas of disbonding or delamination, as directed by DTA, before joint failures can occur.

2.1 Participants in Coupon Specimen Fabrication and Testing

1. Preparation of aluminum substrate plates prior to composite doubler installation was performed by the Sandia Lab's AANC as per Section 2.3.1.

2. The Boron-Epoxy doubler was fabricated and installed on the aluminum substrate by Textron Specialty Materials as per Section 2.3.2.

3. Impact damage was imparted to the appropriate specimens by Lockheed-Martin as per Section 2.3.3.

4. Conditioning (temperature and humidity) of appropriate specimens was performed by Lockheed-Martin as per Section 2.3.4.

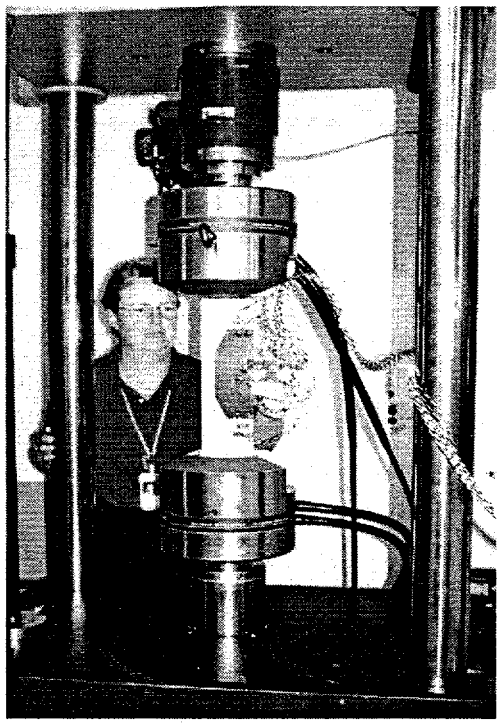

(a)

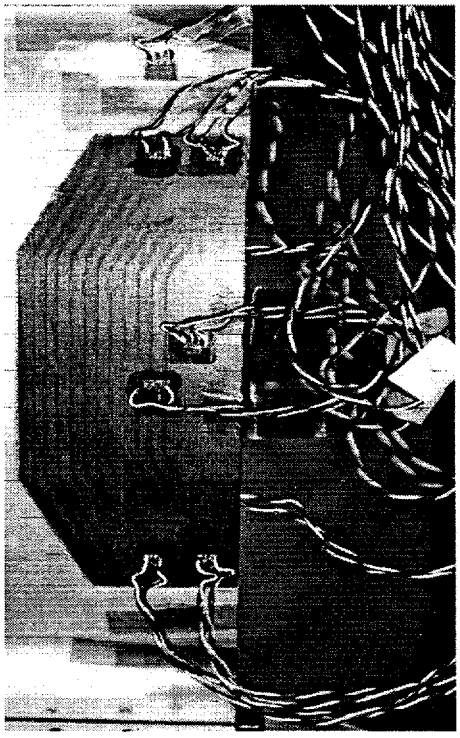

(b)

Figure 6: Set-Up for Damage Tolerance Tests and Close-Up View of Coupon Specimen Mounted in Machine Grips

5. Fatigue and ultimate strength tests were performed by the Sandia Lab's AANC as per Section 2.4.2.

6. Specimen fabrication and subsequent tests were conformed and witnessed by the FAA or its authorized designee as per Section 1.3. The FAA Atlanta Aircraft Certification Office served as the primary point of contact.

2.2 Coupon Configuration

The nine specimen configurations that were tested are described below and summarized in Table 2. Each specimen consisted of an aluminum "parent" plate, representing the original aircraft skin, with a bonded composite doubler. The doubler was bonded over a flaw in the parent aluminum. The specimens had the following basic design configurations:

1. BE-1: Unabated 0.5" fatigue crack at the edge of the aluminum plate; no engineered flaws in composite doubler (Figure 7).
2. BE-2: Stop-drilled, 0.5" sawcut edge crack in the aluminum plate with collocated 0.75" dia. disbond between composite doubler and aluminum; 0.75" dia. disbonds along doubler edge (Figure 8).
3. BE-3: Stop-drilled, 0.5" sawcut edge crack in the aluminum plate with collocated 1.0" dia. disbond between composite doubler and aluminum; 1.0" dia. disbonds along doubler edge (Figure 9).
4. BE-4: Unabated 0.5" fatigue crack at the edge of the aluminum plate with collocated 0.75" dia. disbond between composite doubler and aluminum; 0.75" dia. disbonds along doubler edge (Figure 10).
5. BE-5: 1" dia. hole in aluminum plate; no engineered flaws in composite doubler (Figure 11).
6. BE-6: Unabated 0.5" fatigue crack at the edge of the aluminum plate <u>without a composite doubler</u> (Figure 12). The fatigue crack growth observed in these "baseline" specimens serves as the basis of comparison for the composite reinforced specimens.
7. BE-7: Composite doubler installed with no engineered flaws in the aluminum plate or the composite doubler (Figure 13). This represents the Baseline Specimen with an optimum installation.
8. BE-8: Stop-drilled, 0.5" sawcut edge crack in the aluminum plate with collocated 300 in-lb impact damage from a 1" diameter hemispherical tip; collocated 1" diameter disbond; 160°F hot-wet conditioning (Figure 14).
9. BE-9: Unabated 0.5" fatigue crack at the edge of the aluminum plate with collocated 300 in-lb impact damage from a 1" diameter hemispherical tip; similar impact damage along doubler edge; collocated 1" diameter disbonds at both impact locations; 160°F hot-wet conditioning (Figure 15).

2.3 Specimen Description

1) Material - The parent aluminum plate was 2024-T3. The Boron-Epoxy material was type 5521/4. The specifications for production of the Boron-Epoxy material was as follows: 1) SAE Aerospace Material Specification (AMS) 3865C specification for the fiber, and 2) AMS 3867B and AMS 3867/4A provided requirements for the Boron-Epoxy pre-preg tape material. The adhesive material was FM-73, or accepted substitute AF-163, (0.06 PSF) and the primer was Cytec BR-127.

   [Specimen configurations BE-1 through BE-5 were fabricated using 3M's EC3960 primer (vs. BR-127) and 3M's AF163 (0.06 PSF) adhesive (vs. FM-73). The EC3960 and BR-127 primers are both listed in the Qualified Products List (QPL) for the BMS 5-89 specification; AF163 and FM-73 are both listed in the QPL for the BMS 5-101 specification. Thus, according to the installation specifications cited here they are allowable material substitutions.]

   The Boron-Epoxy composite doubler was a multi-ply lay-up which conformed to the basic design parameters - plies/stiffness ratio - specified in reference [1]. The doublers were a multi-direction lay-up of 13 plies: $[0, +45, -45, 90]_3$ with a 0_o cover ply on top. The plies were cut to different lengths in both in-plane directions in order to taper the thickness of the resulting doubler edges. This produced a more gradual load transfer between the aluminum and the doubler (i.e. reduces the stress concentration in the bondline around the perimeter). A ply taper ratio of approximately 30:1 was utilized; this results in a reduction in length of 30 times the ply thickness. The number of plies and fiber orientations produced an extensional stiffness ratio of Boron-Epoxy to aluminum of 1.2:1 $\{(Et)_{BE} = 1.2\ (Et)_{Al}\}$. See section 2.3.5 for details on how the laminate-to-aluminum extensional stiffness ratio is calculated.

2) Material Thickness - The parent aluminum plate was 2024-T3, 0.071" thick. Each composite doubler had a nominal post-cure thickness of 0.080" (approximately 0.0057" per ply plus a nominal pre-cure adhesive layer of 0.010"; the post-cure adhesive thickness is approximately 0.006").

3) Tension Specimen Dimensions - The specimens were designed for a 4" W X 14" L test area. To accommodate two, 2" deep end grips, the final specimen lengths were 18".

Configuration	Number of Specimens Tested (Specimen Numbers)	Figure	Description
BE-1	1 (Lock1)	7, 16	unabated 0.5″ fatigue edge crack; no engineered flaws in composite doubler installation
BE-2	1 (Lock2)	8, 17	stop-drilled 0.5″ sawcut edge crack with collocated disbond; 0.75″ dia. disbonds in edge of doubler
BE-3	1 (Lock3)	9, 18	stop-drilled 0.5″ sawcut edge crack with collocated disbond; 1.0″ dia. disbonds in edge of doubler
BE-4	1 (Lock4)	10, 19	unabated 0.5″ fatigue edge crack with collocated disbond; 0.75″ dia. disbonds in edge of doubler
BE-5	1 (Lock5)	11, 20	1″ dia. hole in parent aluminum plate; no engineered flaws in composite doubler installation
BE-6	2 (Lock6 - Lock7)	12, 21	unabated 0.5″ fatigue edge crack; aluminum plate with no doubler
BE-7	1 (Lock8 - Lock9)	13, 22	composite doubler installed without any engineered flaws; no flaws in aluminum plate
BE-8	6 (Lock10 - Lock15)	14, 23	stop-drilled 0.5″ sawcut edge crack with collocated impact/disbond damage on doubler; 160°F hot, wet conditioned; tested at room temperature
BE-9	6 (Lock16 - Lock21)	15, 24	unabated 0.5″ fatigue edge crack with collocated impact/disbond damage on doubler; impact/disbond damage on edge of doubler; 160°F hot, wet conditioned; tested at room temperature

Table 2: Composite Coupon Specimen Matrix

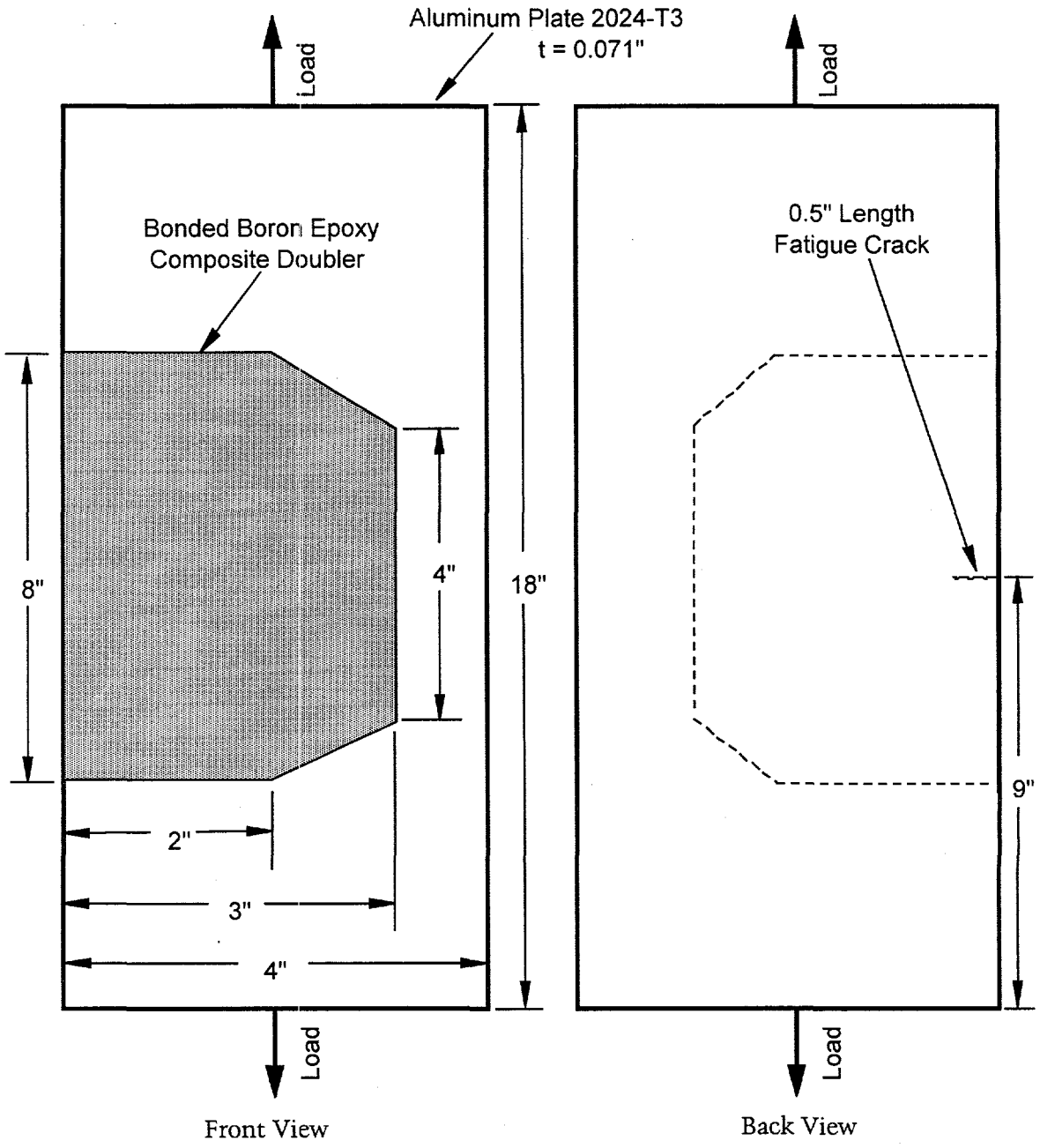

1. 13 Ply Boron/Epoxy doubler
2. $[0, +45, -45, 90]_3$ lay-up (fiber orientation to the load) plus a 0° cover ply on top; longest ply on bottom
3. 30:1 taper ratio drop off
4. Stiffness Ratio, $(Et)_{BE} = 1.2\ (Et)_{Al}$
5. Fatigue crack in skin but no engineered flaws in doubler

Figure 7: Composite Tension Test Coupon - Configuration BE-1

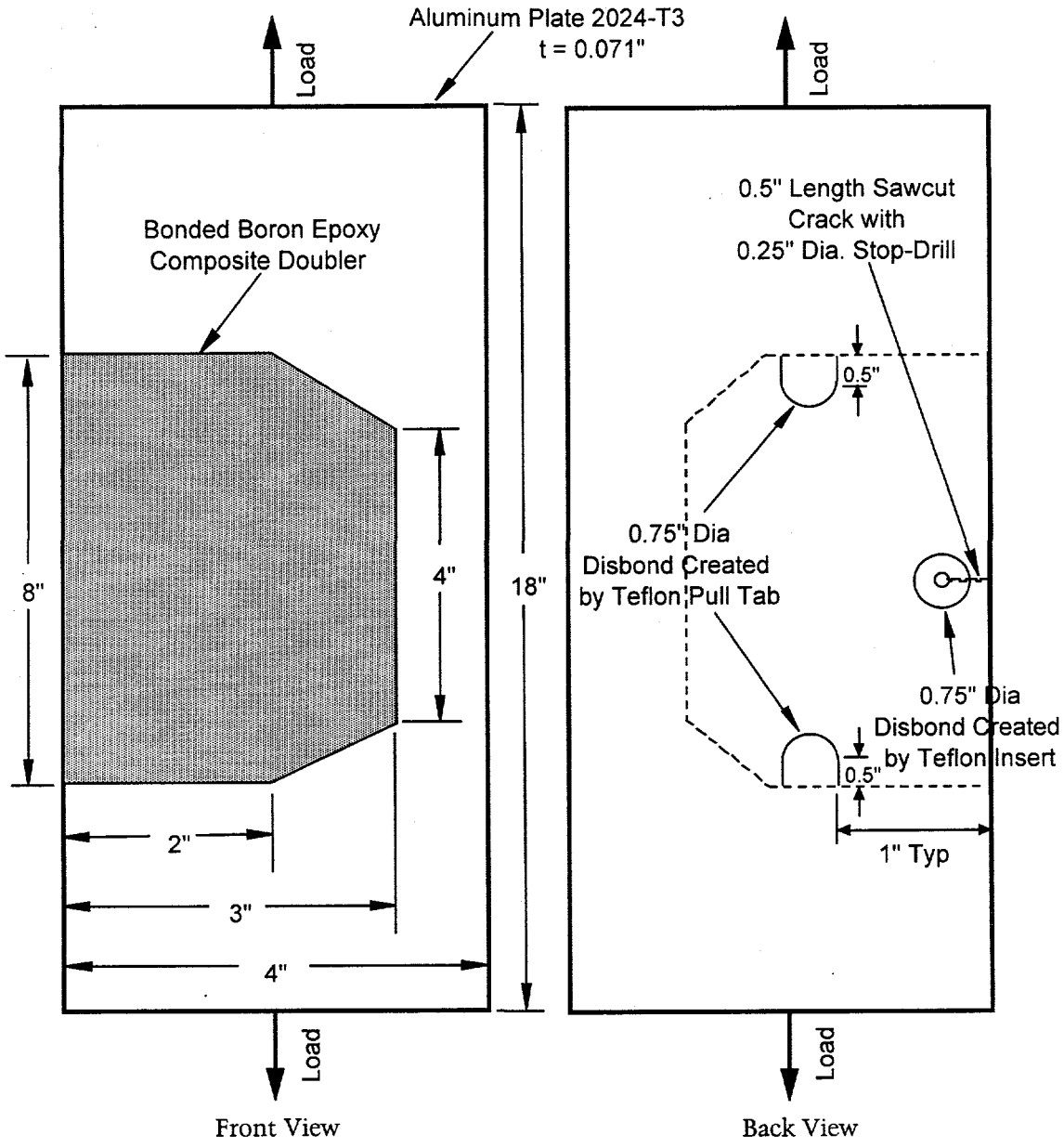

1. **13 Ply Boron/Epoxy doubler**
2. **$[0, +45, -45, 90]_3$ lay-up (fiber orientation to the load) plus a $0°$ cover ply on top; longest ply on bottom**
3. **30:1 taper ratio drop off**
4. **Stiffness Ratio, $(Et)_{BE} = 1.2\ (Et)_{Al}$**
5. **Fatigue crack (stop-drilled) with 0.75" Dia co-located disbond centered over stop-drill hole**
6. **0.75" Dia disbonds in load transfer region of composite doubler (edges of the bondline)**

Figure 8: Composite Tension Test Coupon - Configuration BE-2

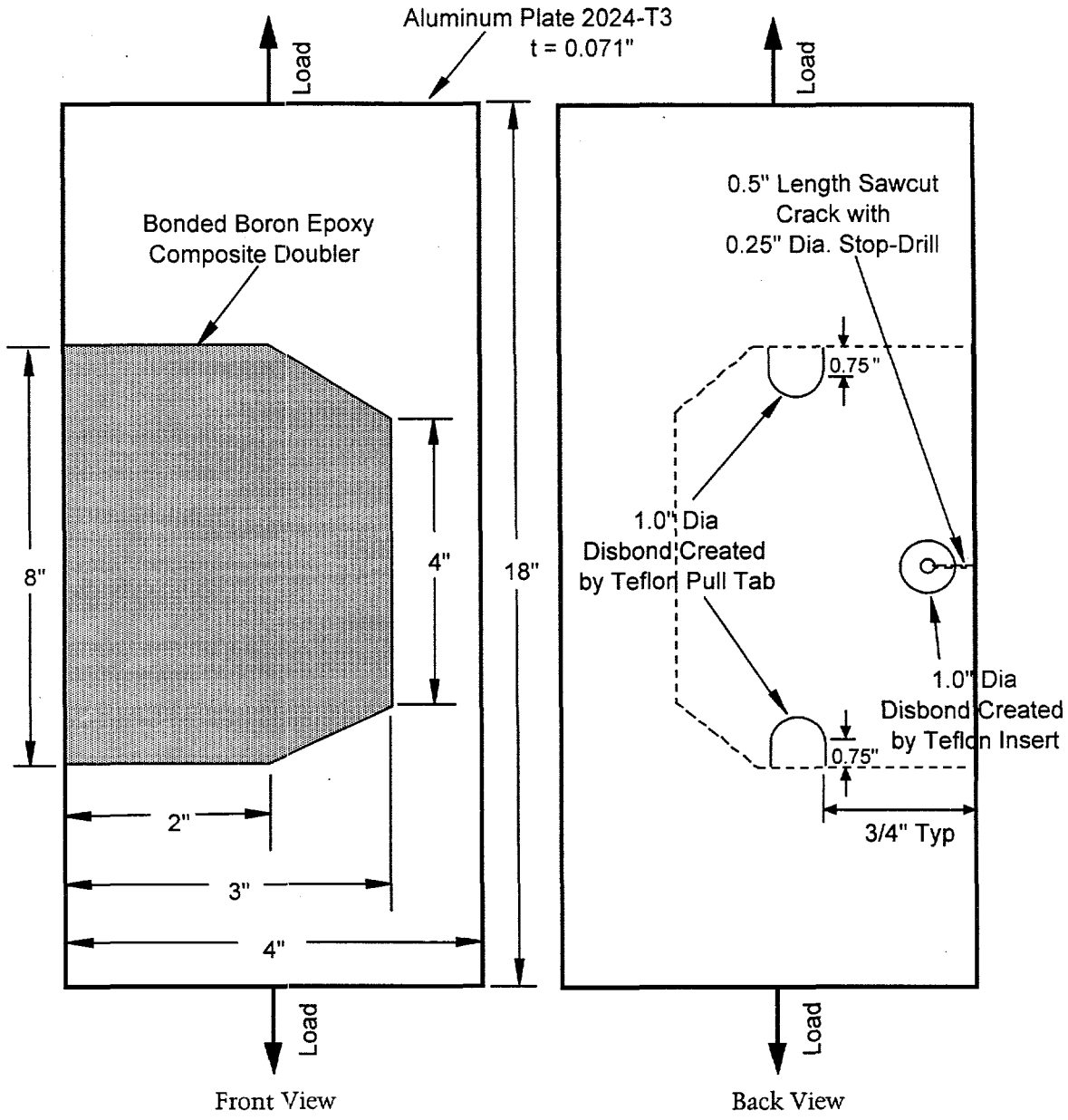

1. 13 Ply Boron/Epoxy doubler
2. [0, +45, -45, 90]$_3$ lay-up (fiber orientation to the load) plus a 0° cover ply on top; longest ply on bottom
3. 30:1 taper ratio drop off
4. Stiffness Ratio, $(Et)_{BE} = 1.2\ (Et)_{Al}$
5. Fatigue crack (stop-drilled) with 1.0" Dia co-located disbond centered over stop-drill hole
6. 1.0" Dia disbonds in load transfer region of composite doubler (edges of the bondline)

Figure 9: Composite Tension Test Coupon - Configuration BE-3

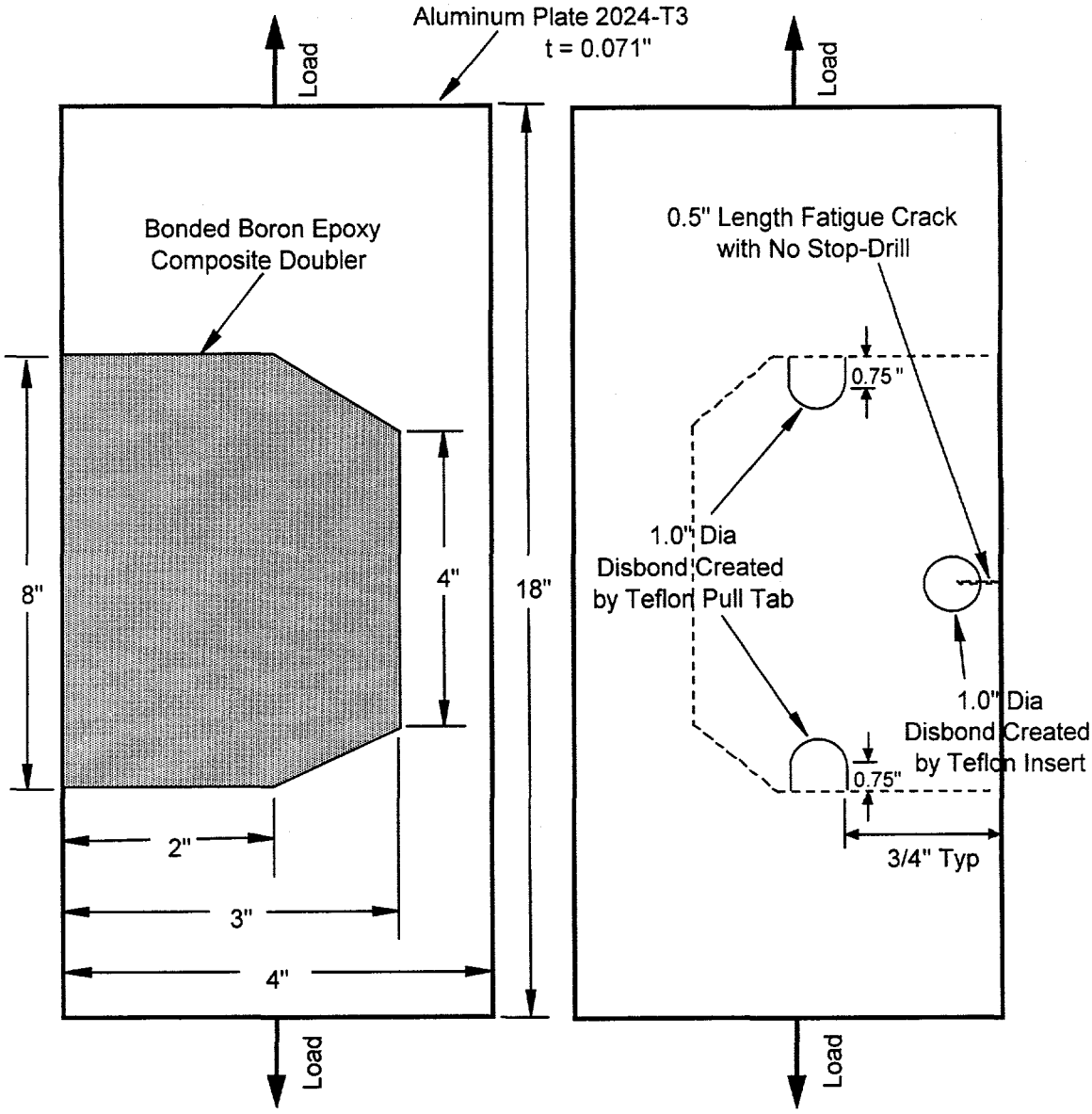

1. **13 Ply Boron/Epoxy doubler**
2. **$[0, +45, -45, 90]_3$ lay-up (fiber orientation to the load) plus a 0° cover ply on top; longest ply on bottom**
3. **30:1 taper ratio drop off**
4. **Stiffness Ratio, $(Et)_{BE} = 1.2\ (Et)_{Al}$**
5. **Fatigue crack (stop-drilled) with 1.0" Dia co-located disbond centered over stop-drill hole**
6. **1.0" Dia disbonds in load transfer region of composite doubler (edges of the bondline)**

Figure 10: Composite Tension Test Coupon - Configuration BE-4

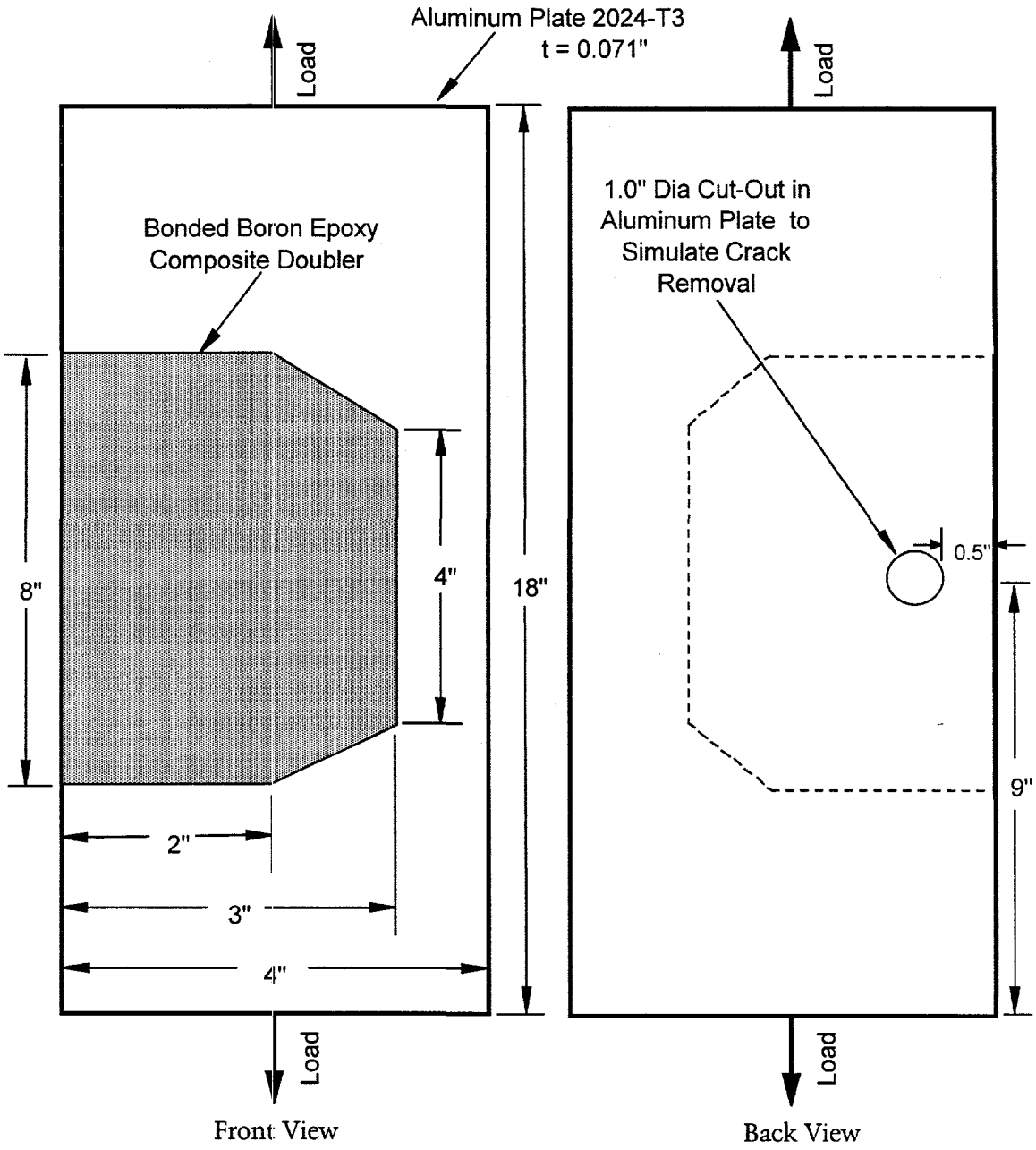

1. 13 Ply Boron/Epoxy doubler
2. [0, +45, -45, 90]$_3$ lay-up (fiber orientation to the load) plus a 0° cover ply on top; longest ply on bottom
3. 30:1 taper ratio drop off
4. Stiffness Ratio, $(Et)_{BE} = 1.2\ (Et)_{Al}$
5. 1.0" Dia cut-out in parent aluminum
6. No engineered flaws in composite doubler installation

Figure 11: Composite Tension Test Coupon - Configuration BE-5

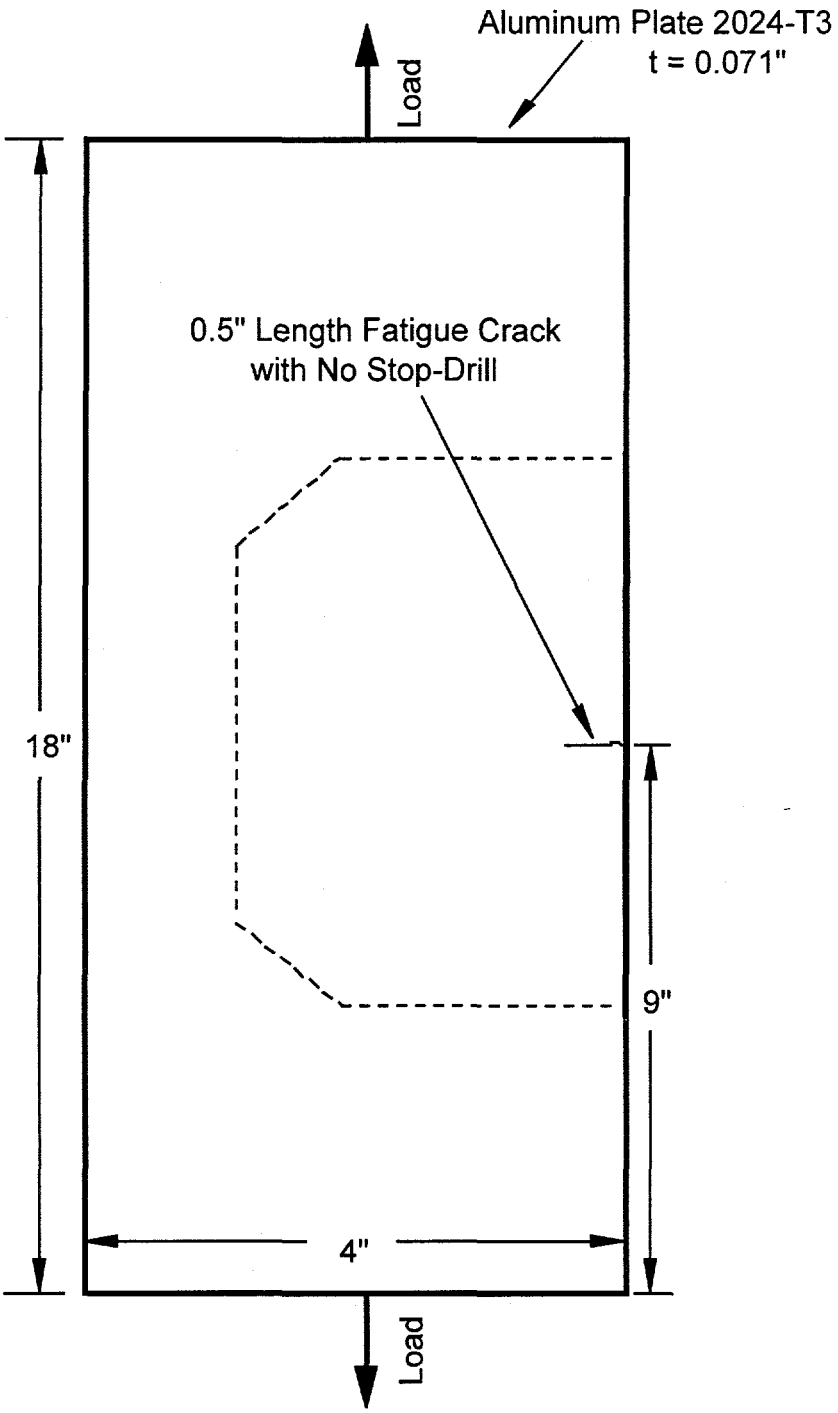

Figure 12: Composite Tension Test Coupon - Configuration BE-6

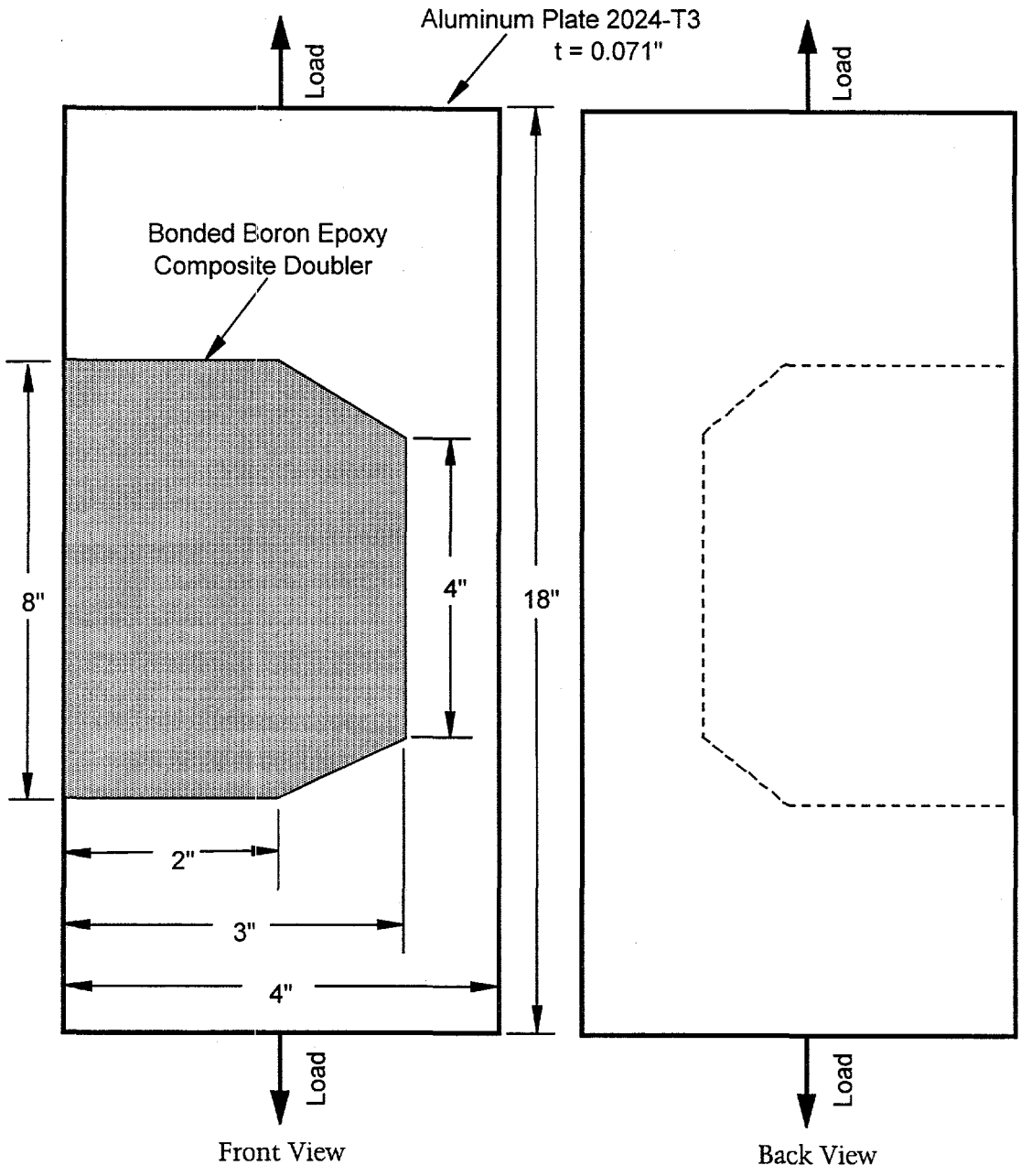

1. 13 Ply Boron/Epoxy doubler
2. [0, +45, -45, 90]$_3$ lay-up (fiber orientation to the load) plus a 0° cover ply on top; longest ply on bottom
3. 30:1 taper ratio drop off
4. Stiffness Ratio, $(Et)_{BE} = 1.2\ (Et)_{Al}$
5. No flaws in parent aluminum
6. No engineered flaws in composite doubler installation

Figure 13: Composite Tension Test Coupon - Configuration BE-7

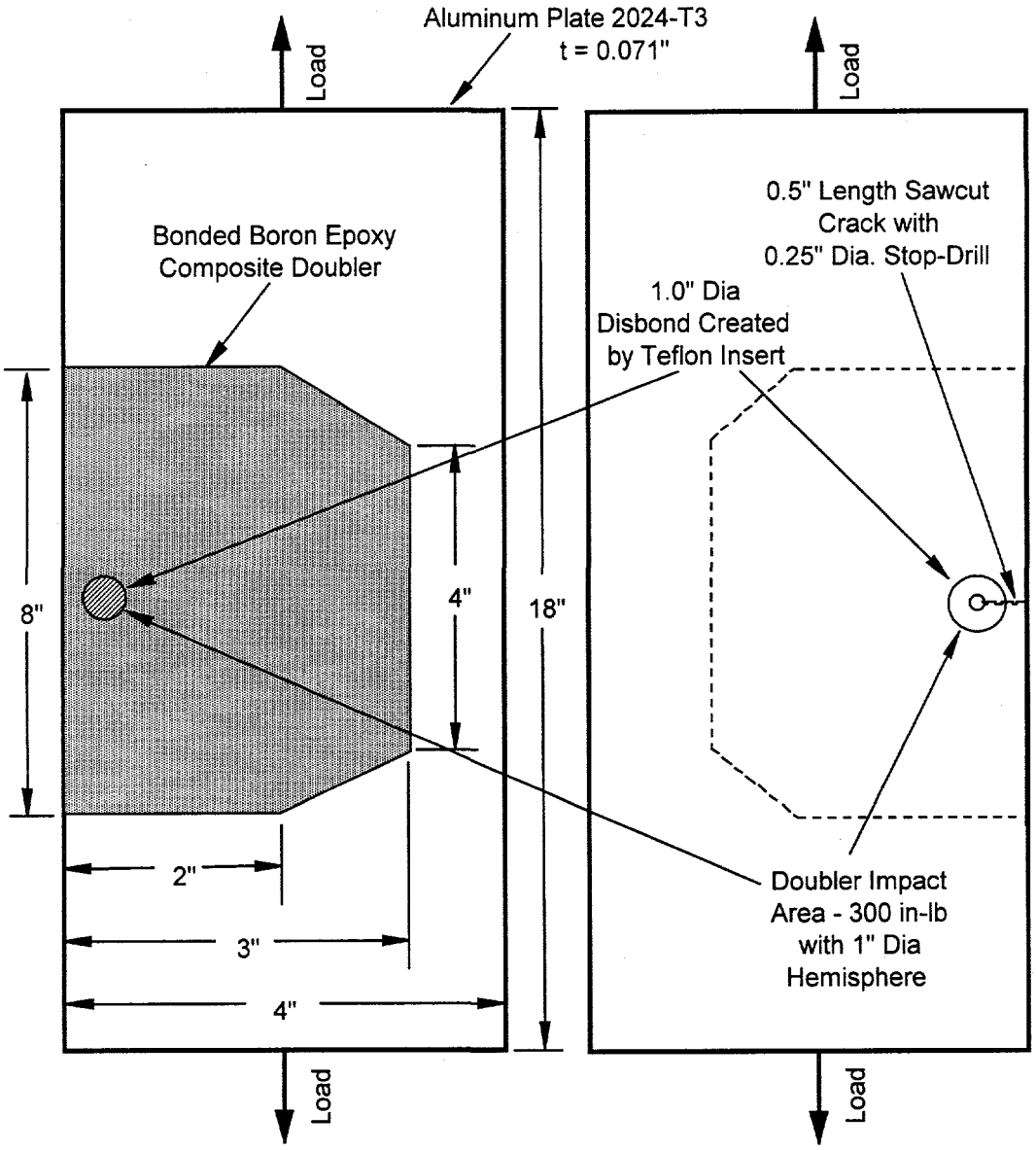

1. **13 Ply Boron/Epoxy doubler**
2. **$[0, +45, -45, 90]_3$ lay-up (fiber orientation to the load) plus a 0° cover ply on top; longest ply on bottom**
3. **30:1 taper ratio drop off**
4. **Stiffness Ratio, $(Et)_{BE} = 1.2\ (Et)_{Al}$**
5. **Crack (stop-drilled) with 1.0" Dia co-located impact damage centered over stop-drill hole; 160°F hot, wet conditioned**
6. **1.0" Dia disbond co-located over fatigue crack and impact damage**

Figure 14: Composite Tension Test Coupon - Configuration BE-8

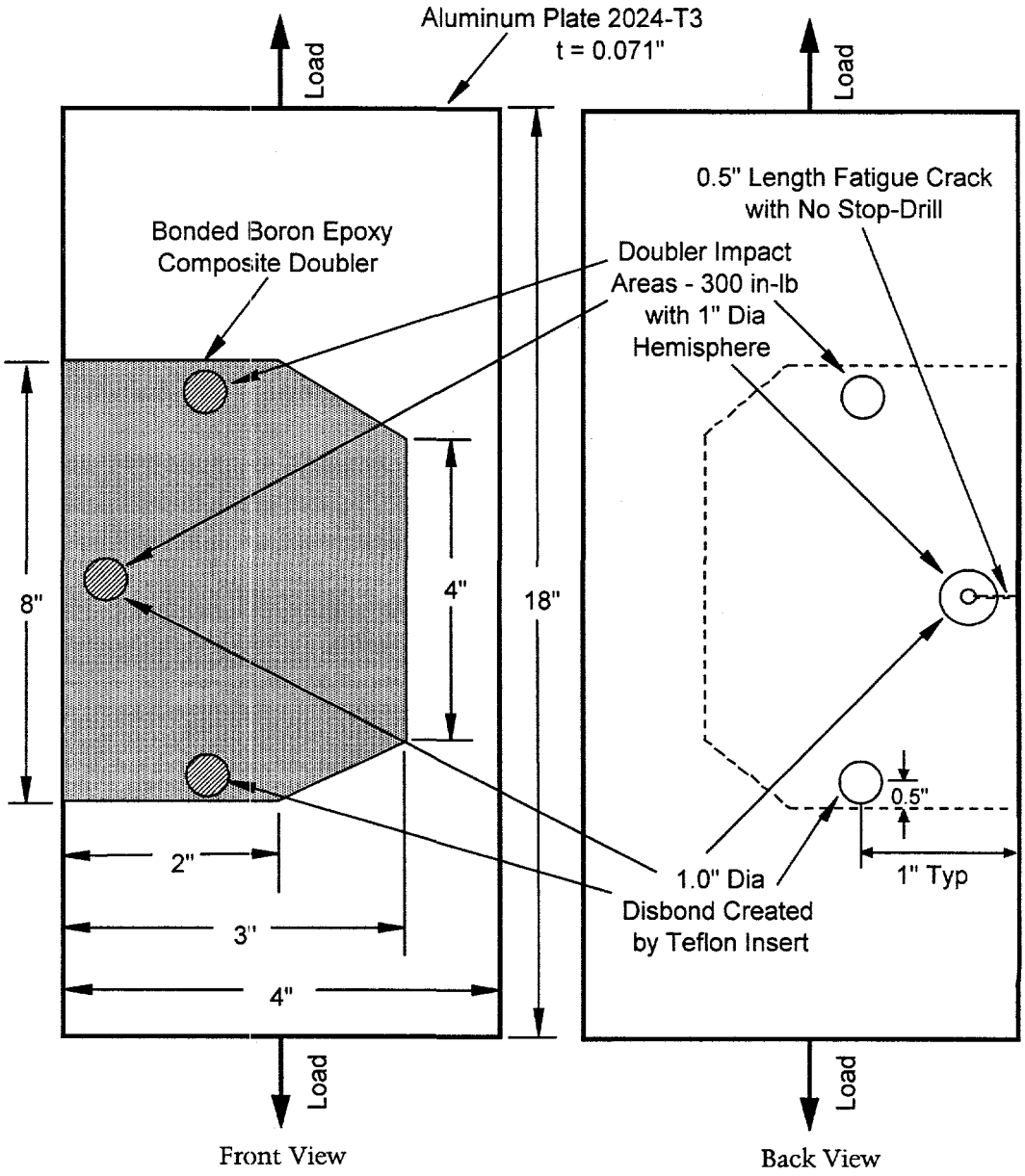

1. **13 Ply Boron/Epoxy doubler**
2. **$[0, +45, -45, 90]_3$ lay-up (fiber orientation to the load) plus a 0° cover ply on top; longest ply on bottom**
3. **30:1 taper ratio drop off**
4. **Stiffness Ratio, $(Et)_{BE} = 1.2\ (Et)_{Al}$**
5. **Crack (stop-drilled) with 1.0" Dia co-located impact damage centered over stop-drill hole; 160°F hot, wet conditioned**
6. **1.0" Dia disbond co-located over fatigue crack; disbond and impact damage in load transfer regions (edges of bondline)**

Figure 15: Composite Tension Test Coupon - Configuration BE-9

2.3.1 Generation of Cracks in Aluminum Substrate Material

Prior to installing the composite doublers, seven of the coupon configurations (BE-1, BE-2, BE-3, BE-4, BE-6, BE-8, and BE-9) had cracks generated in the aluminum substrate plate. Specimen configurations BE-2, BE-3 and BE-8 (specimens Lock2, Lock3, and Lock10-Lock15) had 0.5" sawcut cracks which were stop-drilled using a 0.25" diameter drill bit. Figures 8, 9, and 14 and drawing AANC-1 provide the design, fabrication and inspection details for the abated (stop-drilled) cracks. Specimen configurations BE-1, BE-4, BE-6, and BE-9 (specimens Lock1, Lock4, Lock6, Lock7, and Lock16-21) had a 0.5" fatigue crack which was unabated (i.e. no stop-drill). The fatigue cracks were generated by tension-tension fatigue loads in an MTS Inc. uniaxial, mechanical test machine. A 0.25" length sawcut, imparted as per drawing AANC-1, provided the starter notch for the fatigue crack. The applied fatigue loads were 3.75 ksi to 20.75 ksi (1050 - 5810 lbs. load) to represent the 0 - 17 ksi hoop stress spectrum experienced by the L-1011 fuselage skin during cabin pressurization. The loads applied by the tension test machine were calibrated and traceable to the National Institute of Standards and Technology. Crack lengths were determined using a Bausch and Lomb optical eyepiece measurement device which was applied to the non-composite doubler side of the specimens. The eyepiece produced an image magnification of seven and had an embedded set of crosshairs (tic marks) which provided a resolution of 0.005". The initial, pre-doubler, crack lengths were recorded and used as the initial crack lengths in the subsequent composite coupon fatigue tests.

2.3.2 Surface Preparation and Composite Doubler Installation

All test specimens were prepared using the Phosphoric Acid Non Tank Anodize (PANTA) surface preparation procedure and the Phosphoric Acid Containment System (PACS) equipment. The complete installation procedure is provided in reference [42] and is Textron Specification No. 200008-001 (may also be referenced as the Boeing Specification D658-10183-1). This installation specification was used for the installation of over 150 Boron-Epoxy doublers on fatigue test specimens similar to the ones described in here [41, 43] and for the installation of 25 Boron-Epoxy demonstration doublers on two operational Federal Express 747 aircraft [13]. Specification 200008-001 references a series of FAA-approved Boeing Aircraft Corporation (BAC) processes and Boeing Material Specifications (BMS) that are widely used by Boeing on commercial aircraft. The key installation steps are summarized below.

1. Aluminum Surface Preparation - Solvent clean per BAC 5750. Remove the oxide on the aluminum prior to Phosphoric Acid Anodize using Scotch Brite pads to achieve a 30 second water-break free condition per paragraph 6.6.9.2.2 of specification 200008-001. Phosphoric Acid Anodize (PAA) the aluminum surface using Phosphoric Acid Containment System (PACS) equipment as described in U.S. Patent 4,085,012 and in paragraph 6.6.9.2.2 of specification 200008-001.

2. Primer and Adhesive Process - Prime the PAA aluminum surface using Cytec BR-127 primer (or equivalent: EC3960), type 1, grade A per BMS 5-89. Co-cure the

Cytec FM-73 (or equivalent: AF163) structural film adhesive per BMS 5-101 simultaneously with the Boron-Epoxy doubler.

3. Boron-Epoxy Doubler Installation and Cure - Lay up the 5521/4 Boron-Epoxy doubler in accordance with the application design drawing (AANC-1). Cure for 90 to 120 minutes at 225°F to 250°F at 0.54 ATM vacuum bag pressure (equivalent atmospheric pressure is 7.35 psia) using standard "hot bonder" units as per specification 200008-001, paragraph 7.6.4. Use computer-controlled heater blankets to provide the proper temperature cure profile in the field. Use a series of thermocouples in an active feedback loop to maintain the proper temperature profile.

The Air Force installation procedure [4] is very similar to the process described above except that the Air Force surface preparation step uses a grit blast and silane chemical application.

Following coupon fabrication, the specimens were visually inspected and ultrasonically scanned to determine if there were any disbond or delamination flaws (see also section 2.4.4) other than the ones intentionally engineered into the specimens. The resulting flaw map (location, geometry, and depth) was recorded and the damage locations were marked directly on the specimens for future reference.

2.3.3 Application of Impact Damage to Composite Coupons

Following the composite doubler installation and prior to environmental conditioning (see section 2.3.4), impact damage was imparted to Specimen Configurations BE-8 and BE-9 (specimens Lock10-Lock21). The locations for impact damage were selected to induce the most adverse effect on crack growth mitigation and/or the ability of the doubler to transfer load. Figures 14 and 15 and drawing AANC-1 (see Appendix A) provide the design, fabrication and inspection details. The impact was performed with a 1 inch diameter steel hemisphere tip. A guide tube, lined with Teflon film or equivalent, was used to direct the path of the impact mass. The specimens were fully supported by plates on the front and back side. The plates had appropriate window cut-outs to apply the impact damage.

The magnitude of the impact was 25 $\pm$ 0.5 ft-lb (300 $\pm$ 5 in-lb). The impact damage was applied as per paragraph B.11.3 of the reference [44] NASA specification. Additional guidance was provided by reference [45]. Following impact, the specimens were ultrasonically scanned to determine the extent of the resulting damage (see also section 2.4.4). The resulting flaw map (location, geometry, and depth) was recorded and the damage locations were marked directly on the specimens.

2.3.4 Temperature and Humidity Conditioning

After applying the impact damage, Specimen Configurations BE-8 and BE-9 (specimens Lock10-Lock21) were subjected to temperature and humidity conditioning. The

composite coupons were conditioned per Lockheed Specification 5PTPTT01-A (Section 3.2.4.1.8) in order to simulate end-of-service moisture content. Conditioning of 160°F ± 5°F, 85% ± 5% relative humidity was applied to the test article for a period of time sufficient to achieve saturation moisture content as determined by regular weighing of the test coupons (or regular weighing of the traveler specimens). Temperature and humidity measurements were accurate to applicable ASTM specifications.

Traveler specimens are an experimental aid which are used to assess the condition of the actual test specimens. They are manufactured at the same time and in the same manner as the test coupons. They then remain with and are subjected to the same conditioning environment as the test coupon doublers. There were three (3) traveler specimens. The number of plies (13), the ply lay-up {[0, +45, -45, 90]$_3$, 0}, and doubler materials were the same as the coupon specimens. The traveler specimens were not bonded to an aluminum plate. A 4" X 6" rectangular, untapered laminate was produced for the traveler specimens. This laminate was cut to produce three traveler specimens each having a dimension of 2" X 2". Each traveler specimen was then cleaned and weighed to establish an accurate pre-conditioning weight. The scales used for all test specimen weighings were accurate to applicable ASTM specifications. After the coupon and traveler specimens were conditioned and removed from the environmental chamber, they were stored in sealed polyethylene bags at 75°F ± 5°F and 75% ± 5% relative humidity.

2.3.5 Calculation of Laminate-Aluminum Extensional Stiffness Ratio

The purpose of this section is to describe the method which was used to arrive at the stiffness parameter, $E_x t$, for composite doublers. The calculations used classical laminated plate theory, along with Boron-Epoxy lamina properties, to arrive at the average cured laminate modulus E_x (where x is the direction of the fatigue load).

The Boron-Epoxy lamina properties at room temperature are:

$$E_{11} = 28.0 \text{ X } 10^6 \text{ psi}$$
$$E_{22} = 2.7 \text{ X } 10^6 \text{ psi}$$
$$G_{12} = 0.8 \text{ X } 10^6 \text{ psi}$$
$$\nu_{12} = 0.21$$
$$t_{ply} = 0.0057 \text{ in.}$$

The average laminate properties are calculated using the individual lamina properties listed above along with the following specific lay-up configuration: 1) 13 plies {[0, +45, -45, 90]$_3$, 0}, and 2) laminate thickness t = 0.0741" (13 plies X 0.0057"/ply). The resulting laminate properties were calculated:

$$E_x = 11.873 \text{ X } 10^6 \text{ psi}$$
$$E_y = 10.144 \text{ X } 10^6 \text{ psi}$$
$$G_{xy} = 3.77 \text{ X } 10^6 \text{ psi}$$

$$\nu_{xy} = 0.32$$

Compared to a 0.071" thick, 2024-T3 aluminum plate, the stiffness ratio is,

$$R = (E_x t_{laminate})_{BE} / (E_x t)_{Al} \qquad (11)$$

$$= \frac{(11.873 \text{ X } 10^6 \text{ psi})(0.0741")}{(10.5 \text{ X } 10^6 \text{ psi})(0.071")}$$

$$R = 1.2$$

This method was used to arrive at the 1.2 extensional stiffness ratio listed in Section 2.3.

2.4 Test Loads and Procedures

Tension-tension fatigue tests on the coupon specimens used baseline stress levels of 3.75 KSI to 20.75 KSI (1050 - 5810 lbs. load) to represent the 0 - 17 KSI hoop stress spectrum in the L-1011 fuselage skin during cabin pressurization. The lower stress limit, or test pre-load, was applied to eliminate the residual curvature in the test specimen. The post-installation residual curvature is caused by the different coefficients of thermal expansion between the aluminum and Boron-Epoxy materials. The upper stress limit was used to approximate hoop stresses created in the L-1011 skin due to pressurization. The tests utilized a 220,000 lb uniaxial test machine built by Mechanical Test Systems (MTS). Four inch wide friction grips were used to transmit the machine loads to the test coupons. A Micro Measurements Co. System 4000 data acquisition system and the MTS machine's digital data logging console was used to monitor all loads and strains. The coupon specimens were tested at Room Temperature Ambient (RTA) conditions.

2.4.1 Instrumentation

Load transfer through the composite doubler and stress risers around the defects were monitored using the strain gage layouts shown in Figures 16-24. All strain gage locations indicated in Figure 16-24 have a tolerance of 0.125". Biaxial gages were used to measure both the axial and transverse strains in the anisotropic composite material. Strain readings had an accuracy of $\pm$ 5 microstrain. The strain gages were installed using Micro Measurements Inc. M-bond 200 adhesive which is tolerant to all specimen and environmental test conditions. Crack growth was monitored using optical measurement devices (resolution 0.003") that were applied to the non-composite doubler side of the specimens. Displacement measurements, made in the ultimate failure tests, utilized an LVDT with a resolution of 0.001". Test loads were monitored with a full-bridge load cell which had resolution of 0.1 lb. All load, displacement, and data monitoring electronics were calibrated and traceable to Primary Standards. For Specimen Configurations BE-8

and BE-9 (specimens Lock10-Lock21), test temperature and humidity were also recorded.

2.4.2 Fatigue Tests with Static Strain Measurements

1. A 1050 lb pre-load was applied to eliminate the residual curvature in the test specimens.

2. The 1050 - 5810 lb. cyclic fatigue loads (3.75 - 20.75 ksi stress) were applied at 4 Hz.

3. Each fatigue test was stopped and optical crack growth measurements were made at 36,000, 54,000, and 72,000 fatigue cycles. 72,000 cycles corresponds to two design lifetimes for the L-1011 aircraft. The fatigue tests continued until unstable flaw growth occurred or until a maximum of 144,00 cycles (4X the design objective) were reached. Some of the specimens were fatigue cycled until failure occurred and the crack propagated through the entire width of the specimen.

4. The specimens were inspected with ultrasonic and eddy current NDI techniques at 36,000, 72,000 and 144,000 cycles. The NDI tests (see Section 2.4.4) were performed in-situ to eliminate the removal of the specimens from the tension test machine following each fatigue interval.

5. Static strain measurements were acquired at the following four fatigue test stopping points: 1) Fatigue Cycles = 0, 2) Fatigue Cycles = 72,000, and 3) Fatigue Cycles = 144,000. After pre-loading the specimen to the 1050 lb. pre-load, the strain gage bridges were balanced to produce a zero strain output signal. This data was used as the static tension test starting point (Test Tension Load = 0 lbs.). The tension load was increased to at least the tabulated levels shown below. A load of 4,760 lbs. produced the 17 ksi stress level in the specimen which corresponds to maximum fuselage pressurization. Most specimens were loaded in excess of 4,760 lbs. but below yield stress levels. Strain values were acquired at each load level.

Tension Load	Calculated Strains *
0 lbs	0 με
400	135
800	268
1200	402
1600	537
2000	671
2400	805
2800	839
3200	1073
3600	1207
4000	1341
4400	1476
4760	1596

* *Calculated strain magnitude in the parent aluminum plate away from the composite doubler effects. Strains were tabulated to aid real-time test monitoring. Aluminum plate* $E = 10.5 \times 10^6$ psi.

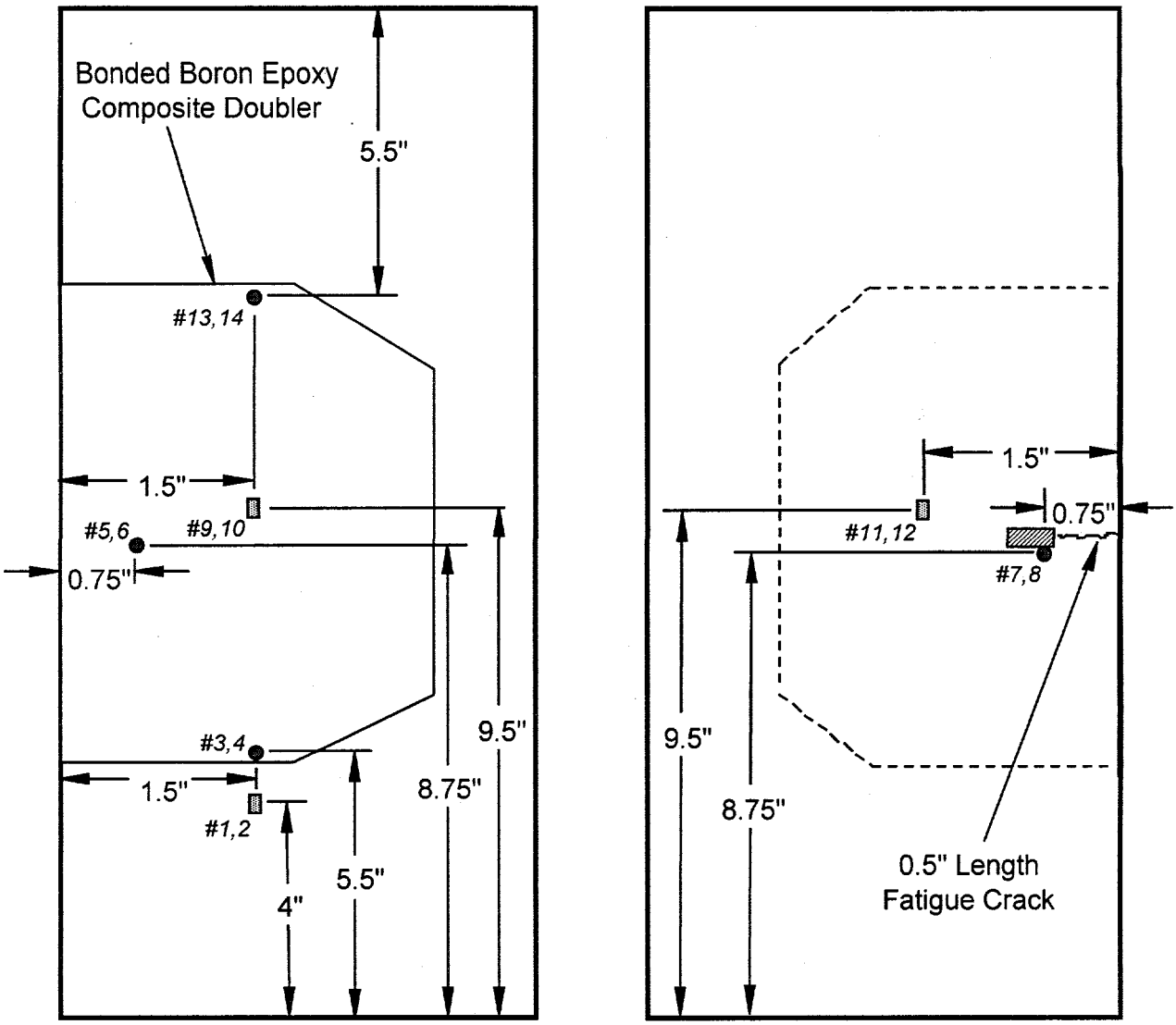

Figure 16: Strain Gage Locations for Composite Tension Test Coupon – Configuration BE-1

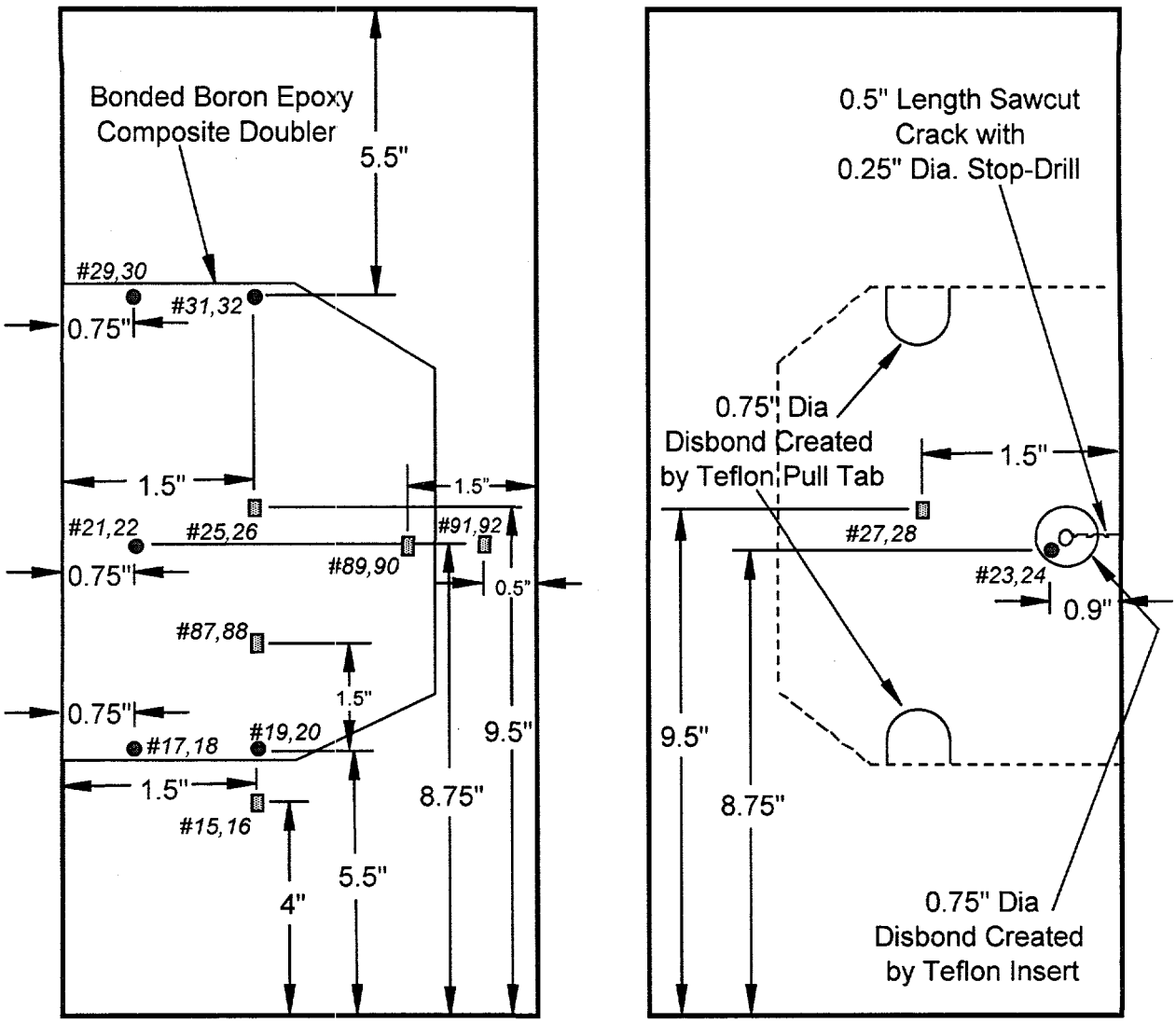

Figure 17: Strain Gage Locations for Composite Tension Test Coupon - Configuration BE-2

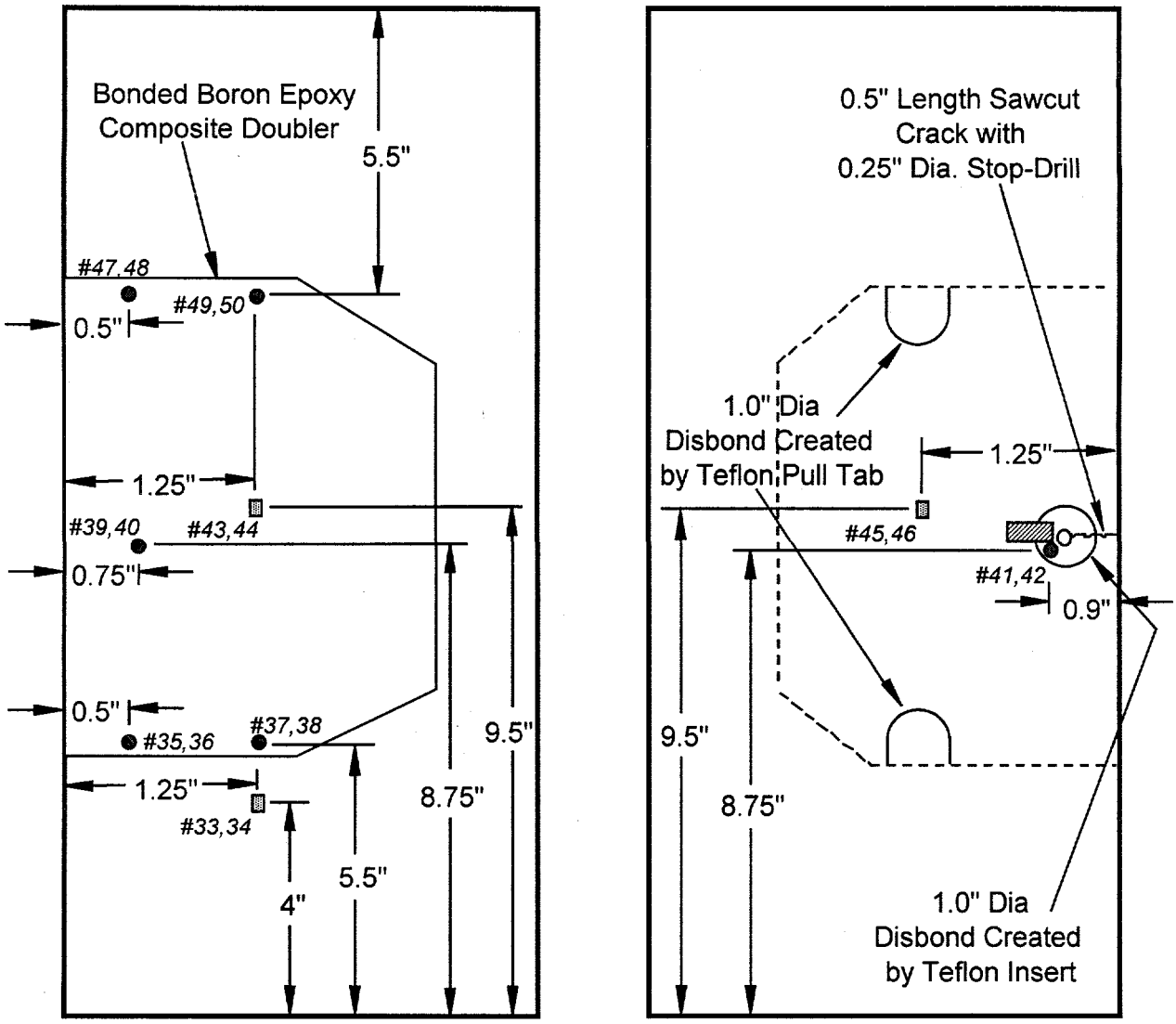

Figure 18: Strain Gage Locations for Composite Tension Test Coupon - Configuration BE-3

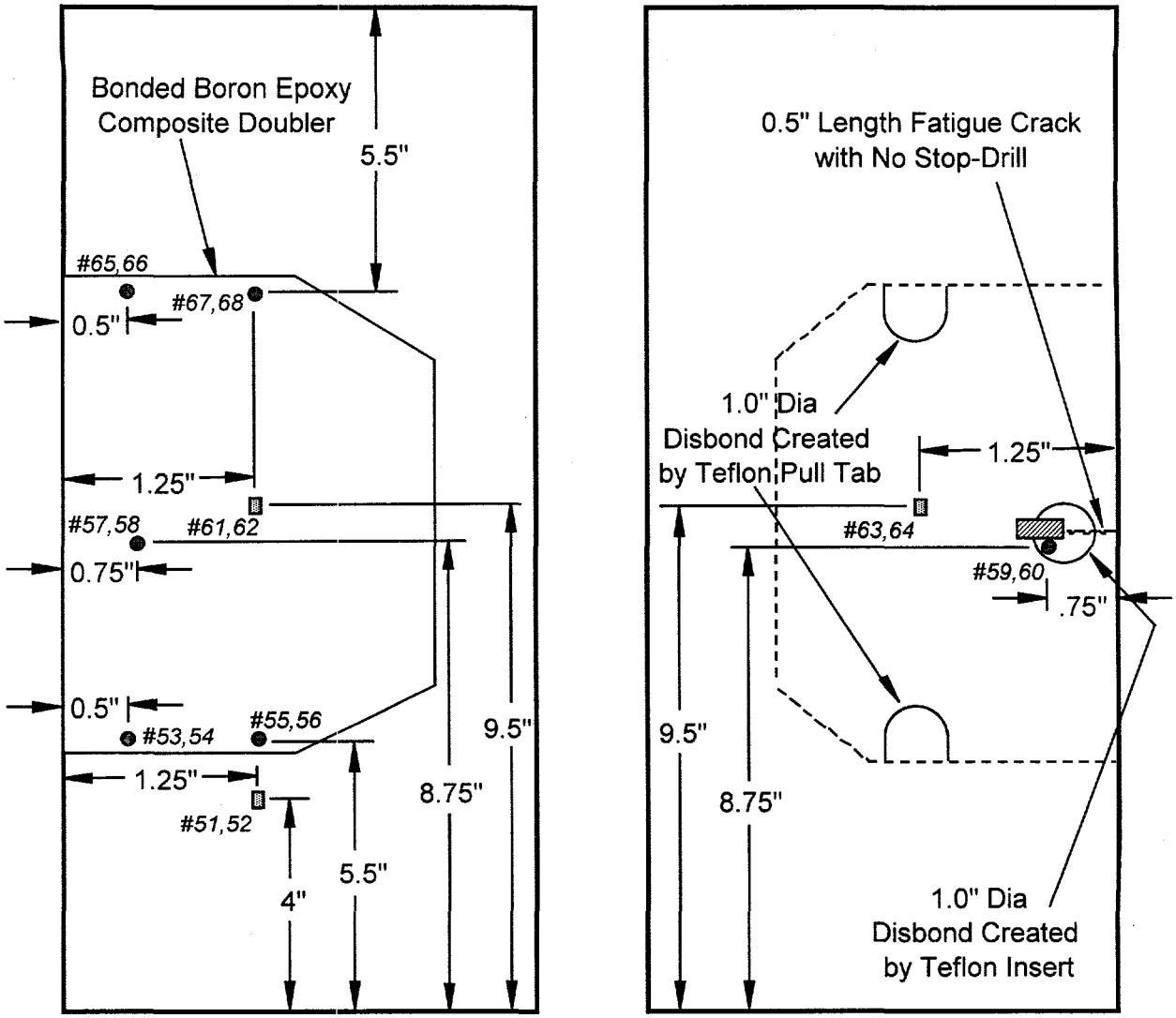

Figure 19: Strain Gage Locations for Composite Tension Test Coupon - Configuration BE-4

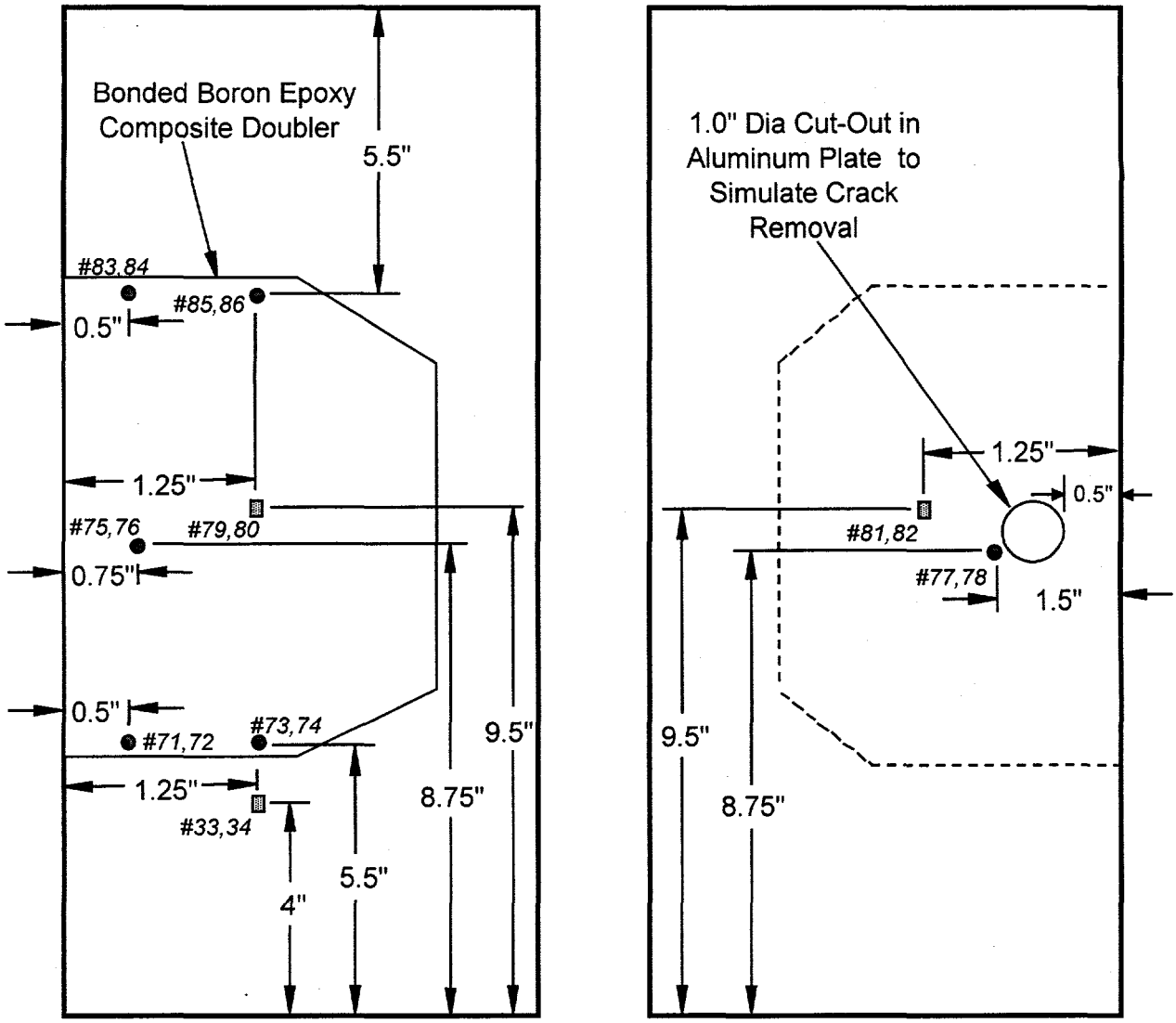

Figure 20: Strain Gage Locations for Composite Tension Test Coupon - Configuration BE-5

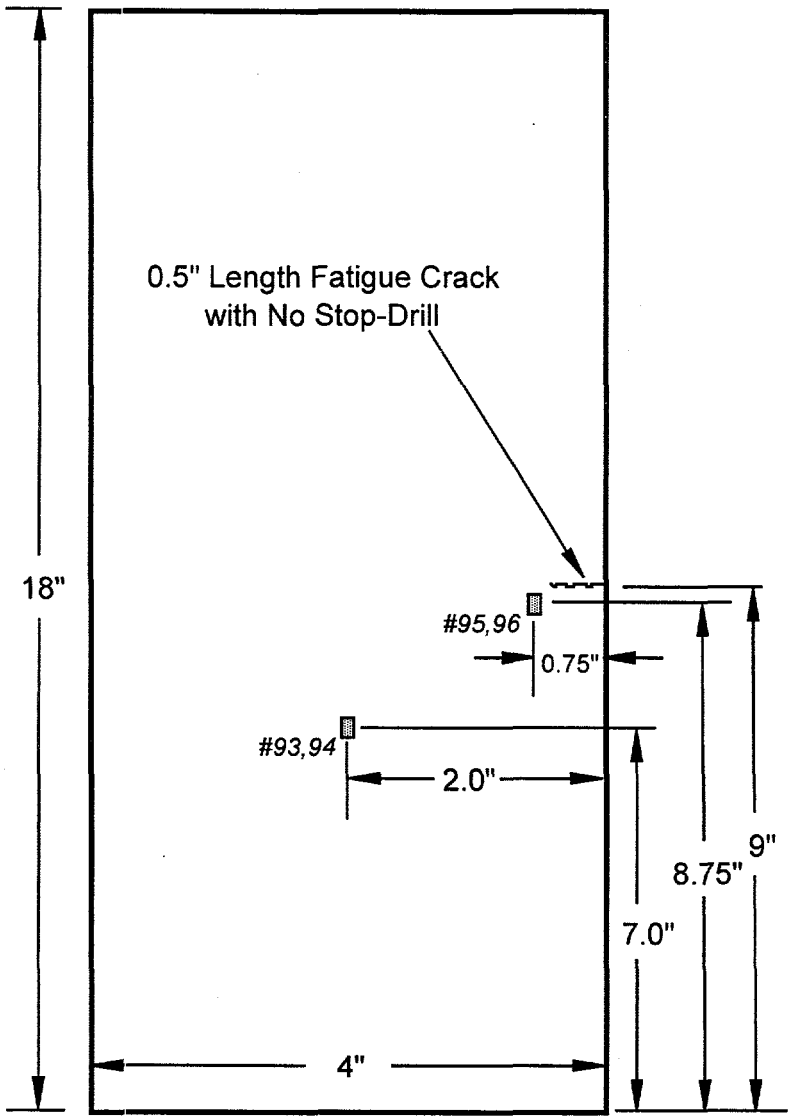

0° - 90° Biaxial 1/8" Gage Length 0° - 90° Biaxial 1/16" Gage Length Crack Propagation Gage	*All Strain Gage Locations are Centered on Axial Gage* *Gage Numbers are Listed in Italics - Even Numbers are Axial Odd Numbers are Lateral*

Figure 21: Strain Gage Locations for Composite Tension Test Coupon - Configuration BE-6

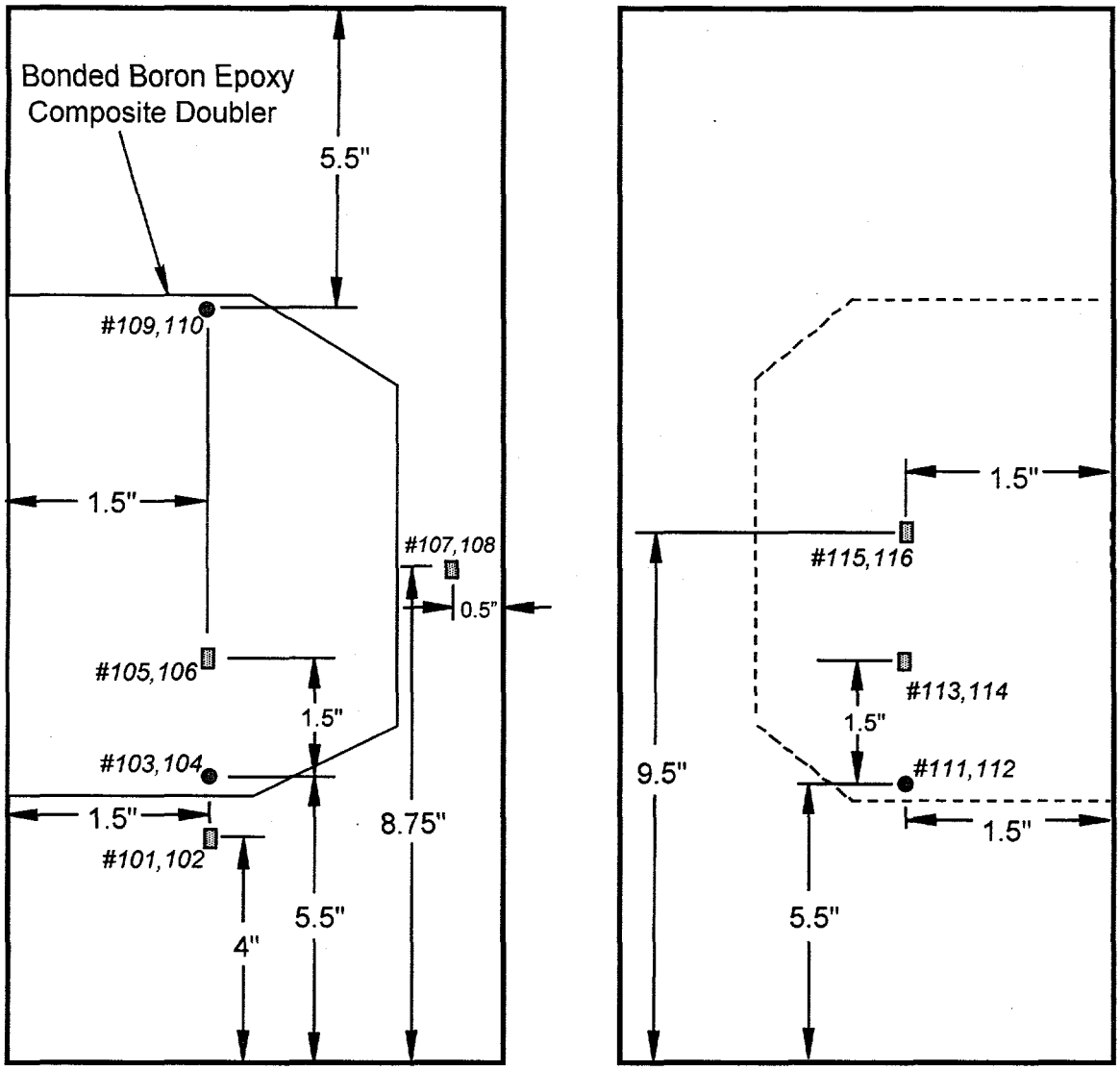

Figure 22: Strain Gage Locations for Composite Tension Test Coupon - Configuration BE-7

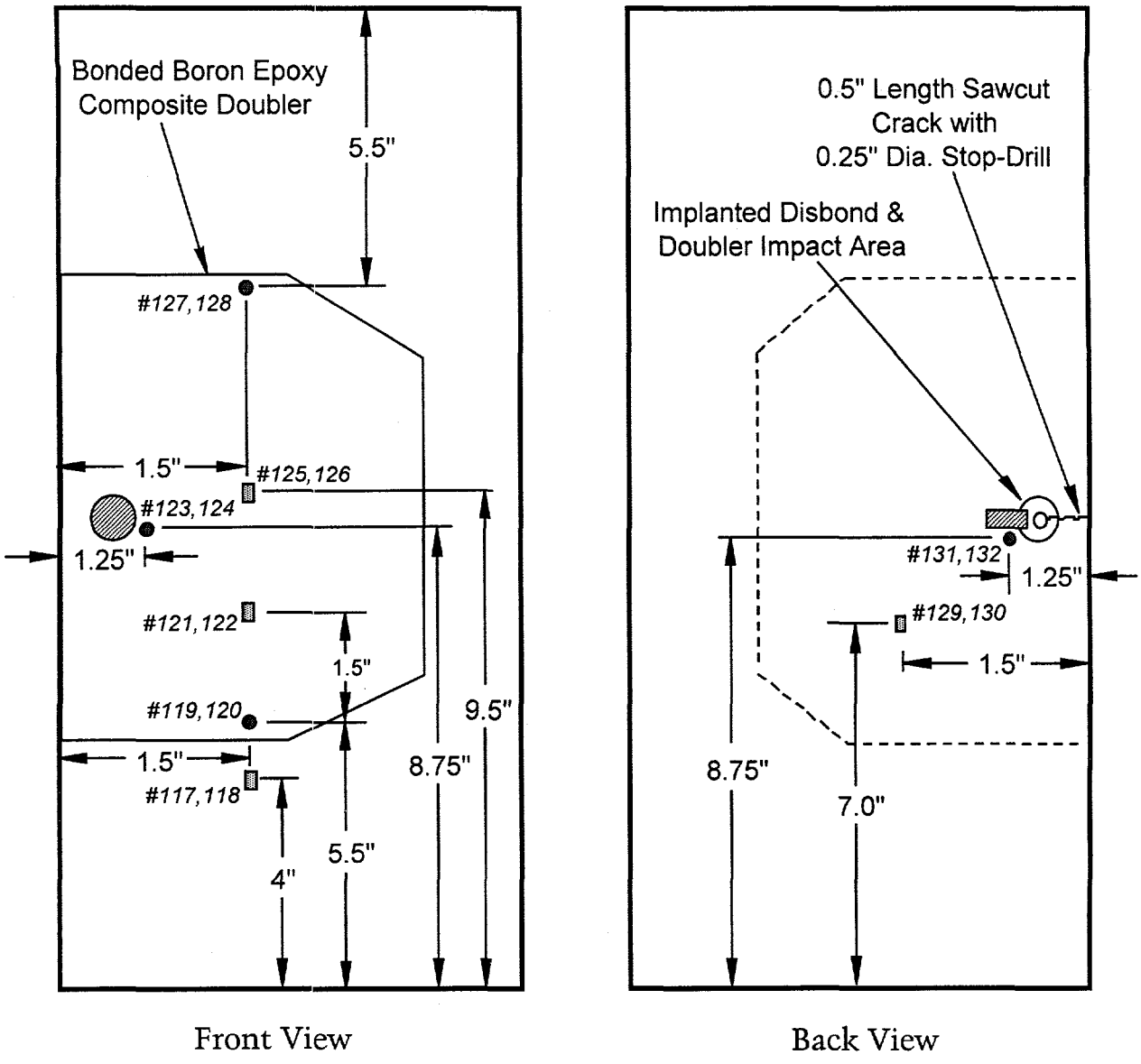

Figure 23: Strain Gage Locations for Composite Tension Test Coupon - Configuration BE-8

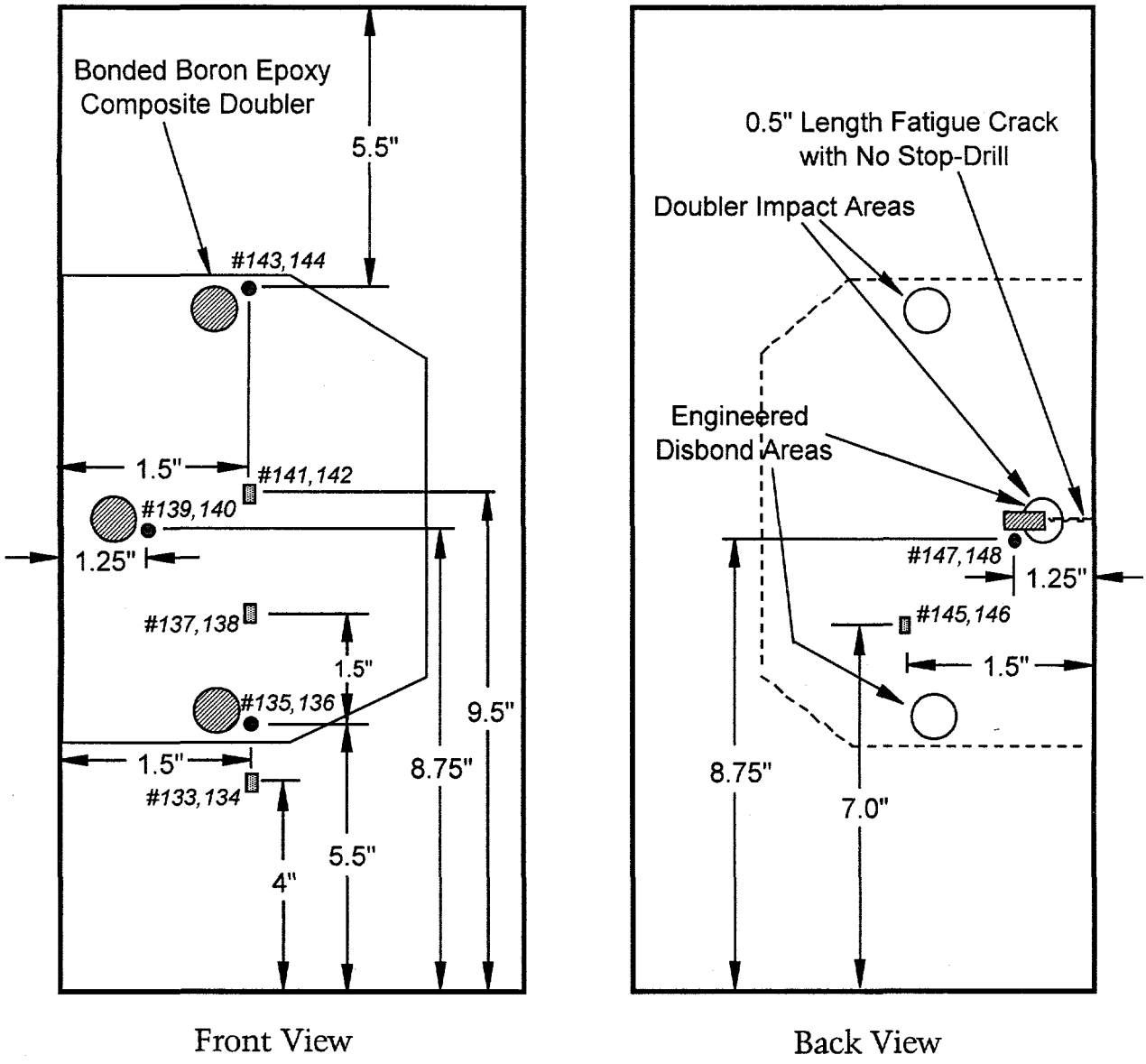

Figure 24: Strain Gage Locations for Composite Tension Test Coupon - Configuration BE-9

2.4.3 Static Tension Ultimate Strength Tests

Several specimens that were fatigued and other specimens that had implanted flaws but were not fatigued were subjected to static ultimate tension tests in order to determine their ultimate strength and failure modes. The test procedures and data acquisition process was as follows.

1. A 1050 lb. pre-load was applied to eliminate the residual curvature in the test specimens. After pre-loading the specimen, the strain gage bridges were balanced to produce a zero strain output signal. This data was used as the tension ultimate test starting point (Test Tension Load = 0 lbs.).

2. The load was increased, using displacement mode control, at a continuous rate of 0.05 inch/minute. Failure was defined as the point where the specimen was unable to sustain an increasing load. The peak load recorded during each failure test was used to calculate the maximum stresses sustained by the flawed specimens (ultimate strength).

3. The machine's crosshead displacement transducer was used to obtain load vs. total displacement curves. In some tests, the biaxial strain gages shown in Figs. 16-24 were continuously monitored to measure the strain fields during specimen failure.

2.4.4 Nondestructive Inspections

The specimens were inspected with visual (optical magnification) and ultrasonic NDI techniques at 36,000, 54,000, 72,000 and 144,000 cycles. The NDI tests were performed in-situ to eliminate the removal of the specimens from the tension test machine following each fatigue interval. The NDI techniques being deployed in this effort were able to detect disbonds, delaminations, and porosity in the composite doubler (ultrasonics), as well as cracks in the parent aluminum material (optical measurements).

Ultrasonic (UT) inspection techniques using the Staveley Bondmaster equipment (resonance mode) and through-transmission ultrasonics were used. The Sandia Labs AANC pulse-echo ultrasonics inspection procedure for bonded composite doublers, AANC-PEUT-Comp-5521/4-004, was also used. The documentation and validation of inspection procedures, as well as the appropriate approvals by the FAA, were handled through reference [18] and the reference [46] inspection procedure under the auspices of this same ACO project number (SP1798AT-Q). Section 3.1.6 contains the results from the inspections conducted before and after the fatigue tests.

3.0 Test Results

The test results supporting this damage tolerance assessment of composite doublers will be presented in four distinct sections: 1) fatigue test results, 2) strain field measurements (evaluation of load transfer), 3) residual strength tests, and 4) ultimate strength tests. Nondestructive inspections, used to relate the above items to flaw initiation and growth, will be discussed in the section on the fatigue test results. The results presented in Section 3.0 provide a comprehensive evaluation of the effectiveness of composite doublers in reducing crack growth in aluminum substructure. Fatigue and strength tests were performed on specimens with various combinations of crack, disbonds, and impact flaws. The flaw sizes, locations, and combinations were engineered to produce extreme worst case conditions. Environmental conditions representing temperature and humidity exposure are also included in the coupon specimens (ref. Section 2.0). Table 2 describes the composite coupon test specimen matrix. Twenty-one specimens representing nine different configurations were tested.

Inspection requirements for the actual on-aircraft installation were established using a Damage Tolerance Analysis [1] and the results from this study. *Disbond, delamination and crack sizes used in these damage tolerance tests were at least twice the size of those which will be detected by the NDI requirements. Thus, there is an inherent safety factor built into this damage tolerance assessment and the doubler performance sited here should be conservative.*

3.1 Fatigue Tests

The results from the fatigue tests on specimens Lock 1 - Lock 21 (configurations BE-1 through BE-9) are summarized in Table 3 and shown graphically in Figures 25 and 26. The results have been broken down according to the specimen's flaw scenario and are provided in sections 3.1.1 to 3.1.6 below.

3.1.1 Stop-Drilled Cracks with Composite Doubler Reinforcement

Specimen configurations BE-2 (Lock2), BE-3 (Lock3), and BE-8 (Lock13, Lock14, & Lock15) showed that crack growth could be substantially reduced or completely eliminated for a number of fatigue lifetimes using composite doubler repairs. This is true in spite of the disbond and impact impediments - both at the critical load transfer region along the doubler's edge and directly over the crack - which were engineered into the specimens.

a. Disbond and Crack Flaws - Note the delay in crack reinitiation until 72,000 and 126,000 cycles in the Figure 25 BE-2 and BE-3 curves. Because of this initial crack growth arrest, specimens Lock2 (BE-2) and Lock3 (BE-3) experienced total crack growths of less than 1.75" up through 144 K fatigue cycles (four design lifetimes of the L-1011 aircraft).

Config.	Description	Fatigue Test Results
BE-1	unabated 0.5″ fatigue edge crack; no engineered flaws in composite doubler installation	• crack propagated 1.78″ in 144 K cycles • no initiation of disbonds • post-fatigue residual strength = 103 ksi
BE-2	stop-drilled 0.5″ sawcut edge crack with collocated disbond; 0.75″ dia. disbonds in edge of doubler	• stop-drilled crack reinitiated after 126 K cycles • crack propagated 0.875″ in 144 K cycles • no growth in disbonds; fracture of adhesive around crack • post-fatigue residual strength = 88 ksi
BE-3	stop-drilled 0.5″ sawcut edge crack with collocated disbond; 1.0″ dia. disbonds in edge of doubler	• stop-drilled crack reinitiated after 72 K cycles (small burr in stop-drilled hole acted as starter notch) • crack propagated 1.71″ in 144 K cycles • no growth in disbonds; fracture of adhesive around crack
BE-4	unabated 0.5″ fatigue edge crack with collocated disbond; 0.75″ dia. disbonds in edge of doubler	• crack propagated 2.21″ in 144 K cycles • fatigue test was extended until specimen failure occurred at 182 K cycles
BE-5	1″ dia. hole in parent aluminum plate; no engineered flaws in composite doubler installation	• 180 K fatigue cycles applied - no fatigue cracks generated • no growth in disbonds

* Crack growth rates in all composite doubler specimens were 10 to 20 times slower than the Control Specimens (BE-6) which had no reinforcing doublers.

Table 3: Composite Doubler Damage Tolerance Fatigue & Ultimate Strength Test Summary

Config.	Description	Fatigue Test Results
BE-6	unabated 0.5″ fatigue edge crack; aluminum plate with no doubler	• crack propagated until specimen failed at 9 K cycles • duplicate specimen failed at 12 K cycles
BE-7	composite doubler installed without any engineered flaws; no flaws in aluminum plate	• two specimens - no crack growth in 144 K and 216 K cycles • no initiation of disbonds • ultimate strength following fatigue = 70 ksi
BE-8	stop-drilled 0.5″ sawcut edge crack with collocated impact/disbond damage on doubler; 160°F hot, wet conditioned; tested at room temperature	• three specimens - cracks reinitiated after 72 K, 90 K, & 90 K cycles • cracks propagated 0.5″ in 144 K cycles • no growth in disbonds • all three ultimate strength tests produced σ_u values in excess of 75 ksi
BE-9	unabated 0.5″ fatigue edge crack with collocated impact/disbond damage on doubler; impact/disbond damage on edge of doubler; 160°F hot, wet conditioned; tested at room temperature	• three specimens - cracks propagated 0.7″ in 144 K cycles • no growth in disbonds • average of three ultimate strength tests produced σ_u value of 72.4 ksi

* Crack growth rates in all composite doubler specimens were 10 to 20 times slower than the Control Specimens (BE-6) which had no reinforcing doublers.

Table 3: Composite Doubler Damage Tolerance Fatigue & Ultimate Strength Test Summary (continued)

b. Disbonds and Cracks with Impact Damage and Hot, Wet Conditioning - Figure 26 shows the fatigue crack growth for the abated crack specimens in the BE-8 configuration. Note the delay in crack reinitiation until 72,000, 90,000, and 72,000 cycles, respectively in the Lock13, Lock14 and Lock15 specimens. In the BE-8 configuration, the disbonds noted above were accompanied by collocated impact damage directly over the crack (see Fig. 14). Prior to testing, the specimens were also subjected to hot, wet conditioning until a 10% (by weight) water absorption was achieved. Specimens Lock13, Lock14 and Lock15 experienced total crack growths of less than 0.060" up through 144,000 fatigue cycles. Note that specimens Lock14 and Lock15 were fatigued beyond the four lifetime test goal to 180,000 cycles (five L-1011 lifetimes). Little or no additional crack growth was observed.

The drop in total crack growth in the impact damaged specimens (config. BE-8) versus the BE-2 and BE-3 configurations can be attributed to the effects of the

deformations produced by the impact. The coupon cracks propagated through the center impact region. Figure 27 shows two views of the typical damage produced by the 300 in.-lb. impact. It can be seen that the aluminum parent material was plastically deformed (cup shaped recess) by the 1" diameter hemisphere used for impact. It is likely that this deformation strain hardened the material and produced beneficial compressive strains that impeded crack growth in the area of impact. In addition, the complex geometry created by the indentation (i.e. lack of flat surface which is in plane with the tension loads) may have also slowed the crack growth in this area. Figure 26 shows that specimen Lock15 reached a plateau where the crack length did not change from 106,000 to 180,000 cycles.

3.1.2 Fatigue Cracks With No Abatement

This includes specimens in the BE-1, BE-4, and BE-9 configurations (Lock1, Lock4, Lock19 - Lock21). The test results showed that large crack mitigation factors can be obtained through the use of composite doublers. Once again, these test results incorporate damage tolerance for bonded Boron-Epoxy doublers since the specimens were intentionally manufactured with worst-case disbond and impact flaws.

a. Disbond and Crack Flaws - Figure 25 shows that specimens Lock1 (BE-1) and Lock4 (BE-4) survived 144,000 fatigue cycles with crack growths of 2" or less. Without any type of crack abatement (e.g. stop-drill at crack tip), crack propagation began shortly after fatigue testing was initiated. The first noticeable change in crack length occurred after approximately 16,000 cycles or 1/2 of an L-1011 lifetime.

   The Lock4 fatigue test was continued beyond the test goals in order to demonstrate that the specimen could survive five L-1011 lifetimes (180,000 cycles) without failure. The cycles-to-failure for this configuration was 182,000 cycles. Once the crack propagated through the width of the aluminum, the adhesive was able to transmit stresses into the doubler which exceeded the material's ultimate strength. At this point, the composite laminate fractured.

   Specimens BE-1 and BE-4 produced very similar crack growth curves. The BE-1 configuration had a good doubler bond along the length of the fatigue crack while the BE-4 configuration had the added impairment of a disbond collocated with the fatigue crack (see Figures 7 and 10). As a result, the initial rate of crack growth was higher in specimen Lock4. However, the two crack growth curves blended into a single propagation rate at a crack length (a) equal to 1.75". In fact, Figure 25 shows that regardless of the initial flaw scenario engineered into the test specimen, all of the flaw growth curves tend to blend into the same outcome as the crack propagates beyond 2" in length. This is because all of the specimens degenerate into the same configuration at this point.

b. Disbonds and Cracks with Impact Damage and Hot, Wet Conditioning - Figure 26 shows the fatigue crack growth for the unabated crack specimens in the BE-9

configuration. In this configuration, the disbonds noted above were accompanied by collocated impact damage directly over the crack and along the edge of the doubler (see Fig. 15). Prior to testing, the specimens were also subjected to hot, wet conditioning until a 10% (by weight) water absorption was achieved. The impact phenomenon discussed above was also present in configuration BE-9; crack growth was arrested in the impact area. Specimens Lock19 and Lock21 experienced total crack growths of 0.70" or less after 144,000 fatigue cycles. The plots of Lock19 and Lock21 in Fig. 26 show that all of the crack growth occurred during the first 90,000 fatigue cycles after which time the crack growth was halted in the impact area.

After three fatigue lifetimes, the Lock20 specimen experienced crack growth of less than 0.80". Thus, an allowable crack length of 1.0" would still not be present after 108,000, post-installation "flight" cycles. Unfortunately, it appears that this specimen had a small notch (manufacturing or handling defect) in the edge of the aluminum skin. The notch may have acted as an initiator for a crack which formed just outside the upper boundary of the composite doubler footprint. This crack, without the benefit of the doubler reinforcement, grew across the aluminum plate and caused a failure of the test specimen outside of the doubler. As a result, no doubler performance data could be obtained beyond 108,000 fatigue cycles.

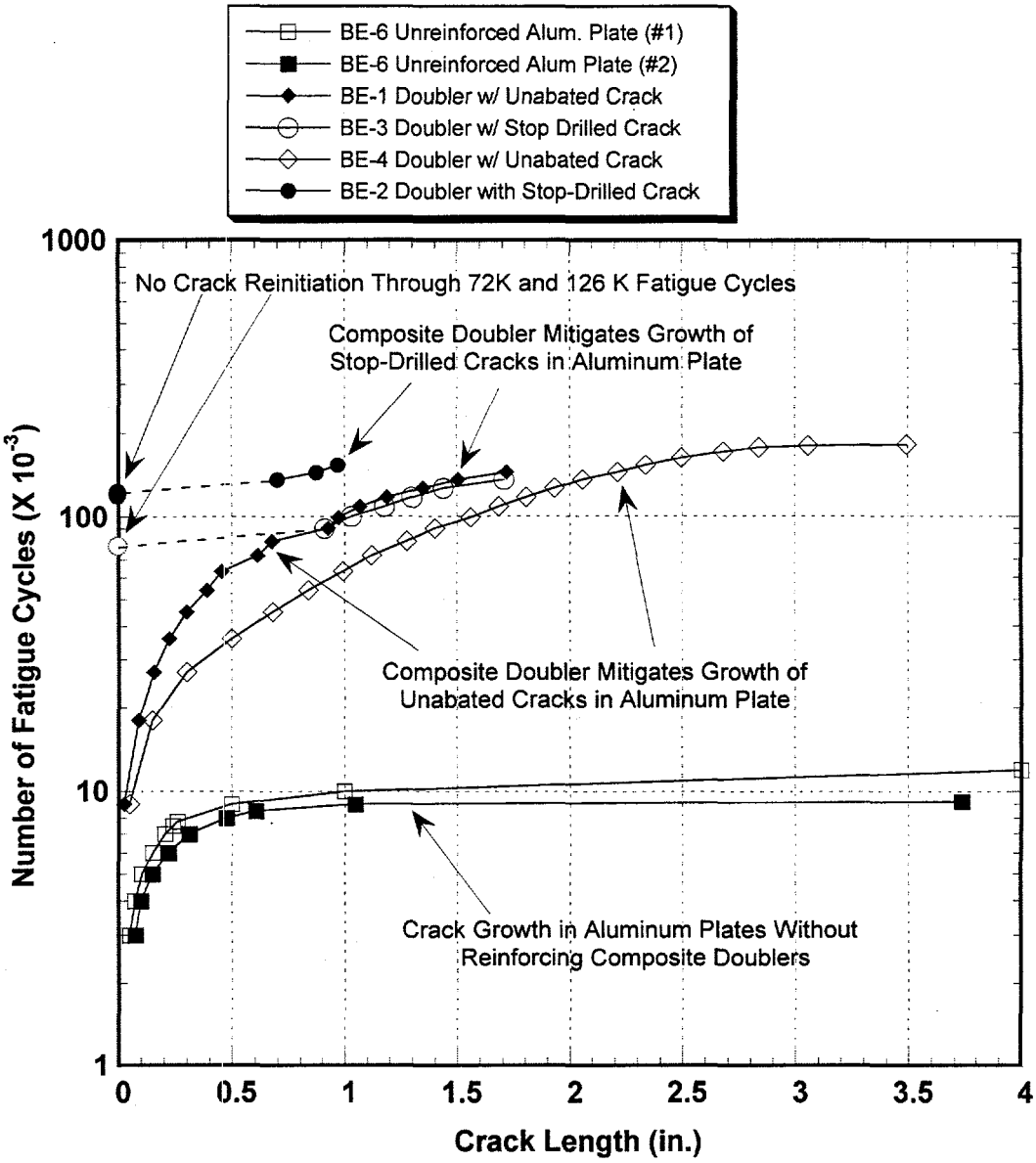

Figure 25: Fatigue Crack Growth in 2024-T3 Plates With and Without Reinforcing Composite Doublers (Configurations BE-1 through BE-6; Specimens Lock1 through Lock7)

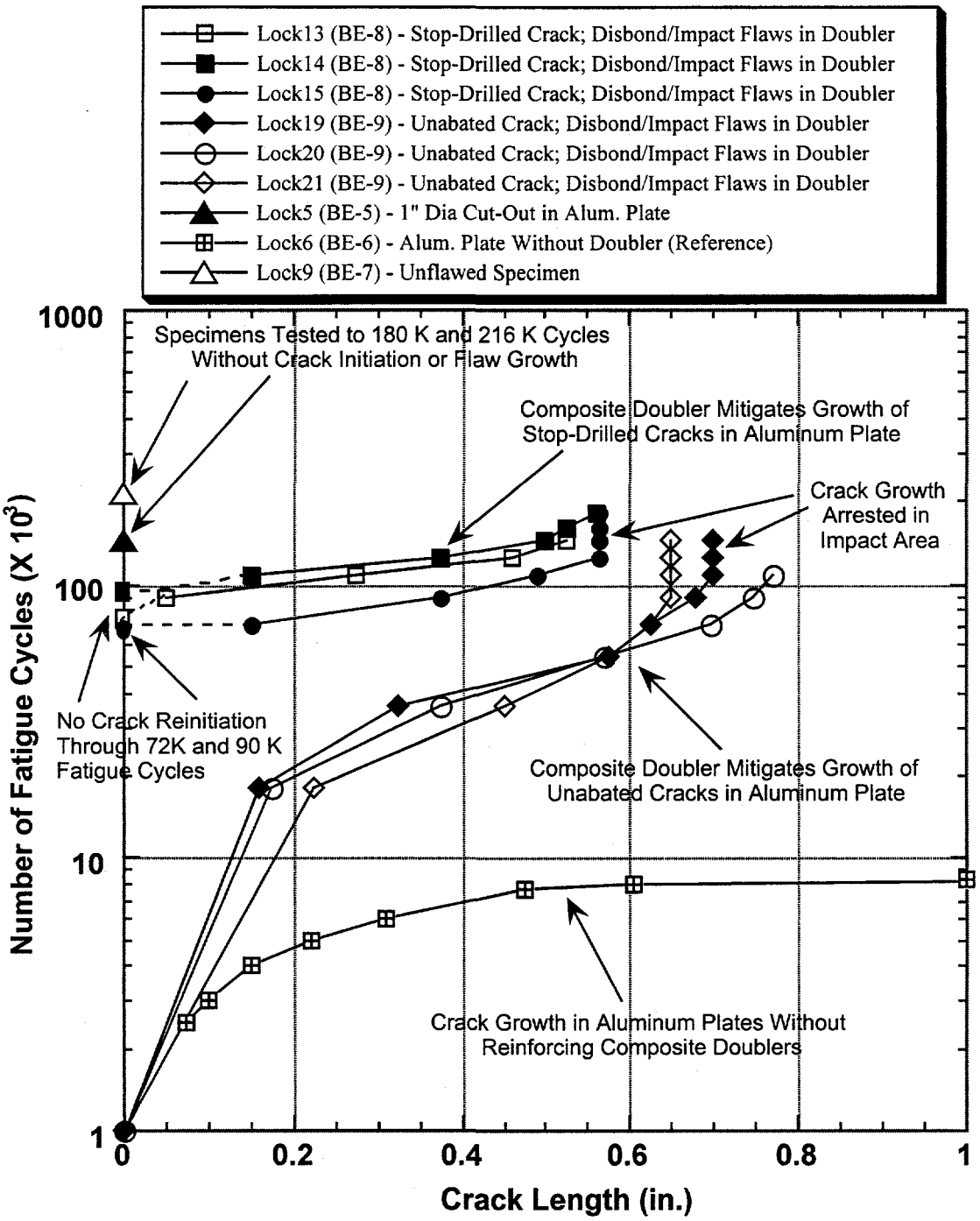

Figure 26: Fatigue Crack Growth in 2024-T3 Plates With and Without Reinforcing Composite Doublers (Configurations BE-6 through BE-9; Spec. Lock6, Lock9, Lock10–12, Lock 16–18)

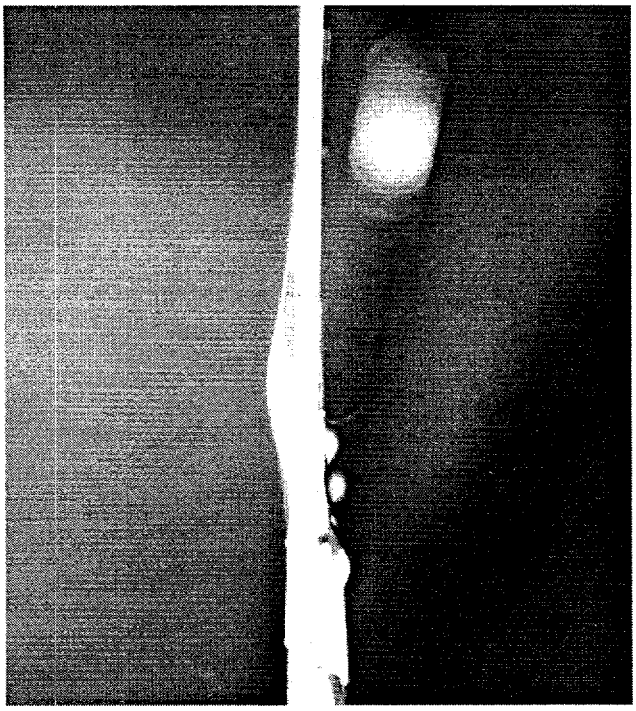

(a) Side View

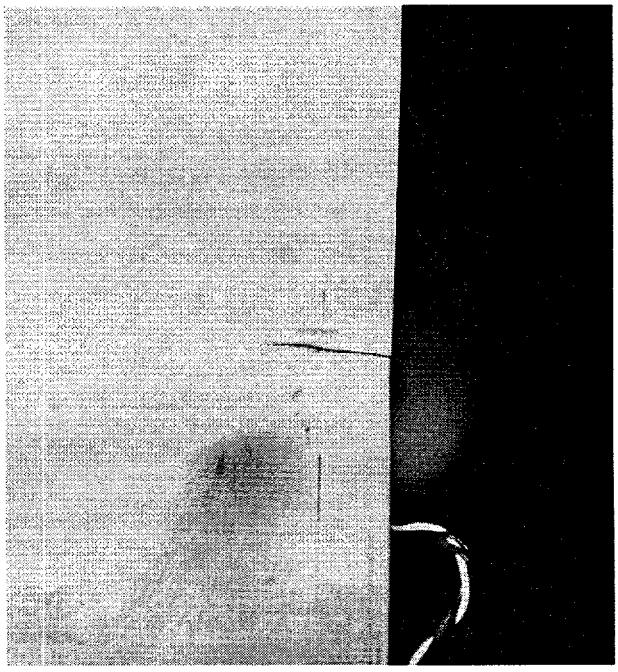

(b) Back View

Figure 27: Impact Damage on Composite Coupons

3.1.3 Material Removed from Parent Plate and Composite Doubler Reinforcement

Specimen Lock5 (configuration BE-5) had a 1" diameter hole simulating the removal of damage (e.g. crack or corrosion) in the parent structure. It could also be considered a stop-drill hole with a very generous radius. In this specimen, a fatigue crack did not initiate during 144,000 fatigue cycles or four L-1011 lifetimes. The bonded composite doubler picked up load immediately adjacent to the cut-out so this type of material removal enhanced the overall performance of the installation. Although the large hole in the parent aluminum created a stress riser, the doubler was able to withstand the high local stresses and prevent any flaws (disbonds, cracks) from developing. Figure 26 shows a data point of zero crack growth after 114,000 cycles for specimen Lock5.

3.1.4 Control Specimens and Comparison of Crack Growth Rates

Two tests were conducted on aluminum "control" specimens which were not reinforced by composite doublers (BE-6 configuration in Table 2). Unabated fatigue cracks were propagated using the same fatigue spectrum applied to the composite reinforced specimens. *Figure 25 shows the crack growth exhibited by the unreinforced plates. In these tests, the fatigue cracks propagated through the width of the BE-6 specimens after 9,000 and 12,000 cycles. By comparison, configuration BE-4 (Lock4), which had a composite doubler, failed after 182,000 cycles. Thus, the fatigue lifetime as defined in the test coupons, was extended by a factor of approximately 20 through the use of composite doublers.* [Again, note that an optimum installation (see 3.1.5 below) or a specimen without a fatigue crack as in BE-5 would be able to sustain much higher fatigue cycles. Therefore, the life extension factor of 20, calculated using flawed doubler installations, is considered conservative.]

In Figures 25 and 26, the number of fatigue cycles are plotted using a log scale because it clearly shows the crack arresting affect of the composite doublers. The unreinforced panels asymptotically approach 10,000 cycles-to-failure while the plates reinforced by composite doublers asymptotically approach 100,000 to 200,000 fatigue cycles. Figures 25 and 26 also show that the crack growth rates for all of the specimens can be approximated by a bilinear fit to the data plotted on a semi-log scale. This simply demonstrates the well known power law relationship between fatigue cycles (N) and crack length (a). The first linear portion extends to (a) = 0.25" in length. The slopes, or crack growth rates, vary depending on the localized configuration of the flaw (e.g. stop-drilled, collocated disbond, presence of doubler). The second linear portion extends to the point of specimen failure. A comparison of these linear approximations shows that the crack growth rate is reduced 20 to 40 times through the addition of a composite doubler. Also, as noted above, all of the doubler specimen crack growth rates are the same after the crack propagates past the initial flaw configuration at the specimen's edge (e.g. engineered disbonds). This occurs at approximately (a) = 1.5" for the non-impact damaged specimens.

3.1.5 Baseline Specimens: Performance of an Optimum Installation

The primary purpose of the damage tolerance tests was to evaluate the performance of Boron-Epoxy doublers in flawed installations. Through experimental demonstrations of acceptable doubler performance in the presence of worst case flaw scenarios, these tests showed that conservatism and appropriate safety factors are inherently built into a Boron-Epoxy doubler design. *However, to complete a comprehensive evaluation of Boron-Epoxy doublers, it is necessary to establish a baseline performance from a normal, unflawed installation. Two specimens with the BE-7 "optimum installation" configuration were subjected to fatigue tests. Both specimens survived 144,000 cycles without flaw initiation of any kind. One of the specimens was subjected to six fatigue lifetimes or 216,000 cycles. Post-test inspections did not reveal any flaws in this specimen* (see 3.1.6 below). Figure 26 plots the fatigue response indicating an absence of cracks (i.e. zero crack growth) throughout the fatigue tests.

3.1.6 Nondestructive Inspection and Propagation of Adhesive Flaws

These damage tolerance tests assessed the potential for loss-of-adhesion flaws (disbonds and delaminations) to initiate and grow in the composite doubler installation. Disbonds can occur between the composite doubler and the aluminum skin while delaminations can develop between adjacent plies of Boron-Epoxy material. It has been shown in related studies that the primary load transfer region, which is critical to the doubler's performance, is around its perimeter [4-6, 21, 24, 32-35, 40]. The purpose of the disbonds in configurations BE-2, BE-3, BE-4, BE-8, and BE-9 were to demonstrate the capabilities of composite doublers when large disbonds exist in the critical load transfer region as well as around the cracks which the doublers are intended to arrest. In this manner, severe worst case scenarios could be assessed and quantitative performance numbers could be established.

a. Initial Assessment of Engineered Flaws in Test Specimens - Each of the fatigue and ultimate strength test coupons was inspected using a C-scan ultrasonic technique [46]. C-scan technology uses information from single point A-scan waveforms to produce an area mapping of the inspection surface. The two-dimensional images are produced by digitizing point-by-point signal variations of an interrogating sensor while it is scanned over a surface [47]. Figures 28 and 29 show C-scan images generated by an ultrasonic inspection of specimens Lock1 (Config. BE-1), Lock 2 (Config. BE-2), Lock11, and Lock12 (both Config. BE-8). Signal variations corresponding to disbonds and delaminations are represented by dark black areas on the images [Note: the NDI system produces color-coded maps, however, for the purposes of this document grey scale plots clearly show the flaws in the test specimens]. The four C-scan images in Figs. 28 and 29 show the specimen flaw profiles prior to fatigue or ultimate strength testing. To provide a point of reference, a shape outline of the Boron-Epoxy doubler is superimposed on the C-scan image. The following observations can be made:

1) The composite laminate in specimen Lock1 contains no flaws; there are no indications of flaws in the C-scan. Although this inspection technique was not set up for crack detection, the small crack at the edge of the specimen (ref. Fig. 7) was imaged in the scan.

2) Specimen Lock2 contains three engineered disbond flaws as shown in Figure 8. The C-scan in Figure 28 shows the three engineered disbonds and reveals that there were no other flaws in the installation.

3) Specimens Lock11 and Lock12 have the same BE-8 configuration: a disbond, centered over a stop-drilled crack, with collocated impact damage as shown in Fig. 14. Figure 29 shows the ability of C-scan ultrasonics to detect the presence of these flaws. The images also demonstrate the ability to consistently produce engineered flaws in the coupons.

b. No Initiation of Disbond Flaws - Although the AANC NDI tests demonstrated the detection of disbonds as small as 0.25" in diameter [18, 47], disbonds of 0.75" and 1.0" diameter were engineered into the test specimens. Inspections performed at 1, 2, 3, 4, 5 and 6 fatigue lifetime intervals revealed that there was no growth in any of the disbonds. Crack propagation in the specimens, and the accompanying displacements as the crack opened each cycle, produced cohesive failure (cracking) in the adhesive. However, this failure was localized about the length of the crack and did not result in any disbonds (adhesive failure). This result was ascertained by visually noting the presence of adhesive on both the aluminum and composite laminate (i.e. adhesive fractured at high strains but it did not disbond). Thus, the full strength of the adhesive was achieved.

   Finally, comparisons between the BE-1 (no disbonds) and the BE-2, 3, 4, 8 and 9 (engineered disbonds) fatigue curves in Figures 25 and 26 show that the large engineered disbonds did not decrease the composite doubler's performance. In fact, many of the specimens with disbonds exhibited *less* crack growth than the BE-1 configuration which had no disbonds.

c. Nondestructive Inspections Show No Change in Engineered Disbonds - Ultrasonic scanning was used to create two-dimensional flaw maps of each test specimen [46]. Once again, signal variations corresponding to disbonds and delaminations are represented by dark black areas on the images. Figures 30-38 show a series of before and after fatigue test images created by NDI. Side-by-side comparisons of the various flawed specimens show that the original engineered flaws, which were detected prior to testing, remained unchanged even after multiple fatigue lifetimes. The following observations can be made:

   1) Specimen Lock3 (Config. BE-3; ref. flaw drawing Fig. 9) - All three implanted flaws are visible and sized correctly in Figure 30. The only discernible change in

the flaw profile during fatigue occurred around the propagating crack. As the crack opened during fatigue loading it produced a fracture of the adhesive. This demonstrates the proper failure mode for a doubler installation. That is, the adhesive should fracture instead of disbonding. This assures that the full strength of the adhesive can be realized in the joint. [Note: the installation process specification [42] requires a wedge test on a composite witness specimen which is installed adjacent to the actual doubler. A successful wedge test result is where adhesive material appears on both the aluminum substrate and the composite doubler. This signifies a good installation and assures that the adhesive layer will fracture at high strains and will not disbond at relatively lower strains.]

2) Specimen Lock4 (Config. BE-4; ref. flaw drawing Fig. 10) - Figure 31 shows that the disbond flaws - located in the critical load transfer region at the doubler's edge - did not grow or change shape during the fatigue tests. This specimen was fatigued beyond the limits of the test goals in order to determine a cycles-to-failure number for this configuration. The crack propagated through the specimen after 182,000 cycles (in excess of five lifetimes). Since the specimen was failed, it was not possible to obtain NDI data in the area of failure as shown in Fig. 31.

3) Specimen Lock 5 (Config. BE-5; ref. flaw drawing Fig. 11) - The 1" diameter cut-out in the aluminum plate is visible in Figure 32. There are no other flaws in the installation. No disbonds initiated during 180,000 fatigue cycles.

4) Specimen Lock9 (Config. BE-7; ref. flaw drawing Fig. 13) - This configuration represents the optimum installation and Figure 33 shows that the test specimens did not have any flaws. Further, post-test inspections revealed that no disbonds or delaminations developed during 216,000 fatigue cycles (six L-1011 lifetimes).

5) Specimens Lock13 and Lock14 (Config. BE-8; ref. flaw drawing Fig. 14) - Figures 34 and 35 contain the before-and-after fatigue test comparisons of NDI results. The ultrasonic scans show: 1) the engineered disbond and impact damage in the original test specimens and, 2) no change in the specimens' flaw profile after 144,000 and 180,000 fatigue cycles.

6) Specimens Lock19, Lock20, and Lock21 (Config. BE-9; ref. flaw drawing Fig. 15) - Figures 36 - 38 contain the before-and-after fatigue test comparisons of NDI results. The ultrasonic scans show: 1) the three disbond and impact damage areas in the original test specimens and, 2) no change in the specimens' flaw profile after 108,000 and 144,000 fatigue cycles.

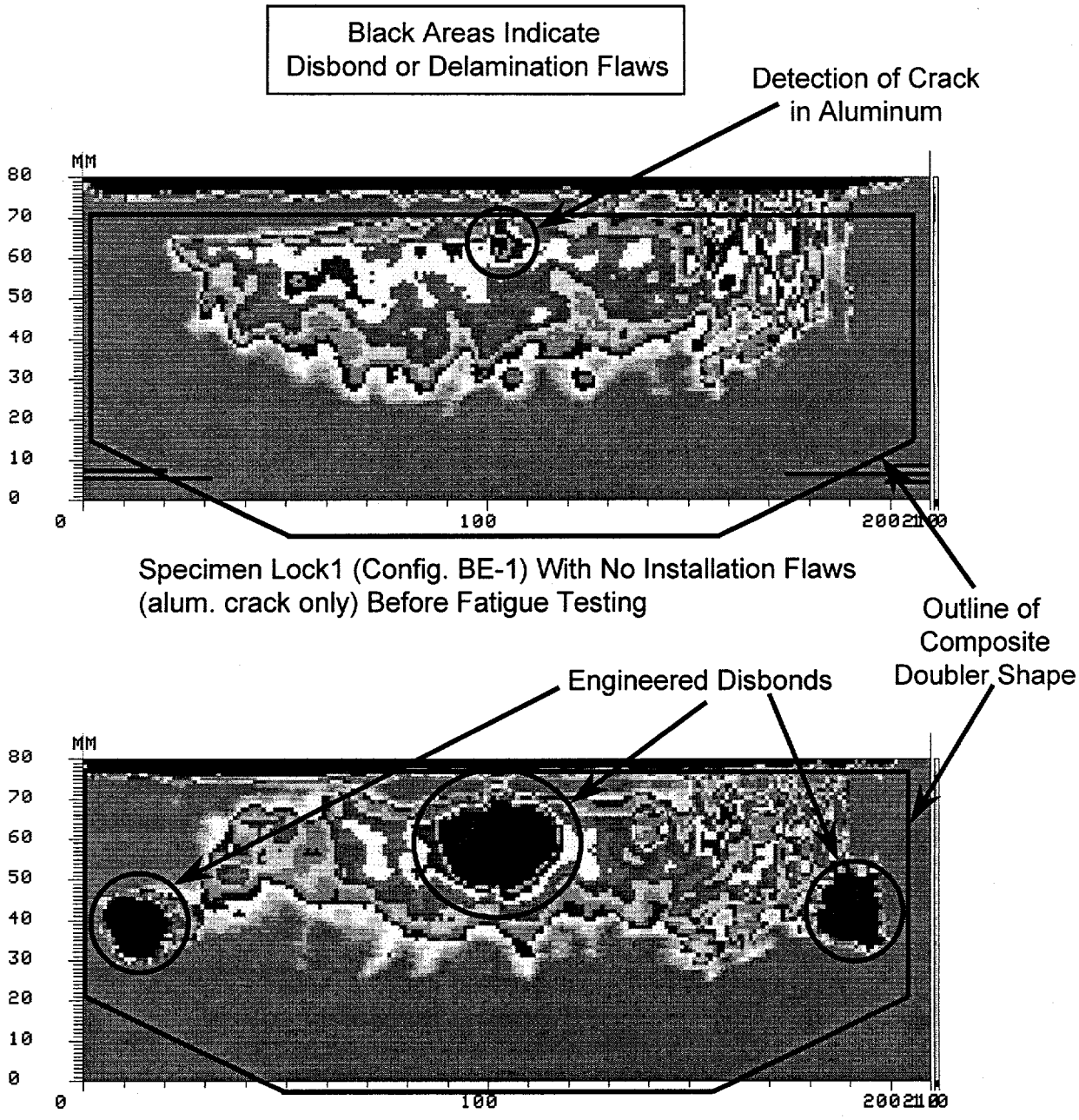

Figure 28: Fatigue Specimens Lock1 and Lock2 Flaw Profiles Before Fatigue Testing; Specimens Were Loaded to Failure After Fatigue Testing

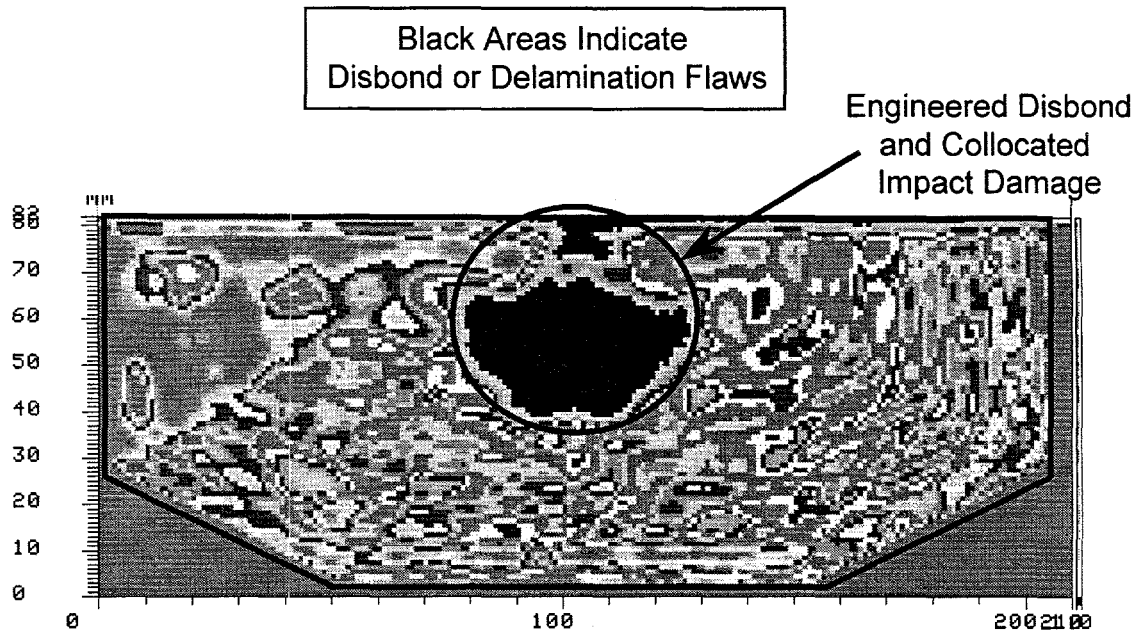

Specimen Lock11 (Config. BE-8) Before Ultimate Strength Test;
Original Damage from Disbond and Collocated Impact

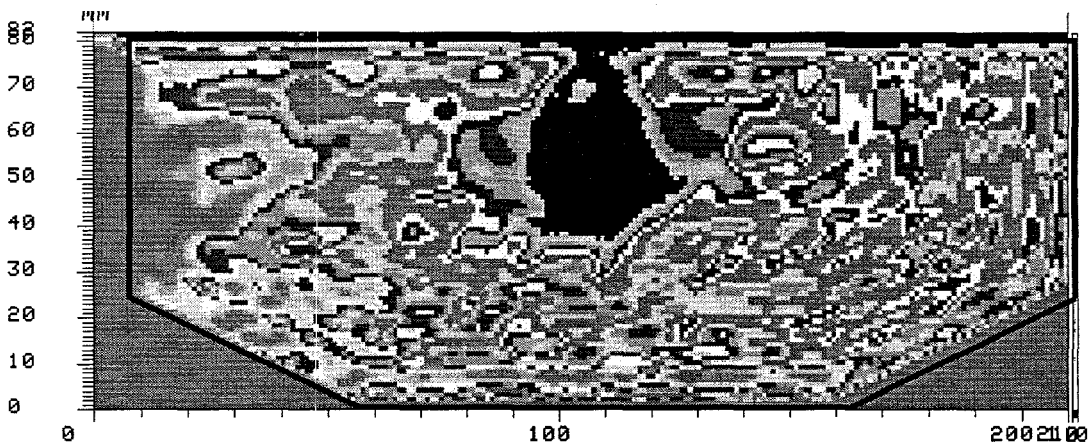

Specimen Lock12 (Config. BE-8) Before Ultimate Strength Test;
Original Damage from Disbond and Collocated Impact

Figure 29: Fatigue Specimens Lock11 and Lock12 (Configuration BE-8) Show Consistency of Engineered Flaw Profiles and Ability to Detect Flaws Via Ultrasonic Inspections

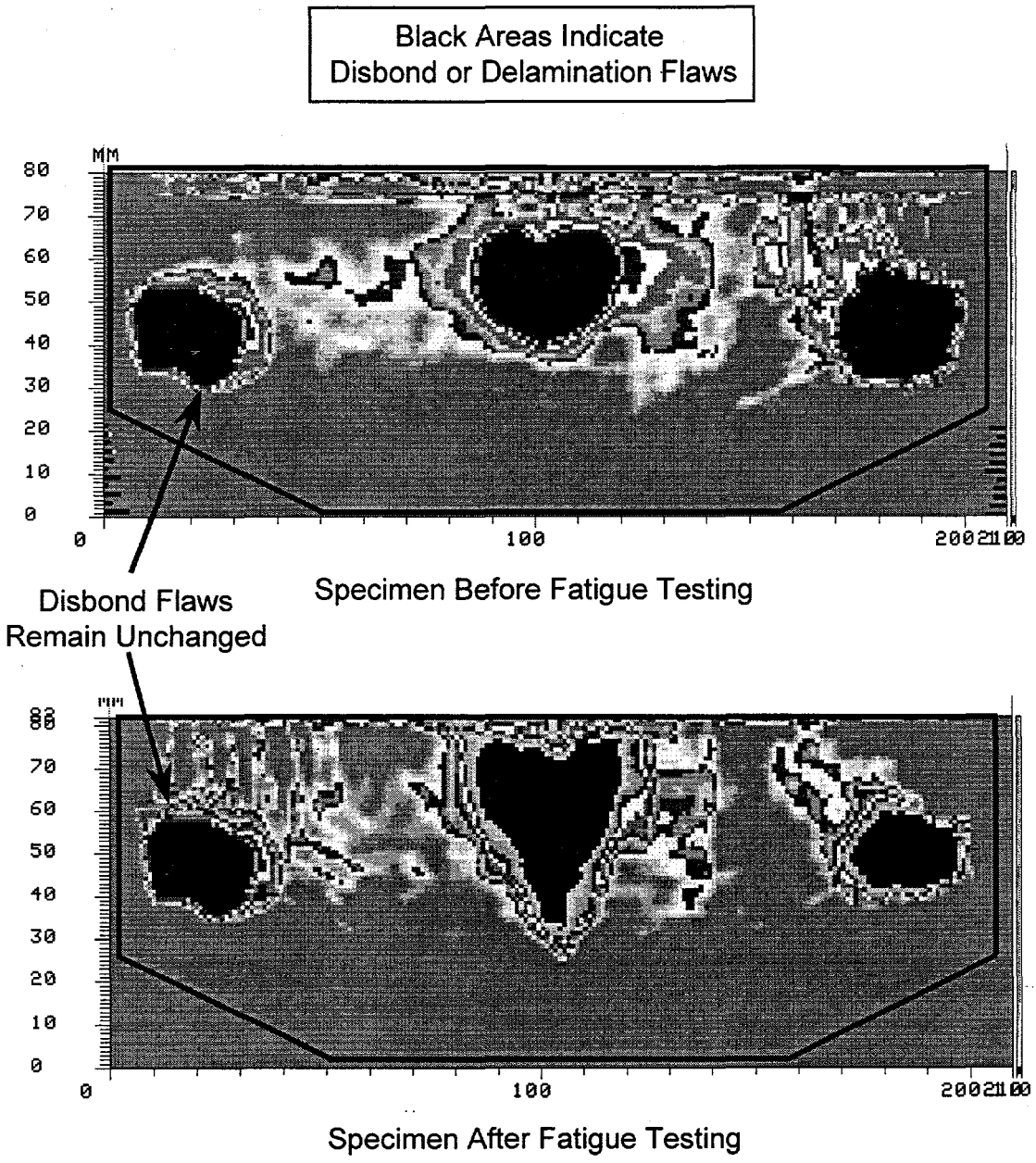

Figure 30: Fatigue Specimen Lock3 (Configuration BE-3) Flaw Profile Before and After 144,000 Fatigue Cycles

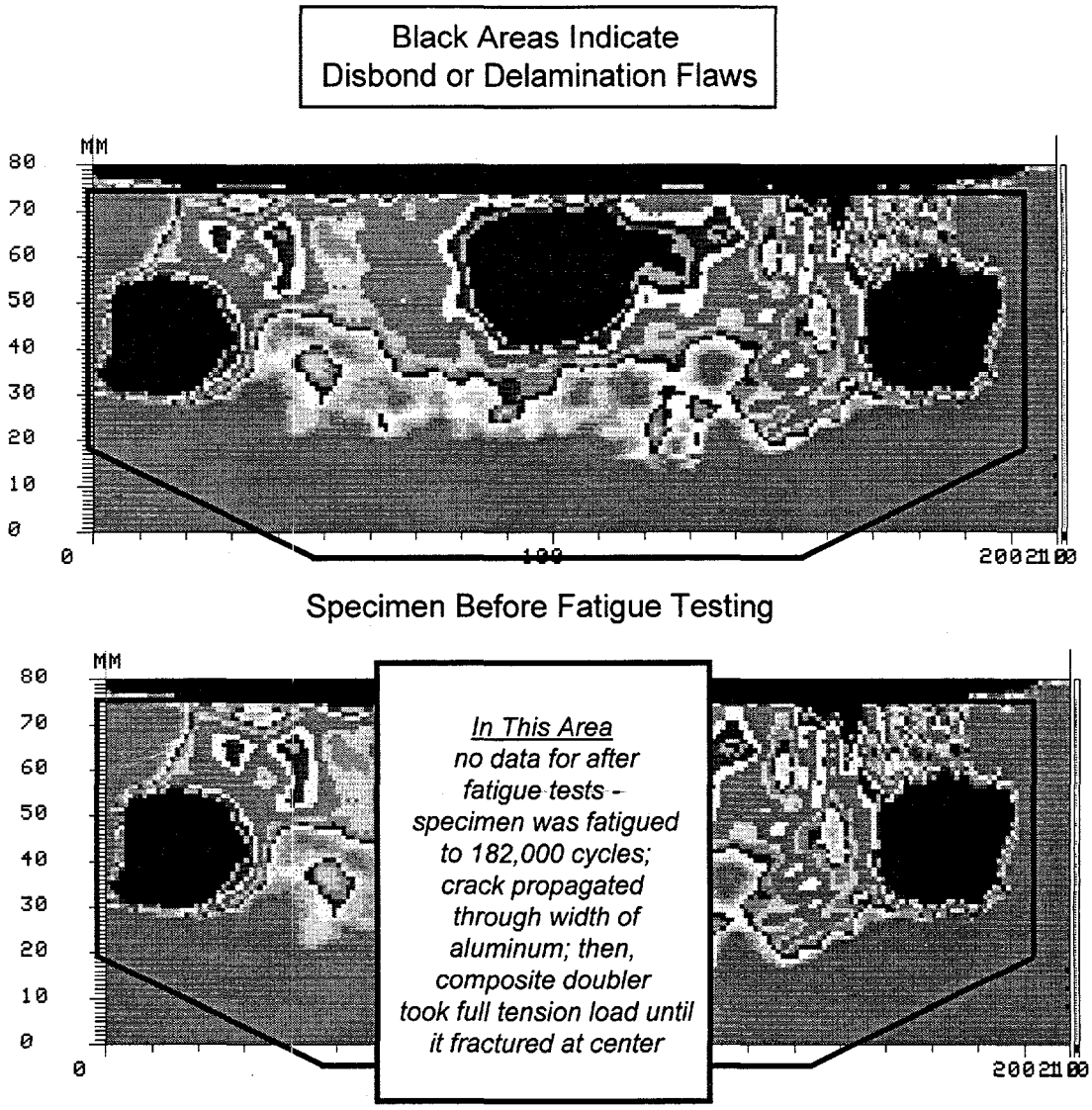

Figure 31: Fatigue Specimen Lock4 (Configuration BE-4) Flaw Profile Before and After 182,000 Fatigue Cycles

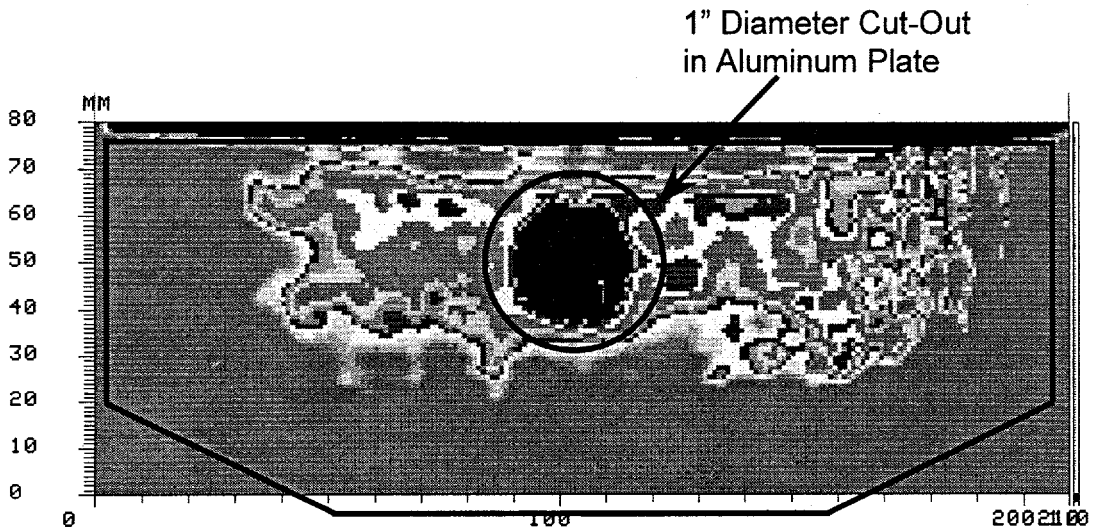

Specimen Before Fatigue Testing

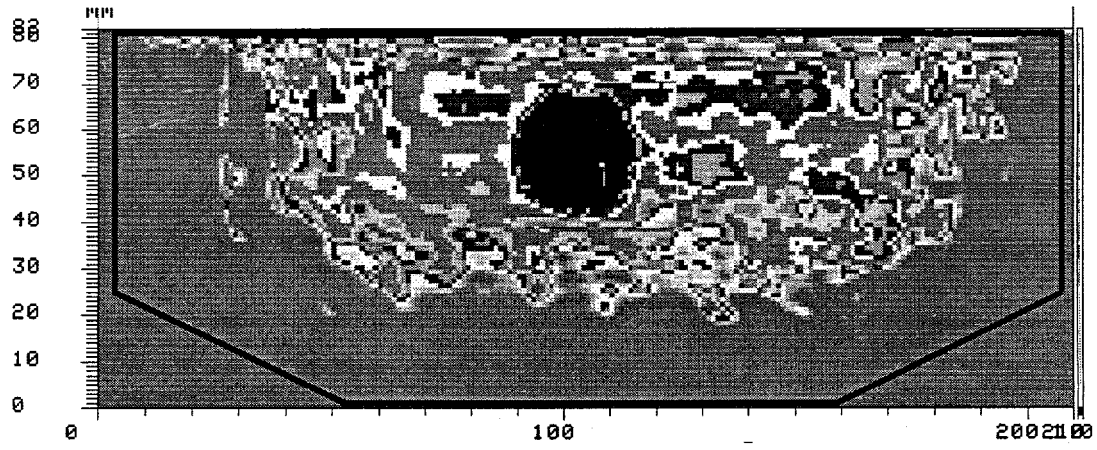

Specimen After Fatigue Testing

Figure 32: Fatigue Specimen Lock5 (Configuration BE-5) Flaw Profile Before and After 180,000 Fatigue Cycles; No Flaw Growth After Five L-1011 Fatigue Lifetimes

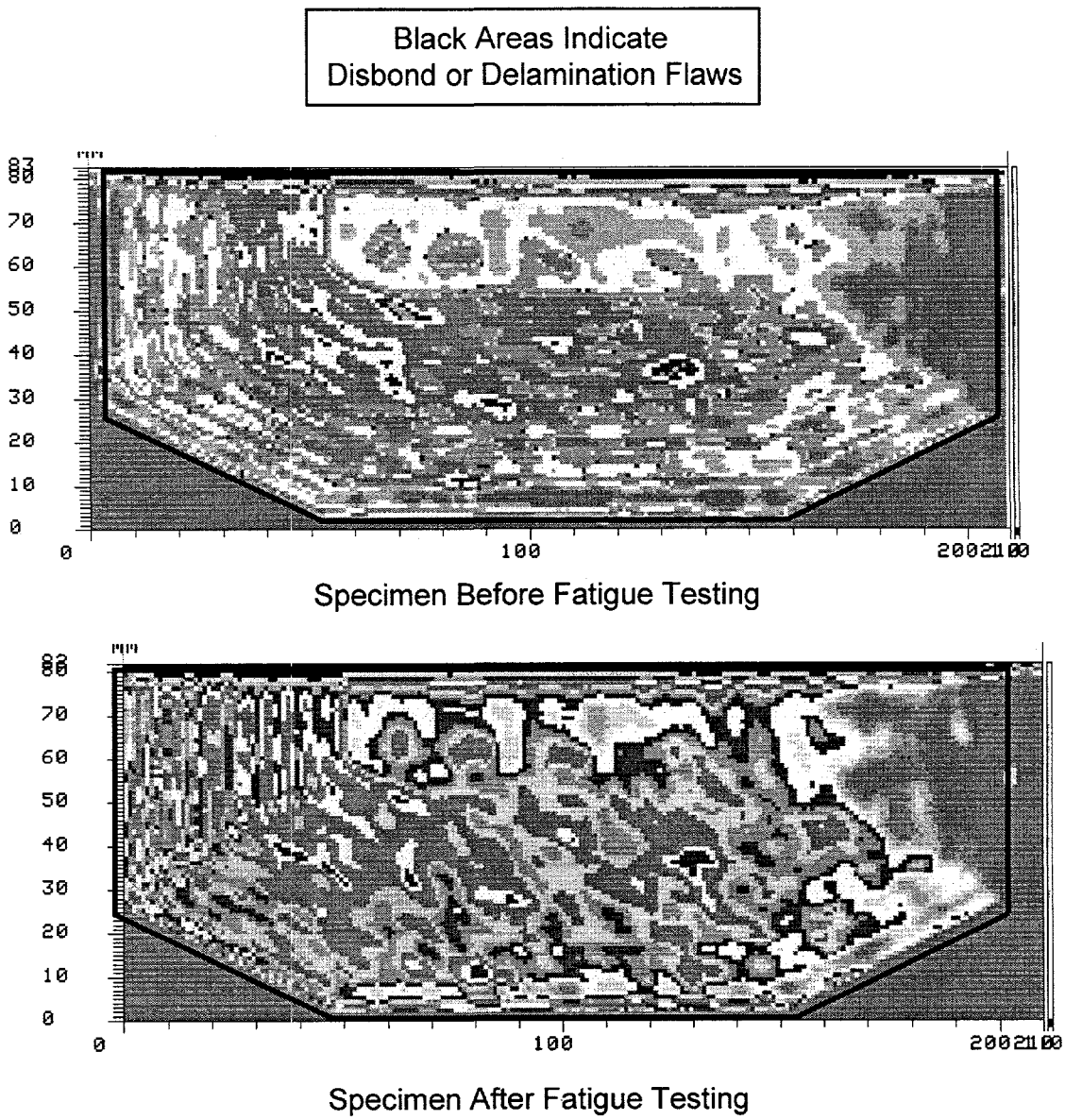

Figure 33: Fatigue Specimen Lock9 (Configuration BE-7) Flaw Profile Before and After 216,000 Fatigue Cycles; No Flaw Growth After Six L-1011 Fatigue Lifetimes

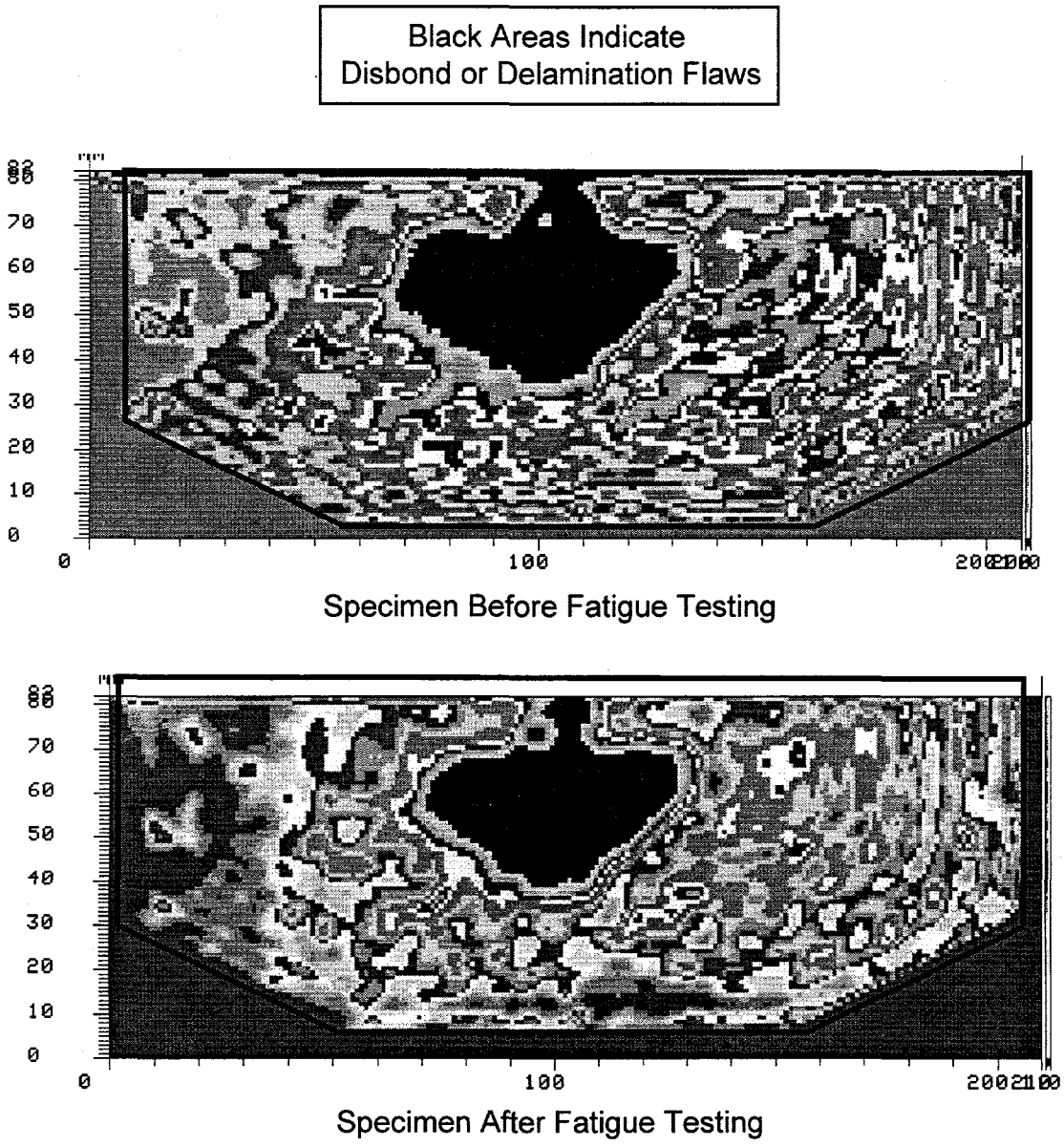

Figure 34: Fatigue Specimen Lock13 (Configuration BE-8) Flaw Profile Before and After 144,000 Fatigue Cycles; No Change in Flaw Profile After Four L-1011 Fatigue Lifetimes

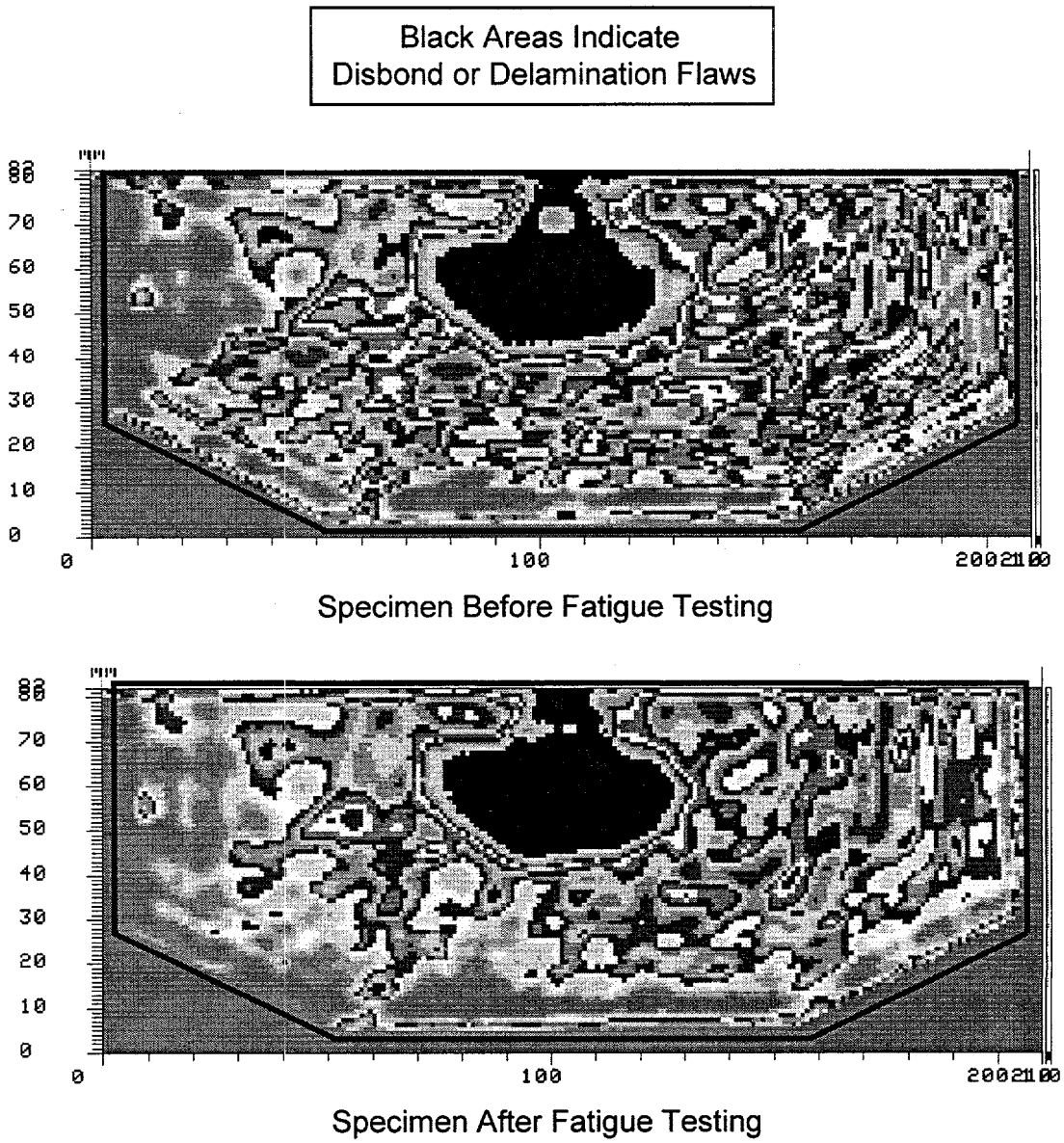

Figure 35: Fatigue Specimen Lock14 (Configuration BE-8) Flaw Profile Before and After 180,000 Fatigue Cycles; No Change in Flaw Profile After Five L-1011 Fatigue Lifetimes

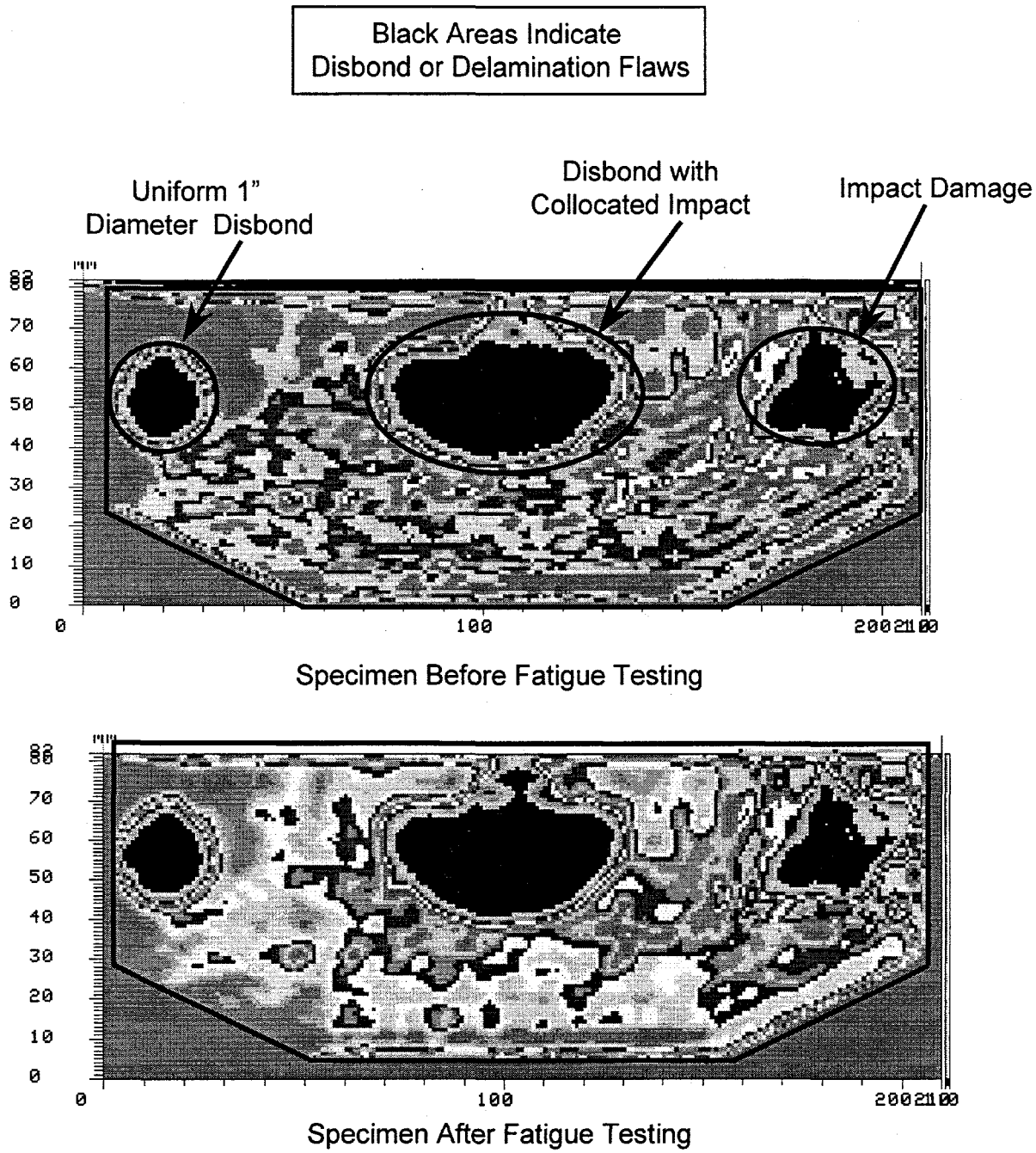

Figure 36: Fatigue Specimen Lock19 (Configuration BE-9) Flaw Profile Before and After 144,000 Fatigue Cycles; No Change in Flaw Profile After Four L-1011 Fatigue Lifetimes

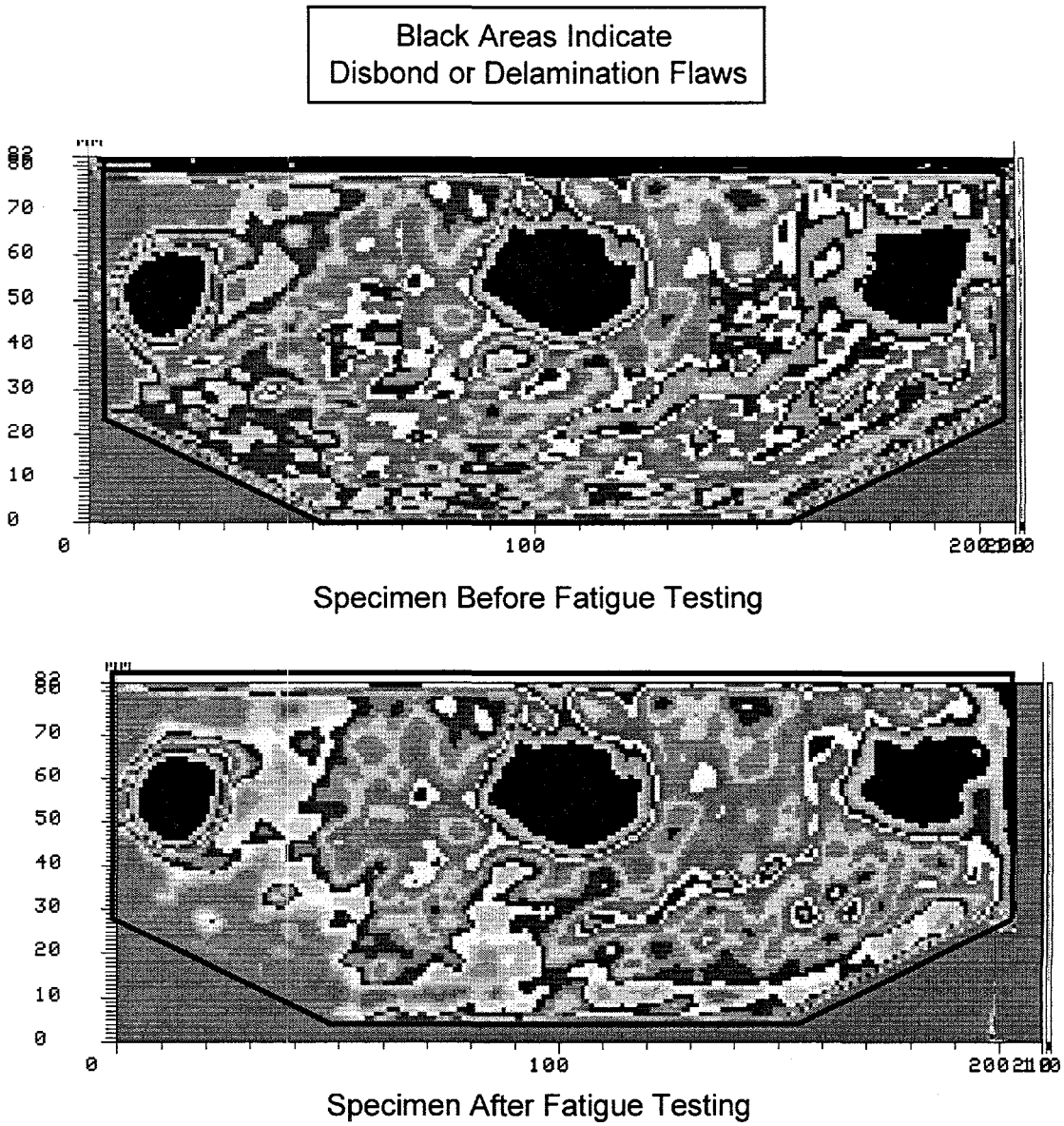

Figure 37: Fatigue Specimen Lock20 (Configuration BE-9) Flaw Profile Before and After 108,000 Fatigue Cycles; No Change in Flaw Profile After Three L-1011 Fatigue Lifetimes

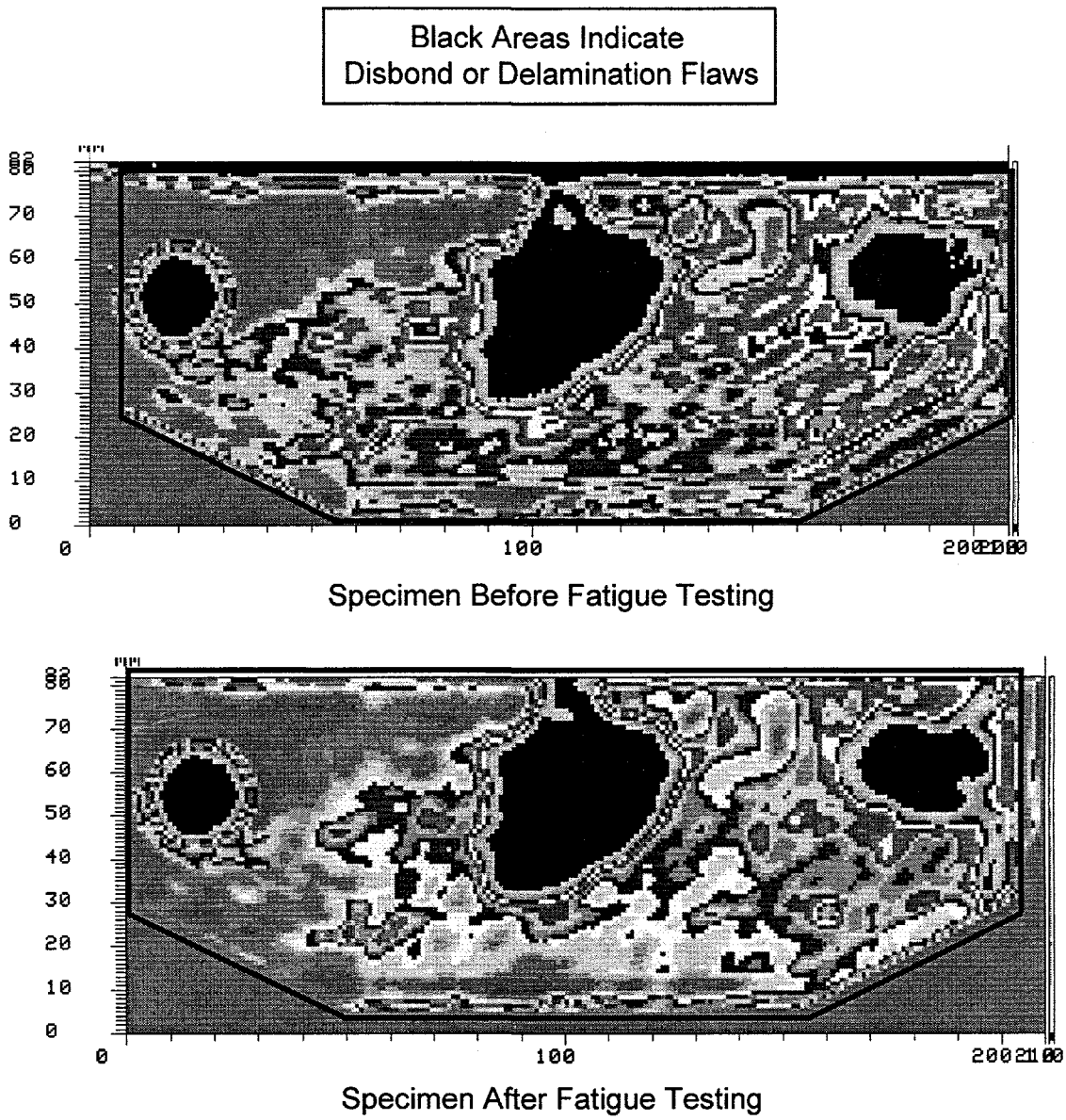

Figure 38: Fatigue Specimen Lock21 (Configuration BE-9) Flaw Profile Before and After 144,000 Fatigue Cycles; No Change in Flaw Profile After Four L-1011 Fatigue Lifetimes

3.1.7 Comments on Fatigue Loading Spectrum and Conservatism of Results

The fatigue tests were conducted using a 3 ksi to 20 ksi sinusoidal load spectrum. The 3 ksi pre-load was intended to eliminate the residual curvature in the test specimens caused by the different coefficients of thermal expansion between the aluminum and boron-epoxy material. However, the pre-load was not able to completely eliminate all of the specimen curvature. As a result, there were bending loads introduced into the tension fatigue tests. The accompanying stress reversals produced a slight amount of "oilcanning" which is not commonly found in aircraft structures. Thus, the fatigue load spectrum exceeded the normal fuselage pressure stresses and the performance values sited here should be conservative. In addition, high strain rates and strain holds were incorporated into the fatigue tests. Since these load characteristics have been shown to be detrimental to a bonded doubler's performance [24], the damage tolerance test results presented here are also conservative from a fatigue implementation standpoint.

3.2 Strain Field Measurements

Figures 16-24 show the strain gage layouts that were used to monitor: 1) the load transfer into the composite doublers and, 2) the strain field throughout the composite laminate and aluminum plate. The stress, strain, and load transfer values presented in this section quantify the doubler performance characteristics discussed above. They provide additional insights into the doubler's ability to: 1) resist crack initiation or mitigate crack growth, and 2) perform acceptably in spite of worst-case installations.

In general, it was observed that all strain responses from the simulated fuselage pressurization loads were linear. No residual strains were noted when the specimens were unloaded. Subsequent failure tests (see Section 3.3 and 3.4 below) showed that the strains induced by the fatigue load spectrum were well inside the linear elastic regime for the 2024-T3 aluminum and Boron-Epoxy composite materials.

The maximum doubler strains were found in the load transfer region around the perimeter (taper region) of the doubler. In all fatigue specimens, the strains monitored in this area were approximately 50% of the total strain in the aluminum plate. This value remained constant over four fatigue lifetimes indicating that there was no deterioration in the bond strength. The strain in the aluminum plate beneath the doubler is reduced in accordance with the strain picked up by the composite doubler. Despite large disbonds which affected approximately 1/3 of the critical load transfer region, the composite doublers maintained acceptable strain fields in the doubler and aluminum material. Furthermore, the doublers were able to pick up the strains necessary to accomplishing their intended purpose of strain reduction and crack mitigation in the parent structure. This performance was achieved in spite of collocated flaw scenarios such as impact and disbond flaws which had been hot, wet conditioned (water absorption/ingress). Note also that these flaws were directly over the cracks which the doublers were intended to arrest.

3.2.1 Strain Field Analysis

A summary of the strain fields in the fatigue test coupons can be seen in the series of curves shown in Figures 39-54. The complete set of strain gage readings for all specimens is tabulated in Appendix B. The maximum total axial strain in the aluminum plate (away from the doubler) was always around 3000 με (for test load P=7,300 lbs.). Axial strains in the aluminum plate beneath the doubler were approximately 50% to 70% of this maximum value while axial strains in the composite doubler ranged from 30% to 50% of the total strain in the specimen. Recall that the axial strains represent the hoop strains in an actual aircraft. The lateral strains in each of the specimens were produced by the Poisson effect and agreed well with the theoretical relation:

$$\varepsilon_a = - (\nu \, X \, \varepsilon_l) \qquad (12)$$

where ν is Poisson's ratio, ε_a represents axial strain and ε_l represents lateral strain. Following is a summary of observations regarding the coupon strain fields from the nine configurations (BE-1 through BE-9) tested.

a. Configuration BE-1 (Specimen Lock1; ref. Fig. 16 for gage locations) - axial strains are shown in Fig. 39; lateral strains are shown in Fig. 40. Strain reduction in aluminum plate (Channels 8 and 12) and the corresponding strain shedding into the doubler (Channels 10 and 14) is evident.

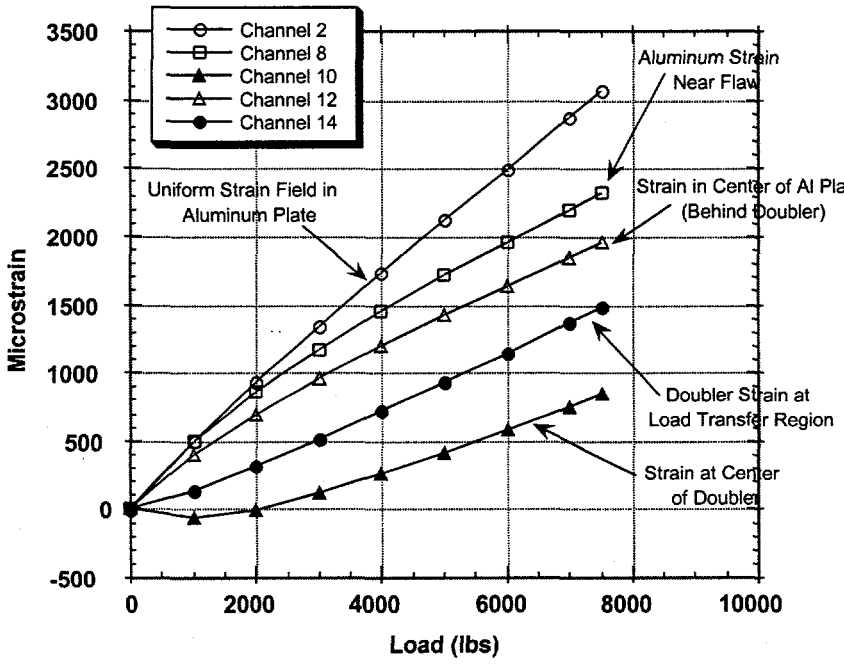

Figure 39: Axial Strain Field in Aluminum and Composite for Configuration BE-1 Specimens (ref. strain gage locations shown in Figure 16)

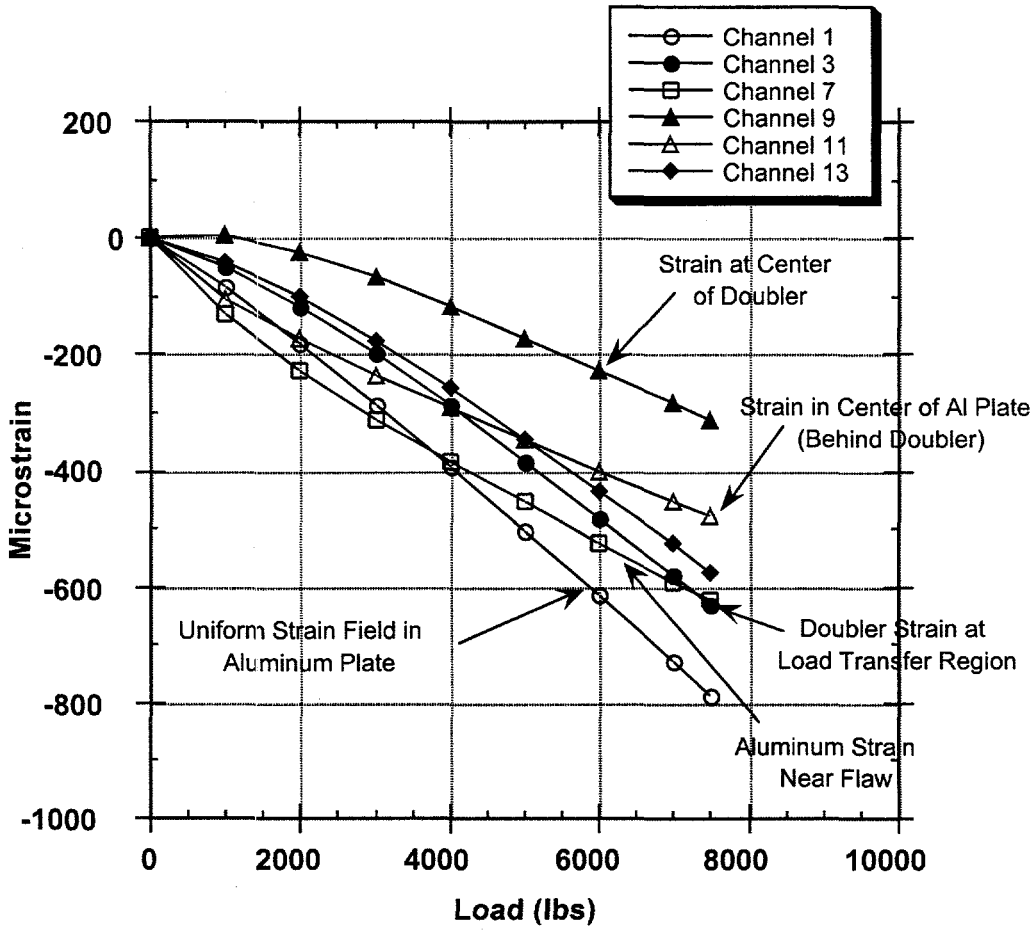

Figure 40: Lateral Strain Field in Aluminum and Composite for Configuration BE-1 Specimens (ref. strain gage locations shown in Figure 16)

b. Configuration BE-2 (Specimen Lock 2; ref. Fig. 17 for gage locations) - axial strains are shown in Fig. 41; lateral strains are shown in Fig. 42. The load transfer is similar at the upper and lower taper regions (compare Ch. 18 and Ch. 30). The strain relief created by disbonds is evidenced by the low strains in Ch. 20 and 32. The large strains in gages immediately adjacent to the disbond (Ch. 18 and Ch. 30) demonstrate that the disbond effects are very localized. The doubler does not create excessive strain risers in the unreinforced aluminum immediately adjacent to the doubler (Ch. 92).

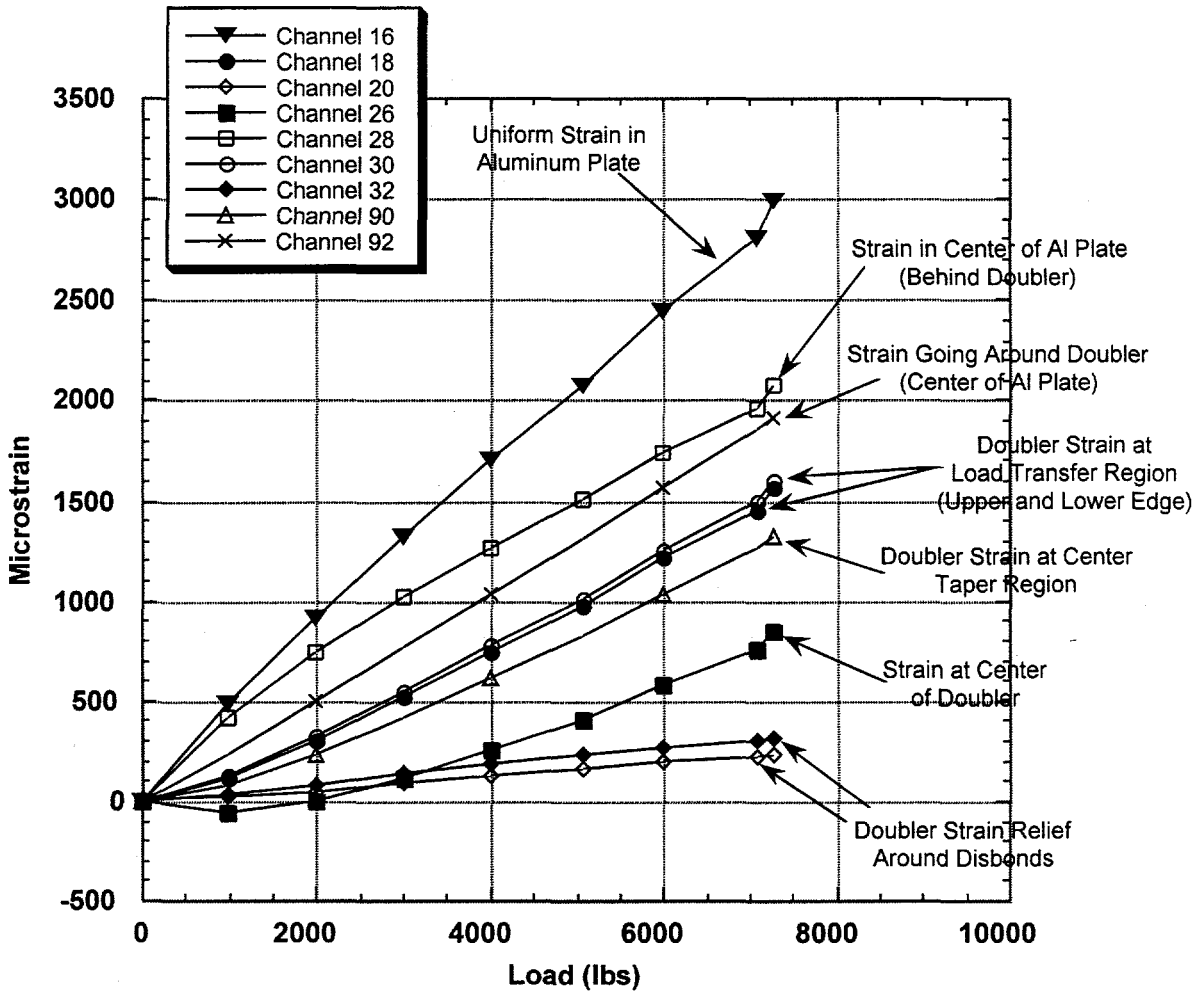

Figure 41: Axial Strain Field in Aluminum and Composite for Configuration BE-2 Specimens (ref. strain gage locations shown in Figure 17)

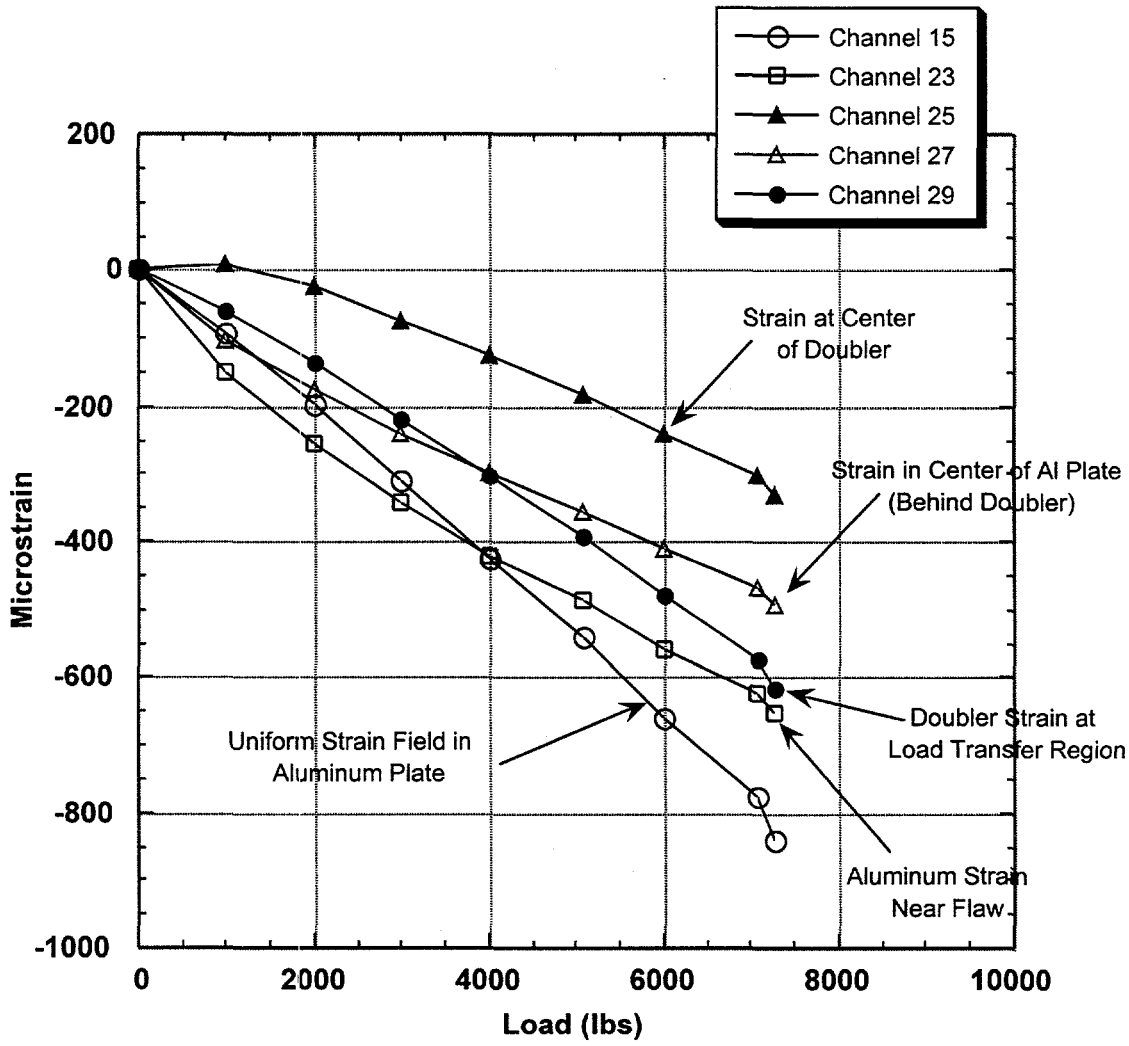

Figure 42: Lateral Strain Field in Aluminum and Composite for Configuration BE-2 Specimens (ref. strain gage locations shown in Figure 17)

c. Configuration BE-3 (Specimen Lock3; ref. Fig. 18 for gage locations) - axial strains are shown in Fig. 43; lateral strains are shown in Fig. 44. The strain fields and insights are similar to the BE-1 and BE-2 results.

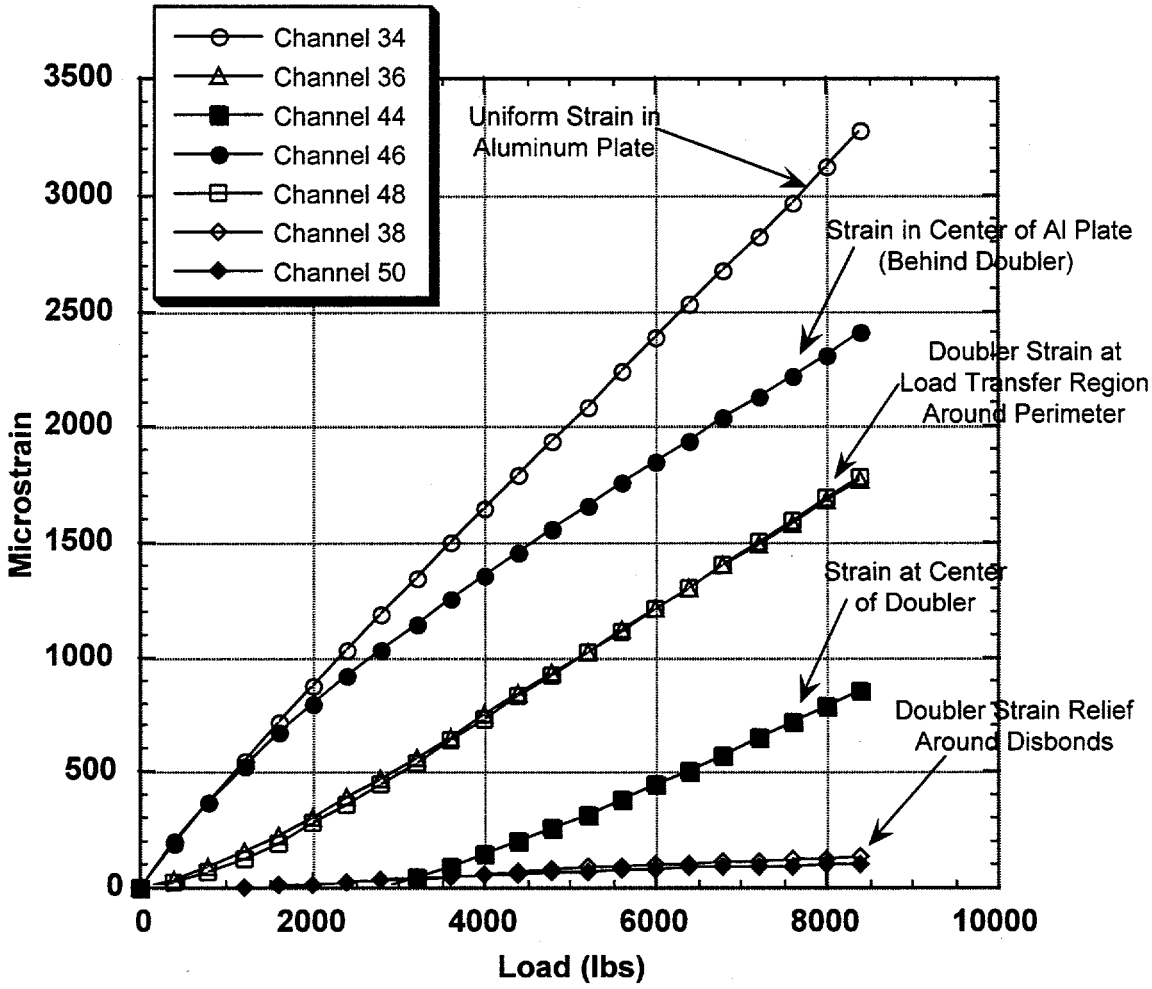

Figure 43: Axial Strain Field in Aluminum and Composite for Configuration BE-3 Specimens (ref. strain gage locations shown in Figure 18)

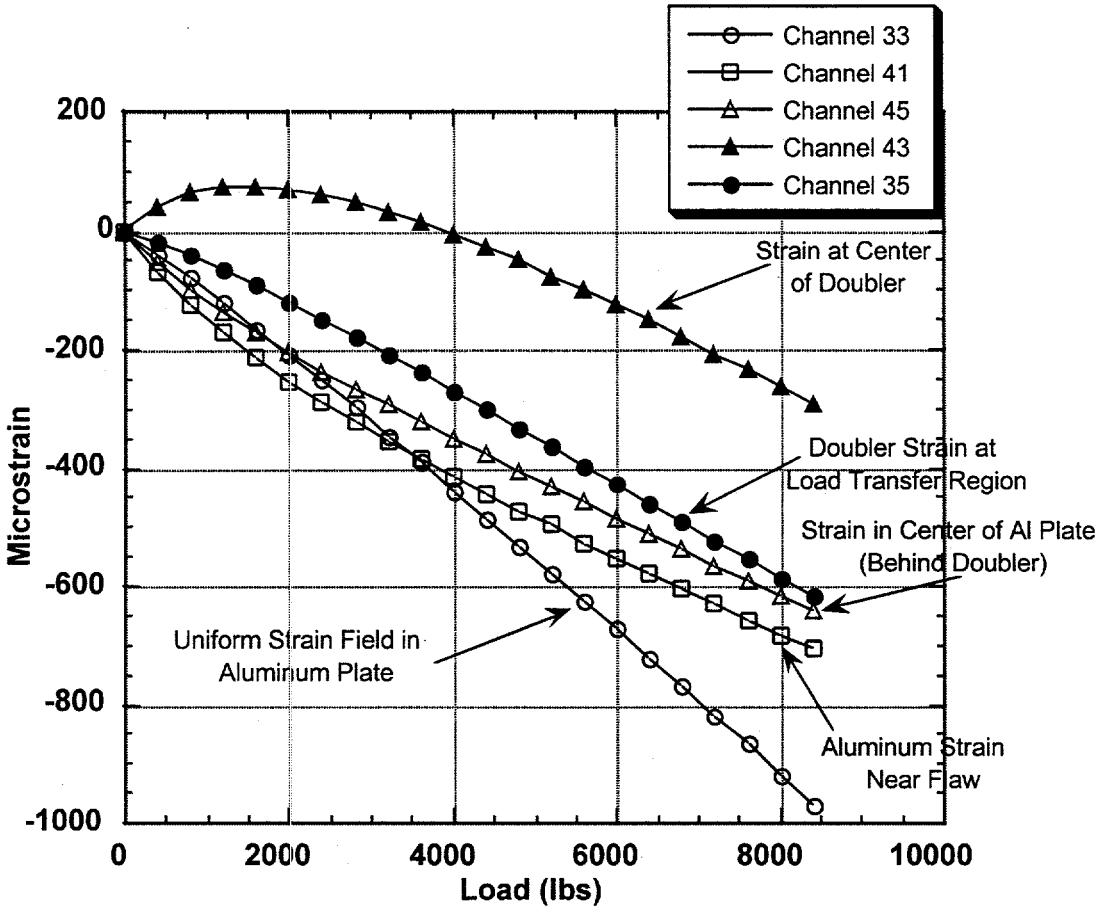

Figure 44: Lateral Strain Field in Aluminum and Composite for Configuration BE-3 Specimens (ref. strain gage locations shown in Figure 18)

d. Configuration BE-4 (Specimen Lock4; ref. Fig. 19 for gage locations) - axial strains are shown in Fig. 45; lateral strains are shown in Fig. 46. The strain fields and insights are similar to the BE-1 and BE-2 results.

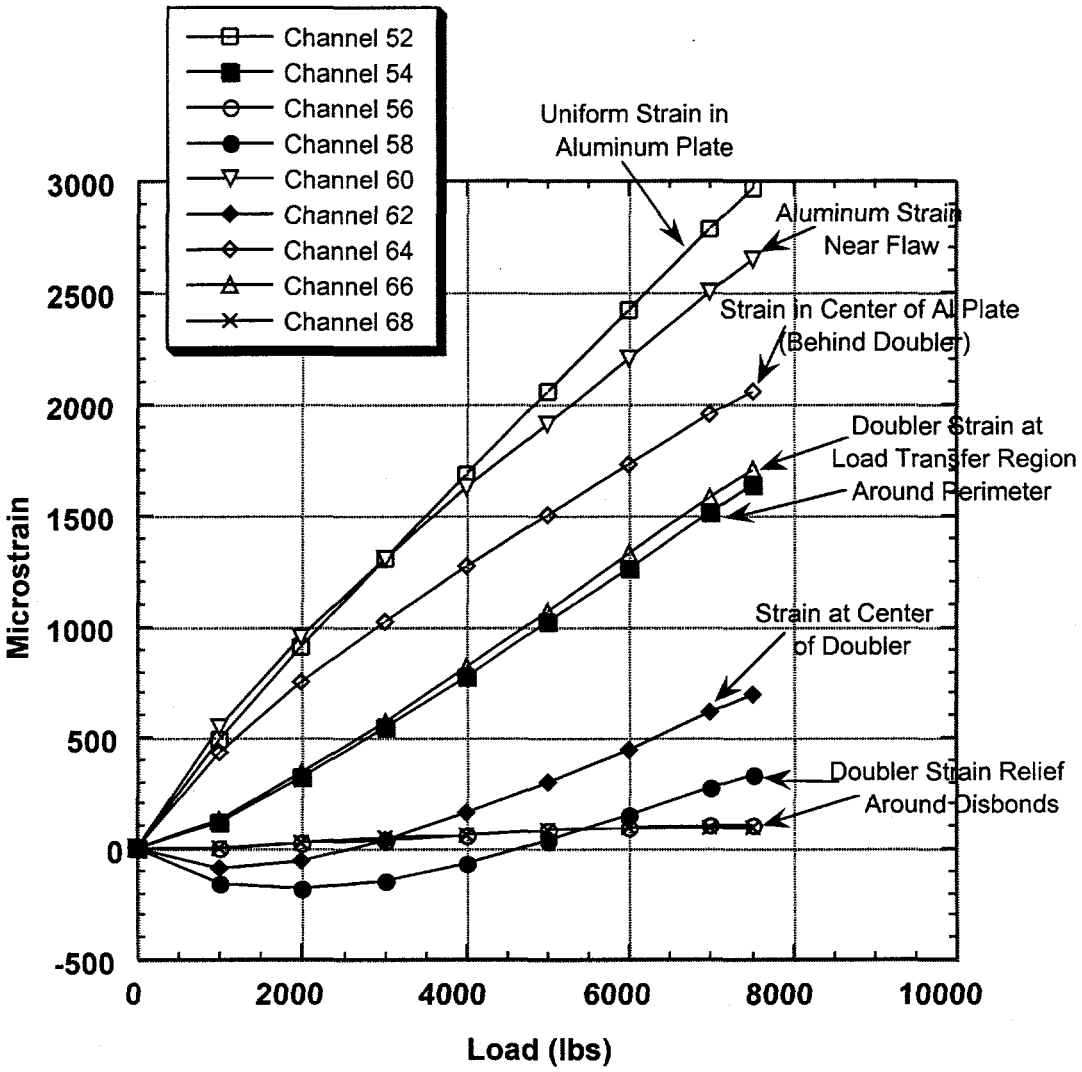

Figure 45: Axial Strain Field in Aluminum and Composite for Configuration BE-4 Specimens (ref. strain gage locations shown in Figure 19)

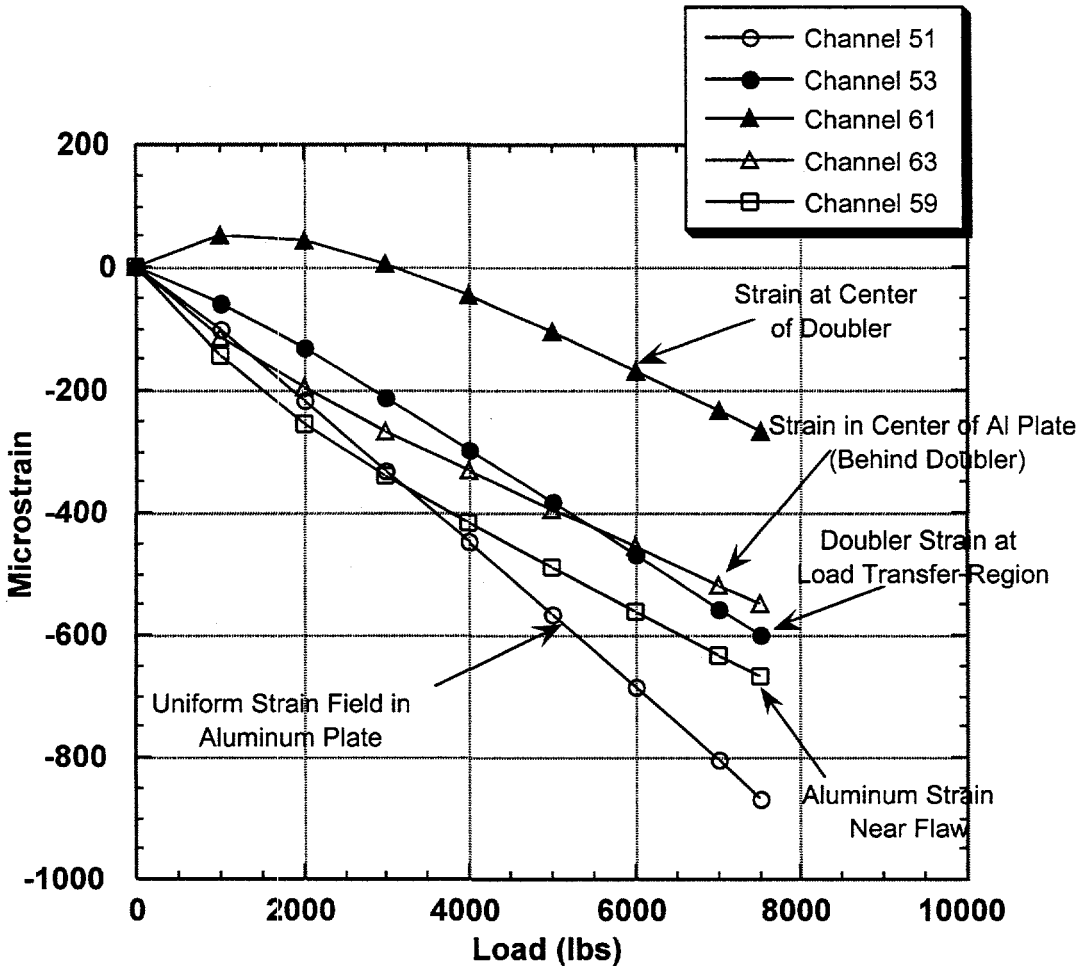

Figure 46: Lateral Strain Field in Aluminum and Composite for Configuration BE-4 Specimens (ref. strain gage locations shown in Figure 19)

e. Configuration BE-5 (Specimen Lock5; ref. Fig. 20 for gage locations) - axial strains are shown in Fig. 47; lateral strains are shown in Fig. 48. The strain fields and insights are similar to the BE-1 and BE-2 results. Note that strain risers around unreinforced holes are generally on the order of three times the uniform strain field away from the hole. Channel 78 shows that the strains at the aluminum cut-out are reduced substantially by the doubler. Rather than exhibiting the normal strain intensification (i.e. 6,000 με = 2 X 3,000 με in uniform field), the strains are reduced below those of the gage outside the doubler area (2,250 με).

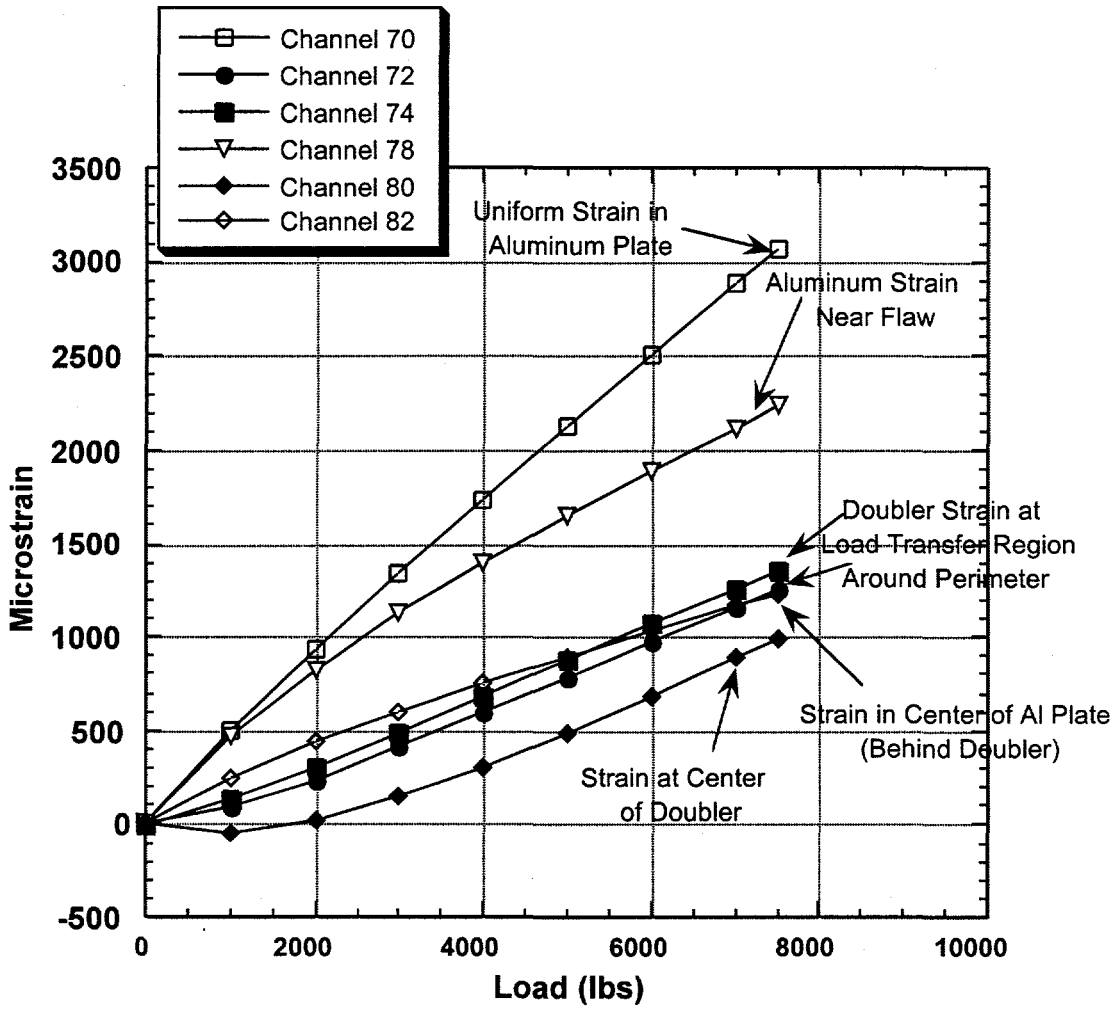

Figure 47: Axial Strain Field in Aluminum and Composite for Configuration BE-5 Specimens (ref. strain gage locations shown in Figure 20)

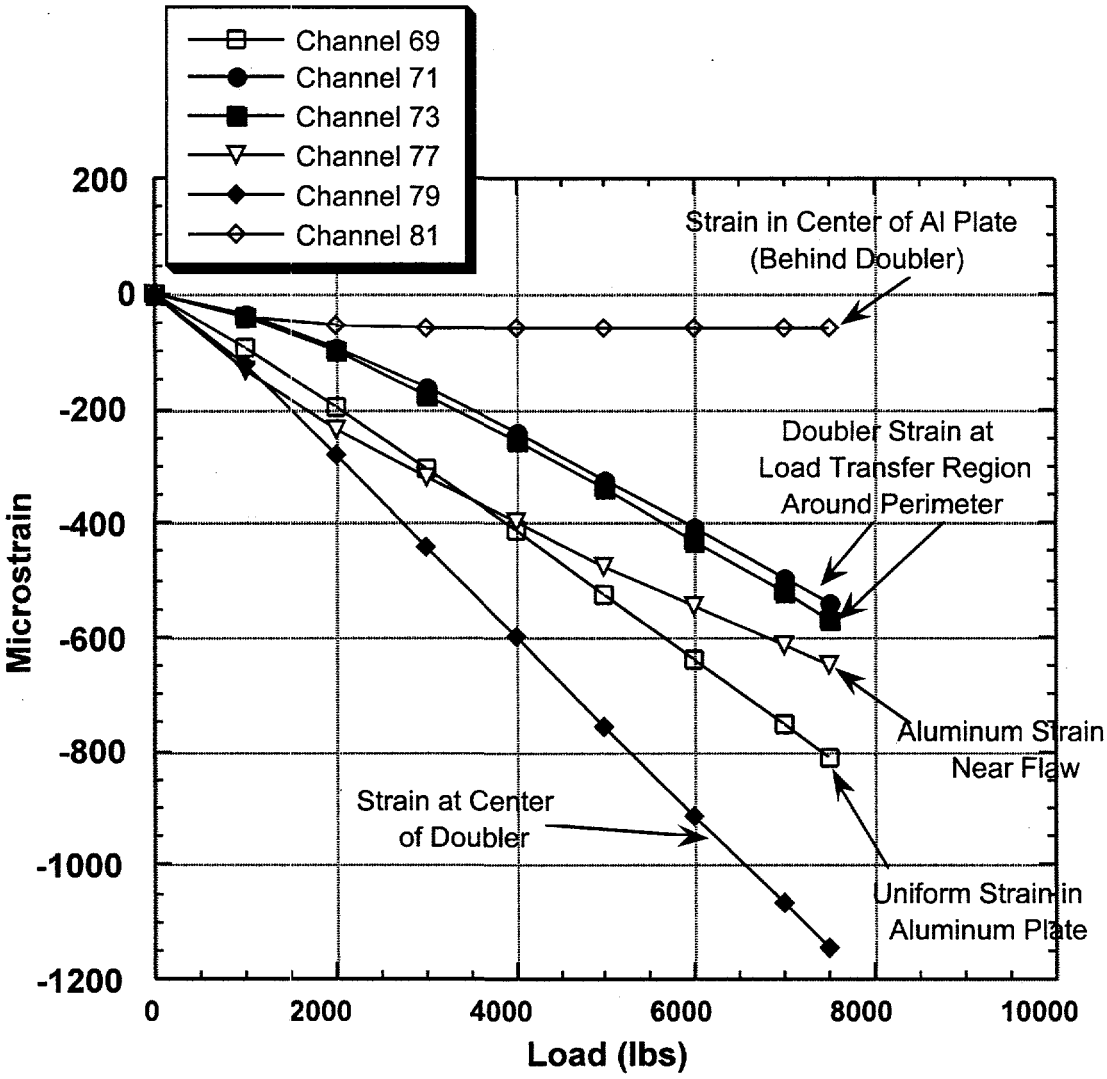

Figure 48: Lateral Strain Field in Aluminum and Composite for Configuration BE-5 Specimens (ref. strain gage locations shown in Figure 20)

f. Configuration BE-6 (Specimen Lock6; ref. Fig. 21 for gage locations) - axial strains are shown in Fig. 49. Strain fields in an aluminum plate without a doubler are in the 2,500 με to 3,500 με range (Ch. 94 and Ch. 96).

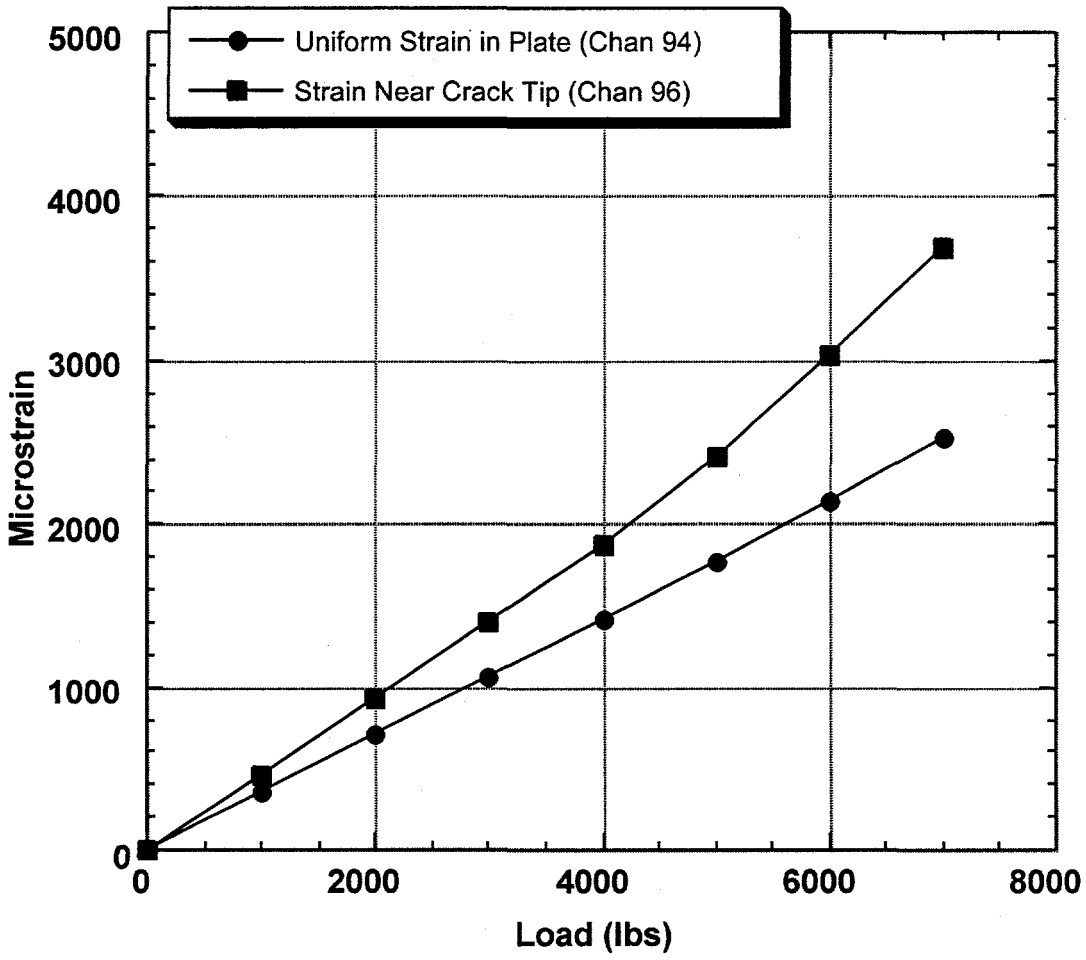

Figure 49: Axial Strain Field in Aluminum and Composite for Configuration BE-6 Specimens (ref. strain gage locations shown in Figure 21)

g. Configuration BE-8 (Specimen Lock14; ref. Fig. 23 for gage locations) - axial strains are shown in Fig. 50. The strain fields and insights are similar to the BE-1 through BE-5 results. The addition of impact damage to the center disbond did not degrade the doubler's ability to absorb a significant portion of the total strain in this region. Figures 29 and 30 show the typical flaw induced in configuration BE-8 specimens. However, channel 124 in Fig. 50 still indicates a 50% load transfer in the flaw area.

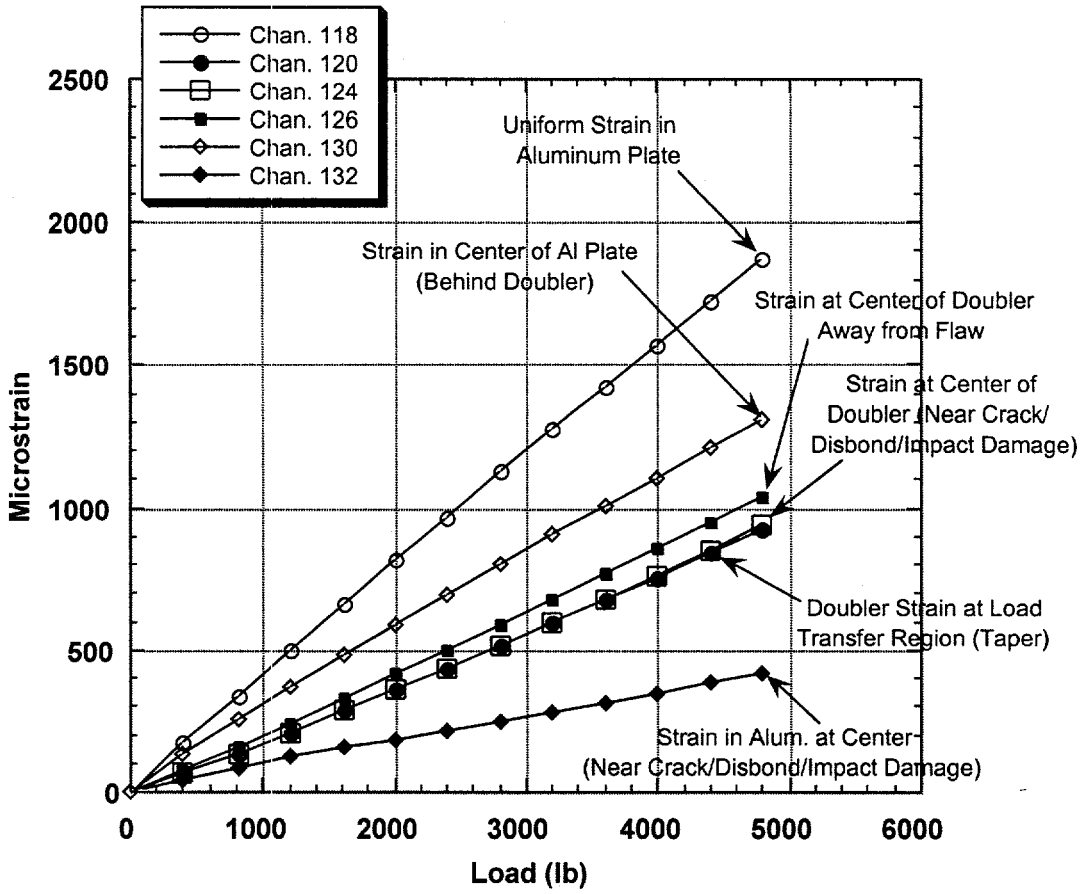

Figure 50: Axial Strain Field in Aluminum and Composite for Configuration BE-8 Specimens (ref. strain gage locations shown in Figure 23)

h. Configuration BE-9 (Specimen Lock20; ref. Fig. 24 for gage locations) - axial strains are shown in Fig. 51; lateral strains are shown in Fig. 52. The strain fields and insights are similar to the BE-1 through BE-5 results. Configuration BE-9 contains three separate disbond and/or impact areas as shown in Figures 36-38. The central impact/disbond area, as in configuration BE-8, achieved a load transfer of almost 50%. The impact damage at the tapered load transfer area (ref. Fig. 27) produced a local strain riser shown by channel 144. Thus, in spite of large plastic deformations in the parent skin and associated disbonds, the doubler is still able to carry significant strains. Large strains immediately adjacent to the lower disbond (Ch. 136) reiterate the fact that relatively large disbond or delamination flaws (up to 1" diameter) in the composite doubler have only localized effects on strain. Overall, the three disbonds in configuration BE-9 appear to have minimal effect on the doubler's ability to transfer load and relieve the parent aluminum plate.

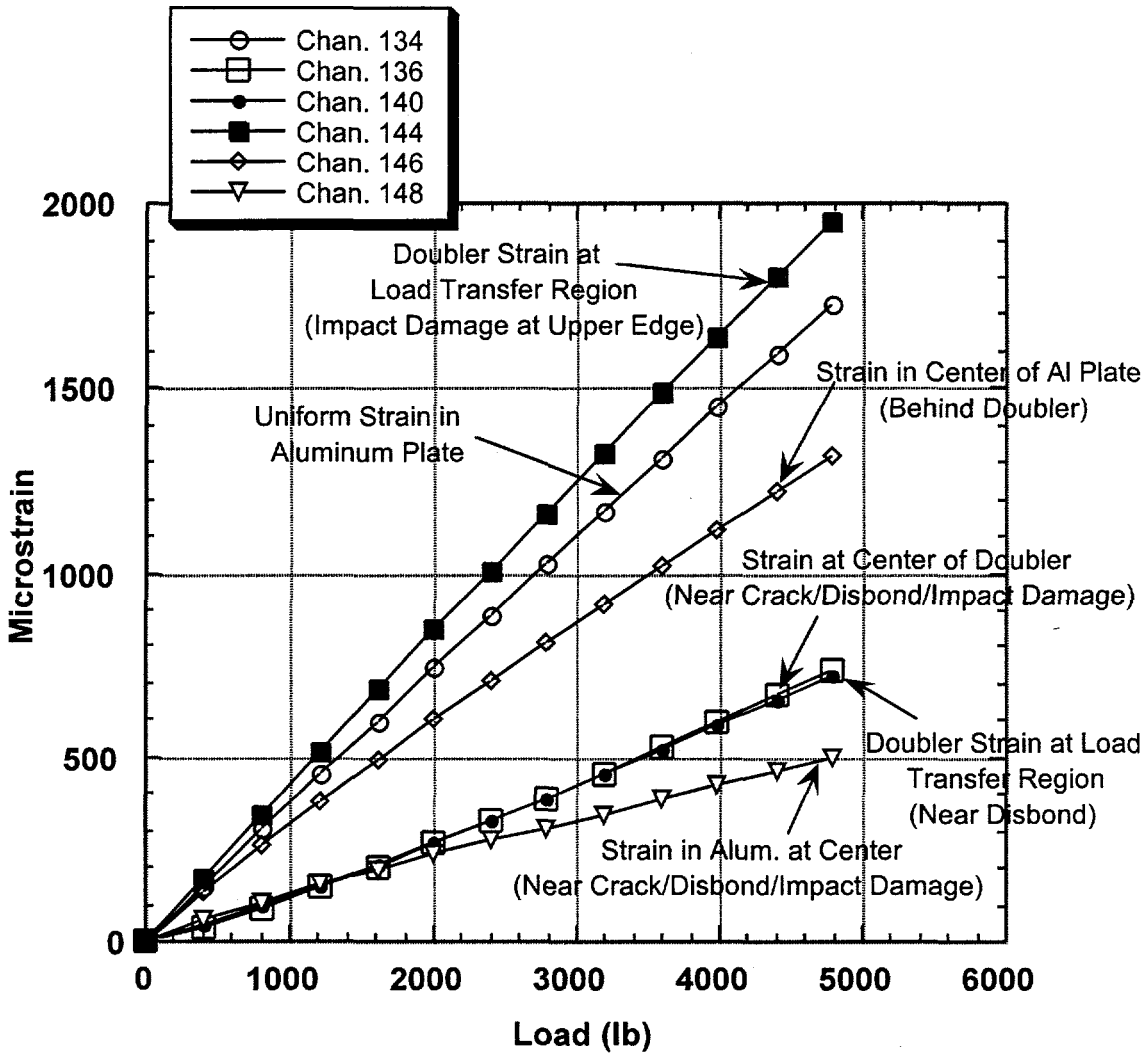

Figure 51: Axial Strain Field in Aluminum and Composite for Configuration BE-9 Specimens (ref. strain gage locations shown in Figure 24)

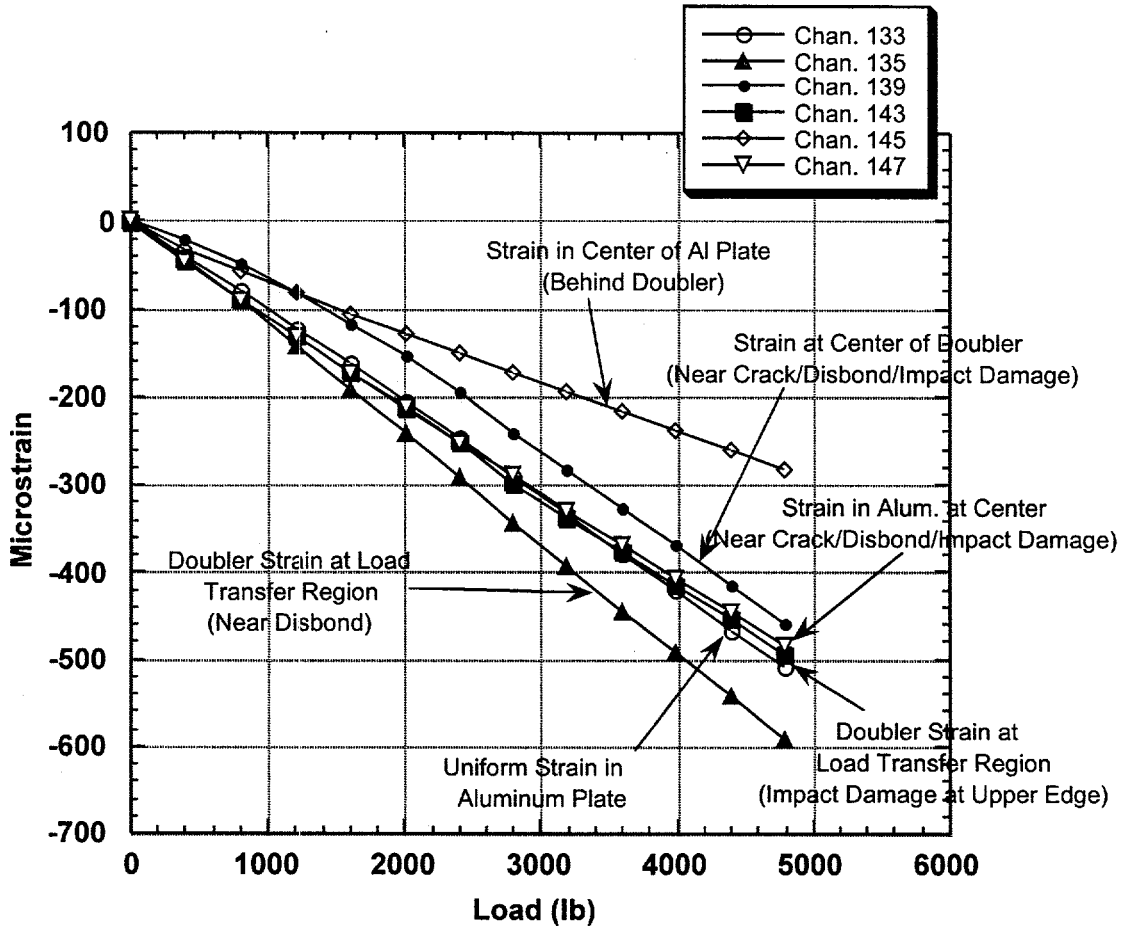

Figure 52: Lateral Strain Field in Aluminum and Composite for Configuration BE-9 Specimens (ref. strain gage locations shown in Figure 24)

i. Configuration BE-7 (Specimen Lock9; ref. Fig. 22 for gage locations) - axial strains are shown in Fig. 53; lateral strains are shown in Fig. 54. The strain fields and insights are similar to the BE-1 through BE-9 results.

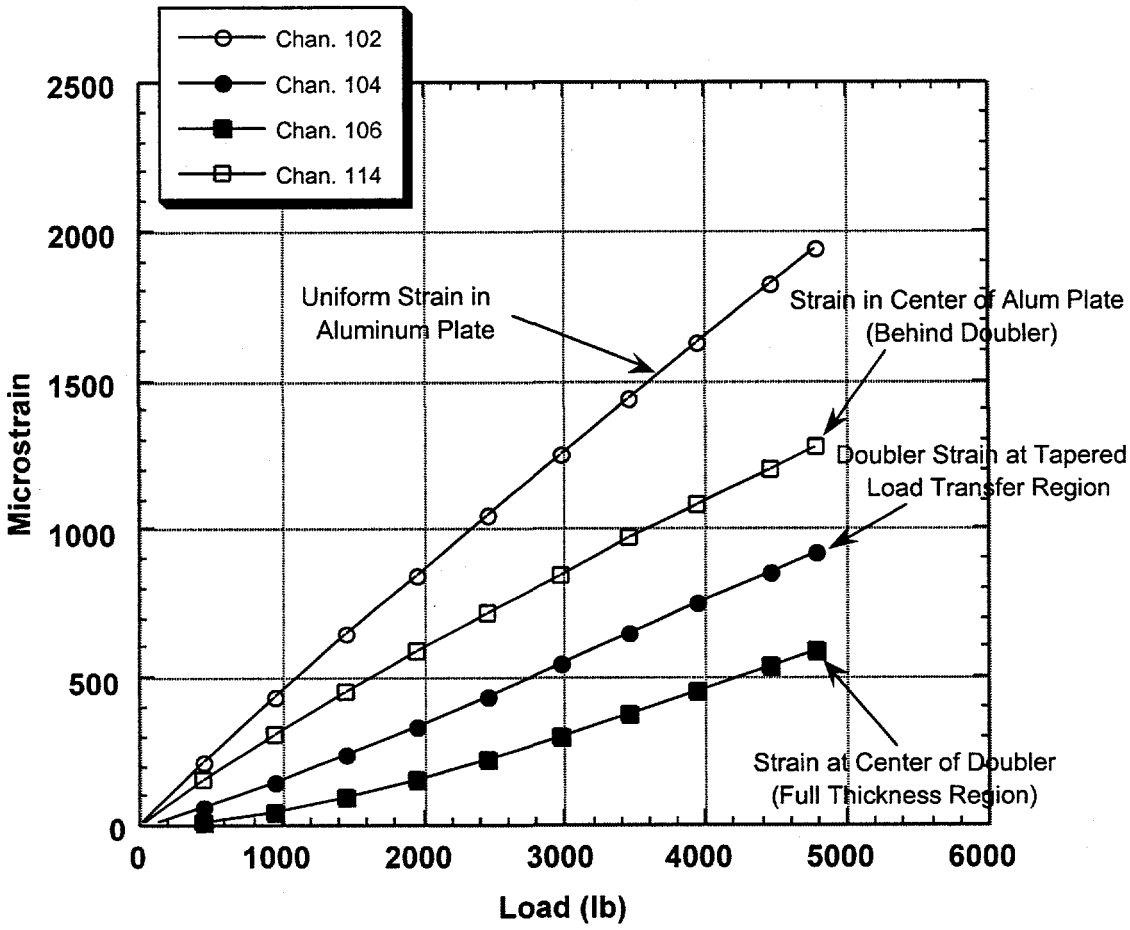

Figure 53: Axial Strain Field in Aluminum and Composite for Configuration BE-7 Specimens (ref. strain gage locations shown in Figure 22)

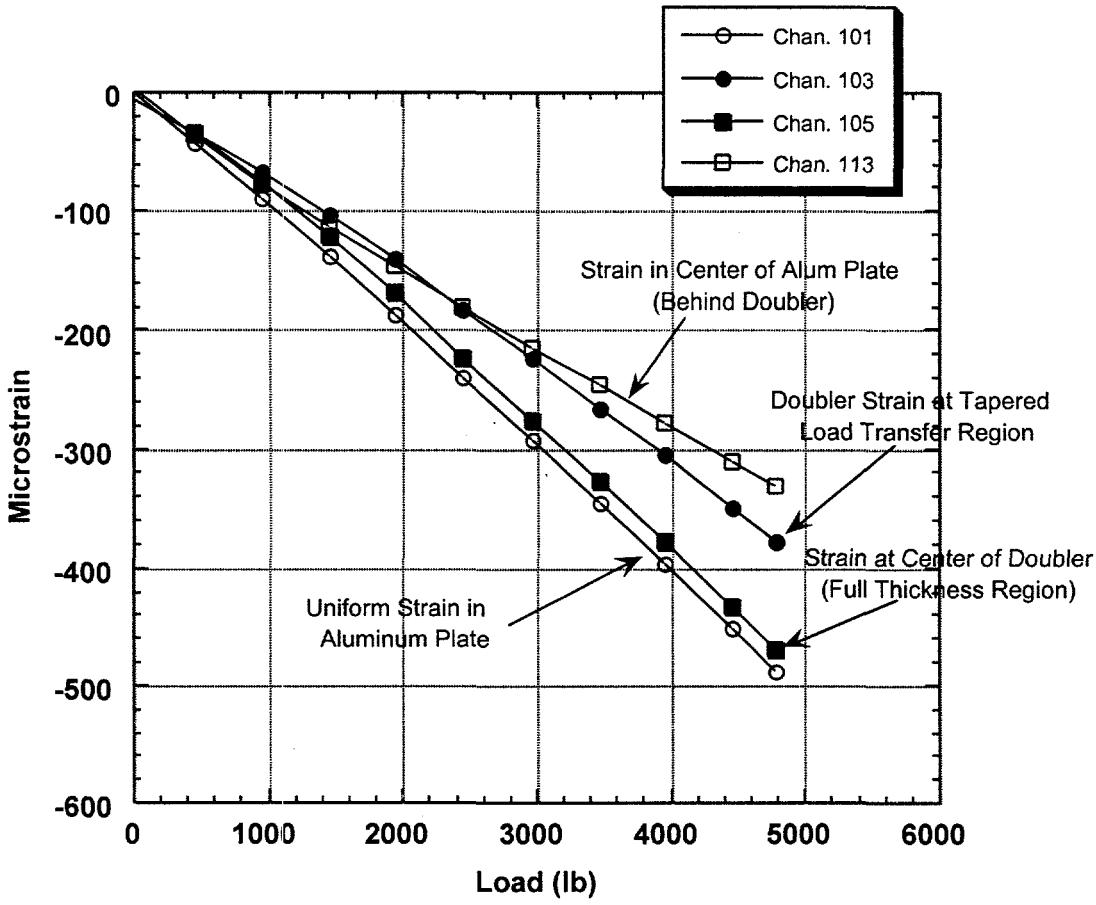

Figure 54: Lateral Strain Field in Aluminum and Composite for Configuration BE-7 Specimens (ref. strain gage locations shown in Figure 22)

The similarity in strain fields between BE-7, which is unflawed, and BE-1 through BE-9, which have crack, disbond and impact flaws along with any detriment brought on by water absorption, indicates that the relatively large flaws produce only a localized effects on the doubler strains and little effect on the overall performance of the doubler. Section 3.1 described how the flawed specimens (BE-1, BE-2, BE-3, BE-4, BE-5, BE-8, and BE-9 configurations) were able to mitigate crack growth in aluminum for up to five L-1011 lifetimes (180,000 cycles).

3.2.2 Stresses in Aluminum Plate and Composite Doubler

To provide a point of reference for any Boron-Epoxy doubler installation, various stresses sustained by the fatigue test specimens are listed in Table 4. Strain data collected from the biaxial (axial and lateral) gages were used to calculate stresses in the composite

doubler and parent aluminum skin. Strains measured from these gages were used to calculate the corresponding membrane stresses through the following equations:

$$\sigma_a = \frac{E}{1-\nu^2}(\varepsilon_a + \nu\varepsilon_l) \tag{13}$$

$$\sigma_l = \frac{E}{1-\nu^2}(\varepsilon_l + \nu\varepsilon_a) \tag{14}$$

where E is the modulus of elasticity, ν is Poisson's ratio, σ_a is the axial stress in the skin, σ_l is the longitudinal stress in the skin, ε_a is the hoop strain, and ε_l is the longitudinal strain. From Mil-Handbook 5, the modulus of elasticity and Poisson's ratio for 2024-T3 aluminum are: E =10.5 X 10^6 psi and ν =0.33, respectively. As stated in Section 2.3.5, the properties of the Boron-Epoxy laminate are E_x = 11.87 X 10^6 psi and ν = 0.32.

Table 4 shows that uniform stresses of 17 ksi, representing maximum hoop stresses during flight pressurization, or higher were achieved in the parent skin for each specimen configuration. Away from the fatigue crack, the maximum stresses in the aluminum beneath the doubler were roughly one-third the yield stress for 2024-T3. The maximum stresses in the composite doublers occurred at the edge of the doubler (load transfer region) and never exceeded 10 ksi. Stress risers near fatigue cracks, which normally amount to two or three times the uniform strain field away from the flaw, were essentially eliminated by the composite doubler. The maximum aluminum stresses immediately adjacent to the fatigue cracks were less than, or in two cases approximately equal to, the uniform stress field outside the doubler. A comparison of the stresses at zero and after 100,000 to 180,000 fatigue cycles shows that the doublers picked up additional stresses when the fatigue crack growth reduced the load carrying capacity of the parent aluminum (i.e. stress relief occurred in aluminum).

3.2.3 Load Transfer

Plots of percent load transfer were obtained by calculating the ratio between doubler strains and strains in corresponding portions of the aluminum parent skin. Figures 55 - 62 show the resulting load transfer plots for various doubler and aluminum reference channels $\{\varepsilon_{doubler} / \varepsilon_{alum(ref)}\}$. *The curves indicate that the load transfer into the doubler - and away from the aluminum - was similar in all fatigue specimens regardless of the type and degree of damage in the specimen. In the tapered portion of the doubler, the load transfer was consistently in the 50 - 60 % range. In the center, where the doubler reaches its maximum thickness of 13 plies, the load transfer was in the 30 - 50% range.* Table 5 summarizes the load transfer results at maximum load (max fuselage pressurization). The spectrum of fatigue specimens ranged from unflawed (optimum

consistency of load transfer values across the full spectrum of specimens despite the large variations in flaw scenarios. Furthermore, these load transfer values remained constant over four fatigue lifetimes. This indicates that there was no deterioration in the bond strength.

Spec. No. (Config.)	Biaxial Channels	Peak Load (lbs) *	Stress at Zero Cycles (psi)	Stress After Fatigue (psi)	No. of Cycles	Location on Test Specimen
Lock1 (BE-1)	1, 2	5,000	23,010	22,450	144,000	Aluminum Away from Doubler
	5, 6	5,000	3,520	14,350	144,000	Doubler Near Flaw
	7, 8	5,000	18,410	No Data	144,000	Aluminum Near Flaw
	9, 10	5,000	4,700	9,510	144,000	Doubler Center (full thickness)
	11, 12	5,000	15,359	1,100	144,000	Aluminum Center Beneath Doubler
	13,14	5,000	13,340	10,420	144,000	Doubler Edge (upper taper region)
Lock2 (BE-2)	15, 16	6,000	26,200	26,562	144,000	Aluminum Away from Doubler
	17, 18	6,000	14,530	10,900	144,000	Doubler Edge (lower taper region)
	21, 22	6,000	2,270	5,180	144,000	Doubler Near Flaw
	23, 24	6,000	25,070	2,510	144,000	Aluminum Near Flaw
	25, 26	6,000	6,660	4,180	144,000	Doubler Center (full thickness)
	27, 28	6,000	18,840	19,000	144,000	Aluminum Center Beneath Doubler
Lock3 (BE-3)	33, 34	4,800	20,780	20,150	144,000	Aluminum Away from Doubler
	35, 36	4,800	10,859	10,875	144,000	Doubler Edge (lower taper region)
	39, 40	4,800	-47	6,030	144,000	Doubler Near Flaw
	41, 42	4,800	23,280	22	144,000	Aluminum Near Flaw
	43, 44	4,800	3,186	5,310	144,000	Doubler Center (full thickness)
	45, 46	4,800	16,760	1,930	144,000	Aluminum Center Beneath Doubler

* Load of 4,800 lbs produces skin stress of 17 ksi - this corresponds to hoop stress at maximum L-1011 fuselage pressure levels.

Table 4: Stresses in Aluminum and Composite Doubler at Maximum Fuselage Pressure Loads

Spec. No. (Config.)	Biaxial Channels	Peak Load (lbs) *	Stress at Zero Cycles (psi)	Stress After Fatigue (psi)	No. of Cycles	Location on Test Specimen
Lock4 (BE-4)	51, 52	5,000	22,048	21,490	144,000	Aluminum Away from Doubler
	53, 54	5,000	11,850	11,380	144,000	Doubler Edge (lower taper region)
	59, 60	5,000	20,670	260	144,000	Aluminum Near Flaw
	61, 62	5,000	3,470	8,450	144,000	Doubler Center (full thickness)
	63, 64	5,000	16,200	700	144,000	Aluminum Center Beneath Doubler
Lock5 (BE-5)	69, 70	5,000	22,930	22,820	144,000	Aluminum Away from Doubler
	73, 74	5,000	10,110	10,010	144,000	Doubler Edge (lower taper region)
	75, 76	5,000	5,450	5,440	144,000	Doubler Near Flaw
	77, 78	5,000	17,580	17,670	144,000	Aluminum Near Flaw
	79, 80	5,000	3,250	3,430	144,000	Doubler Center (full thickness)
	81, 82	5,000	10,300	9,970	144,000	Aluminum Center Beneath Doubler
Lock9 (BE-7)	101,102	4,800	20,940	21,150	144,000	Aluminum Away from Doubler
	103, 104	4,800	10,540	10,730	144,000	Doubler Edge (lower taper region)
	105, 106	4,800	5,790	5,930	144,000	Doubler Center (full thickness)
	113, 114	4,800	13,770	13,880	144,000	Aluminum Center Beneath Doubler

* Load of 4,800 lbs. produces skin stress of 17 ksi - this corresponds to hoop stress at maximum L-1011 fuselage pressure levels

Table 4: Stresses in Aluminum and Composite Doubler at Maximum Fuselage Pressure Loads (continued)

Spec. No. (Config.)	Biaxial Channels	Peak Load (lbs) *	Stress at Zero Cycles (psi)	Stress After Fatigue (psi)	No. of Cycles	Location on Test Specimen
Lock14 (BE-8)	117, 118	4,800	19,810	20,800	180,000	Aluminum Away from Doubler
	119, 120	4,800	9,380	9,520	180,000	Doubler Edge (lower taper region)
	123, 124	4,800	9,840	11,010	180,000	Doubler Near Flaw
	131, 132	4,800	3,180	5,630	180,000	Aluminum Near Flaw
	125, 126	4,800	12,640	14,380	180,000	Doubler Center (full thickness)
	129, 130	4,800	14,270	13,560	180,000	Aluminum Center Beneath Doubler
Lock20 (BE-9)	133, 134	4,800	18,390	18,460	99,000	Aluminum Away from Doubler
	135, 136	4,800	7,240	6,770	99,000	Doubler Edge (lower taper region)
	139, 140	4,800	7,600	8,010	99,000	Doubler Near Flaw
	147, 148	4,800	3,980	7,080	99,000	Aluminum Near Flaw
	141, 142	4,800	8,070	8,850	99,000	Doubler Center (full thickness)
	145, 146	4,800	14,370	14,210	99,000	Aluminum Center Beneath Doubler

* Load of 4,800 lbs. produces skin stress of 17 ksi - this corresponds to hoop stress at maximum L-1011 fuselage pressure levels

Table 4: Stresses in Aluminum and Composite Doubler at Maximum Fuselage Pressure Loads (continued)

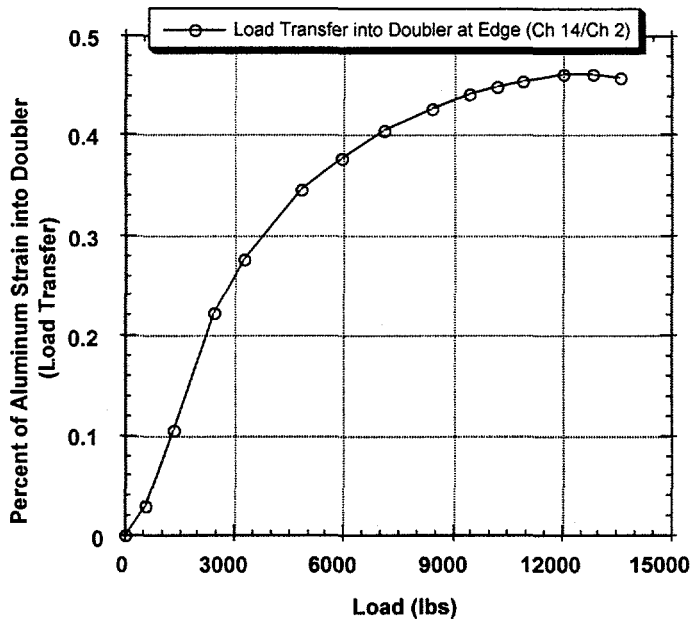

Figure 55: Load Transfer into Doubler for Configuration BE-1

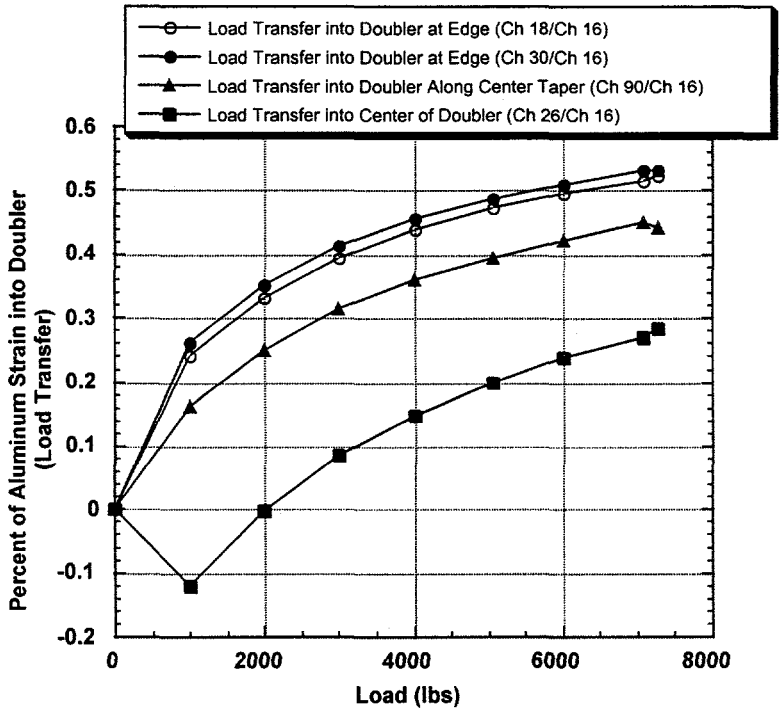

Figure 56: Load Transfer into Doubler for Configuration BE-2

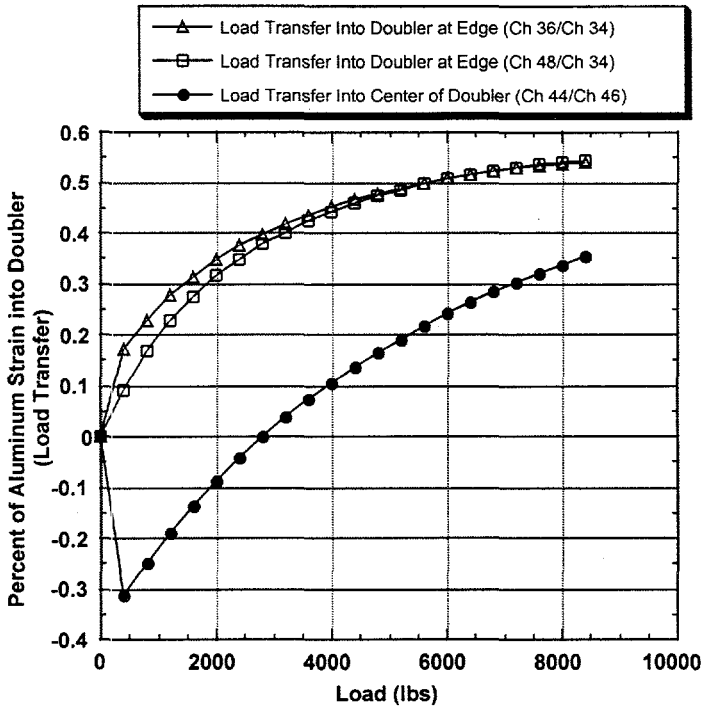

Figure 57: Load Transfer into Doubler for Configuration BE-3

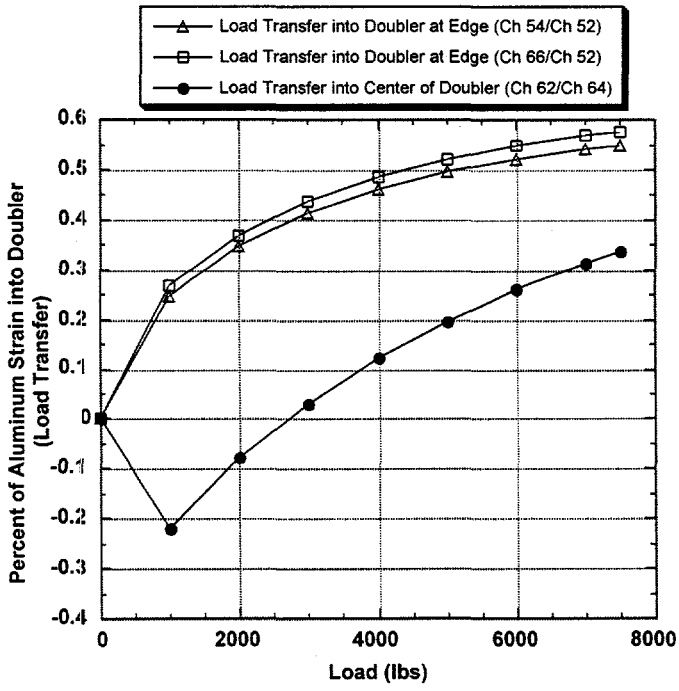

Figure 58: Load Transfer into Doubler for Configuration BE-4

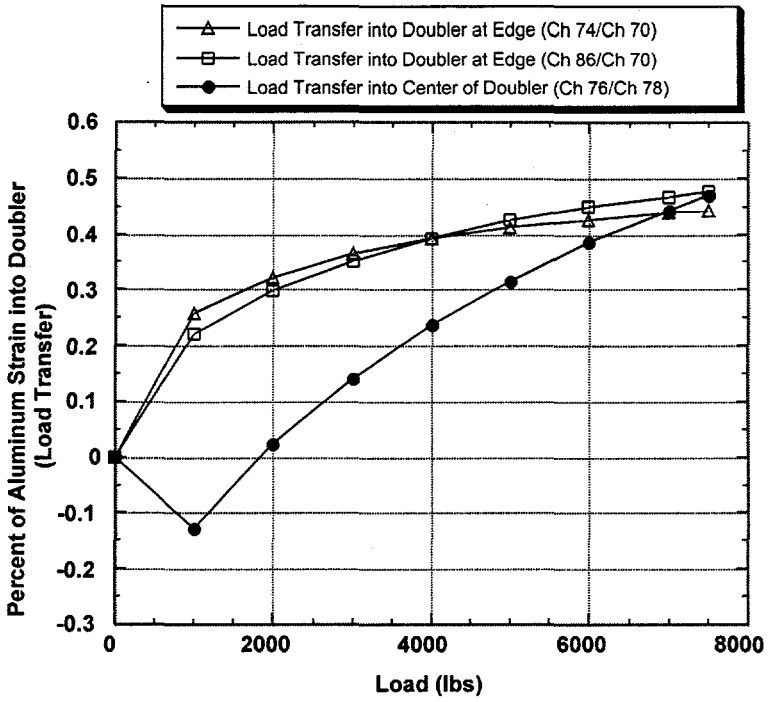

Figure 59: Load Transfer into Doubler for Configuration BE-5

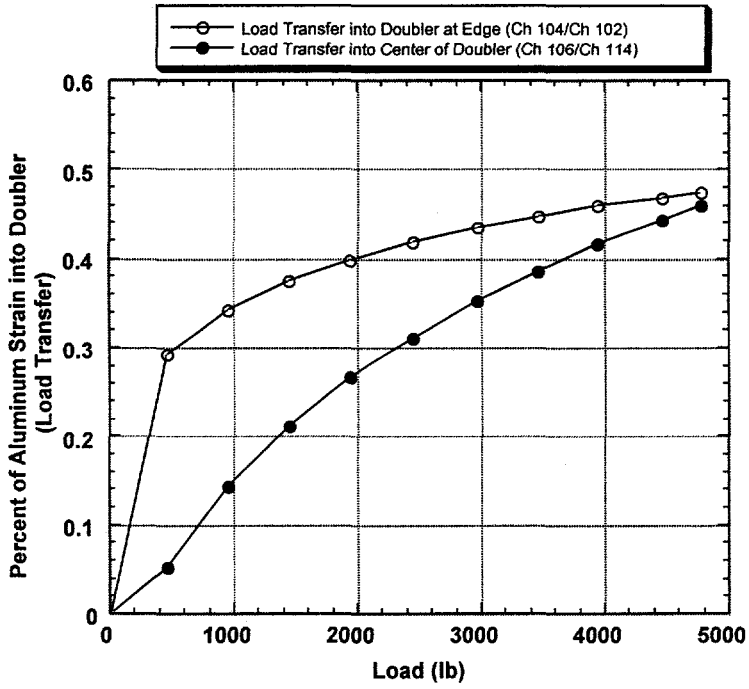

Figure 60: Load Transfer into Doubler for Configuration BE-7

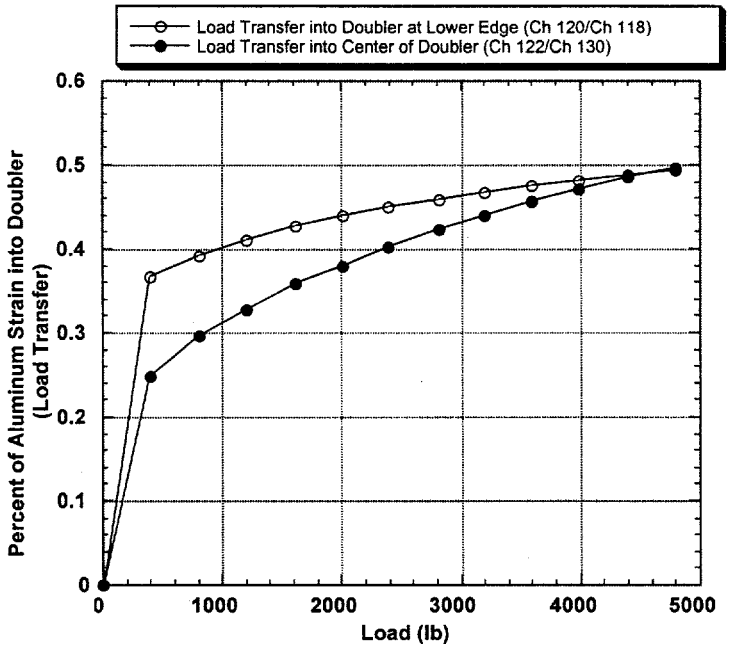

Figure 61: Load Transfer into Doubler for Configuration BE-8

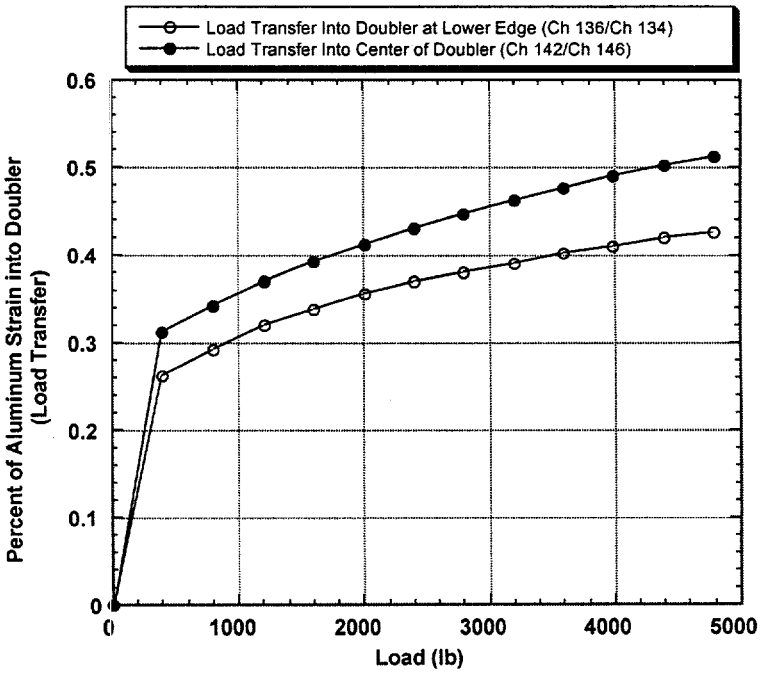

Figure 62: Load Transfer into Doubler for Configuration BE-9

Specimen Config.	Doubler Channel	Alum. Ref. Channel	Peak Load (lbs)	Load/Strain Transfer Ratio	Location on Composite Doubler
BE-1	14	2	13,600	62.3 %	Edge (upper taper region)
BE-1	10	2	13,600	45.7	Center (full thickness)
BE-2	30	16	7,300	53.4	Edge (upper taper region)
BE-2	18	16	7,300	52.3	Edge (lower taper region)
BE-2	26	28	7,300	40.7	Center (full thickness)
BE-3	48	34	8,400	54.5	Edge (upper taper region)
BE-3	36	34	8,400	54.2	Edge (lower taper region)
BE-3	44	46	8,400	35.5	Center (full thickness)
BE-4	66	52	7,500	57.5	Edge (upper taper region)
BE-4	54	52	7,500	55.0	Edge (lower taper region)
BE-4	62	64	7,500	33.7	Center (full thickness)
BE-5	86	70	7,500	47.5	Edge (upper taper region)
BE-5	74	70	7,500	44.2	Edge (lower taper region)
BE-5	76	78	7,500	47.0	Center (full thickness)
BE-7	110	102	4,800	47.4	Edge (upper taper region)
BE-7	104	102	4,800	49.1	Edge (lower taper region)
BE-7	106	114	4,800	46.0	Center (full thickness)
BE-8	128	118	4,800	49.4	Edge (upper taper region)
BE-8	120	118	4,800	49.4	Edge (lower taper region)
BE-8	122	130	4,800	49.7	Center (full thickness)
BE-9	136	134	4,800	42.6	Edge (lower taper region)
BE-9	142	146	4,800	51.3	Center (full thickness)

Table 5: Load/Strain Transfer Ratio - Percent of Aluminum Strain into Adjacent Composite Doubler at Maximum Load

3.2.4 Effects of Multiple Fatigue Lifetimes on Strain Fields

In each of the fatigue specimens, the vast majority of the strain field remained unchanged over the course of the fatigue tests. Several of the specimen configurations showed no change in strain levels from 0 fatigue cycles to 216,000 fatigue cycles. The only strain changes noted in any of the specimens were caused by crack propagation.

a. No Change in Strain Field - Configurations BE-5 (aluminum cut-out damage), BE-7 (unflawed specimen), BE-8 (impact and disbond over fatigue crack), and BE-9 (multiple impacts and disbond over fatigue crack) exhibited little or no change in strain field during the course of their fatigue tests. The NDI before-and-after results in Figures 32-38 show that the initial "programmed" flaws did not change shape nor did any new flaws develop as a result of the fatigue loads. Quantitatively, the strain gage values acquired before and after fatigue testing substantiate the NDI results. Figure 63 plots the strain field for configuration BE-5 (specimen Lock5) before and

after 144,000 fatigue cycles. The before-and-after plots lie on top of each other demonstrating an unchanged strain field. Similarly, Figure 64 shows that the strains in the BE-7 configuration (specimen Lock9) were undisturbed by 144,000 fatigue cycles. Figures 65 and 66 show that, for the most part, configurations BE-8 (Lock14) and BE-9 (Lock20) were unaffected by the fatigue cycles. However, both configurations showed slight changes around the center crack growth area. In configuration BE-8, the strains increased in doubler channel 124 and aluminum channel 132 (ref. Fig. 65). Both of these channels are adjacent to the implanted fatigue crack which grew 0.56" in 180,000 cycles. Configuration BE-9 displayed the same phenomena where doubler channel 144 and aluminum channel 148 increased slightly as the fatigue crack grew 0.77" in 99,000 cycles (ref. Fig. 66).

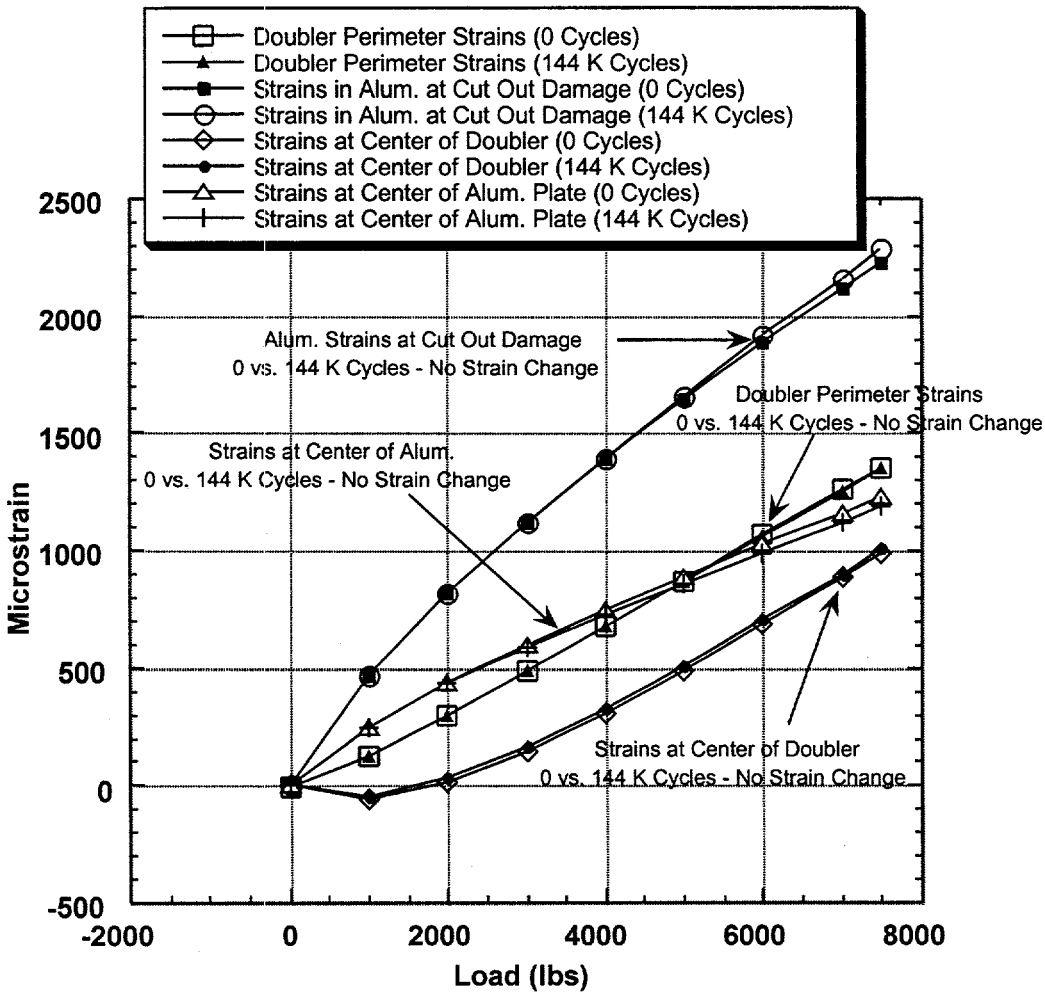

Figure 63: Strain Field in Configuration BE-5 (Lock5) Remains Unchanged Over 144,000 Fatigue Cycles - No Flaw Growth in Doubler Installation

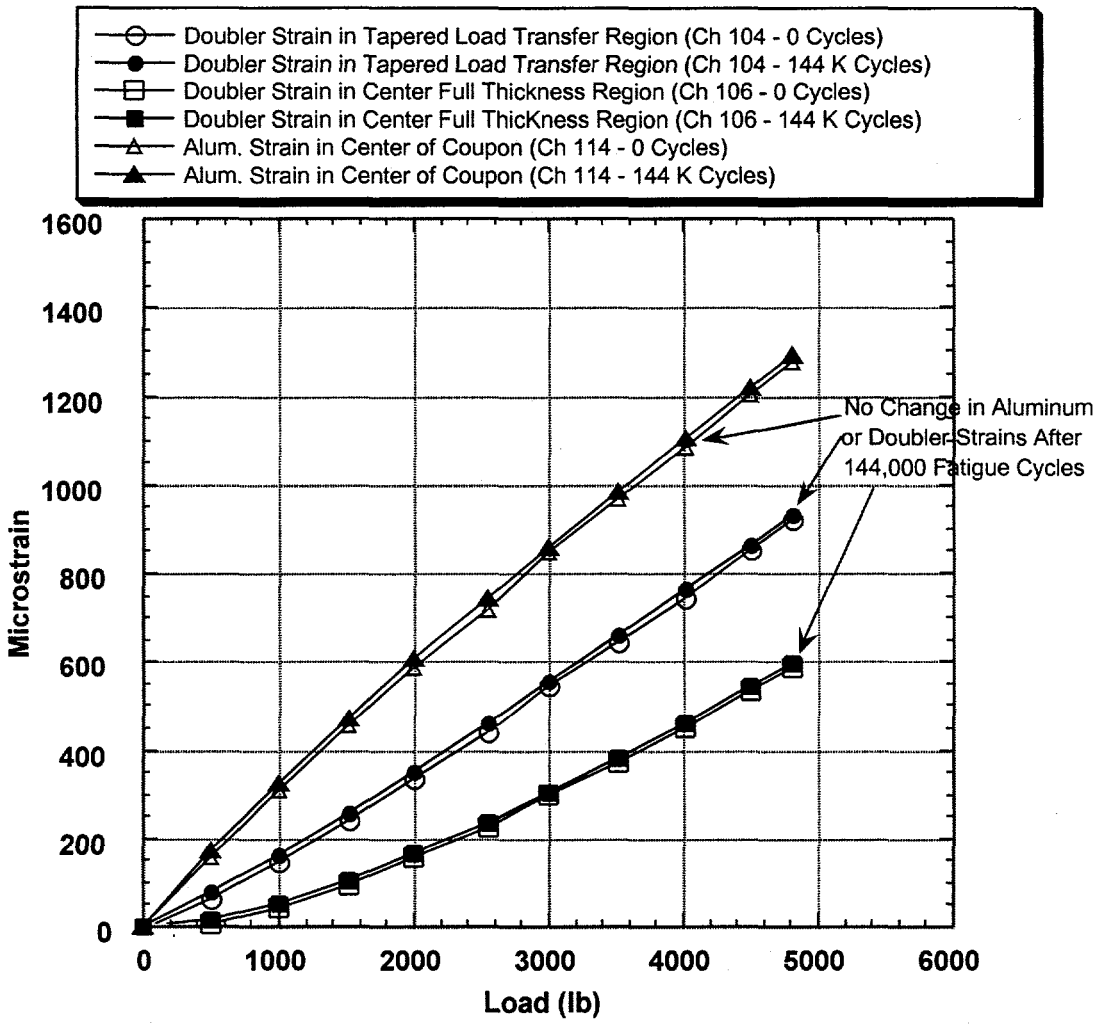

Figure 64: Strain Field in Configuration BE-7 (Lock9) Remains Unchanged Over 144,000 Fatigue Cycles - No Flaw Growth in Doubler Installation

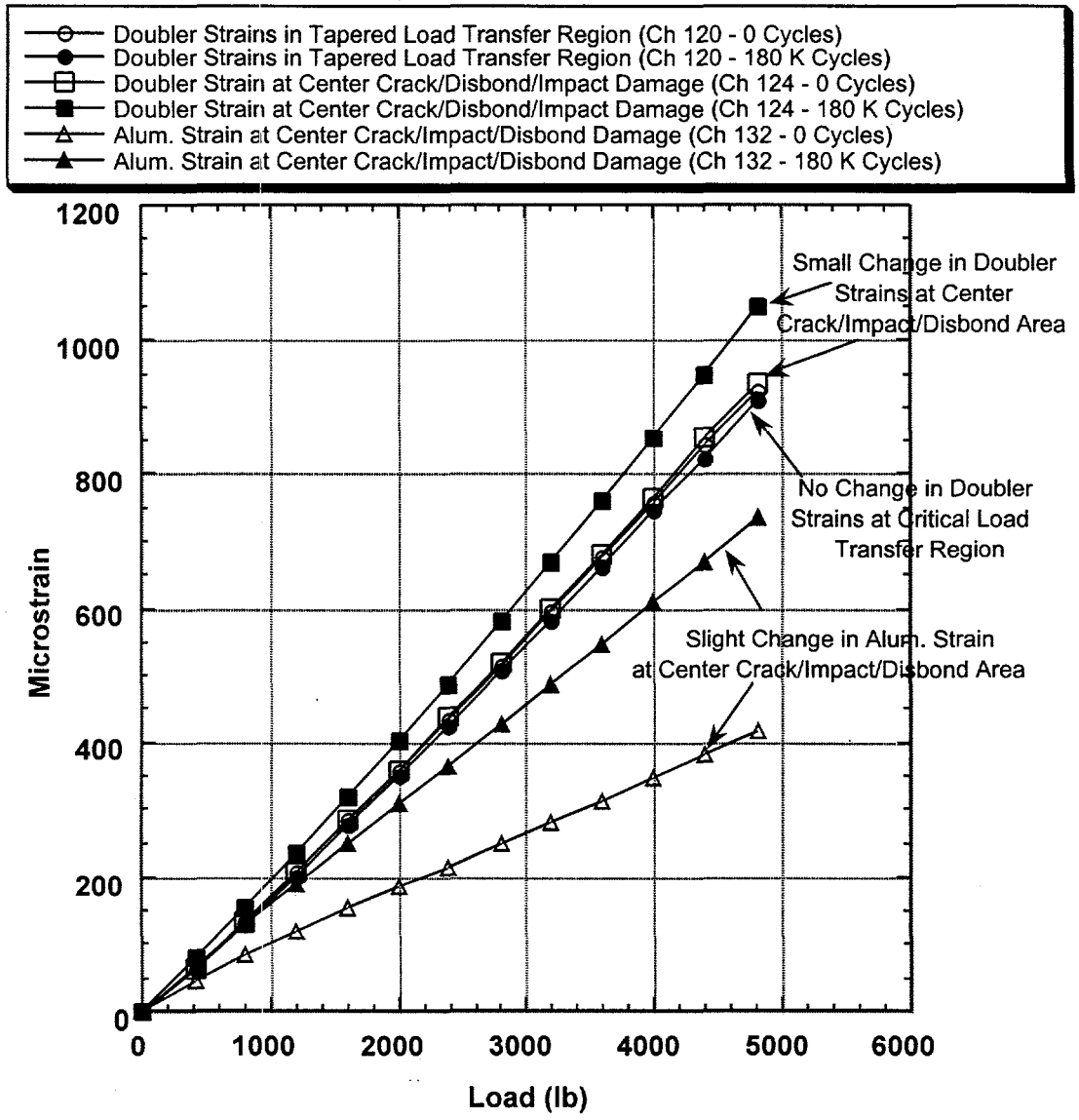

Figure 65: Strain Field in Configuration BE-8 (Lock14) Undergoes Slight Changes Due to Aluminum Crack Growth - No Flaw Growth in Doubler Installation

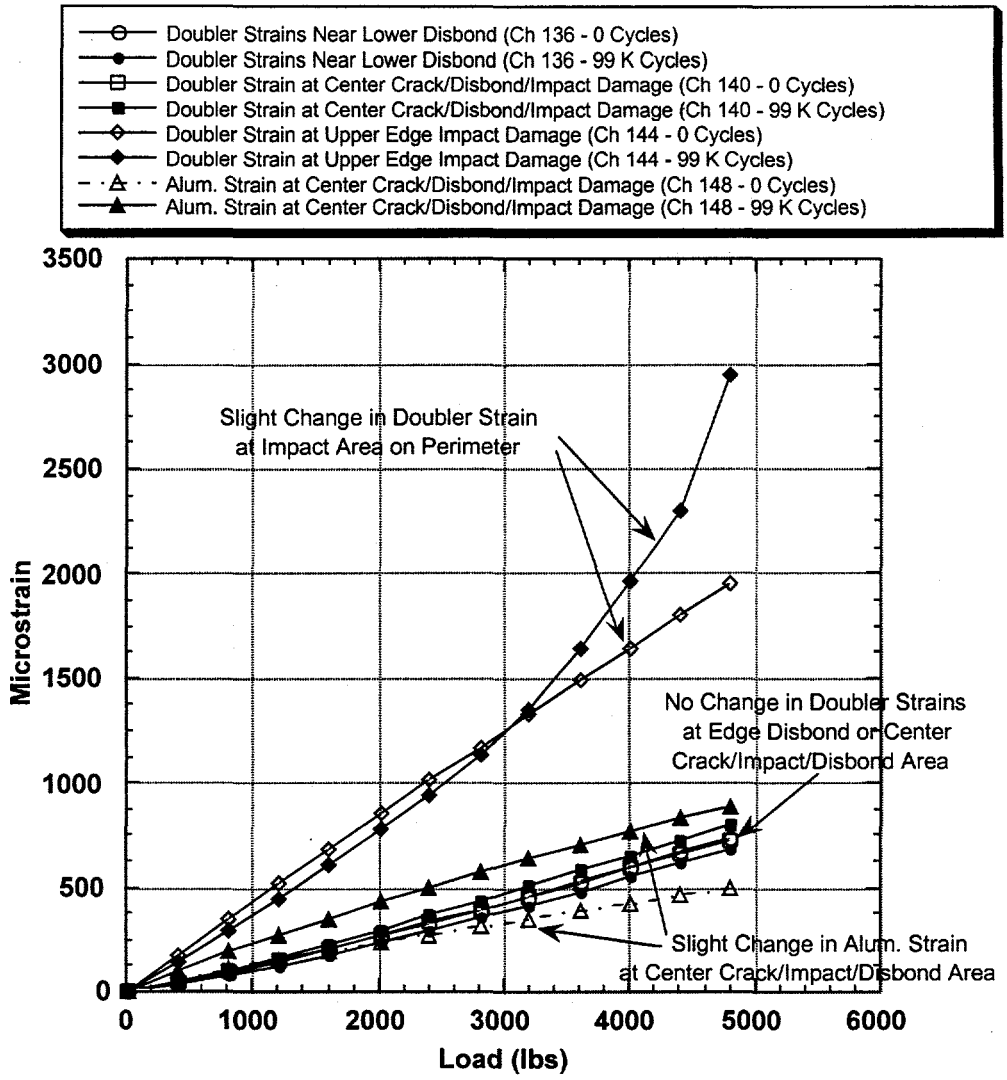

Figure 66: Strain Field in Configuration BE-9 (Lock20) Undergoes Slight Changes Due to Aluminum Crack Growth - No Flaw Growth in Doubler Installation

b. Strain Changes Caused by Fatigue Cracks - In the specimens where crack growth grew beyond the perimeters of the implanted disbond flaw, significant strain changes were observed in the immediate area of the propagating crack. The results, however, highlight the ability of the composite doubler to pick up additional load in response to a loss of strength in the parent structure.

The NDI results in Figure 30 show how the propagating crack produced a fracture in the adhesive layer in configuration BE-3. Similar changes were observed in the BE-1, BE-2, and BE-4 configuration specimens which all experienced a crack growth of

1" or more. Once again, the strain gage results quantify and verify the NDI assessments. Although the strains remained constant in the critical load transfer region, Figures 67 and 68 show that there were several localized changes in the strain fields due to the propagation of the crack through the aluminum plate.

Figure 67 points out the increasing load picked up by the composite doubler as the aluminum crack propagates in the BE-1 configuration. At N= 0 cycles, the strains at the center of the doublers amounted to 30% of the total strain in the aluminum plates. At N = 144,000 cycles, however, the same strain gages registered 60% to 70% of the total strain in the plate. The N = 0 and N = 144,000 cycles curves in Figure 67 show how the doubler picks up more load as the crack propagates and the plate relieves its load (ref. channel 10). The related reduction in plate strains can be seen by looking at the channel 12 strains before and after the fatigue tests (drop from 67% of total strain to less than 3% of total strain in plate). Figure 68 shows the similar results obtained in configuration BE-4.

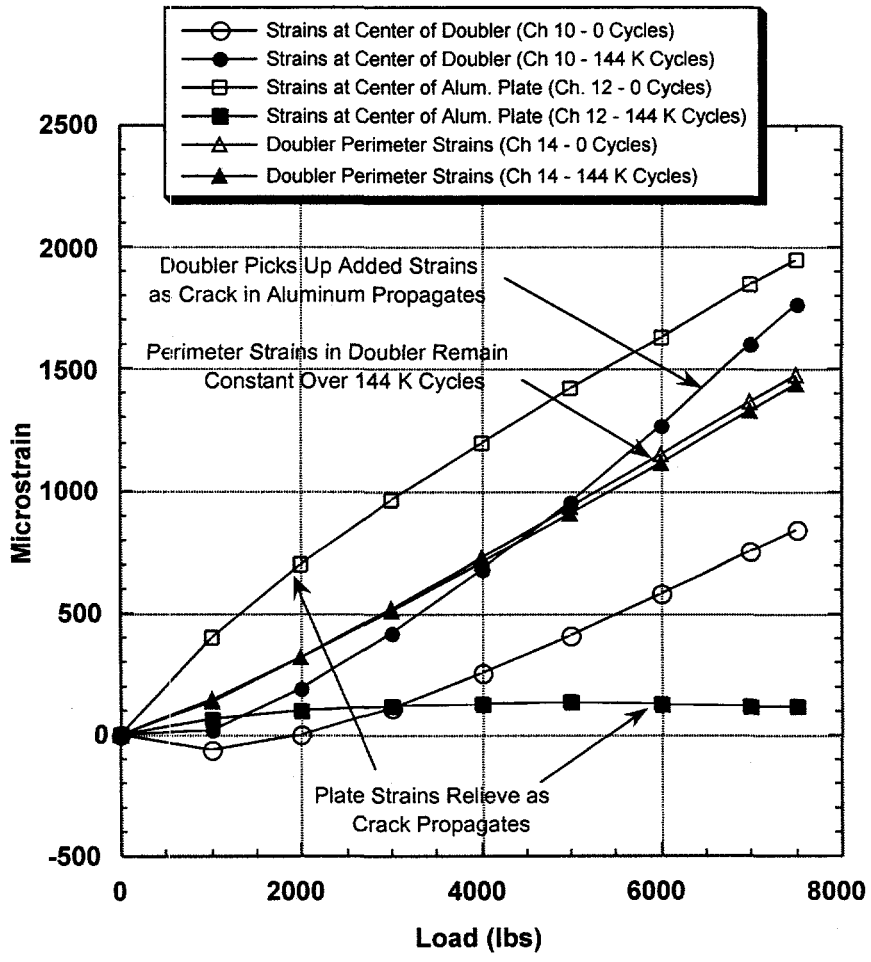

Figure 67: Performance of Composite Doubler Over Crack - Crack Propagation Causes Aluminum to Off Load Strain to Doubler; Configuration BE-1 (Lock1)

It is important to note three items regarding this change in strain field: 1) the composite doubler was able to meet its design objectives and absorb additional load as required, 2) the effects were localized about the crack (i.e. the strains around the perimeter - especially in the critical load transfer region - remained unchanged), and 3) the change in flaw shape (ref. Fig. 30) was caused by a cohesive failure of the adhesive, not a growth in the implanted disbond. This latter point is key because the cohesive failure indicates that the installation was good and that the full strength of the adhesive was achieved. Disbonds, indicated by a lack of adhesive on either the laminate or aluminum mating surface, are undesirable since they can occur at lower loads.

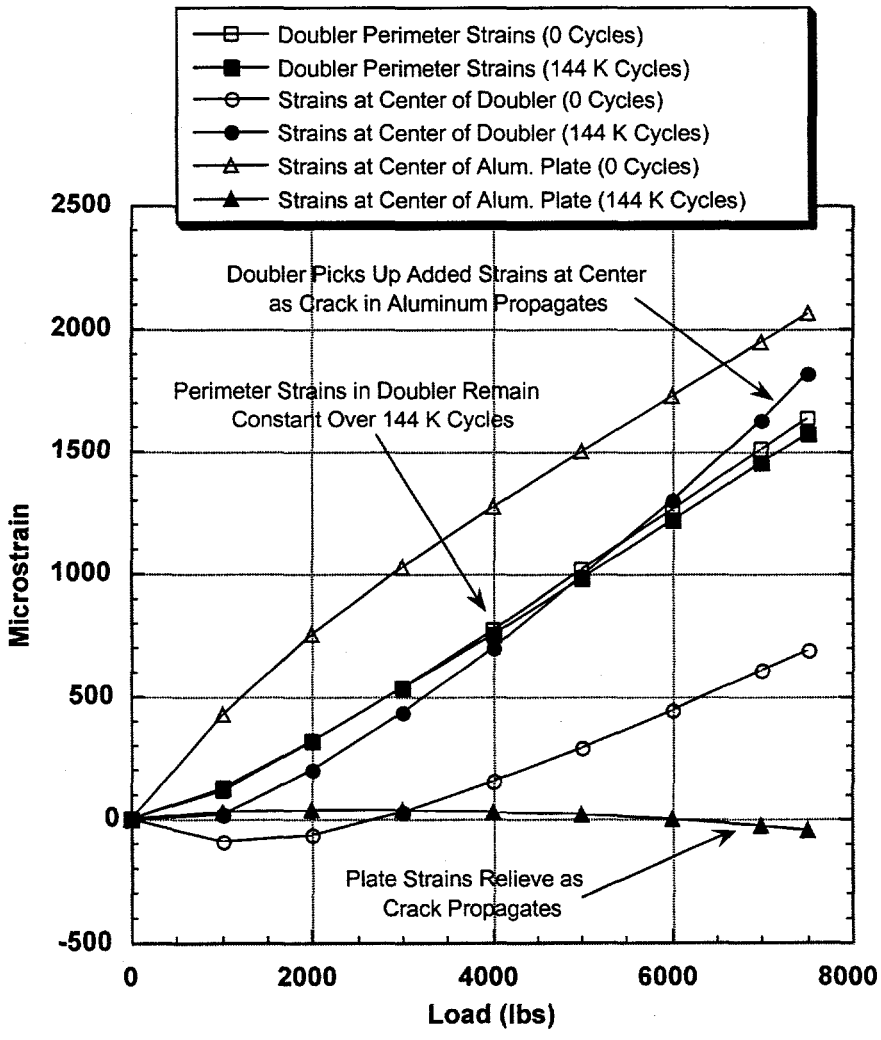

Figure 68: Performance of Composite Doubler Over Crack - Crack Propagation Causes Aluminum to Off Load Strain to Doubler; Configuration BE-4 (Lock4)

3.3 Static Tension Residual Strength Tests

Two of the specimens, Lock 1 (configuration BE-1) and Lock 2 (configuration BE-2), which were subjected to 144,000 fatigue cycles (four L-1011 lifetimes) were subsequently tested to determine their static residual tensile strength. These were not ultimate strength tests since the specimens were tested after flaws were engineered into the specimens and the implanted cracks were subsequently grown. By using the maximum load at failure and the original crossection area at the start of the static residual strength test, the resulting "residual tensile strength" numbers are conservative.

Both specimens, BE-1 and BE-2, had plate crack reinitiation during the course of their fatigue tests (ref. Fig. 25). Their failure modes were identical: crack propagation and associated cohesive bond failure through the aluminum plate. The doubler separated from the aluminum plate through a cohesive fracture of the adhesive. Thus, there was no disbond growth and adhesive was found on both the aluminum and composite laminate. The crack and adhesive fracture propagated up to the point where the composite laminate tapered to only a 3 ply thickness. At this point, the composite laminate fractured vertically producing enough deformation in the specimen to release the load.

Figure 69 shows the strain field in specimen BE-2 up through failure. The aluminum plate away from the doubler (channel 16) began to yield at approximately 12,000 lbs. while the doubler continued to increase its load in a linear fashion. This load/response process continued until failure occurred at 103 ksi and the specimen could no longer sustain an increasing load. *Figure 69 illustrates that the composite doubler was able to transmit stresses in the plastic regime and that extensive yielding/loading beyond the initial yield level was required to fail the installation.*

In calculating the ultimate tensile stress, the cross-sectional dimensions of the aluminum and the bonded doubler were used.

1. Specimen BE-1: fatigue testing propagated the unabated crack to 2.25" in length; measured static ultimate tensile strength was 103 ksi.
2. Specimen BE-2: fatigue testing propagated the stop-drilled crack (crack reinitiation at 126,000 cycles) to 1.625" in length; measured static ultimate tensile strength was 88 ksi.

Even in the presence of severe worst case installations (disbonds) and extensive damage growth (fatigue cracks extending through 50% of the specimen width), it was seen that the doubler-reinforced-plates were able to achieve residual tensile strengths (i.e. post-damage tensile strength) which exceeded the 70 ksi Mil handbook listing for the ultimate tensile strength of 2024-T3 material. Thus, the Boron-Epoxy doubler was able to return the parent structure to its original strength (i.e. load carrying capability).

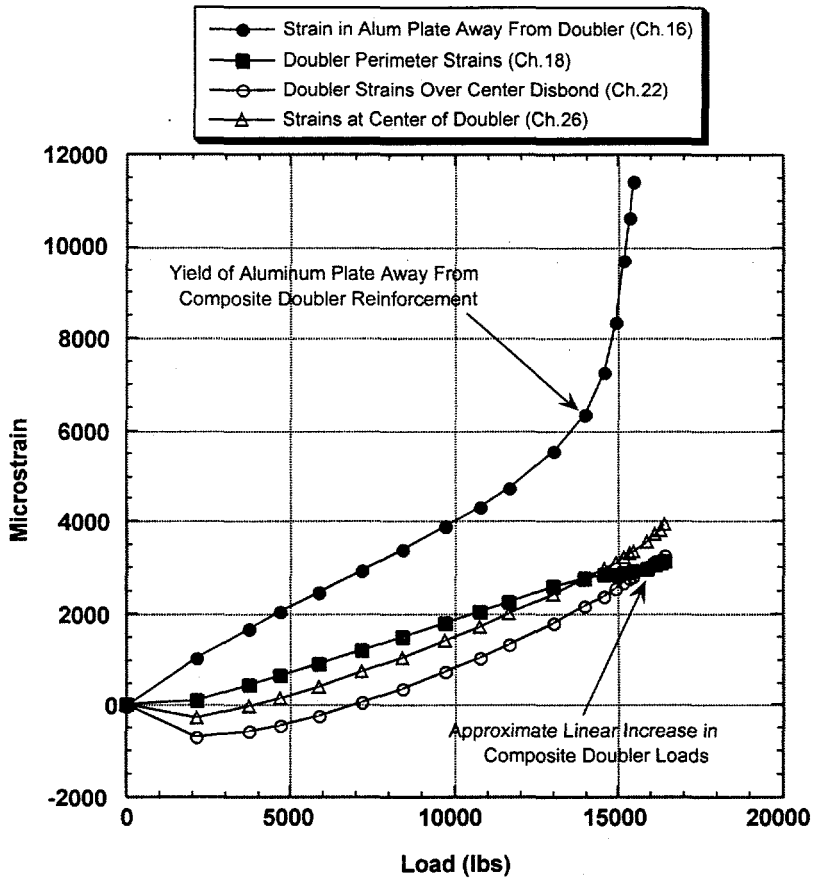

Figure 69: Strain Fields in Composite Doubler and Aluminum Plate During Ultimate Failure Test (Configuration BE-2)

3.4 Static Tension Ultimate Strength Tests

Six specimens, Lock 13-15 (configuration BE-8) and Lock 19-21 (configuration BE-9), were subjected to the ultimate tensile strength tests without prior fatigue loading. Although these specimens were not fatigued they did contain engineered flaws as per the BE-8 and BE-9 configurations (ref. Figs. 14 and 15). Ultimate strength values are normally associated with test-to-failure on optimum, unflawed materials. Thus, these tests results are conservative. To provide a basis of comparison, ultimate strength tests were also conducted on control specimens (unreinforced aluminum coupons) and baseline specimens (unflawed doubler installations).

3.4.1 Ultimate Tensile Strength Values

The ultimate strength values for each of the specimens tested was essentially the same regardless of the flaw scenario. Table 6 lists the ultimate tensile strength values obtained in this test series; the average values are summarized below. Duplicate tests on similar

specimens showed that the results were repeatable. The maximum scatter within a single specimen configuration was 1.9%. The maximum scatter across all of the ultimate strength results was 7.0%.

Test Specimen	Avg. Ult. Strength
1. Plain 2024-T3 (unreinforced)	72.3 ksi
2. Unflawed composite doubler installation	70.5 ksi
3. Impact/disbond doublers over a stop-drilled crack	75.4 ksi
4. Multiple impact/disbond flaws over an unabated crack`	72.4 ksi

[Mil handbook ultimate strength value for 2024-T3 material = 70 ksi]

These ultimate strength tests further demonstrated the ability of a Boron-Epoxy composite doubler to return a damaged aluminum structure to its original load carrying capacity. Ultimate strengths in excess of Mil handbook values were produced by the doubler-reinforced plates. Again, these desirable strength values were determined despite the large installation flaws which were engineered into the specimens (worst-case conditions).

Specimen Configuration	Specimen Number	Flaw Summary	Ultimate Tensile Strength (psi) ⊕
BE-6	6A *	No flaws	72,570
BE-6	7A *	No flaws	72,060
BE-7	9 Δ	Unflawed doubler installation	70,530
BE-8	10	Impact/disbond doubler over a stop-drilled crack	75,490
BE-8	11	Impact/disbond doubler over a stop-drilled crack	75,480
BE-8	12	Impact/disbond doubler over a stop-drilled crack	75,310
BE-9	16	Multiple impact/disbond flaws over an unabated crack	72,450
BE-9	17	Multiple impact/disbond flaws over an unabated crack	73,010
BE-9	18	Multiple impact/disbond flaws over an unabated crack	71,680

⊕ Mil-Hndbk-5 Value for 2024-T3 Aluminum = 70,000 psi

* Non-fatigued aluminum coupons without composite doubler

Δ Post-fatigue test but specimen was still unflawed

Table 6: Results from Ultimate Tensile Strength Failure Tests

3.4.2 Ultimate Failure Mode

Figure 70 shows a front and back view of a failed specimen from the BE-8 configuration (Lock 12). The implanted, 1" diameter disbond is clearly visible as is the stop drilled crack. Each of the ultimate tensile strength tests produced the same failure mode which can be described as follows. Upon reaching the yield stress, the aluminum parent skin began to yield (ref. Fig. 69). Initially, the yielding was primarily in the exposed, unreinforced area of the coupon. As the load was increased further, the aluminum beneath the doubler also began to yield and elongate. The yield zone traveled from the tapered edge of the doubler toward the center of the specimen. This caused the aluminum to sequentially pull away from the doubler which was not yielding or stretching at the same rate as the parent aluminum.

The result was a rolling wave of cohesive failure in the adhesive layer. *There was no disbond growth in the specimen as evidenced by the presence of adhesive on both the aluminum and mating composite doubler in Fig. 70. Again, this indicates that the installation was successful and the full strength of the adhesive was achieved.* During the course of the test it was possible to hear popping sounds corresponding to the fracture of the adhesive. When this cohesive failure (as opposed to adhesive, or disbond, failure) in the adhesive reached the center crack of the coupon, half of the aluminum plate was left without doubler reinforcement. At that point, the crack in the aluminum propagated rapidly across the entire width of the test specimen. Thus, the aluminum was severed in half, as shown in Fig. 70, but the doubler remained in one piece. The contrast between the 1" diameter disbonded area, which has no adhesive, and the adjacent adhesive fracture area, which contains a layer of the adhesive material, is also evident on the aluminum skin in Fig. 70.

Figure 71 shows the common failure mode experienced across the set of BE-9 configuration specimens. The engineered disbonds at the center and lower edge of the doubler are visible. The cohesive failure of the adhesive, indicating that the full strength of the adhesive material was realized, is also apparent due the presence of adhesive on both the aluminum and composite skins. One case where the impact damage included fracture of the composite laminate is shown. The damage tolerance tests demonstrated that the loss of doubler integrity at the critical load transfer region produced only localized effects and did not reduce the overall performance of the doubler.

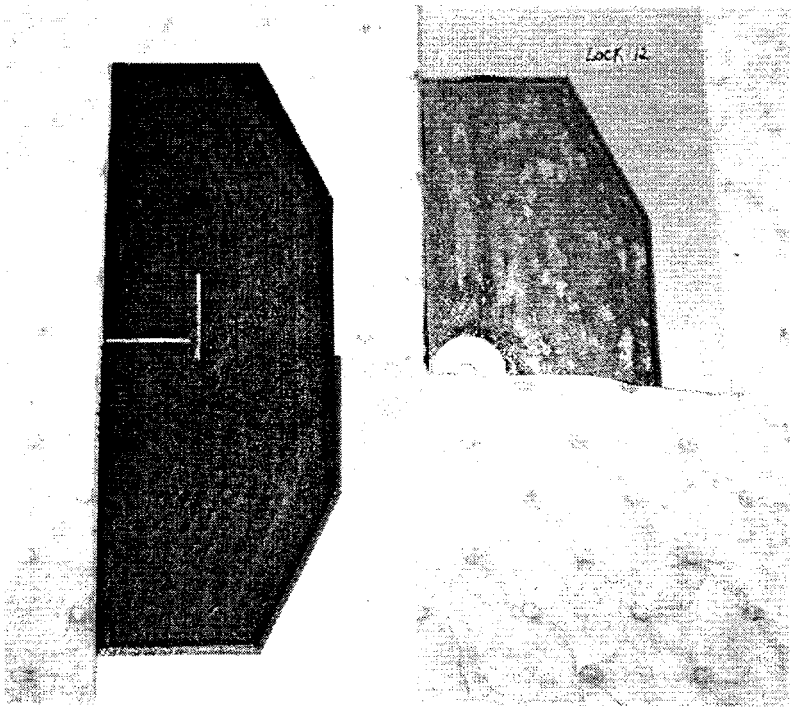

(a) Front View Showing Doubler Intact

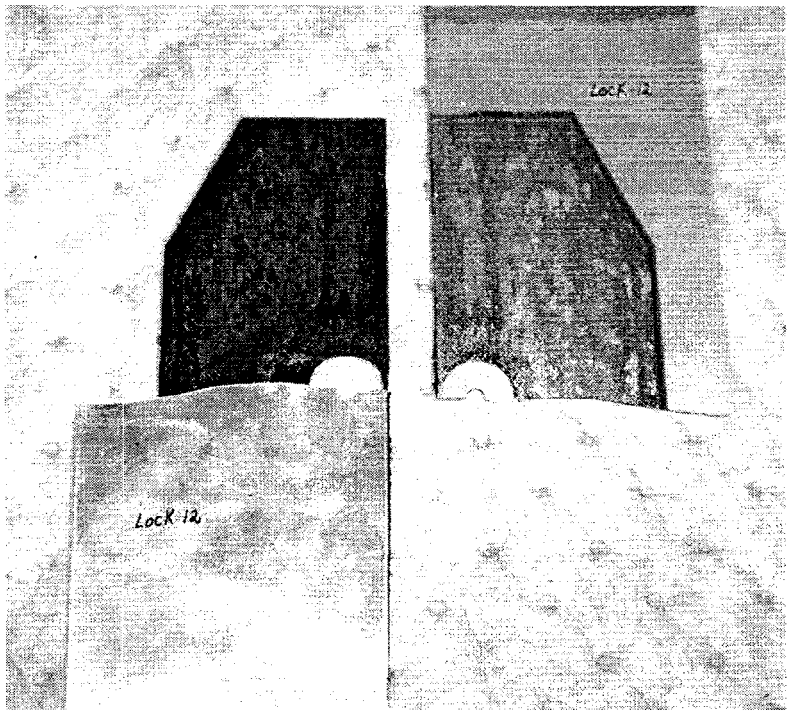

(b) Back View of Doubler/Plate Shows Adhesive on Both Mating Skins

Figure 70: Ultimate Failure of BE-8 Configuration (Lock12) Showing: 1) failure mode of the specimen, 2) fracture of the adhesive and 3) implanted disbond

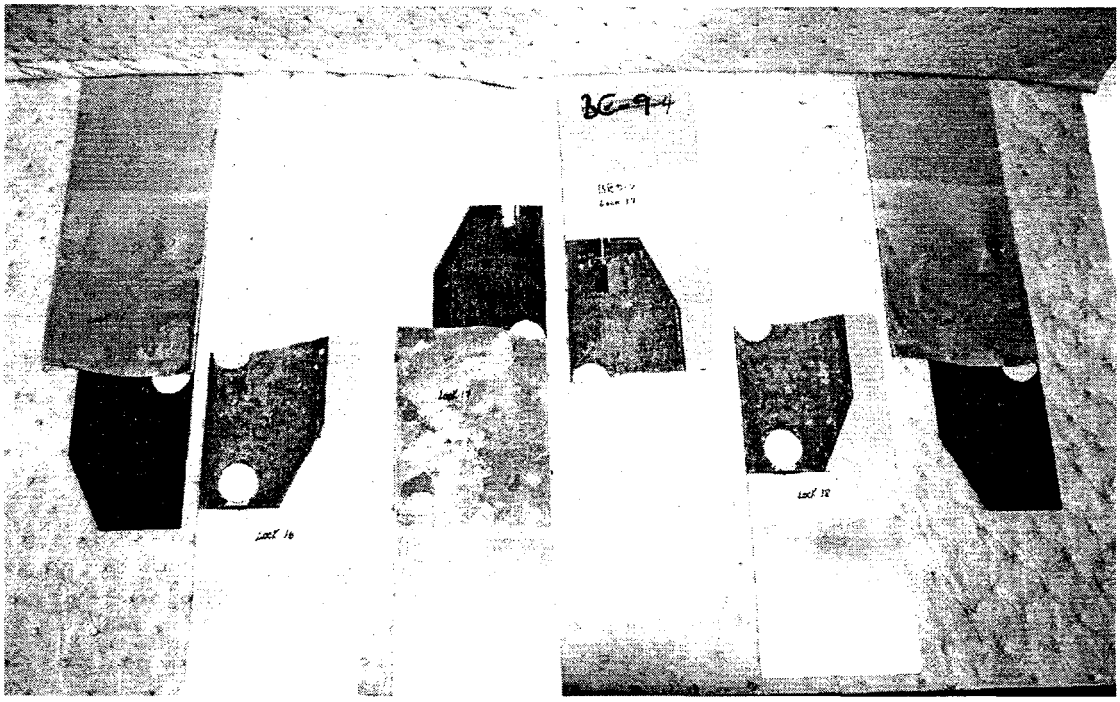

(a) Common Failure in Doubler Specimens

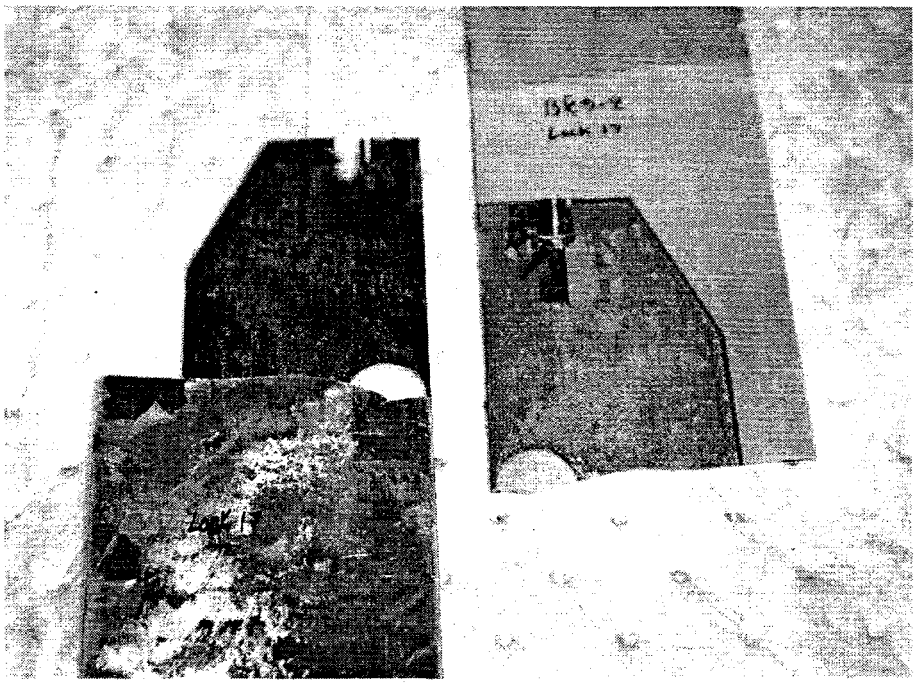

(b) Close-Up View of Doubler Fracture Caused by Impact

Figure 71: Ultimate Failure of BE-9 Configuration - 1) cohesive fracture of adhesive indicates full strength was realized, and 2) fracture caused by impact did not effect overall performance of composite doubler

This Page Left Intentionally Blank

4.0 Conclusions

The overall purpose of this joint project between the FAA and the aviation industry was to evaluate the viability of bonded composite doublers for commercial aircraft repairs. The resulting data will allow the FAA to formally certify the use of composite doublers and to provide suitable requirements for the design, installation and subsequent inspection for continued integrity. This effort focused on the use of Boron-Epoxy composite material.

In recent years, the military has experienced several successful applications of bonded Boron-Epoxy doublers. However, composite doublers have not been certified for use on the U.S. commercial aircraft fleet. One of the concerns surrounding composite doubler technology pertains to long-term survivability, especially in the presence of non-optimum installations. This test program demonstrated the damage tolerance capabilities of bonded composite doublers. The fatigue and strength tests quantified the structural response and crack abatement capabilities of Boron-Epoxy doublers in the presence of worst case flaw scenarios. The engineered flaws included cracks in the parent material, disbonds in the adhesive layer, and impact damage to the composite laminate. Environmental conditions representing temperature and humidity exposure were also included in the coupon tests. Other critical issues such as design, installation, quality assurance, and inspection have been addressed in other FAA reports under this same FAA ACO project (SP-1798AT-Q).

General Use of Results - The objective of this damage tolerance analysis was to obtain a generic assessment of the ability of Boron-Epoxy doublers to reinforce and repair cracked aluminum structure. Although the first commercial application of this technology is the L-1011 door frame discussed above, the results from this study can be applied to any application. By designing the specimens using the nondimensional stiffness ratio, it is possible to extrapolate these results to various parent structure and composite laminate combinations. The number of plies and fiber orientations used in these tests resulted in an extensional stiffness ratio of 1.2:1 $\{(Et)_{BE} = 1.2\ (Et)_{Al}\}$. Independent Air Force [39] and Boeing studies [40-41] have determined that stiffness ratios of 1.2 to 1.5 produce effective doubler designs. Lockheed-Martin has also used this range of stiffness ratios in military composite doubler designs. The stress analysis which accompanies the repair design will be able to determine the optimum stiffness ratio.

Summary of Damage Tolerance Assessment in Light of Inspection Requirements - Large strains immediately adjacent to the doubler flaws emphasize the fact that relatively large disbond or delamination flaws (up to 1" diameter) in the composite doubler have only localized effects on strain and minimal effect on the overall doubler performance (i.e. undesirable strain relief over disbond but favorable load transfer immediately next to disbond). This statement is made relative to the inspection requirement which will result in the detection of disbonds/delaminations of 0.5" diameter or greater [49-50]. Obviously, disbonds will effect the capabilities of composite doublers once they exceed some percentage of the doubler's total footprint area. The point at which disbonds

become detrimental depends upon the size and location of the disbond and the strain field around the doubler. This study did not attempt to determine a "flaw size vs. effect" relation. Rather, it used flaws which were twice as large as the detectable limit to demonstrate the ability of composite doublers to tolerate potential damage.

Similarly, the crack mitigation capabilities of Boron-Epoxy doublers were evaluated using crack sizes which exceeded the inspection threshold. The current inspection requirement calls for inspection intervals and sensitivity to detect cracks of 1" length [48]. The damage tolerance tests presented in this document looked at crack growth beneath doublers of up to 3". The doublers were able to mitigate the crack growth by a factor of 20 versus the unrepaired aluminum. Test results showed that it would take two to three L-1011 fatigue lifetimes (72,000 - 108,000 cycles) for a crack to propagate 1" beneath a reinforcing composite doubler. Finally, these tests showed that Boron-Epoxy composite doublers are able to achieve this performance level (i.e. reinforce and mitigate crack growth) even in the presence of extreme worst-case flaw scenarios. This is the strongest evidence of the damage tolerance of bonded Boron-Epoxy doublers.

Fatigue Tests: Flawed Specimens - The composite doublers produced significant crack growth mitigation when subjected to simulated pressure tension stress cycles. Even specimens with unabated fatigue cracks and collocated disbonds and impact damage were able to survive 144,000 fatigue cycles without specimen failure (less than 2" crack growth). During the course of fatigue cycling, all crack growth occurred in the aluminum plates. No fractures were found in any of the composite laminates. Comparisons with control specimens which did not have composite doubler reinforcement showed that the fatigue lifetime was extended by a factor of 20.

Fatigue Tests: Baseline (Unflawed) Specimens - The best basis of comparison for the performance characteristics discussed above was provided by specimens with normal installation and no flaws. These unflawed specimens showed that crack growth and disbonds/delaminations could be eliminated for at least 216,000 fatigue cycles.

Adhesive Disbonds - The fatigue specimens contained engineered disbonds of 3 to 4 times the size detectable by the doubler inspection technique [46]. Despite the fact that the disbonds were placed above fatigue cracks and in critical load transfer areas, it was observed that there was no growth in the disbonds over 144,000 to 216,000 fatigue cycles (four to six L-1011 lifetimes). In addition, it was demonstrated that the large disbonds, representing almost 30% of the axial load transfer perimeter, did not decrease the overall composite doubler performance.

Performance of Adhesive Layer - Previous analyses of bonded doublers have demonstrated that the most critical part of the repair installation is the adhesive [4-6, 21, 24,30, 39-41, 43]. It must transfer the load to the composite doubler and hold up under many load cycles. The adhesive must also resist moisture and other environmental effects. In order to obtain the optimal adhesive strength and assure a satisfactory performance over time, it is essential to strictly comply with the installation process [42].

Surface preparation is one of the key steps in the installation process. This study demonstrated the ability of the accepted adhesives (AF-163 and FM-73 as per Ref. [48]) to transfer loads over multiple fatigue lifetimes of a commercial aircraft. Strain field analyses and fatigue tests showed that large disbonds - in excess of those which will be detected by NDI - and Boron-Epoxy water absorption did not effect the performance of the adhesive layer.

Stress/Strain Fields - The maximum doubler strains were found in the load transfer region around the perimeter (taper region) of the doubler. In all nine doubler configurations, the strains monitored in this area were 45% - 55% of the total strain in the aluminum plate. This value remained constant over four fatigue lifetimes indicating that there was no deterioration in the bond strength. During crack propagation, the stresses in the doubler increased to pick up the loads released by the plate. Data acquired during failure tests showed that the composite doubler was able to transmit stresses in the plastic regime and that extensive yielding of the aluminum was required to fail the installation. Also, stress risers, normally observed around flaws, were eliminated by the doubler.

Residual Strength - Post-fatigue load-to-failure tests produced residual strength values for the composite-aluminum specimens. Comparisons of the test results with tabulated values for 2024-T3 ultimate tensile strength, which do not use flawed specimens, should be conservative. Even the existence of disbonds and fatigue cracks did not prevent the doubler-reinforced-plates from achieving static ultimate tensile strengths in excess of the 70 ksi Mil handbook listing for 2024-T3 material. Thus, the composite doubler was able to restore the structure to its original load carrying capability.

Ultimate Strength - The ultimate strength values for each of the specimens tested was essentially the same regardless of the flaw scenario. Ultimate strengths in excess of Mil handbook values were produced by the doubler-reinforced plates. The high strain levels experienced during the failure tests did not produce disbond growth in the specimen. The failure mode was extensive aluminum yielding followed by fracture in the adhesive layer. This indicates that the installation was successful and that the full strength of the adhesive was achieved. Finally, these results are conservative since they were obtained in the presence of severe flaw scenarios which were engineered into the specimens.

Overall Evaluation of Bonded Boron-Epoxy Composite Doublers: Crack Mitigation and Damage Tolerance - By combining the ultimate strength results with the crack mitigation results, it is possible to truly assess the capabilities and damage tolerance of bonded Boron-Epoxy composite doublers. In this test series, relatively severe installation flaws were engineered into the test specimens in order to evaluate Boron-Epoxy doubler performance under worst case, off-design conditions. The engineered flaws were at least two times larger than those which can be detected by NDI. It was demonstrated that even in the presence of extensive damage in the original structure (cracks, material loss) and in spite of non-optimum installations (adhesive disbonds), the composite doubler allowed the structure to survive more than four design lifetimes of fatigue loading. Installation flaws in the composite laminate did not propagate over 216,000 fatigue cycles.

Furthermore, the added impediments of impact (severe enough to deform the parent aluminum skin) and hot-wet exposure did not effect the doubler's performance. Since the tests were conducting using extreme combinations of flaw scenarios (sizes and collocation) and excessive fatigue load spectrums, the performance parameters presented here were arrived at in a conservative manner.

Finally, it should be noted that despite the successful results achieved in this damage tolerance assessment effort, the use of composite doubler repairs includes a number of potential pitfalls and engineering challenges. In addition to assuring a quality installation, design and analysis efforts must address difficult issues such as thermally induced residual stresses and stress risers around the doubler's outer perimeter. This paper adds to the growing database of composite doubler performance characteristics, however, a comprehensive engineering approach is always necessary to ensuring the safe application of these aircraft repairs.

REFERENCES

1. Jones, K.M., and Shah, S., "Composite Repair - Upper Forward Corner of P-3 Door - Model L-1011 Aircraft, Strength and Damage Tolerance Analysis", Report No. LG95ER0157, Part of Documentation Package for FAA Atlanta Aircraft Certification Office Project No. SP1798AT-Q, analysis plan December 1995, final report October 1996.
2. Baker, A.A., "Bonded Composite Repair of Metallic Aircraft Components", AGARD-CP-550 Composite Repair of Military Aircraft Structures, 1994.
3. Lynch T.P., "Composite Patches Reinforce Aircraft Structures", Design News, April 1991.
4. Sandow, F.A. and R. K. Cannon, "Composite Repair of Cracked Aluminum Alloy Aircraft Structure", Air Force Wright Aeronautical Laboratories Report AD-A190 514, Sept. 1987.
5. Baker, A.A. and Jones, R., Bonded Repair of Aircraft Structures, Martinus Nijhoff Pub., The Netherlands, 1988.
6. Atluri, S.N., Park, J.H., Punch, E.F., O'Donoghue, P.E., Jones, R., "Composite Repairs of Cracked Metallic Aircraft Structures", Dept. of Transportation Report No. DOT/FAA/CT-92/32, May 1993
7. Elvidge, R., "Structures in Service – An Airline Point of View," Canadian Aeronautics and Space Journal, Vol. 30, December 1984
8. Jones, R. and Callinan, R., "A Design Study in Crack Patching," Fibre Science and Technology, Vol. 14, 1981.
9. Bakuckas, Jr, J.G., Chen, C.C., Yu, J., Tan, P.W., and Bigelow, C.A., "Engineering Approach to Damage Tolerance Analysis of Fuselage Skin Repairs," Dept. of Transportation Report No. DOT/FAA/AR-95/75, November 1996.
10. Davis, M., "The Development of an Engineering Standard for Composite Repairs," AGARD-CP-550, Proceedings of AGARD Meeting, Seville, October 1994.
11. Christian Jr., T., Hammond, D., and Cochran, J., "Composite Material Repairs to Metallic Airframe Components," Journal of Aircraft, Vol. 29, 1992.
12. Roach, D., "DC-10 Composite Doubler Repair Status Report," AANC-FAA document, July 1998.
13. Belason, E.B., "Status of Bonded Boron-Epoxy Doublers for Military and Commercial Metallic Aircraft Structures," Airframe Finishing, Maintenance and Repair Conference, SAE Paper 951145, Bellevue, WA, March 1995.
14. Sivam, T.P., Edwards, D., Mason, S., and Guy, P., "The Evolution of Composite Patch Repair Technology at CTAS in Meeting the Challenges of the C141-B Drop-In-Repair Program for WRALC," SAE Airframe Maint. and Repair Conf, SAE Paper No. SAE-961255, August 1995.
15. Baker, A.A., and Chester, R.J., "Recent Advances in Bonded Composite Repair Technology for Metallic Aircraft Components," Proc. Int'l Conf. on Adv. Composite Materials, 1993.
16. Molent, L., Callinan, R.J., and Jones, R., "Design of an All Boron/Epoxy Doubler Reinforcement for the F-111C Wing Pivot Fitting: Structural Aspects," *Composite Structures*, Vol. 11, 1989.

17. Roach, D.P., and Walkington, P., "Full Scale Structural and NDI Validation Tests on Bonded Composite Doublers for Commercial Aircraft Applications", Sandia National Laboratories/ Dept. of Energy Report No. SAND98-1015 , November 1998
18. Roach, D.P., and Walkington, P., "Development and Validation of Nondestructive Inspection Techniques for Composite Doubler Repairs on Commercial Aircraft Applications", Sandia National Laboratories/ Dept. of Energy Report No. SAND98-1014 , May 1998.
19. Roach, D.P., "Results from FAA Program to Validate Bonded Composite Doublers for Commercial Aviation Use," SAE Paper 972622, SAE Airframe Maintenance and Repair Conference, August 1997.
20. Roach, D.P. "Use of Composite Doublers to Repair DC-10 Aircraft Structure," AANC proposal to the FAA, November 1997.
21. Baker, A.A., "Fatigue Studies Related to Certification of Composite Crack Patching for Primary Metallic Aircraft Structure," FAA-NASA Symposium on Continued Airworthiness if Aircraft Structures, Dept. of Transportation Report No. DOT/FAA/AR-97-2,I, July 1997.
22. Fredell, R.S., "Damage Tolerant Repair Techniques for Pressurized Aircraft Fuselages", PhD Dissertation, Delft University, 1994.
23. Rice, R., Francini, R., Rahman, S., Rosenfeld, S., Rust, S., Smith, S., and Broek, D., "Effects of Repair on Structural Integrity", Dept. of Transportation Report No. DOT/FAA/CT-93/79, December 1993.
24. Jones, R., Chiu, C., Paul, J., "Designing for Damage Tolerant Bonded Joints," *Composite Structures*, Vol. 25, 1993
25. Chiu, W.K., Rees, D., Chalkley, P., and Jones, R., "Designing for Damage Tolerant Repairs," ARL Aircraft Structures Report 450, August 1992.
26. Grills, R.H., and Mullis, T., "C-141 Weep Hole External Inspection of Bonded Boron Patches", Air Force 3rd Aging Aircraft Conference, Sept. 1995.
27. Roach, D.P., Moore, D., and Walkington, P., "Nondestructive Inspection of Bonded Composite Doublers for Aircraft", Proceedings of SPIE Conference on Nondestructive Evaluation of Aging Aircraft, December 1996.
28. Gieske, J.H., Roach, D.P., Walkington, P.D., "Ultrasonic Inspection Technique for Composite Doubler/Aluminum Skin Bond Integrity for Aircraft," SPIE Nondestructive Evaluation Techniques for Aging Infrastructure & Manufacturing Conf., vol. 3258, April 1998.
29. Fredell, R.S., van Barnveld, W., and Vlot, A., "Analysis of Composite Crack Patching of Fuselage Structures: High Patch Modulus Isn't the Whole Story", SAMPE Int'l Symposium 39, April 1994.
30. Rose, L.R., "Influence of Disbonding on the Efficiency of Crack Patching", *Theoretical Applied Fracture Mechanics*, vol. 7 , 1987.
31. Baker, A.A., "Growth Characterization of Fatigue Cracks Repaired with Adhesively Bonded Boron/Epoxy Patches," Proc. Of Int'l Conf. Fracture, ICF-9, April 1997.
32. Rose, L.R., "A Cracked Plate Repaired by Bonded Reinforcements," Int'l Journal of Fracture, Vol. 18, 1982.
33. Sun, C.T., Klug, J., and Arendt, C., "Analysis of Cracked Aluminum Plates Repaired with Bonded Composite Patches," AIAA Journal, Vol. 34, February 1996.

34. Callinan, R.J., Rose, L.R., and Wang, C.H., "Three Dimensional Stress Analysis of Crack Patching," Proc. Of Int'l Conf. Fracture, ICF-9, April 1997.
35. Rose, L.R., "Design Analysis and Validation for a Bonded Composite Repair to Primary Aircraft Structure," Proc. Of Int'l Conf. Fracture, ICF-9, April 1997.
36. Davis, M.J., "A Call for Minimum Standards in Design and Application Technology for Bonded Structural Repairs", Int'l Symposium on Composite Repair of Aircraft Structures in concert with ICCM-10, August 1995.
37. Fredell, R.S., and Marr, J., "An Engineering Approach to the Design and Analysis of Fuselage Crack Patching with the Computer Program CalcuRep for Windows", Int'l Symposium on Composite Repair of Aircraft Structures in concert with ICCM-10, August 1995.
38. Xiong, X., Raizenne, D., "A Design Methodology and PC-Based Software for Bonded Composite Repair in Aircraft Structure", Int'l Symposium on Composite Repair of Aircraft Structures in concert with ICCM-10, August 1995.
39. Schweinberg, W., Jansen, R., and Fiebig, J., "Advanced Composite Repairs of the C-141 Wing Structure", Int'l Symposium on Composite Repair of Aircraft Structures in concert with ICCM-10, August 1995.
40. Klemczyk, C., and Belason, E.B., "Analysis of Maximum Stresses Associated with a Boron/Epoxy Doubler Bonded to Aluminum", Boeing Report under contract 6-1171-10A3397R4, January 1994
41. Rutherford, P., Berg, S., Miller, M. and Mazur, C. "Boron Epoxy Field Repair Doubler for Commercial Aircraft," Boeing Report under contract 6-1171-10A3397R4, January 1995.
42. Berg, S.D., "Process Specification for the Fabrication and Application of Boron-Epoxy Doublers onto Aluminum Structures", Textron Specialty Materials Specification No. 200008-001 (may also be referenced as the Boeing Specification D658-10183-1 which was written for Textron), dated November 30, 1995, Textron Specialty Materials, Lowell, MA, 01851.
43. Belason, E.B., "Fatigue and Static Ultimate Tests of Boron-Epoxy Doublers Bonded to 7075-T6 Aluminum with a Simulated Crack", Int. Conf. on Aeronautical Fatigue, Melbourne, Australia, May 1995.
44. ACEE Composite Project Office, "NASA/Aircraft Industry Standard Specification for Graphite Fiber/Toughened Thermoset Resin Composite Material," NASA Reference Publication 1142, Langley Research Center, 1985.
45. Suppliers of Advanced Composite Materials Association (SACMA) Recommended Test Method for Compression After Impact Properties of Oriented Fiber-Resin Composites, SRM 2-28.
46. Walkington, P., and Roach, D., "Ultrasonic Inspection Procedure for Bonded Boron-Epoxy Composite Doublers," Sandia Labs AANC Specification AANC-PEUT-Comp-5521/4-004, Sandia National Laboratories, Albuquerque, NM; also included in FAA Document SNL96ER0007 under Atlanta ACO Project SP1798AR-Q, FAA approval January 1997.
47. Roach, D., Moore, D., and Walkington, P., "Nondestructive Inspection of Bonded Composite Doublers for Aircraft", SPIE Int'l Conf. on NDI of Aging Aircraft, December 1996.

48. Huang, J., Reeve, S., and Shah, S., "Boron/Epoxy Material Allowables for L-1011 Repair", Report No. LG95ER0193, Part of Documentation Package for FAA Atlanta Aircraft Certification Office Project No. SP1798AT-Q, November 1995.
49. Herderich, D., Shah, S., and Izquierdo, I., "Doubler-Composite Reinforcement, P-3 PAX Door, UPR FWD Corner, Composite Reinforcement", Lockheed-Martin Aeronautical Systems Drawing No. LCC-7622-378, April 1996.
50. Belason, E.B., Rutherford, P., Miller, M., and Raj, S., "Evaluation of Bonded Boron/Epoxy Doublers for Commercial Aircraft Aluminum Structures", FAA/NASA Int. Symposium on Aircraft Structural Integrity, May 1994.

Appendix A

Engineering Drawings for Damage Tolerance Test Program

This Page Left Intentionally Blank

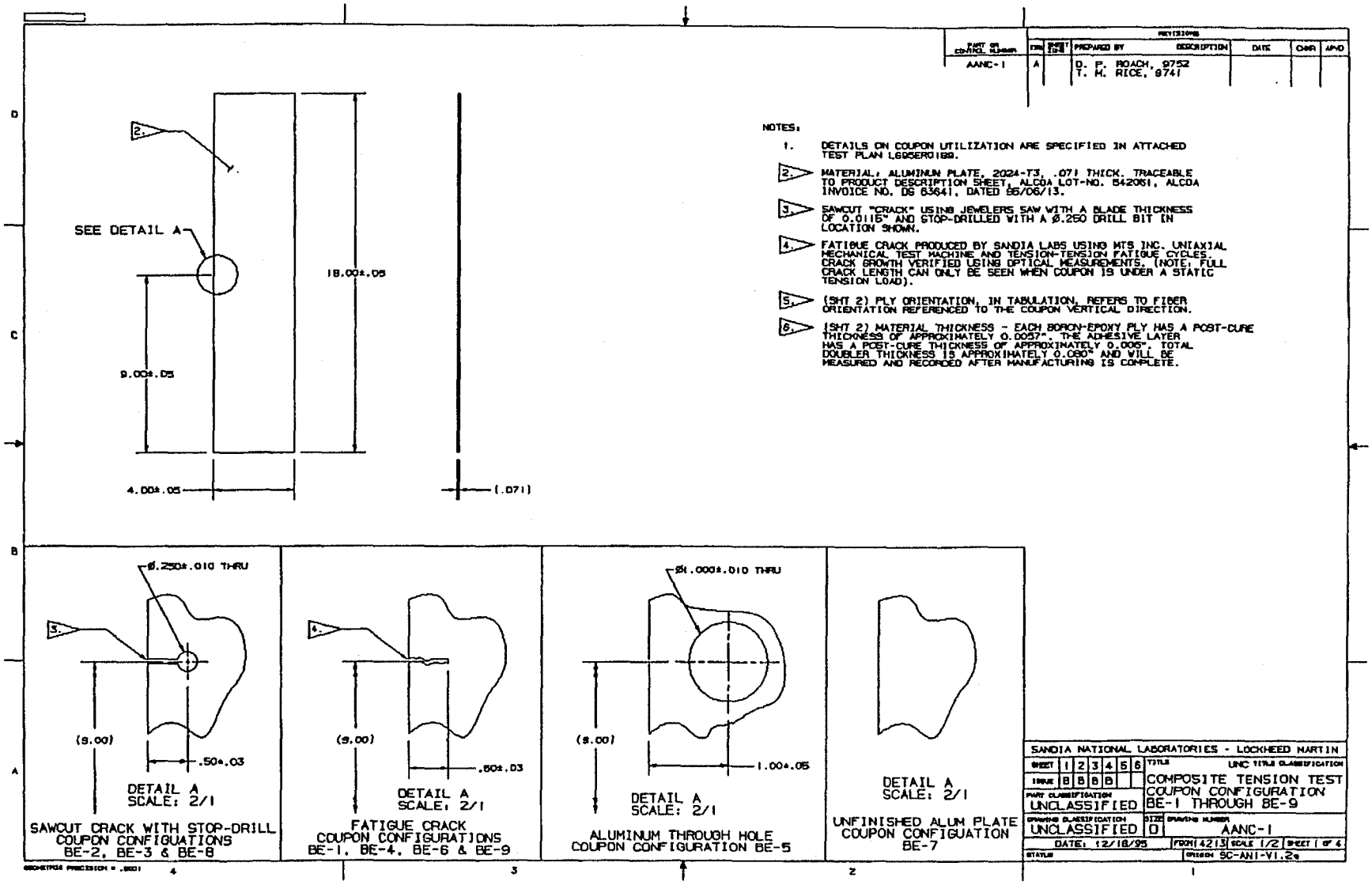
PART OR CONTROL NUMBER
REVISIONS
ZONE
SHEET
PREPARED BY
DESCRIPTION
DATE
CHKR
APVD
AANC-1
A
D. P. ROACH, 9752
T. H. RICE, 9741
NOTES:
1. DETAILS ON COUPON UTILIZATION ARE SPECIFIED IN ATTACHED TEST PLAN L695ER0189.
2. MATERIAL: ALUMINUM PLATE, 2024-T3, .071 THICK. TRACEABLE TO PRODUCT DESCRIPTION SHEET, ALCOA LOT-NO. 542061, ALCOA INVOICE NO. DS 63641, DATED 86/06/13.
3. SAWCUT "CRACK" USING JEWELERS SAW WITH A BLADE THICKNESS OF 0.0115" AND STOP-DRILLED WITH A Ø.250 DRILL BIT IN LOCATION SHOWN.
4. FATIGUE CRACK PRODUCED BY SANDIA LABS USING MTS INC. UNIAXIAL MECHANICAL TEST MACHINE AND TENSION-TENSION FATIGUE CYCLES. CRACK GROWTH VERIFIED USING OPTICAL MEASUREMENTS. (NOTE: FULL CRACK LENGTH CAN ONLY BE SEEN WHEN COUPON IS UNDER A STATIC TENSION LOAD).
5. (SHT 2) PLY ORIENTATION, IN TABULATION, REFERS TO FIBER ORIENTATION REFERENCED TO THE COUPON VERTICAL DIRECTION.
6. (SHT 2) MATERIAL THICKNESS - EACH BORON-EPOXY PLY HAS A POST-CURE THICKNESS OF APPROXIMATELY 0.0057". THE ADHESIVE LAYER HAS A POST-CURE THICKNESS OF APPROXIMATELY 0.005". TOTAL DOUBLER THICKNESS IS APPROXIMATELY 0.080" AND WILL BE MEASURED AND RECORDED AFTER MANUFACTURING IS COMPLETE.
SEE DETAIL A
18.00±.05
9.00±.05
4.00±.05
(.071)
Ø.250±.010 THRU
(9.00)
.50±.03
DETAIL A
SCALE: 2/1
SAWCUT CRACK WITH STOP-DRILL
COUPON CONFIGUATIONS
BE-2, BE-3 & BE-8
FATIGUE CRACK
COUPON CONFIGURATIONS
BE-1, BE-4, BE-6 & BE-9
Ø1.000±.010 THRU
1.00±.05
ALUMINUM THROUGH HOLE
COUPON CONFIGURATION BE-5
UNFINISHED ALUM PLATE
COUPON CONFIGUATION
BE-7
SANDIA NATIONAL LABORATORIES - LOCKHEED MARTIN
SHEET 1 2 3 4 5 6
ISSUE 8 8 8 8
TITLE
UNC TITLE CLASSIFICATION
COMPOSITE TENSION TEST
COUPON CONFIGURATION
BE-1 THROUGH BE-9
PART CLASSIFICATION
UNCLASSIFIED
DRAWING CLASSIFICATION
UNCLASSIFIED
SIZE
D
DRAWING NUMBER
AANC-1
DATE: 12/18/95
FSCM 42131
SCALE 1/2
SHEET 1 OF 6
STATUS
SPECIFICATION SC-ANI-V1.2a

TABULATION

BREAKOUT	ORIENTATION	DIM. A	DIM. B	DIM. C	DIM. D	DIM. E	MATERIAL
ADHESIVE	N/A	5.000	8.000	4.000	2.000	3.000	TYPE AF163 (0.06 PSF), BE-1 THRU BE-5 TYPE FM-73 (0.06 PSF), BE-7 THRU BE-9
PLY 1	0°	5.000	8.000	4.000	2.000	3.000	BORON-EPOXY TYPE 5521/4
PLY 2	+45°	5.180	7.840	3.915	1.889	2.820	BORON-EPOXY TYPE 5521/4
PLY 3	-45°	5.360	7.280	3.830	1.778	2.640	BORON-EPOXY TYPE 5521/4
PLY 4	90°	5.540	6.920	3.745	1.666	2.460	BORON-EPOXY TYPE 5521/4
PLY 5	0°	5.720	6.560	3.660	1.555	2.280	BORON-EPOXY TYPE 5521/4
PLY 6	+45°	5.900	6.200	3.575	1.444	2.100	BORON-EPOXY TYPE 5521/4
PLY 7	-45°	6.080	5.840	3.490	1.333	1.920	BORON-EPOXY TYPE 5521/4
PLY 8	90°	6.260	5.480	3.405	1.221	1.740	BORON-EPOXY TYPE 5521/4
PLY 9	0°	6.440	5.120	3.320	1.110	1.560	BORON-EPOXY TYPE 5521/4
PLY 10	+45°	6.620	4.760	3.235	0.999	1.380	BORON-EPOXY TYPE 5521/4
PLY 11	-45°	6.800	4.400	3.150	0.888	1.200	BORON-EPOXY TYPE 5521/4
PLY 12	90°	6.980	4.040	3.065	0.776	1.020	BORON-EPOXY TYPE 5521/4
PLY 13	0°	5.000	8.000	4.000	2.000	3.000	BORON-EPOXY TYPE 5521/4

TABULATION NOTES: DIMENSIONS HAVE A TOLERANCE OF ±0.050" AND REFLECT A PLY DROP-OFF OF 0.180". TABULATION FOR COUPONS BE-1 THRU BE-5 AND BE-7 THRU BE-9. COUPON BE-6 HAS NO ADHESIVE OR BORON-EPOXY DOUBLER.

7. REFER TO SHEET 3 FOR TEFLON INSTALLATION ON COUPON CONFIGURATIONS BE-2, BE-3 AND BE-4 BEFORE DOUBLER INSTALLATION.

8. COMPOSITE DOUBLER INSTALLATION - REFER TO TEXTRON SPECIALTY MATERIALS SPECIFICATION (TSM) 200008-001 (MAY ALSO BE REFERENCED AS BOEING SPECIFICATION WRITTEN FOR TEXTRON NO. D658-10183-1).

A. ALUMINUM SURFACE PREPERATION - SOLVENT CLEANED PER BOEING AIRCRAFT SPECIFICATION (BAC) 5750; PHOSPHORIC ACID ANODIZE USING PHOSPHORIC ACID CONTAINMENT SYSTEM (PACS) AS DESCRIBED IN U.S. PATENT 4,085,012 AND IN PARAGRAPH 6.6.9.2.2 OF TSM SPEC. 200008-001.

B. ADHESIVE PROCESS - ALUMINUM SURFACE IS TO BE PRIMED WITH CYTEC MATERIAL BR-127 PER BOEING MATERIALS SPECIFICATION (BMS) 5-89; CO-CURE THE TYPE II STRUCTURAL ADHESIVE MATERIAL CYTEC FM-73 (0.06 PSF) PER BMS 5-101 SIMULTANEOUSLY WITH THE BORON-EPOXY DOUBLER MATERIAL 5521/4. COUPON CONFIGURATION BE-1 THRU BE-5, ALREADY FABRICATED, USED 3M PRIMER EC3960 AND 3M ADHESIVE AF163 (0.06 PSF) THESE MATERIALS ARE ALSO LISTED IN THE QUALIFIED PRODUCTS LIST (QPL) OF THE CITED INSTALLATION SPECS. BMS 5-89 & BMS 8-101 & ARE CONSIDERED ALLOWABLE MATERIAL SUBSTITUTIONS.

C. DOUBLER INSTALLATION - BORON-EPOXY DOUBLER IS LAID UP IN ACCORDANCE WITH THE APPLICATION DESIGN DRAWINGS, CURE FOR 90 TO 120 MINUTES AT 225°F TO 250°F AT 0.54 ATM VACUUM BAG PRESSURE (7.35 PSIA) AS SPECIFIED IN TSM SPEC. 200008-001 PARAGRAPH 7.6.4.

D. DO NOT APPLY TOPCOAT OR EDGE SEALANT AFTER DOUBLER CURE.

E. POST DOUBLER INSTALLATION INSPECTION FOR DISBONDS AND DELAMINATIONS BY TEXTRON SPECIALTY MATERIALS, USING ULTRASONIC (UT) NDI METHODS. CONDUCT UT INSPECTIONS AS PER STANDARD PROCEDURES RECOMMENDED BY THE EQUIPMENT MANUFACTURER. SANDIA INSPECTION PROCEDURE AANC-UT-COMP-5521/4-002 WILL ALSO BE USED.

9. 5521/4 BORON-EPOXY SHALL BE USED, AS MANUFACTURED BY TEXTRON SPECIALTY MATERIALS, LOWELL MA. PER SAE AMS SPECIFICATION NUMBERS 3665C, 3667B AND 3867/4A.

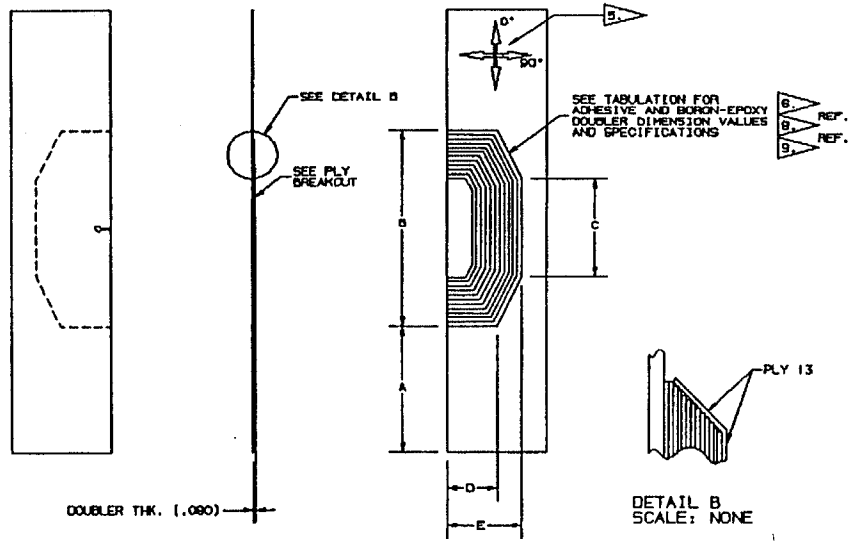

DETAIL B
SCALE: NONE

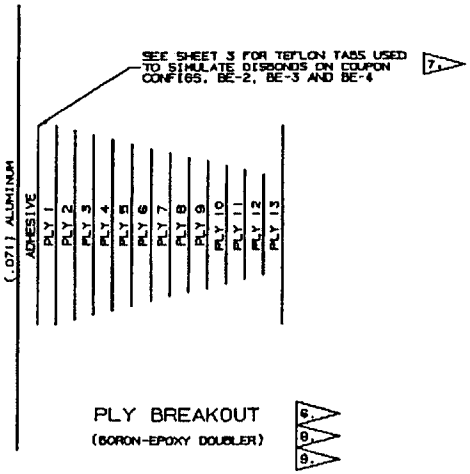

PLY BREAKOUT
(BORON-EPOXY DOUBLER)

DRAWING NUMBER	AANC-1	
DRAWING CLASSIFICATION	UNCLASSIFIED	
SIZE D	FSCM 14213	SCALE 1/2
STATUS	ISSUE B	SHEET 2 OF 4

GEOMETRIC PRECISION ± .XXX

NOTES:

12. COUPON CONFIGURATIONS BE-8 AND BE-9 TO UNDERGO IMPACT DAMAGE, HOT-WET CONDITIONING AND POST INSPECTION AS FOLLOWS:

A. IMPACT DAMAGE AS PER PARAGRAPH 8.113 OF NASA REFERENCE PUBLICATION 1142 USING 1.0" DIAMETER STEEL HEMISPHERE. IMPACT ENERGY WILL BE 25 ± 0.5 FT-LB (300 ± 6 IN-LB). COUPON WILL BE SUPPORTED WHILE IMPARTING IMPACT DAMAGE. (HARDWARE FOR IMPARTING IMPACT DAMAGE SUPPLIED BY LOCKHEED.)

B. HOT-WET CONDITIONED AS PER LOCKHEED SPECIFICATION EPTPTT01-A SECTION 3.2.4.1.8. CONDITIONING WILL BE AT 160°F ± 5°F, 85% ± 5% RELATIVE HUMIDITY.

C. POST IMPACT INSPECTION FOR DISBONDS AND DELAMINATIONS WILL BE PERFORMED USING ULTRASONIC (UT) NDI METHODS. CONDUCT UT INSPECTIONS AS PER STANDARD PROCEDURES RECOMMENDED BY THE EQUIPMENT MANUFACTURER. SANDIA INSPECTION PROCEDURE AANC-UT-COMP-552174-002 WILL ALSO BE USED.

13. AFTER THE COUPON SPECIMENS AND TRAVELER SPECIMENS ARE CONDITIONED FOR TEMPERATURE AND HUMIDITY, THEY CAN BE REMOVED FROM THE ENVIRONMENTAL CHAMBER AND STORED IN SEALED POLYETHALENE BAGS AT 75°F ± 5°F AND 75% ± 5% RELATIVE HUMIDITY.

14. ALL COUPON SPECIMENS ARE PERMANENTLY IDENTIFIED BY ENGRAVING THEIR UNIQUE PART NUMBER INTO THE ALUMINUM PLATE.

COUPON BE-8

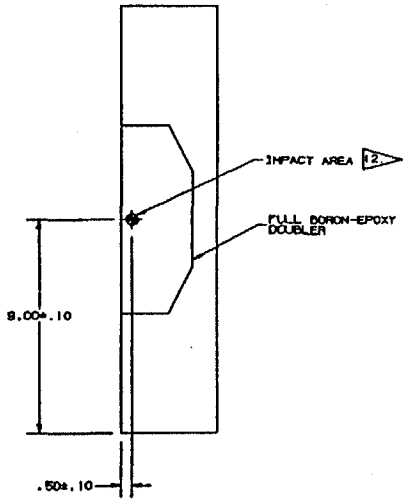

COUPON BE-9

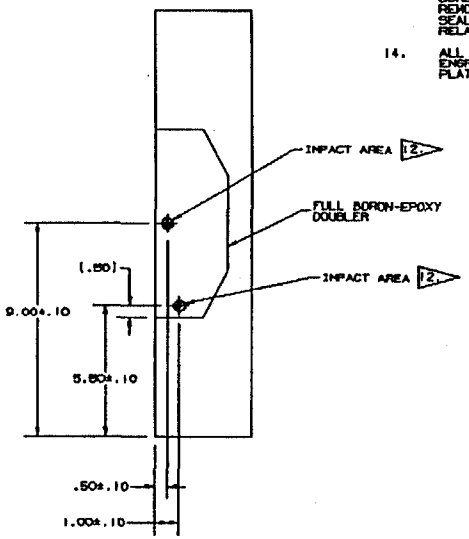

DRAWING NUMBER	AANC-1
DRAWING CLASSIFICATION	UNCLASSIFIED
SIZE D	FSCM 16213 SCALE 1/2
	ISSUE B SHEET 4 OF 4
STATUS	

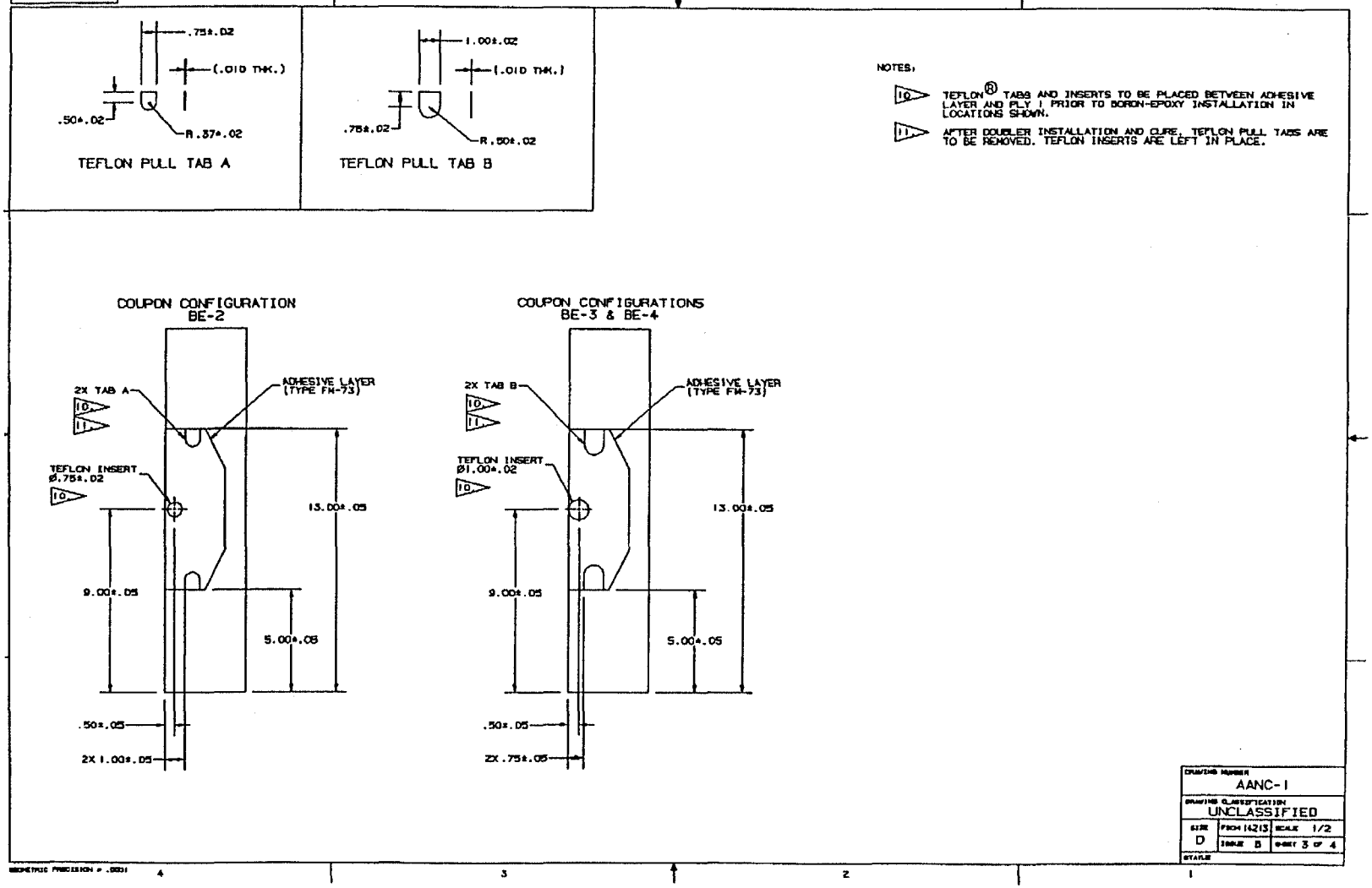
.75±.02
(.010 THK.)
.50±.02
R.37±.02
TEFLON PULL TAB A
1.00±.02
(.010 THK.)
.75±.02
R.50±.02
TEFLON PULL TAB B
NOTES:
10 TEFLON® TABS AND INSERTS TO BE PLACED BETWEEN ADHESIVE LAYER AND PLY 1 PRIOR TO BORON-EPOXY INSTALLATION IN LOCATIONS SHOWN.
11 AFTER DOUBLER INSTALLATION AND CURE, TEFLON PULL TABS ARE TO BE REMOVED. TEFLON INSERTS ARE LEFT IN PLACE.
COUPON CONFIGURATION BE-2
2X TAB A
10
11
ADHESIVE LAYER (TYPE FM-73)
TEFLON INSERT Ø.75±.02
10
13.00±.05
9.00±.05
5.00±.05
.50±.05
2X 1.00±.05
COUPON CONFIGURATIONS BE-3 & BE-4
2X TAB B
10
11
ADHESIVE LAYER (TYPE FM-73)
TEFLON INSERT Ø1.00±.02
10
13.00±.05
9.00±.05
5.00±.05
.50±.05
2X .75±.05
AANC-1
UNCLASSIFIED
D
FSCM 14213
SCALE 1/2
ISSUE B
SHEET 3 OF 4
4
3
2
1

Appendix B

Strain Data from Damage Tolerance Tests

This Page Left Intentionally Blank

	Load (lbs)	Channel 1	Channel 2	Channel 3	Channel 4	Channel 5	Channel 6	Channel 7
0	0	0	-1	0	3e+37	13	0	1
1	1002	-85	499	-48	3e+37	-328	-114	-132
2	2000	-182	938	-117	3e+37	-327	-89	-229
3	3000	-286	1346	-199	3e+37	-275	-4	-311
4	4000	-393	1736	-288	3e+37	28	114	-386
5	5000	-504	2119	-384	3e+37	48	251	-454
6	6000	-615	2494	-481	3e+37	46	399	-523
7	7000	-728	2871	-581	3e+37	46	558	-591
8	7500	-787	3060	-632	3e+37	-272	639	-624

	Channel 8	Channel 9	Channel 10	Channel 11	Channel 12	Channel 13	Channel 14
0	0	0	0	0	0	-1	0
1	495	7	-61	-104	400	-41	131
2	866	-23	-1	-175	700	-103	312
3	1177	-68	112	-236	957	-177	512
4	1450	-119	253	-293	1193	-259	720
5	1712	-173	411	-347	1418	-346	934
6	1954	-228	577	-400	1631	-435	1148
7	2202	-285	753	-452	1846	-527	1368
8	2326	-314	842	-479	1951	-574	1475

Strain Data for Specimen Configuration BE-1

	Load (lbs)	Channel 15	Channel 16	Channel 17	Channel 18	Channel 19	Channel 20	Channel 21
0	0	0	0	0	0	-3	6	2
1	992	-91	484	-36	115	-35	18	34
2	1990	-198	916	-89	305	-55	51	19
3	3000	-311	1319	-151	521	-63	87	-16
4	4000	-425	1699	-218	746	-63	125	-60
5	5060	-541	2072	-285	979	-45	159	-113
6	6000	-659	2441	-355	1213	-20	192	-167
7	7080	-777	2804	-423	1446	27	221	-228
8	7280	-839	2990	-455	1564	68	230	-264

	Channel 22	Channel 23	Channel 24	Channel 25	Channel 26	Channel 27	Channel 28	Channel 29
0	2	0	1	1	1	0	0	1
1	-160	-152	556	8	-59	-104	420	-59
2	-175	-257	985	-25	-1	-177	741	-135
3	-119	-343	1355	-73	113	-240	1018	-218
4	-26	-420	1687	-126	253	-299	1267	-302
5	93	-488	2005	-182	411	-356	1506	-391
6	225	-559	2312	-242	581	-412	1735	-480
7	371	-624	2621	-301	755	-467	1963	-572
8	453	-654	2777	-331	846	-494	2077	-616

	Channel 30	Channel 31	Channel 32	Channel 87	Channel 88	Channel 89	Channel 90	Channel 91
0	0	-6	5	1	2	1	1	-1
1	126	-15	34	-11	-16	-44	79	-82
2	321	-12	84	-47	57	-103	230	-164
3	544	0	136	-91	170	-164	414	-246
4	774	17	187	-137	303	-224	611	-327
5	1009	53	229	-186	449	-283	818	-409
6	1247	93	269	-236	602	-341	1030	-489
7	1490	167	301	-290	775	-404	1264	-576
8	1596	217	307	-307	826	-419	1324	-595

	Channel 92
0	0
1	237
2	495
3	762
4	1028
5	1306
6	1564
7	1856
8	1916

Strain Data for Specimen Configuration BE-2

	Load (lbs)	Channel 33	Channel 34	Channel 35	Channel 36	Channel 37	Channel 38	Channel 39
0	0	0	-1	0	0	0	1	0
1	400	-38	193	-17	33	-28	-3	17
2	800	-78	374	-38	86	-48	-2	23
3	1200	-120	547	-63	152	-63	3	23
4	1604	-164	716	-91	225	-75	8	14
5	2000	-207	877	-119	304	-82	16	5
6	2400	-252	1035	-148	388	-84	24	-8
7	2800	-298	1189	-177	473	-83	33	-21
8	3200	-345	1344	-208	562	-78	41	-36
9	3600	-391	1494	-239	653	-70	51	-54
10	4000	-438	1644	-270	745	-60	60	-71
11	4400	-485	1794	-302	837	-45	68	-89
12	4800	-532	1939	-333	928	-28	76	-108
13	5200	-579	2086	-365	1021	-8	85	-131
14	5600	-626	2234	-397	1115	15	92	-151
15	6000	-673	2379	-428	1208	41	99	-170
16	6400	-721	2525	-460	1301	71	105	-192
17	6800	-768	2669	-492	1396	106	112	-213
18	7200	-817	2817	-524	1490	142	117	-234
19	7600	-865	2963	-555	1583	179	123	-255
20	8000	-919	3119	-588	1679	223	129	-278
21	8400	-971	3272	-618	1772	267	133	-302

Strain Data for Specimen Configuration BE-3

	Channel 40	Channel 41	Channel 42	Channel 43	Channel 44	Channel 45	Channel 46	Channel 47
0	1	0	0	1	1	0	-1	1
1	-88	-68	237	41	-62	-53	199	-20
2	-143	-124	449	64	-93	-98	373	-45
3	-174	-172	641	75	-100	-136	529	-74
4	-186	-214	814	76	-92	-172	670	-105
5	-184	-253	975	71	-70	-205	800	-137
6	-171	-289	1124	61	-39	-236	919	-168
7	-150	-323	1266	48	-1	-265	1035	-200
8	-123	-356	1404	32	44	-294	1145	-232
9	-90	-385	1537	13	92	-322	1253	-264
10	-53	-415	1667	-7	144	-350	1357	-296
11	-12	-445	1792	-28	200	-378	1458	-327
12	31	-472	1917	-50	257	-404	1556	-358
13	80	-496	2039	-76	317	-430	1656	-390
14	129	-526	2160	-100	380	-457	1751	-421
15	178	-554	2277	-125	444	-484	1844	-451
16	233	-577	2396	-151	508	-510	1939	-481
17	287	-604	2518	-179	575	-536	2033	-510
18	344	-631	2637	-207	644	-564	2125	-539
19	401	-657	2753	-234	712	-590	2217	-567
20	462	-682	2874	-263	782	-616	2310	-595
21	523	-705	2994	-293	852	-642	2403	-621

	Channel 48	Channel 49	Channel 50
0	0	0	0
1	18	-31	-4
2	63	-54	-1
3	124	-71	4
4	196	-86	9
5	276	-96	17
6	361	-100	24
7	449	-100	32
8	540	-99	39
9	634	-94	47
10	730	-85	54
11	823	-73	61
12	918	-57	68
13	1013	-39	73
14	1112	-17	78
15	1208	9	83
16	1303	40	86
17	1400	75	90
18	1497	113	92
19	1592	153	95
20	1690	200	97
21	1784	249	98

Strain Data for Specimen Configuration BE-3 (Continued)

	Load (lbs)	Channel 51	Channel 52	Channel 53	Channel 54	Channel 55	Channel 56	Channel 57
0	0.00000e+00	-1	-1	0	-1	-2	2	0
1	1.00200e+03	-103	485	-58	120	-57	1	38
2	2.00000e+03	-215	914	-133	318	-73	18	33
3	3.00000e+03	-331	1308	-214	541	-63	39	10
4	4.00000e+03	-448	1688	-298	777	-32	60	-23
5	5.00000e+03	-566	2058	-383	1019	18	78	-61
6	6.00000e+03	-685	2423	-469	1264	89	91	-103
7	7.00000e+03	-806	2788	-556	1510	179	100	-147
8	7.50000e+03	-867	2971	-599	1633	230	102	-172

	Channel 58	Channel 59	Channel 60	Channel 61	Channel 62	Channel 63	Channel 64	Channel 65
0	0	0	1	1	-1	-1	0	0
1	-157	-146	541	53	-94	-114	428	-72
2	-182	-253	959	43	-59	-196	753	-155
3	-142	-340	1309	6	31	-267	1026	-239
4	-67	-417	1623	-46	155	-332	1273	-325
5	32	-488	1915	-105	296	-395	1505	-408
6	145	-560	2203	-168	449	-457	1729	-490
7	268	-633	2499	-234	612	-520	1950	-570
8	333	-669	2646	-267	695	-550	2060	-608

	Channel 66	Channel 67	Channel 68
0	-1	-2	-1
1	130	-57	4
2	337	-79	23
3	574	-79	43
4	821	-59	62
5	1073	-21	76
6	1327	38	87
7	1582	119	93
8	1709	167	95

Strain Data for Specimen Configuration BE-4

	Load (lbs)	Channel 69	Channel 70	Channel 71	Channel 72	Channel 73	Channel 74	Channel 75
0	0.00000e+00	0	0	0	0	0	-1	0
1	1.00200e+03	-93	492	-34	85	-38	127	-53
2	2.00000e+03	-197	931	-93	236	-101	300	-120
3	3.00000e+03	-306	1345	-164	411	-176	489	-193
4	4.00000e+03	-416	1736	-242	593	-256	681	-266
5	5.00000e+03	-527	2120	-324	783	-342	874	-337
6	6.00000e+03	-639	2501	-408	972	-431	1068	-408
7	7.00000e+03	-754	2879	-495	1162	-523	1259	-478
8	7.50000e+03	-813	3070	-539	1259	-570	1357	-514

	Channel 76	Channel 77	Channel 78	Channel 79	Channel 80	Channel 81	Channel 82	Channel 83
0	1	0	0	1	1	0	0	0
1	-60	-135	468	-125	-56	-40	250	-31
2	18	-235	821	-279	16	-54	438	-82
3	159	-321	1124	-441	148	-58	600	-144
4	329	-401	1394	-599	308	-59	750	-209
5	520	-476	1649	-757	488	-59	894	-280
6	726	-546	1887	-913	685	-59	1033	-351
7	938	-614	2117	-1067	888	-62	1165	-424
8	1048	-648	2231	-1144	993	-61	1230	-461

	Channel 84	Channel 85	Channel 86
0	0	1	0
1	54	-34	108
2	191	-88	278
3	365	-155	474
4	557	-227	683
5	762	-304	899
6	974	-383	1120
7	1191	-466	1345
8	1300	-507	1458

Strain Data for Specimen Configuration BE-5

	Load (lbs)	Channel 93	Uniform Strain in Plate (Chan 94)	Channel 95	Strain Near Crack Tip (Chan 96)
0	0.00000e+00	1	0	0	0
1	1.00000e+03	-120	348	-70	457
2	2.00000e+03	-242	701	-136	925
3	3.00000e+03	-364	1056	-198	1394
4	4.00000e+03	-486	1408	-263	1863
5	5.00000e+03	-611	1769	-350	2405
6	6.00000e+03	-744	2139	-461	3027
7	7.00000e+03	-885	2519	-613	3695

Strain Data for Specimen Configuration BE-6

	Load (lb)	Chan. 101	Chan. 102	Chan. 103	Chan. 104	Chan. 105	Chan. 106	Chan. 107
0	-6.0000	0.0000	1.0000	-6.0000	-5.0000	-5.0000	-5.0000	0.0000
1	457.00	-43.000	216.00	-35.000	63.000	-35.000	8.0000	-39.000
2	952.00	-90.000	433.00	-68.000	148.00	-75.000	44.000	-83.000
3	1455.0	-138.00	645.00	-104.00	242.00	-121.00	96.000	-128.00
4	1946.0	-188.00	845.00	-141.00	336.00	-169.00	156.00	-173.00
5	2451.0	-239.00	1047.0	-183.00	437.00	-223.00	223.00	-219.00
6	2966.0	-293.00	1248.0	-224.00	542.00	-276.00	297.00	-266.00
7	3462.0	-346.00	1440.0	-266.00	643.00	-327.00	373.00	-312.00
8	3948.0	-397.00	1625.0	-306.00	745.00	-379.00	451.00	-357.00
9	4456.0	-452.00	1817.0	-349.00	851.00	-433.00	533.00	-404.00
10	4777.0	-488.00	1938.0	-378.00	918.00	-470.00	588.00	-435.00

	Chan. 108	Chan. 109	Chan. 110	Chan. 111	Chan. 112	Chan. 113	Chan. 114	Chan.115
0	-2.0000	-6.0000	-5.0000	2.0000	-1.0000	3.0000	-1.0000	3.0000
1	110.00	-41.000	67.000	-38.000	150.00	-37.000	157.00	-39.000
2	239.00	-81.000	156.00	-81.000	305.00	-77.000	309.00	-78.000
3	375.00	-122.00	253.00	-124.00	460.00	-113.00	453.00	-112.00
4	509.00	-164.00	351.00	-165.00	608.00	-147.00	585.00	-144.00
5	650.00	-212.00	454.00	-208.00	761.00	-180.00	717.00	-174.00
6	793.00	-259.00	562.00	-250.00	915.00	-215.00	845.00	-204.00
7	931.00	-304.00	669.00	-291.00	1062.0	-247.00	967.00	-233.00
8	1067.0	-350.00	773.00	-331.00	1207.0	-278.00	1083.0	-261.00
9	1209.0	-398.00	883.00	-374.00	1356.0	-311.00	1202.0	-290.00
10	1301.0	-430.00	951.00	-400.00	1453.0	-331.00	1278.0	-307.00

	Chan. 116
0	-2.0000
1	150.00
2	291.00
3	420.00
4	538.00
5	654.00
6	767.00
7	872.00
8	973.00
9	1077.0
10	1144.0

Strain Data for Specimen Configuration BE-7

	Load (lb)	Chan. 118	Chan. 120	Chan. 122	Chan. 124	Chan. 126	Chan. 128	Chan. 130
0	5.0000	-1.0000	-1.0000	0.0000	-1.0000	-1.0000	-1.0000	0.0000
1	400.00	169.00	62.000	32.000	63.000	74.000	63.000	129.00
2	809.00	339.00	133.00	75.000	134.00	157.00	135.00	253.00
3	1204.0	499.00	205.00	121.00	206.00	240.00	206.00	369.00
4	1619.0	663.00	283.00	174.00	284.00	329.00	284.00	485.00
5	2004.0	815.00	358.00	225.00	358.00	415.00	358.00	592.00
6	2395.0	965.00	434.00	280.00	436.00	500.00	434.00	696.00
7	2809.0	1124.0	516.00	340.00	519.00	592.00	517.00	805.00
8	3199.0	1272.0	595.00	398.00	598.00	679.00	595.00	906.00
9	3599.0	1422.0	675.00	459.00	680.00	769.00	676.00	1008.0
10	3990.0	1569.0	756.00	520.00	763.00	855.00	757.00	1106.0
11	4404.0	1725.0	842.00	586.00	853.00	949.00	842.00	1208.0
12	4789.0	1869.0	924.00	648.00	936.00	1036.0	924.00	1304.0

	Chan. 132
0	-1.0000
1	44.000
2	85.000
3	119.00
4	153.00
5	184.00
6	215.00
7	248.00
8	279.00
9	311.00
10	345.00
11	381.00
12	415.00

Strain Data for Specimen Configuration BE-8

	Load (lb)	Chan. 133	Chan. 134	Chan. 135	Chan. 136	Chan. 137	Chan. 138	Chan. 139
0	5.0000	0.0000	0.0000	0.0000	0.0000	0.0000	1.0000	0.0000
1	397.00	-40.000	153.00	-44.000	40.000	-17.000	24.000	-21.000
2	799.00	-80.000	304.00	-91.000	89.000	-38.000	58.000	-49.000
3	1210.0	-122.00	455.00	-142.00	146.00	-61.000	101.00	-82.000
4	1608.0	-163.00	599.00	-192.00	203.00	-84.000	146.00	-117.00
5	2009.0	-206.00	744.00	-241.00	265.00	-108.00	197.00	-155.00
6	2406.0	-248.00	887.00	-291.00	329.00	-133.00	250.00	-194.00
7	2789.0	-291.00	1025.0	-345.00	389.00	-158.00	302.00	-242.00
8	3196.0	-334.00	1169.0	-395.00	457.00	-183.00	360.00	-284.00
9	3593.0	-379.00	1310.0	-445.00	526.00	-208.00	419.00	-327.00
10	3990.0	-421.00	1449.0	-494.00	595.00	-234.00	479.00	-370.00
11	4402.0	-467.00	1593.0	-544.00	668.00	-259.00	543.00	-415.00
12	4794.0	-510.00	1729.0	-591.00	737.00	-284.00	604.00	-460.00

	Chan. 140	Chan. 141	Chan. 142	Chan. 143	Chan. 144	Chan. 145	Chan. 146	Chan. 147
0	0.0000	0.0000	0.0000	-1.0000	0.0000	1.0000	0.0000	1.0000
1	45.000	-10.000	42.000	-45.000	173.00	-31.000	135.00	-46.000
2	96.000	-24.000	89.000	-89.000	345.00	-58.000	260.00	-89.000
3	152.00	-40.000	141.00	-132.00	516.00	-83.000	381.00	-131.00
4	209.00	-56.000	194.00	-174.00	682.00	-107.00	494.00	-172.00
5	269.00	-73.000	249.00	-214.00	847.00	-130.00	604.00	-212.00
6	331.00	-90.000	306.00	-254.00	1008.0	-152.00	710.00	-252.00
7	390.00	-107.00	363.00	-300.00	1162.0	-173.00	812.00	-290.00
8	455.00	-125.00	424.00	-338.00	1326.0	-195.00	917.00	-330.00
9	521.00	-143.00	485.00	-377.00	1485.0	-218.00	1018.0	-369.00
10	588.00	-161.00	547.00	-415.00	1640.0	-239.00	1117.0	-407.00
11	656.00	-179.00	611.00	-455.00	1801.0	-261.00	1218.0	-447.00
12	723.00	-196.00	673.00	-496.00	1951.0	-282.00	1313.0	-485.00

	Chan. 148
0	-1.0000
1	58.000
2	108.00
3	154.00
4	195.00
5	236.00
6	274.00
7	308.00
8	346.00
9	385.00
10	423.00
11	461.00
12	498.00

Strain Data for Specimen Configuration BE-9

DISTRIBUTION:

1 Ron Atmur
FAA-Los Angeles ACO
ANM-12 OL
3960 Paramount Blvd.
Lakewood, CA 90712-4137

1 Alan Baker
Aeronaut. & Maritime Research Lab
506 Lorimer St Fishermens Bend
P.O. Box 4331
Melbourne, Victoria, Australia 03001

1 Dorenda Baker
DOT/FAA
Northwest Mountain Region
1601 Lind Ave. S. W. ANM-109
Renton, WA 98055-4056

1 Oksana Bardygula
1538 Girard Ave. #4
Bourbonneas, IL 60914

1 Bob Bell
Lockheed-Martin
86 South Cobb Dr.
D/73-25 Zone 0160
Marietta, GA 30063-0160

1 Cathy Bigelow
FAA Hughes Technical Center
AAR-433
Atlantic City Int'l. Airport, NJ 08405

1 Brett Bolan
AFRL/MLSA
2179 Twelfth St., Rm. 122
Wright-Pat. AFB, OH 45433-7718

1 John Brausch
AFRL/MLSA
2179 Twelfth St., Rm. 122
Wright-Pat. AFB, OH 45433-7718

1 Al Broz
FAA-New England, ANE 105N
12 New England Exec, Dev. Park
Burlington, MA 01803

1 Ronald Cairo
Pratt & Whitney
MS 714-03
P.O. Box 109600
West Palm Beach, FL 33410-9600

1 Tom Collins
Boeing North American
12214 Lakewood Blvd
MC-AB70
Downey, CA 90242

1 Tobey Cordell
AFRL/MLLP
2230 Tenth St.
Wright-Pat. AFB, OH 45433-7817

1 Bill Cusato
Federal Express
7401 World Way West
Los Angeles, CA 90045

1 Isaac Daniel
Center for Qual. Eng. & Failure Prev.
Northwestern Univ.
2137 N. Campus Dr.
Evanston, IL 60208-3020

1 Gregg Delker
USAir
4001 N. Liberty St.
Winston-Salem, NC 27156

1 Capt. Jason Denney
USAF
WL/FIBE, Bldg. 65
2790 D Street, Room 504
Wright-Patt. AFB, OH 45433-7402

1 Gerry Doetkott
Northwest Airlines
MS C- Dept. C8840
St. Paul, MN 55111-3034

1 Cong Duong
Boeing
Mail Code 71-34
2401 E. Wardlow Road
Long Beach, CA 90807-5309

1 Bob Eastin
FAA National Resource Specialist Fatigue
FAA- Los Angeles ACO
ANM-12 OL
3960 Paramount Blvd.
Lakewood, CA 90712-4137

1 Jennifer Elmore
NAVAIRSYSCOM
Bldg. 2187, Suite 2380
48110 Shaw Rd. Unit 5
Patuxent River, MD 20670

1 John Fabry
FAA Hughes Technical Center
AAR-433
Atlantic City Int'l. Airport, NJ 08405

1 Mike Favaloro
Textron Systems Division
201 Lowell St., MS-5128
Wilmington, MA 01887

1 Allen Fawcett
Boeing Commercial Airplane Group
P.O. Box 3707 MC 0K-UC
Seattle, WA 98124-2207

1 Jay Fiebig
WR-ALC/TIED
255 2nd St., Ste. 122
Robins AFB, GA 31098-1637

1 Tom Flournoy
FAA Hughes Technical Center
AAR-430
Atlantic City Int'l. Airport, NJ 08405

1 Major Rob Fredell
USAF Academy
HQ USAFA/DFEM
2354 Fairchild Dr., Suite 6H2
USAF Academy, CO 80840-6240

1 Stephen Galea
Aeronautical & Maritime Res. Lab
GPO Box 4331
Melbourne, Victoria 3001
Australia

5 Dave Galella
FAA Hughes Technical Center
AAR-433
Atlantic City Int'l. Airport, NJ 08405

1 Joe Gallagher
AFRL/ML Bldg. 45
2130 8th St, Suite 1
Wright-Pat. AFB, OH 45433-7542

1 Wriley Gay
Naval Aviation Depot
Commanding Officer Code 4.3.4.4
PSC Box 8021
Cherry Pt., NC 28533-0021

1 Thomas Gogel
Lufthansa Technik
FRA WA42
Lufthansa Base
60546 Frankfurt
Germany

1 Ulf Goranson
Boeing Commercial Airplane Group
Structures Lab & Tech. Standards
P.O. Box 3707, M/S 4510
Seattle, WA 98124-2207

1 Kim Graebner
The Boeing Company
1218 Armstrong Ct.
Derby, KA 67037

1 Ken Griess
Boeing Customer Service
Box 3707 MS 2J-62
Seattle, WA 98124-2207

1 Bob Grills
SAIC Ultra Image International
Two Shaw Cove
New London, CT

1 Don Hagemaier
Boeing
2401 East Wardlow Rd
Mail Code 71-12
Long Beach, CA 90807-5309

1 Michael J.Hoke
Abaris Training
5401 Longley Lane
Suite 49
Reno, NV 89511

1 David Hsu
Iowa State University
1915 Scholl Rd.
ASCII
Ames, IA 50011

1 Jun Hun
Boeing
3855 Lakewood Blvd.
Mail Code 35-35
Long Beach, CA 90846

1 Larry Ilcewicz
FAA Nat. Resource Specialist Composites
1601 Lund Ave. SW
ANM-115N
Renton, WA 98055

1 William Jappe
Boeing
2401 East Wardlow Rd
MC C078-013
Long Beach, CA 90807-5309

1 Kevin Jones
Schwartz Engineering
11503 Jones Maltsberger
Suite 200
San Antonio, TX 78216

1 Jeff Kollgaard
Boeing Commercial Airplane Group
P.O. Box 3707 MS 9U-EA
Seattle, WA 98124-2207

1 Bob Lamson
Aviation Partners
Box 81107
Seattle, WA 98108

1 Steve LaRiviere
Boeing
P.O. Box 3707, M/S 9U-EA
Seattle, WA 98136

2 Jess Lewis
FAA
P.O. Box 882
Mustang, OK 73064

1 Jack Lincoln
USAF/TOGAA
ASC/ENE Bldg. 125
2335 Seventh St., Ste. G
Wright Patterson AFB, OH 45933

1 Gordon Lindstrom
Saab Aircraft
S-581 88 Linkoping
Sweden

1 John Marshall
Delta Air Lines, Inc.
Dept. 563, 1500 Aviation Blvd.
Hartsfield Atlanta Int'l. Airport
Atlanta, GA 30320

1 Jim Mazza
AFRL/MLSA
2179 Twelfth St., Rm. 122
Wright-Pat. AFB, OH 45433-7718

1 Glae McDonald
US Airways
Maintenance Hangar
5020 Hangar Rd., P.O. Box 19004
Charlotte, NC 28219

1 Pamela McDowell
Boeing Defense & Space Group
P.O. Box 3707
MS 4X-56
Seattle, WA 98124-2207

1 Matthew Miller
Boeing Commercial Airplane Group
P.O. Box 3707, MS 6M-67
Seattle, WA 98124-2207

1 Tommy Mullis
WR-ALC/TIEDM
420 2nd St. Suite 100
Robins AFB, GA 31098

1 George Murphy
Federal Express
7401 World Way West
Los Angeles, CA 90045

1 Amir Nasruddin
US Airways
Pittsburgh Int'l Airport
P.O. Box 12346, MC Pit/D345 Hangar 3
Pittsburgh, PA 15231-0346

1 Arnold Nathan
Israel Aircraft Industries
Eng. Div. Dept. 4441
Ben Gurion Int'l. Airport, Israel

1 Burl Nethercutt
American Airlines
Maintenance & Eng. Center
P.O. Box 582809, MD 23
Tulsa, OK 74158-2809

1 Jim Newcomb
FAA Hughes Technical Center
AAR-433
Atlantic City Int'l. Airport, NJ 08405

1 Tom O'Connor
ARTI
One Ridgmar Centre
6500 West Freeway
Fort Worth, TX 76116-2187

1 Don Oplinger
FAA Hughes Technical Center
ACD-220, Bldg. 210
Atlantic City Int'l Airport, NJ 08405

1 John Oxenford
Syncrude Canada Ltd.
9421 – 17 Ave.
Edmonton, Alberta T6N 1H4

1 Don Palmer
Boeing
P.O. Box 516
MC 102-1111
St. Louis, MO 63166

1 David Rashi-Dian
Boeing
Internal Mail Code 35-35
3855 Lakewood Blvd
Long Beach, CA 90846

1 Francis Rose
Aeronaut. & Maritime Research Lab
506 Lorimer St Fishermens Bend
P.O. Box 4331
Melbourne, Victoria, Australia 03001

1 Paul Rutherford
Boeing Defense and Space Group
P.O. Box 3999
MS 4X-56
Seattle, WA 98124-2499

1 Lt. Jim Ryan
AFRL/VASE
2790 D St., Rm. 504
Wright-Pat. AFB, OH 45433-7402

1 Forrest Sandow
AFRL/VASA Bldg. 45
2130 8th St., Suite 1
Wright-Pat. AFB, OH 45433

1 Christine Scala
Aeronaut. & Maritime Research Lab
506 Lorimer St Fishermens Bend
P.O. Box 4331
Melbourne, Victoria, Australia 03001

1 Bill Schweinburg
WR-ALC/TIED
420 Second St., Ste. 100
Robins AFB, GA 31098

1 Paul Sconyers
DOT/FAA
Atlanta Aircraft Cert. Office
1701 Columbia Ave., Ste. 2-160
College Park, GA 30337-2748

1 Nick Shah
Boeing
2401 E. Wardlow Rd.
Long Beach, CA 90807-5309

1 Surendra Shah
Lockheed-Martin Aero. Systems
1465 Sumter Drive
Marietta, GA 30064

1 Tom Shahood
Textron Systems Division
201 Lowell St., MS-1113
Wilmington, MA 01887-2941

2 William Shurtleff
Iowa State University
1915 Scholl Road
Ames, IA 50011

1 Chris Smith
FAA Hughes Technical Center
AAR-430
Atlantic City Int'l. Airport, NJ 08405

5 Fred Sobeck
FAA Flight Standards
AFS 330D
800 Independence Ave. SW
Washington, DC 20591

1 Barry Spigel
Southwest Research Institute
P.O. Drawer 28510
San Antonio, TX 78228-0510

1 Paul Tan
FAA Hughes Technical Center
AAR-433
Atlantic City Int;l. Airport, NJ 08405

1 Bob Thomas
Wayne State University
Institute for Manufacturing
66 W. Hancock 242 Physics
Detroit, MI 48201

1 Patrick Walter
Texas Christian University
Engineering Dept., Box 298640
Ft. Worth, TX 76129

1 Mike Waddell
AFRL/MLMP
2977 P St., Bldg. 653, Suite 6
Wright-Pat. AFB, OH 45433-7739

1 Hans Weber
Weber Technology Applications
7916 Laurelridge Rd
San Diego, CA 92120

1 Bud Westerman
Boeing Defense & Space Group
P.O. Box 3707
MS 4X-56
Seattle, WA 98124-2207

1 Raymond Worley
Delta Air Lines, Inc.
1500 Aviation Blvd. TOC-1
Dept. 521/NDI
Hartsfield Atlanta Int'l. Airport
Atlanta, GA 30320

1 Dwight Wilson
Boeing
2401 East Wardlow Rd
MC C071-0013
Long Beach, CA 90807-5309

1 Nancy Wood
Boeing
P.O. Box 516
MC 1-2-1111
St. Louis, MO 63166

1 Rich Yarges
FAA-ANM 112
1601 Lind Ave. SW
Renton, WA 98055-4099

1 Jin Yu
Boeing
2401 East Wardlow Rd
MC 71-34
Long Beach, CA 90807-5309

1	MS-0958	Carol Adkins, 1472
1	MS-0958	Tommy Guess, 1472
1	MS-0724	Joan Woodard, 6000
1	MS-0766	Dori Ellis, 6300
1	MS-0767	Henry Abeyta, 6312
1	MS-0615	Dick Perry, 6352
1	MS-0615	Mike Ashbaugh, 6352
1	MS-0615	Larry Dorrell, 6352
1	MS-0615	Ken Harmon, 6352
1	MS-0615	Craig Jones, 6352
1	MS-0615	David Moore, 6352
20	MS-0615	Dennis Roach, 6352
1	MS-0615	Mike Valley, 6352
5	MS-0615	Phil Walkington, 6352
1	MS-0829	Floyd Spencer, 12323
1	MS-9018	Central Technical Files, 8940-2
2	MS-0899	Technical Library, 4916
2	MS-0619	Review & Approval Desk, 12690
		For DOE/OTSI